SCIENTIFIC CONFERENCE
Le Bourget-du-Lac – July 2022

PRE-PRINT 2021

SYMPOSIUM 03
Cave deposits

Internal microstratigraphy and lamination pattern as a tool for deciphering past hydrological conditions: a study case of a Middle Pleistocene stalagmite (Grotte de l'Été, Saône-et-Loire, France)

Jonathan AVELLAN, <u>Christine PERRIN</u> & Christian PERRENOUD

Muséum National d'Histoire Naturelle, HNHP UMR7194, CERP Tautavel Avenue Léon-Jean Grégory, 66720 Tautavel France
<u>cperrin@mnhn.fr</u> (corresponding author)

Abstract

Stalagmite growth is governed by the water flux, the CO_2 saturation of drip water relative to the cave atmosphere, and temperature. These parameters are inter-related and linked to both climate and site-specific conditions of the karst hydrological dynamics. Petrography and microstratigraphy of speleothems have thus the potential to provide clues for deciphering the relationships between stalagmite fine-scale internal architecture and the hydrological conditions of stalagmite feeding, in particular variability of drip rate which in turn yields important climatic information.

We report here on a lower-Middle-Pleistocene calcite stalagmite from the "Grotte de l'Été" (Saône-et-Loire). In our approach, we combine successive morphologies of the stalagmite apex, variations of stalagmite width, nature and occurrence of discontinuities and growth interruptions, facies and lamination characteristics, frequency of laminae, in order to infer their significance in terms of microenvironmental and hydrological changes.

The results show that the integration of this information provides a consistent picture of the evolution of the rate of infiltration, its variability, and the state of saturation of the feed water, thus making it possible to reconstitute the history of the hydrology of the seepage site at the time of speleothem deposition.

Résumé

Architecture interne et patron de lamination pour déchiffrer les conditions paléohydrologiques: étude d'une stalagmite du Pléistocène moyen (Grotte de l'Été, Saône-et-Loire, France)

La croissance des stalagmites est gouvernée par le débit d'alimentation, la pression partielle de CO_2 de l'eau d'infiltration par rapport à celle de l'air de la cavité, et la température. Ces paramètres sont interdépendants et liés au climat et aux conditions spécifiques du site en termes de dynamique hydrologique. La pétrographie et la microstratigraphie des stalagmites permettent ainsi d'appréhender les relations entre leur architecture interne et les conditions hydrologiques de leur alimentation, en particulier la variabilité du débit d'alimentation, qui à son tour livre des informations importantes sur le paléoclimat.

Les travaux présentés ici portent sur une stalagmite calcitique du Pléistocène moyen inférieur de la Grotte de l'Été (Saône-et-Loire). L'approche analytique combine l'évolution de la morphologie sommitale et de la largeur de la concrétion, la nature et l'occurrence des discontinuités et des arrêts de croissance, les caractéristiques des faciès et de la lamination, pour en déduire des informations sur les changements environnementaux et hydrologiques.

Les résultats montrent que l'intégration de ces informations constitue une image cohérente de l'évolution du taux d'infiltration, de sa variabilité et de l'état de saturation de l'eau d'alimentation, permettant ainsi de reconstituer l'histoire hydrologique du site d'infiltration au moment de la formation du spéléothème.

1. Introduction

Stalagmite growth is governed by climate at global and regional scales, and site-specific conditions of the karst hydrological dynamics, which in turn constrain the feeding drip conditions of each individual stalagmite. Beside climate, both physical (i.e., conditions of feeding water-flow) and chemical (i.e., geochemistry of groundwater) properties of water feeding speleothems exert strong controls on the crystal precipitates and thereby on petrographic and geochemical characteristics of speleothems. Therefore, reliable interpretation of proxies requires the prior understanding of the relationship between proxy and one or several climate parameters. For this purpose, a widely used method is cave monitoring, which allows present-day site-specific cave parameters to be linked to the external climatic and environmental conditions, as well as the driving factors of carbonate formation to be determined. However, these relationships may evolve through time and their present-day state may differ from those prevailing at the time of

speleothem growth. Within the soil-karst-cave system, the groundwater flow feeding speleothems commonly bears two components: a rather diffuse slow long-residence time, high-storage infiltration, and a more rapid fissure-driven, short-residence time, low-storage flow component. Change in the functioning of the karst system can induce significant changes in the infiltration conditions and in the feeding pattern of stalagmites at any drip site.

Petrography and microstratigraphy of speleothems have the potential to provide clues for deciphering the relationships between stalagmite fine-scale internal architecture and the local conditions of stalagmite feeding, in particular

variations of drip rate together with hydrological information about the infiltration conditions and drip rate feeding the stalagmite at the time of its formation. This in turn yields valuable information about the local and regional past climate conditions.

For this study, an integrated approach has been developed for inferring past conditions of speleothem growth and local conditions of hydrological setting. This approach was then applied to a large stalagmite from the Été Cave in the Macônnais region which has been dated back from the lower Middle Pleistocene.

2. Materials and methods

The "Grotte de l'Été" is located in the Macônnais massif, north of Mâcon and two km north of the Azé Caves (Fig. 1), which belong to the same karst system (BARRIQUAND *et al.* 2011, DAUTUN *et al.* 2014). The cave is developed in limestones from the lower-middle Bajocian and Aalenian. "Grotte de l'Été" was discovered in 2014 by speleologists exploring the tunnel drilled in the early 1930's to transport water from the Goulouze source to the village of Saint-Gengoux-de-Scissé. The explored part of "Grotte de l'Été" corresponds to a large-sealed fossil gallery partly filled with coarse detrital and clay sediments, in which a flowstone, bearing the studied stalagmite ÉTÉ 1 was found. The base and top of this speleothem were dated by uranium-thorium and the ages obtained are at the limit of this technique (>400 ka). However, TOMBRET *et al.* (2017) showed that this speleothem probably formed between 500 and 600 ka.

The general methodological approach combines observations of nature and occurrence of discontinuities and growth interruptions, facies and lamination characteristics, successive morphologies of the stalagmite apex, variations of stalagmite widths, frequency of laminae, for inferring their significance in terms of microenvironmental and hydrological changes during speleothem growth. Observations of polished slabs parallel to the general median growth axis were performed with a stereomicroscope. Large thin sections were prepared continuously along the median growth axis of the stalagmite and observed with an optical microscope. Minerals were identified from their optical properties under the

transmissive light microscope and from Raman microspectrometry operating with a 535.2 nm exciting line and a spectral window of 130-1800 cm^{-1}.
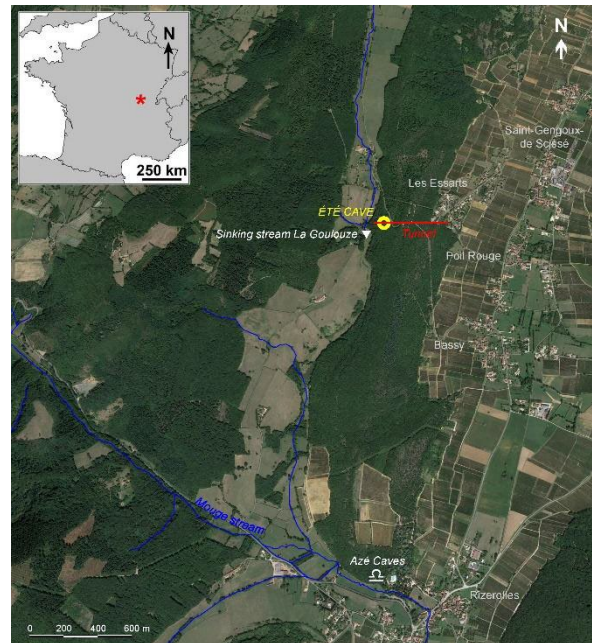

Figure 1: Localisation of the "Grotte de l'Été" (aerial view Google Earth).

3. Results

Mineralogical identifications show that the speleothem is entirely formed by calcite. Small amounts of detrital material, chiefly clay, are included at level of some surfaces of discontinuities.

Facies and lamination
Two main petrofacies, both consisting of columnar calcite, can be easily recognized in the ÉTÉ 1 speleothem (Fig. 2). The compact columnar calcite has a brown-translucent aspect in the polished slabs and a transparent appearance under the optical microscope. The intra- and intercrystalline porosity is very low. The second facies corresponds to an open columnar calcite with high intracrystalline and intercrystallite primary microporosity. The elongated pores

likely correspond to ancient and now-empty fluid inclusions. Variations of pore density from one level to the next form the lamination. This open columnar calcite has a rather white or whitish aspect on the polished slab and a more or less dark appearance under the light microscope.

Discontinuities and growth interruptions
Based on typology of discontinuities defined by previous authors (RAILSBACK *et al.* 2013, PERRIN *et al.* 2014, MARTÍN-CHIVELET *et al.* 2017), three main types of surfaces were identified in the studied sample: discontinuities associated with partial dissolution or type E surfaces *sensu* RAILSBACK *et al.* (2013), surfaces marked by a detrital clay deposit, and discontinuities resulting from abrupt facies change. Seven main surfaces of discontinuities (S1-S7) are clearly observed

in the speleothem (Fig. 2). They form the boundaries of microstratigraphic units or sub-units.

Growth units
The speleothem displays five successive growth units (Fig. 2). The first two (U1 and U2) correspond to the formation of flowstone dominated by the brown-translucent columnar

fabrics. Units 3 and 4 represent transition phases between flowstone and stalagmite, and unit 5 reflects stalagmite growth. This succession therefore expresses major changes in feeding modes of the speleothem, from a lateral, mainly continuous flow feeding flowstone (units 1 and 2) to a drip-water fed stalagmite (unit 5).
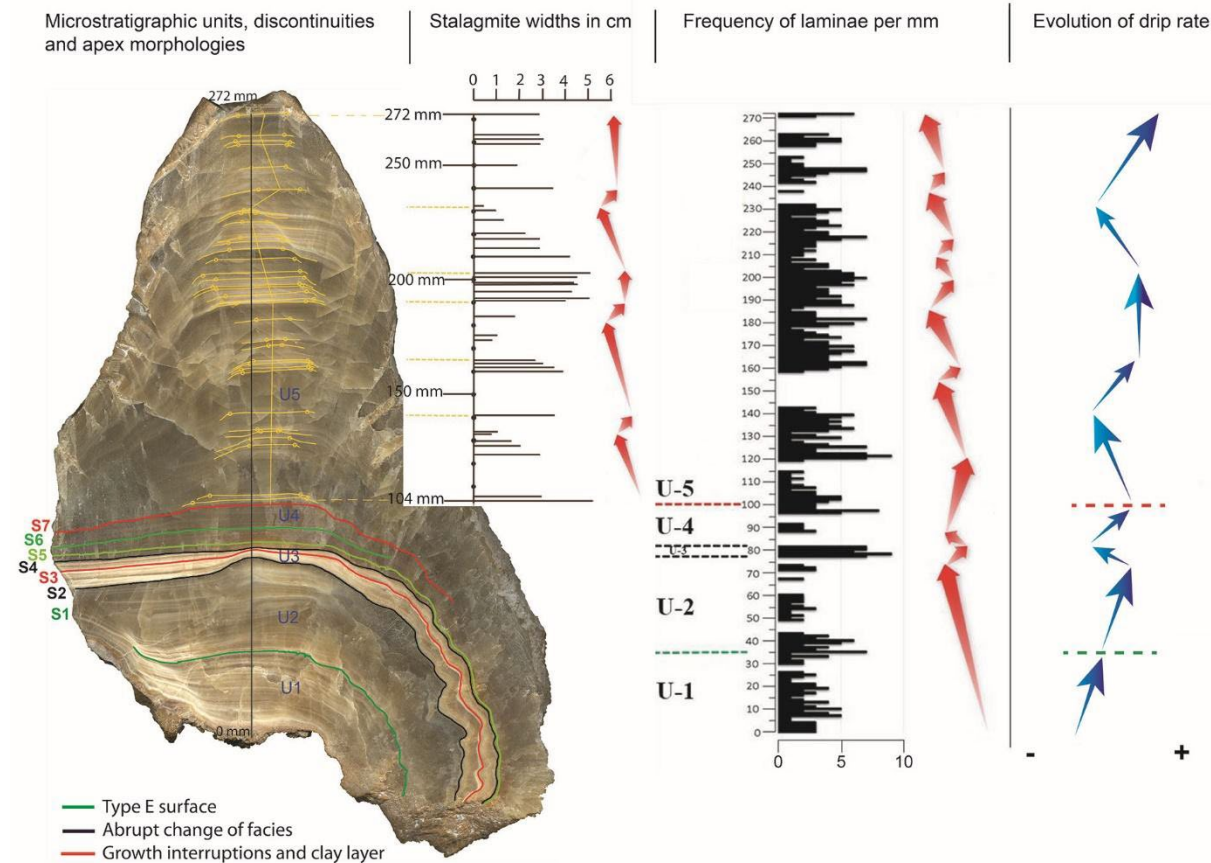

Figure 2: Summary of results obtained from the speleothem ÉTÉ 1 and interpretation in terms of variation of drip rate during speleothem growth. Red arrows denote trends of successive stalagmite width and frequency of laminae per mm, respectively. Blue arrows highlight the inferred evolution of drip rate.

Internal microstratigraphic features

We analyzed in detail some particular architectural speleothem features, which are known to be related to drip rate variability, following methodologies developed by BERTHAUX *et al.* (2002), MUÑOZ-GARCÍA *et al.* (2016), and MARTÍN-CHIVELET *et al.* (2017).

During the stalagmite phase, the apex morphology changes from flat-topped meseta shape to frilled trilobal forms and vice versa. Concomitantly, variations of stalagmite widths show retractional, progradational and aggradational stacking patterns (Fig. 2).

Significance in terms of hydrological changes and drip rate variability
All these features combined provide a coherent picture of the evolution of drip rate, drip rate variability and saturation state of water feeding the speleothem through time.
During the flowstone phase (U1 and U2), the water supply feeding the speleothem was regular and increased successively in both units; enhanced degassing conditions of the thin water film favored the regular growth of compact columnar calcite crystals. The transition phase from flowstone to stalagmite (U3 and U4) corresponds to drastic changes in hydrological conditions characterized by a relatively high variability of water supply to the speleothem ÉTÉ 1. This is shown by abrupt facies changes from compact to open columnar calcite (and vice-versa), by the relatively high frequency of discontinuities (type E surfaces) and growth interruptions, and by the high variability of the number of laminae by thickness unit. During the stalagmite

phase (U5), changes of the apex shape and stacking pattern reflect the succession of two decrease-increase cycles in drip water supply, separated by a period of rather constant drip rate (Fig. 2).

4. Conclusion

The speleothem ÉTÉ 1 records the growth of a flowstone which gradually evolves into a large stalagmite as a consequence of change in the source of water feeding the speleothem (i.e., lateral water flow to drip site). Some petrographic and microstratigraphic elements reflect the hydrological history of the speleothem and can be used to infer variability and regularity of water flow feeding the speleothem.

These first results are expected to provide an efficient tool for interpretation of the isotopic and geochemical data in terms of climatic and environmental changes. They also emphasize the value of such integrated approach for documenting hydrological history of drip site, in particular for fossil (e.g., non-still growing) speleothems or those for which *in situ* monitoring could not be undertaken or did not appear relevant.

Acknowledgments

References

BARRIQUAND L., BARRIQUAND J., ARGANT A., FLOSS H., GALLAY A., GUÉRIN C., GUILLOT L., JEANNET M., NYKIEL C., QUINIF Y. (2011) Le site des grottes d'Azé. *Quaternaire*, H.S. n°4, 15-25.

BERTHAUX J., SONDAG F., SANTOS R., SOUBIÈS F., CAUSSE C., PLAGNES V., LE CORNEC F., SEIDEL A. (2002) Paleoclimatic record of speleothems in a tropical region: study of laminated sequences from a Holocene stalagmite. *Quaternary International*, 89, 3-16.

DAUTUN S., BARRIQUAND L., GUILLOT L., SILVA S. (2014) Fonctionnement hydrogéologique du système karstique des Grottes d'Azé, mise en place d'un suivi hydrochimique et traçages colorimétriques. *Actes 24ème Rencontre d'octobre*, Azé, 117–134.

MARTÍN-CHIVELET J., MUÑOZ-GARCÍA M.B., CRUZ J.A., ORTEGA A.I., TURRERO M.J. (2017) Speleothem Architectural Analysis: Integrated approach for stalagmite-based paleoclimate research. *Sedimentary Geology*, 353, 28–45.

MUÑOZ-GARCÍA M.B., CRUZ J., MARTÍN-CHIVELET J., ORTEGA A.I., TURRERO M.J., LOPEZ ELORZA M. (2016) Comparison of speleothem fabrics and microstratigraphic stacking patterns in calcite stalagmites as indicators of paleoenvironmental change. *Quaterny International*, 407, 74-85.

PERRIN C., PRESTIMONACO L., SERVELLE G., TILHAC R., MAURY M., CABROL P. (2014) Aragonite–Calcite Speleothems: Identifying Original and Diagenetic Features. *Journal of Sedimentary Research*, 84, 245–269.

RAILSBACK L., AKERS P., WANG L., HOLDRIDGE G., VOARINTSOA N.R. (2013) Layer-bounding surfaces in stalagmites as keys to better paleoclimatological histories and chronologies. *International Journal of Speleology*, 42, 167–180.

TOMBRET O., GHALEB B., BAHAIN J.J. (2017) *Résultats d'analyse U-Th et calculs d'âge pour des échantillons de carbonates issus d'une stalagmite de la Grotte de l'Eté à Azé (Bourgogne)*. Rapport non publié UMR 7194 HNHP.

The Story behind the fluvial deposits in the Caumont chalk caves, France

Daniel BALLESTEROS[1], Andrew FARRANT[2], Diana SAHY[2], Kim GENUITE[1], Ingrid BEJARANO[1] & Carole NEHME[1]

(1) UMR 6266 IDEES, University of Rouen Normandy / CNRS, Mont St-Aignan CEDEX, France, ballesteros@geol.uniovi.es, kim.genuite@univ-rouen.fr, ingridbejarano.geo@gmail.com, carole.nehme@univ-rouen.fr (corresponding author)
(2) British Geological Survey, Keyworth, Nottingham, NG12 5GG, United Kingdom, arf@bgs.ac.uk, dihy@bgs.ac.uk

Abstract

The particular history of Caumont quarries and caves resulted in the availability of suitable stratigraphical sections of infill to study the cave evolution. In this sense, the stratigraphy of 16 sections were detailed and combined with microscopical observations, XRD analyses and U/Th datings of speleothems. The results helped us define four stratigraphical units. Both units 1 and 2 resulted from the erosion of the cave bedrock before from 300 to 127 ka, while the unit 3 included allochthonous sediments originally from the topographical surface. These sediments were introduced into the system through solution pipes during the Upper Pleistocene. Finally, the muddy unit 4 was deposited under slack-waters conditions. Overall, the infill of Caumont caves recorded the evolution of the karst during the last 300 ka, revealing the efficient connection between the endokarst and the plateau surface after 127 ka.

Résumé

Les dépôts fluviatiles dans les grottes de la craie de Caumont (Normandie, France). Les carrières et les grottes de Caumont présentent la particularité de recéler des remplissages dont la stratigraphie permet de reconstituer l'histoire. Dans ce but, les stratigraphies de 16 sections sont examinées au moyen d'observations microscopiques, d'analyses XRD et de datations U/Th de spéléothèmes. Ainsi, quatre unités stratigraphiques peuvent être identifiées qui permettent de reconstituer l'évolution de ce karst sur les 300.000 dernières années.

1. Introduction

Protected from surface weathering and erosion, cave deposits are superb archives of information on landscape and environmental change. They can provide the evidence required to unravel the evolution of karst systems and regional landscapes over 10^5-10^6 year timescales. However, this requires access to suitable deposits. Often, researchers are only able to access limited parts of any sedimentary deposits, usually those located at the top of detrital sections. The older parts and their internal characteristics often remain hidden unless revealed by natural processes or human excavation. This is especially true for caves formed in Upper Cretaceous Chalk, which are typically formed under paragenetic conditions (FARRANT et SMART, 2011). Most chalk caves are small and sediment filled.

This study documents the caves and their sediments revealed by underground stone extraction at Caumont, in northern France. Here, quarrying for building stone has cut through a network of natural, often sediment-filled cave passages. Caumont caves (Fig. 1) were discovered through the historical underground quarrying that lasted from the medieval period to the 19th century. Between 2018 and 2020, the IDEES Laboratory of the University of Rouen-Normandie conducted the *Archéomateriaux, Territoire, Patrimoine* (ATP) project to study the historical underground quarries with the cooperation of the *Comité Régional de Spéléologie de Normandie* (CRSN) of the *Fédération Française de Spéléologie*. Caumont quarries supplied a particular type of high-quality chalk building stone since Gallo-Roman times (Ballesteros et al., 2021). In Caumont, quarrymen mined 12 km of galleries, intercepting active karst conduits filled with cave sediments. Speleologists subsequently explored these caves, often by partially excavating the cave infill (e.g., RODET, 1997; RODET et STAIGRE, 2019), discovering over two kilometers of natural cave passages. The discovery of this complex cave system has made Caumont caves a key site for the speleological community in Normandy (e.g., BEAUFILS, 2018) as no other karst caves in the Chalk areas of northern France rival the large development of Caumont system.

The caves and cave sediments at Caumont were first studied by RODET (1985, 2007, 2010), establishing their origin and development. The present research builds on this earlier work, aiming to reconstruct the regional paleoclimate and paleoenvironment of the Normandy region through the analysis of cave geomorphology and their associated speleothem and detrital deposits. NEHME *et al.* (2020) showed that cave development is linked to the incision of the Seine River over the past million years. Initial cave development was focused on certain low-permeability stratigraphical horizons in the Chalk succession including marl seams (thin clay beds), sheet flints and hardgrounds (mineralized beds that represents past seafloors). Groundwater flow concentration and subsequent mixing dissolution on these horizons, initiated conduit

development (BALLESTEROS *et al.,* 2020). These stratigraphical inception horizons are particularly numerous and well developed in Normandy, compared to southern England, where chalk caves are less common and smaller. Evidence from river terrace deposits and other caves in the Seine Valley suggest Caumont caves were initially formed c. 500-600 ka (NEHME et al., 2020). Uranium-thorium dating of a flowstone from the lowest level of Caumont system gives a minimum age of 301 ± 20 ka BP for base-level lowering and passage abandonment.

The focus of the current research is the reconstruction of the evolution of Caumont cave system from the Chibanian (Middle Pleistocene) to the present and linking this with the fluvial incision. This work combines geomorphological, geological, geochemical, and geochronological techniques to determine the speleogenesis of the system.
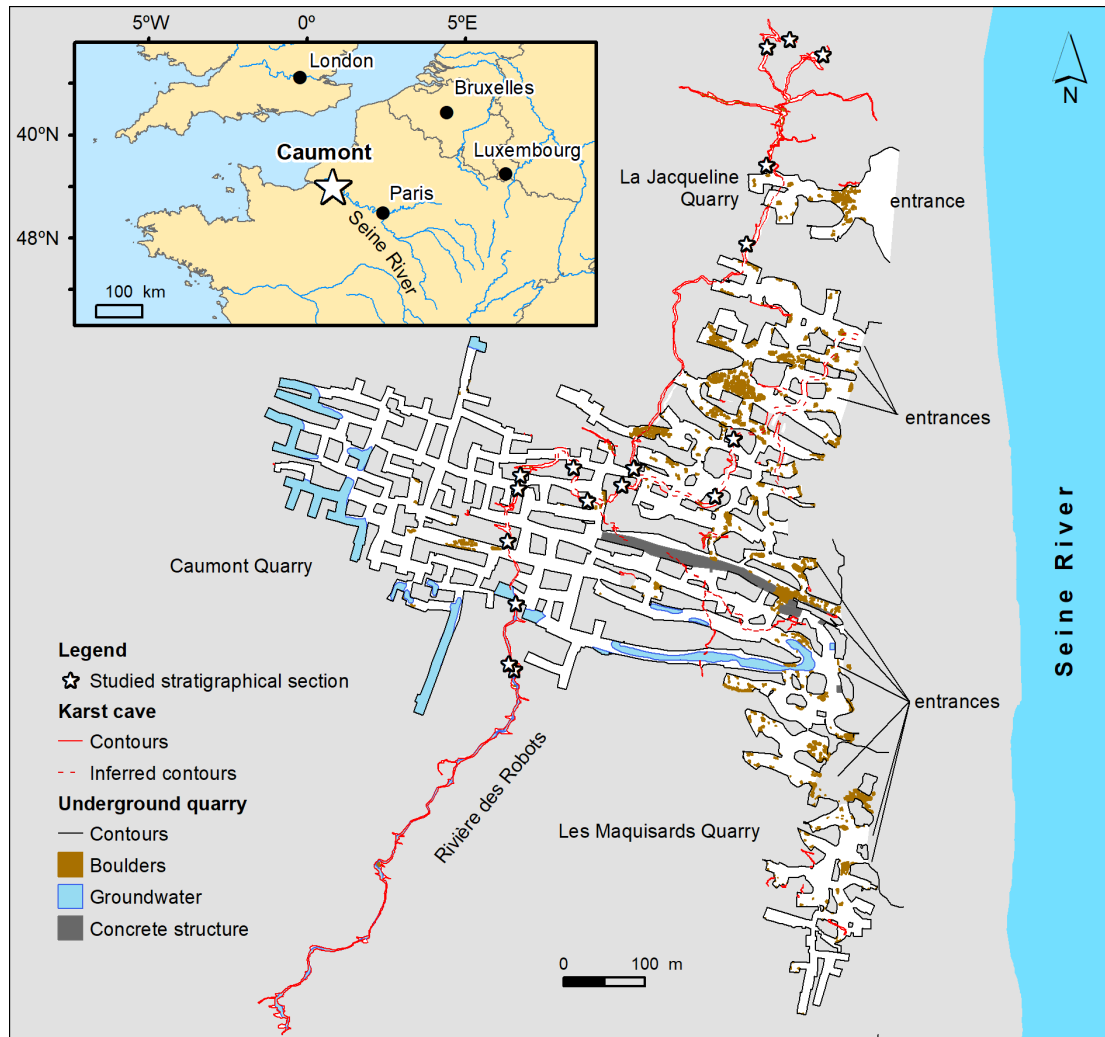

Figure 1: Location of Caumont quarries and caves in Normandy, northern France.

2. Materials and methods

This study used multiple techniques to reconstruct the cave geometry, to describe the mineralogy and texture of the sediments, and to constrain the age of the deposits. Together, the data enabled us to reconstruct a conceptual model of the evolution of the cave and its associated deposits. This work comprised five steps.

Step 1 was to undertake an accurate survey of the cave system and the quarry (Fig. 1) using a distometer laser range finder. The raw survey data was then computed using Compass software to create the georeferenced survey in a geographical information system.

Step 2 was the identification and description of fifteen sediment sections within the caves (Fig. 1). Detailed stratigraphical descriptions (lithology, texture, structure,

thickness) helped defining similar sedimentary units between different sections throughout the cave system.

The third step was the analysis of thin sections. Ten thin sections of detrital layers were analyzed using an optical microscope (Leica) to identify the structure and texture of sediments, and to characterize the various minerals and clasts. A specific identification of certain key mineral phases, for example, metamorphic, igneous, and biogenic quartz, helped identifying the sources of the cave sediments.

Phase 4 was the analysis via X-Ray Diffraction (XRD) to identify the clay minerals. The abundance and/or absence of particular clay minerals can be related to the sedimentary environment and the paleoclimatic context of its deposition. The final step was to constrain the age of the deposits using

uranium-series dating. Speleothems located on the top of the sediments or within interbedded layers were dated to

constrain the minimal and maximal age of sediment deposition.

3. Preliminary results and interpretations

Field evidence and more detailed observations enabled us to define four distinct and laterally continuous stratigraphical units separated by erosive uniformities. From the bottom to the top, the units are:

Unit 1: up to 0.5 m of dark orange-brown coarse sand to silt, showing up-fining sequences. Erosive channels, cross bedding and ripple lamination are locally present. Thin sections and clast lithology analysis show that the sand grains in Unit 1 are comprised of sub-angular igneous and metamorphic quartz, as well as flint (chert). These characteristics indicate that this unit corresponds to thalweg and channel facies, in which sediments were transported and deposited by streams.

Unit 2: 0.1 to 1 m of brown, frequently massive or thinly laminated silt and clay. The silt is comprised of igneous and metamorphic quartz. The sedimentary characteristics of Unit 2 correspond to active channel deposits associated with streams. A flowstone precipitated on the top of Unit 2, dated to 127 ka, has been partially eroded. The sediments were also eroded, leaving the remaining flowstone perched above the deposits as a false floor. This evidence suggests that Units 1 and 2 were deposited before 127 ka.

Unit 3 overlies units 1 and 2 and comprises 0.1 to 1 m of brownish-yellow silt and fine sand, with interbedded

pebbles. These sediments constitute up-fining sequences with small pebbles defining an erosive surface at the bottom. Ripple and parallel lamination are recognized along the sequences, as well as interbedded Clay-with-Flint type deposits. The thin sections indicate that both the silt and sand grains are subangular and exhibit moderate sorting. Most of the grains are composed of metamorphic quartz. Flint, chalk, speleothem fragments and Eocene limestone clasts are also present. The unit is frequently overlain by speleothems. The up-fining sequences, sedimentary structures and clear channel facies indicate that the sediments were deposited in cave streams under high discharge conditions. Such flood events eroded previous speleothems and earlier sediments. The moderate sorting and restricted grain size suggest that much of the sediment was originally derived from the erosion of the Clay-with-Flints and aeolian deposits that cover much of the surrounding Normandy plateau. Here, the Clay-with-flint and aeolian sediments were introduced into the endokarst by debris-flow and collapse processes, probably via dissolution pipes. Two uranium-series dates of flowstone constrain the age of the Unit 3 to between 127 and 10 ka.
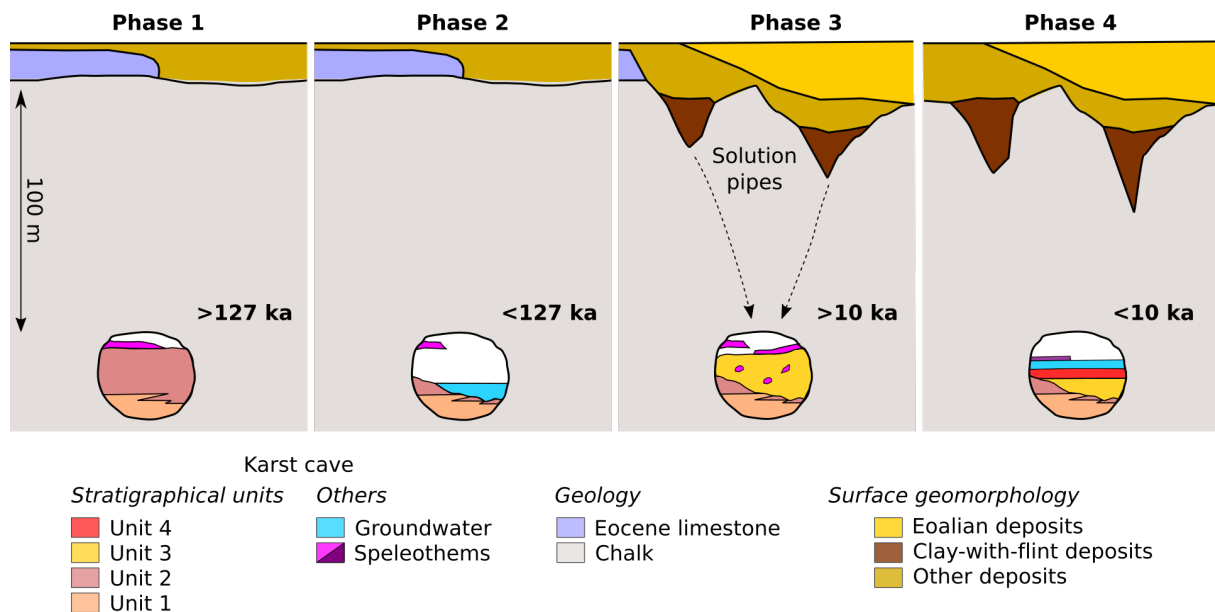

Figure 2: Conceptual model showing the evolution of Caumont caves: (a) Phase 1 with deposition of units 1 and 2 and the precipitation of a flowstone at 127 ka; (b) Phase 2 causing the partial erosion of previous units the flowstone formed 127 ka ago, remaining perched on sediment fills; (c) Phase 3 defined by the deposition of unit 3, involving allogenic sediments and clasts; and (d) phase 4, when cave passages were partially filled by groundwater, triggering the decanting of unit 4.

Unit 4: 5 to 90 cm of brown, sometimes silty massive clay. This unit is deposited directly over the bedrock or on the top of Units 2 and 3. The deposition of Unit 4 is most likely to have occurred in conduits partially or totally filled by water. This ponding is either due to a general water table rise by aggradation at the resurgence, or local ponding within the

cave by other deposits, for example a rock-fall, that acted as a dam. A uranium-series dating suggests that the Unit 4 was formed mainly during the Holocene.

The identification of the four stratigraphical units enabled the construction of a preliminary history of the infill of

Caumont caves since the Chibanian (Fig. 2). The evolution of the cave deposits can be divided into four phases:

The first phase was the deposition of Units 1 and 2 during the period between the estimated formation of the Caumont caves at c. 500-600 ka (Nehme *et al.*, 2020) and 127 ka (Fig. 2). This was most likely during the onset of an interglacial period when underground drainage systems were active. The apparent lack of allochthonous sediments suggests that both units derived mainly from the erosion of the bedrock and autogenic surface deposits, with few if any allogenic inputs from outside the Caumont area. This phase of sedimentation ended with the draining of the cave and deposition of speleothems.

Phase 2 marked a change to erosion, with much of the previous Units 1 and 2 deposits being eroded. The overlying flowstone was locally undermined, causing the partial collapse of the flowstone deposits, the remains of which are preserved in the cave walls and floors (Fig. 2). This phase suggests changes in the drainage (e.g., lowering of the Seine river and sea level, wetter conditions).

The third phase was the deposition of Unit 3 under fluvial conditions during the Upper Pleistocene, sometime between 127 and 10 ka. The provenance of Unit 3 includes allochthonous materials including aeolian deposits and Eocene limestones, indicating a link to the surface (Fig. 2). Fragments of speleothems indicate some reworking of previous deposits.

The final phase prior was the partial erosion of previous deposits and infilling of the conduit by slack-water facies, probably after 10 ka BP (Fig. 2). This may relate to paragenetic sedimentation following base-level rise related to the Holocene sea-level rise and aggradation in the adjacent Seine Valley.

The intersection of the Caumont caves by quarrying and subsequent exploration has led to a reactivation of the conduit and flushing out of some of the sediments, creating the sections observed in this study.

4. Conclusions

The intersection of caves developed in Upper Cretaceous Chalk by quarrying has revealed sediment sections than can be used to decipher the history of cave development. Preliminary results identify four distinct stratigraphical units, deposited since the Chibanian. The initial phase of sedimentation, characterized by the deposition of coarse fluvial sand, silt and pebbles resulting from the erosion of the bedrock, was followed by a period of speleothem deposition. After 127 ka, groundwater floods eroded part of the cave infill. Renewed fluvial activity introduced allogenic sediments from the overlying plateau surface, including Eocene limestone, Clay-with-Flint and aeolian sediments. The final phase involved partial erosion of the sediment and the deposition of a slack-water facies, possibly related to Holocene aggradation of the Seine Valley.

Acknowledgments

References

BALLESTEROS D., FARRANT A., NEHME C., WOODS M., TODISCO D., MOURALIS D. (2020). Stratigraphical influence on chalk cave development in Upper Normandy, France: implications for chalk hydrogeology. *International Journal of Speleology*, n°49, 187-208.

BALLESTEROS D., PAINCHAULT A., NEHME C., TODISCO D., VARANO M., MOURALIS D. (2021). Normand Chalkstone (France): geology and historical uses from quarries to monuments. *Episodes*, doi: 10.18814/epiiugs/2020/0200s03.

FARRANT, A.R. and SMART, P.L., 2011. Role of sediment in speleogenesis; sedimentation and paragenesis. *Geomorphology*, n°134, 79-93.

NEHME C., FARRANT A., BALLESTEROS D., TODISCO D., RODET J., SAHY D., GRAPPONE J.M., STAIGRE J., MOURALIS, D. (2020). Reconstructing fluvial incision rates based upon palaeo-water tables in Chalk karst networks along the Seine valley (Normandy, France). *Earth Surface Processes and Landforms*, doi: 10.1002/esp.4851

RODET J. (1985). Le développement du karst dans la craie de Normandie et ses conséquences sur la protection des eaux souterraines (Normandie, France). *Annales de la Société Géologique de Belgique*, n°108, 31-41.

RODET J. (1997). À la limite de la Spéléologie, la Karstologie de la Craie. *Spelunca* n°23, 73-75.

RODET J. (2007). Chalk karst and aquifer of Normandy. *European Journal of Water Quality*, n°38, 11-21.

RODET J. (2010). Les karsts du bassin de Paris. *Karstologia Mémoires*, n°9, 148-153.

RODET J., STAIGRE J.-C. (2019). Désobstruction et spéléologie en Normandie. Actes du premier colloque francophone Histoires de désob', *Spelunca Mémoires* n°38, Fédération Française de Spéléologie, Azé, pp. 180-207.

Dating speleothems in Southern Italy (Apulia and Sardinia): palaeoclimate implications and speleogenetic clues

Andrea COLUMBU[1], John HELLSTROM[2], Carlos PÉREZ-MEJÍAS[3], Hsun-Ming HU[4,5],
Russell DRYSDALE[6], Jon WOODHEAD[2], Hai CHENG[3], Chuan-Chou SHEN[4,5],
Jo DE WAELE[1], Veronica CHIARINI[1], Laura SANNA[7] & Mario PARISE[8]

(1) Department of Biological, Geological and Environmental Sciences, University of Bologna, Via Zamboni 67, 40126, Bologna, Italy, andrea.columbu2@unibo.it (corresponding author), veronica.chiarini3@gmail.com, jo.dewaele@unibo.it

(2) School of Earth Sciences, University of Melbourne, Vic, 3010, Australia, john@ionium.net, jdwood@unimelb.edu.au

(3) Institute of Global Environmental Change, Xi'an Jiaotong University, Xi'an, 710049, China, perezmegias@mail.xjtu.edu.cn, cheng021@xjtu.edu.cn

(4) High-precision Mass Spectrometry and Environment Change Laboratory (HISPEC), Department of Geosciences, National Taiwan University, Taipei, 10617, Taiwan, ROC, hsunming.hu@gmail.com, river@ntu.edu.tw

(5) Research Center for Future Earth, National Taiwan University, Taipei 10617, Taiwan, ROC, hsunming.hu@gmail.com; river@ntu.edu.tw

(6) School of Geography, University of Melbourne, 221 Bouverie Street, VIC, 3010, Melbourne, Australia, rnd@unimelb.edu.au

(7) CNR-IGAG, National Research Council of Italy, Institute of Environmental Geology and Geoengineering, Via Marengo 2, 09123 Cagliari, Italy, laura.sanna@igag.cnr.it

(8) Department of Earth and Environmental Sciences, Università "Aldo Moro", Via Orabona 4, 70125, Bari, Italy, mario.parise@uniba.it

Abstract

This study reports the results of a comprehensive radiometric dating campaign carried out on 51 speleothems from caves in Apulia and Sardinia during the last ~7 years. Around 230 ages were produced by exploiting the U-Th method. Sampling targeted 5 caves in Apulia and 12 caves in Sardinia. All caves are located ~41˚N (±1˚) latitude, representing an ideal location for the understanding speleothem deposition in relation to past Mediterranean climate. U-Th dates can be used as minimum age for the caves in which they formed, hence providing geochronological constraints on speleogenetic processes. The preliminary results attest that in both regions: 1) there is evidence of speleothem deposition since 600-800 thousand years before present (ka), implying that speleogenesis occurred beforehand. According to cave morphology observations, and in relation to local geology, the formation of most of the explored caves is estimated to have occurred several millions of years before present; 2) speleothem deposition occurred during glacial (last glacial, MIS6, MIS8, MIS10) and interglacial (Holocene, MIS5, MIS7, MIS9, MIS13) stages over the last ~500 ka. This implies that climate during the glacial stages was never too cold and dry to impede speleothem deposition, as has been the case in other parts of Europe.

Résumé

Datations de spéléothèmes dans le Sud de l'Italie (Apulie et Sardaigne) : implications paléoclimatiques et indices spéléogénétiques. Cette étude porte sur les résultats d'une campagne de datation radiométrique menée sur 51 spéléothèmes prélevés pendant les 7 dernières années dans 5 grottes d'Apulie et 12 de Sardaigne. Ces grottes sont situées à proximité du 41 °N, localisation idéale pour comprendre les conditions de formation des spéléothèmes en fonction des climats passés de la Méditerranée. Les dates U-Th peuvent donner un âge minimum pour les grottes dans lesquelles se trouvent les spéléothèmes, contraignant ainsi le cadre géochronologique de la spéléogenèse. Ces résultats préliminaires montrent que dans les deux régions : i) des spéléothèmes se sont formés depuis 600.000 à 800.000 ans, impliquant que les grottes sont plus anciennes. Les observations des formes souterraines en fonction de la géologie locale montrent que la majorité des grottes explorées se sont formés il y a plusieurs millions d'années ; ii) la formation des spéléothèmes s'est faite durant les périodes glaciaires (LGM, MIS 6, MIS 8, MIS 10) et interglaciaires (Holocène, MIS 5, MIS 7, MIS 9, MIS 13) durant les derniers 500.000 ans. Cela implique que le climat durant cette période ne fut jamais trop froid ni trop sec pour empêcher la formation des spéléothèmes, comme cela a été le cas dans d'autres régions d'Europe.

1. Introduction

Dating speleothems provides the twofold opportunity to: 1) understand the relation between cave calcite deposition and past climates (FAIRCHILD & BAKER, 2012); and 2) attribute minimum ages to the caves in which speleothems

formed (SASOWSKY, 1998). Regarding point 1, $CaCO_3$ precipitation is only possible if the precipitation /evapotranspiration (PE) ratio is > 1 at a certain location, and meteoric water is able to percolate into the karst reservoir. Additionally, soils must provide CO_2 (and/or bedrock pyrite oxidation must provide H_2SO_4) to the infiltrating water in order to trigger the dissolution of the bedrock and the consequent precipitation of calcite once the seepage reaches the vadose cave environment (FRISIA & BORSATO, 2010). Accordingly, climate periods that better sustain a regular and continuous deposition of speleothems are those characterized by relatively humid (= abundance of precipitation, i.e., no aridity) and warm (=high soil bioproductivity, i.e., no bare soils) conditions, especially at middle latitudes. Regarding point 2, the age of "voids" can be estimated by dating the deposits they contain. Speleothems often represent the most suitable samples to chronologically constrain cave formation, considering that other datable deposits such as allochthonous sediments and/or dissolution by-products (i.e. alunite and/or dolomite, POLYAK, 1998; POLYAK et al., 2016) are not as common as cave calcite.

Additionally, speleothem dating using the U-Th method has seen remarkable technical improvements in recent times

and can be extremely precise (HELLSTROM, 2006; CHENG et al., 2016).

This work presents an extensive U-Th chronological dataset, reporting the age of numerous speleothems sampled in two southern Italian regions: Sardinia and Apulia. The first is an island strategically located at the centre of the western Mediterranean Sea, while the second, comprising the "heel" of the Italian "boot", is representative of the southern portion of the Peninsula. Speleothem-based research has been intense in Italy over the last ~20 years, although it mostly focused on the north of the country (FRISIA et al., 2005; ZANCHETTA et al., 2007; BELLI et al., 2013; REGATTIERI et al, 2019; JOHNSTON et al., 2018; ISOLA et al., 2019; POZZI et al., 2019; DRYSDALE et al., 2020). Accordingly, this work fills the gap of the existing literature by procuring novel information on this underrepresented portion of the territory. It also represents an occasion to explore the environmental conditions favoring speleothem deposition at southern European latitudes with respect to climate change occurring at global scale (i.e., glacial vs interglacial shifts), and provides a preliminary investigation regarding the age of speleogenesis in several cave systems in Sardinia and Apulia
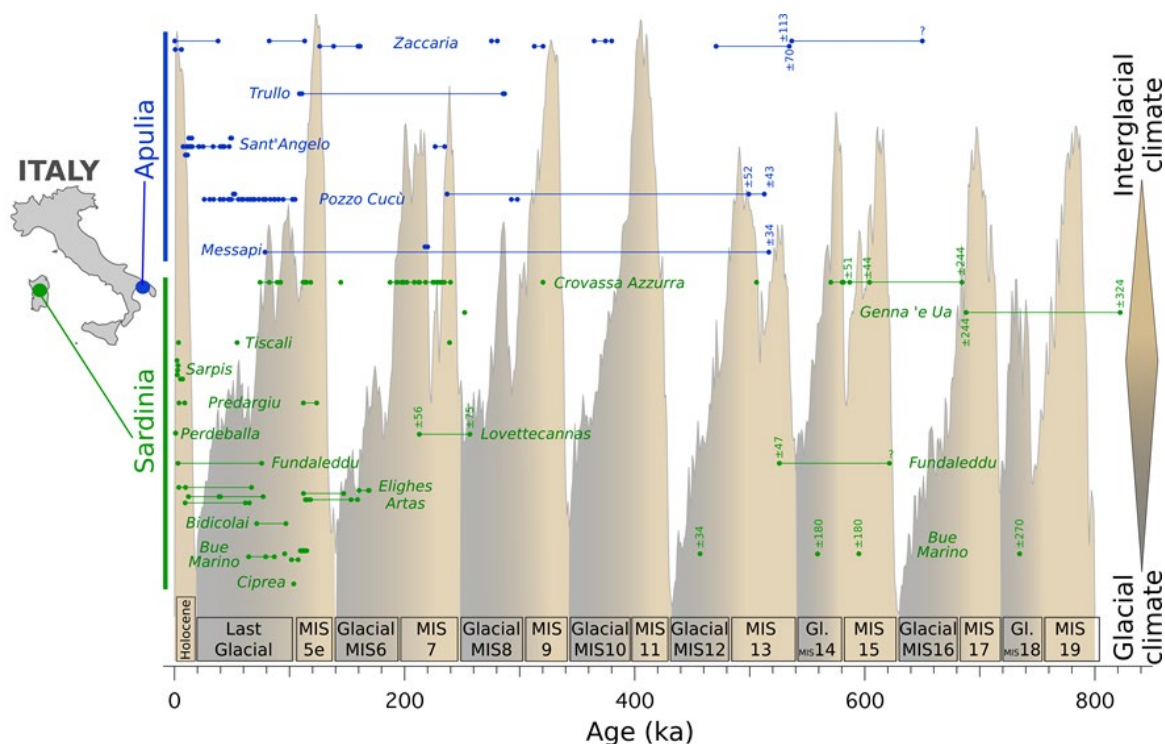.

Figure 1: Age distribution of the dated speleothems vs climate variations. Dots indicate the obtained ages, while horizontal lines connect bottom to top of each speleothem. Caves' names are reported in blue (Apulia) and green (Sardinia); numbers indicate age uncertainties only in the case of relatively large errors. Samples marked with "?" did not deliver a precise age because of the method limit. Global stack benthic δ18O curve (LISIECKI & RAYMO, 2005) in the background is here taken as reference for interglacial vs glacial climate changes over the last ~800 ka (scale has been omitted for simplicity). The bottom reports glacial vs interglacial periods referred as Marine Isotope Stages (MIS).

2. Materials and methods

Karst terrains are widespread in both Sardinia and Apulia. In the first region, calcareous rocks outcrop mostly in the central-eastern part and southern-western corner of the

island, often forming well recognizable table-topped mountainous morphologies (De Waele et al., 2012). Apulia is instead an extensive karst plateau with relatively small

altitude variations (Parise, 2011). The caves visited during the last ~7 years are Crovassa Azzurra, Bue Marino, Genna e' Ua, Tiscali, Sarpis, Predargiu, Lovettecannas, Perdeballa, Fundaleddu, Elighe Artas, Bidicolai and Ciprea in Sardinia, and Zaccaria, Trullo, Sant'Angelo, Pozzo Cucù and Messapi in Apulia. All caves are located around or below ~41˚N latitude. A total of 51 speleothems were sampled, 21 from Apulia and 30 from Sardinia. For the conservation of the cave environment, only broken speleothems were collected during explorations. All speleothems were dated by the uranium-thorium (U-Th) method, which has a limit of around 600 ka. Dating mostly targeted the bottom and top of each speleothem, in order to evaluate the growth period. However, a few samples were used for proxy-based palaeoclimate research and thus dated with higher resolution (COLUMBU et al., 2020; see these last works for the U-Th method details). Analyses were mostly performed at the School of Earth Sciences of the University of Melbourne, (Australia) and at the Institute of Global Environmental Change of the Xi'an Jiaotong University (China), as well as at the Department of Geosciences of the National Taiwan University (Taiwan).

3. Results

U-Th results attest that almost all speleothems grew during the last ~800 ka (Fig. 1). Because of natural attrition, younger speleothems (i.e. <150 ka) dominate. However, analyses returned several ages at the limit of the U-Th method. For this reason, ages of ~500 ka or older are characterized by a relatively large uncertainty (Fig. 1). In only one case, the precise age was not constrained because of its antiquity, so it has been arbitrarily set at around 600 ka (reported with a "?" in fig. 1). The U-Th ages show that, in both Sardinia and Apulia, carbonate deposition occurred during glacial (last glacial, MIS6, MIS8, MIS10) and interglacial (Holocene, MIS5, MIS7, MIS9, MIS13) climate stages, and possibly even during older glacial/interglacial periods (although the age uncertainties of the older speleothems do not allow a reliable assessment)

4. Discussions and final remarks

This work demonstrates that carbonate deposition at mid- to low European latitudes (i.e., at or below ~41˚N) is efficient during both glacial and interglacial climates. This contrasts with results obtained in western and central Europe, where glacial-age speleothems are extremely rare (LECHLEITNER et al., 2018). In detail, the dating of speleothems from Apulia already suggested that carbonate deposition during the last glacial was continuous, with no significant hiatuses (COLUMBU et al., 2020). The same is likely true also for Sardinian speleothems, as well as those Apulian speleothems where dating was targeted at top and bottom of stalagmites only, with the latter age corresponding to last glacial, MIS6, MIS8 and MIS10 (fig. 1). Continuous speleothem deposition during glacial climate is rather rare even on the Mediterranean side of the Iberian peninsula, which possibly represents the best counterpart with respect to southern Italy. For example, the most representative, but incomplete/intermittent, last glacial speleothem records are from Ejulve and Cueva Victoria Caves in Iberia (PÉREZ-MEJÍAS et al., 2019; BUDSKY et al., 2019); however, none of these speleothems grew during full glacial conditions. In contrast, continuous deposition of speleothems during glacial periods is attested in the eastern side of the Mediterranean basin, in Sofular (BADERTSCHER et al., 2011) and Soreq-Pequiin Caves (BAR-MATTHEWS et al., 2003). From a palaeoclimate/environmental perspective, this work implies that glacial conditions in Sardinia and on the Italian peninsula at least below ~41˚N were milder than continental Europe, in terms of rainfall and average temperature. Specifically, these southern Italian territories were not characterised by enduring periods of glacial aridity, and rainfall was able to efficiently recharge the karst aquifers. Concurrently, average temperatures were higher than northern Italy and Europe, possibly with the same latitudinal temperature gradient existing today.

This work provides the first preliminary chronological constraint for the explored karst systems. In both regions, there is evidence of speleothem deposition since at least ~600 ka, implying that speleogenesis occurred beforehand. Ahead of more detailed studies, geological considerations and morphological observations in caves suggest that all explored karst systems formed in more remote times, possibly several millions of years ago. Regarding Sardinia, the oldest dates belong to Genna e' Ua Cave (~700-800 ka), a fossil cave nowadays found at several hundred meters above the current river stream. In Apulia, the oldest dates belong to Zaccaria Cave (~600 ka), which nowadays lies at around ~120 metres a.s.l. and around 6 km from the modern coastline. It is likely that several million years ago, the local base level was at the same altitude of Genna e' Ua Cave in Sardinia and the palaeo coastline was adjacent to Zaccaria Cave in Apulia. Finally, the case of Crovassa Azzurra Cave in Sardinia is different because morphological observations relate this karst system to hypogenic hydrothermal speleogenesis. Detailed studies have suggested that speleogenetic inception for this cave might even be traced back to the Cambrian (GÁZQUEZ et al., 2018).

This preliminary work confirms speleothem dating as a precious tool for both palaeoclimate/environmental and speleogenetic studies, as long as it is carried out on multiple speleothems from a large number of caves.

References

BADERTSCHER S., FLEITMANN D., CHENG H., EDWARDS R. L., GÖKTÜRK O.M., ZUMBÜHL A., LEUENBERGER M., TÜYSÜZ O. (2011) Pleistocene water intrusions from the Mediterranean and Caspian seas into the Black Sea: *Nature Geoscience*, 4(4), 236-239.

BAR-MATTHEWS M., AYALON A., GILMOUR M., MATTHEWS A., HAWKESWORTH C. J. (2003) Sea–land oxygen isotopic relationships from planktonic foraminifera and speleothems in the Eastern Mediterranean region and their implication for paleorainfall during interglacial intervals: *Geochimica et Cosmochimica Acta*, 67(17), 3181-3199.

BELLI R., FRISIA S., BORSATO A., DRYSDALE R., HELLSTROM J., ZHAO J.X., SPÖTL C. (2013) Regional climate variability and ecosystem responses to the last deglaciation in the northern hemisphere from stable isotope data and calcite fabrics in two northern Adriatic stalagmites: *Quaternary Science Reviews*, 72, 146-158.

BUDSKY A., WASSENBURG J. A., MERTZ-KRAUS R., SPÖTL C., JOCHUM K. P., GILBERT L., SCHOLZ D. (2019) Western Mediterranean climate response to Dansgaard/Oeschger events: new insights from speleothem records: *Geophysical Research Letters*, 46(15), 9042-9053.

CHENG H, EDWARDS RL, SINHA A, SPÖTL C, YI L, CHEN S, KELLY M, KATHAYAT G, WANG X, LI X. (2016) The Asian monsoon over the past 640,000 years and ice age terminations. *Nature*, 42(7609), 640-646.

COLUMBU A., CHIARINI V., SPÖTL C., BENAZZI S., HELLSTROM J., CHENG H., DE WAELE J. (2020) Speleothem record attests to stable environmental conditions during Neanderthal-Modern Human turnover in Southern Italy. *Nature Ecology & Evolution*, 4(9), 1188-1195.

DE WAELE J, FERRARESE F, GRANGER D, SAURO F. (2012). Landscape evolution in the tacchi area (central-east Sardinia, Italy) based on karst and fluvial morphology and age of cave sediments: *Geografia Fisica e Dinamica Quaternaria*, 35, 119-127.

DRYSDALE R., COUCHOUD I., ZANCHETTA G., ISOLA I., REGATTIERI E., HELLSTROM J., (…) (2020) Magnesium in subaqueous speleothems as a potential palaeotemperature proxy. *Nature Communications*, 11(1), 1-11.

FAIRCHILD I. J., BAKER A. (2012) *Speleothem science: from process to past environments.* John Wiley & Sons, Chichester.

FRISIA S., BORSATO A. (2010) Karst. In: carbonates in continental settings. (Ed. Alonso-Zarza A.M. & Tanner L.H.): *Developments in sedimentology* (Ed: Van Loon, A.J.), Vol. 61, Carbonates in continental settings (Ed: Alonso-Zarza A.M. & Tanner L.H.), 269-318.

FRISIA S., BORSATO A., SPÖTL C., VILLA I. M., CUCCHI F. (2005) Climate variability in the SE Alps of Italy over the past 17000 years reconstructed from a stalagmite record. *Boreas*, 34(4), 445-455.

GAZQUEZ F., COLUMBU A., DE WAELE J., BREITENBACH S., HUANG C.-R., SHEN CC., LU Y., CALAFORRA JM., VAUTRAVERS M, HODELL D.A. (2018) Quantification of paleo-aquifer changes using clumped isotopes in subaqueous carbonate speleothems. *Chemical Geology*, 497, 246-257.

HELLSTROM J. (2006) U–Th dating of speleothems with high initial 230Th using stratigraphical constraint. *Quaternary Geochronology*, 1(4), 289-295.

ISOLA I., RIBOLINI A., ZANCHETTA G., BINI M., REGATTIERI E., DRYSDALE R.N., HELLSTROM J.C., BAJO P., MONTAGNA P., PONS-BRANCHU E. (2019) Speleothem U/Th age constraints for the Last Glacial conditions in the Apuan Alps, northwestern Italy *Palaeogeography, Palaeoclimatology, Palaeoecology*, 518, 62-71.

JOHNSTON V.E., BORSATO A., FRISIA S., SPOTL C., DUBLYANSKY Y., TOCHTERLE P., HELLSTROM J.C., BAJO P., EDWARDS R.L., CHENG H (2018) Evidence of thermophilisation and elevation-dependent warming during the Last Interglacial in the Italian Alps. *Scientific Reports*, 8(1), 2680.

LECHLEITNER F., AMIRNEZHAD-MOZHDEHI S., COLUMBU A., COMAS-BRU L., LABUHN I., PEREZ-MEJIAS C., REHFELD K. (2018) The Potential of Speleothems from Western Europe as Recorders of Regional Climate: a Critical Assessment of the SISAL Database. *Quaternary*, 1(3), 1-31.

LISIECKI L.E., RAYMO M.E. (2005) A Pliocene-Pleistocene stack of 57 globally distributed benthic δ 18O records. *Paleoceanography*, 20(1), 1-17.

PARISE M. (2011) Surface and subsurface karst geomorphology in the Murge (Apulia, southern Italy). *Acta Carsologica*, 40 (1), 79-93.

PEREZ-MEJIAS C., MORENO A., SANCHO C., MARTIN-GARCIA R., SPÖTL C., CACHO I., CHENG H., EDWARDS L. (2019) Orbital-to-millennial scale climate variability during Marine Isotope Stages 5 to 3 in northeast Iberia. *Quaternary Science Reviews*, 224, 105946.

POLYAK, V. J. (1998) Age and Origin of Carlsbad Cavern and Related Caves from ⁴⁰Ar/³⁹Ar of Alunite. *Science*, 279(5358), 1919-1922.

POLYAK V. J., PROVENCIO P., ASMEROM Y. (2016) U-Pb dating of speleogenetic dolomite: A new sulfuric acid speleogenesis chronometer. *International Journal of Speleology*, 45(2), 103-109.

POZZI J. P., ROUSSEAU L., FALGUERES C., MAHIEUX G., DESCHAMPS P., SHAO Q., KACHI D., BAHAIN J.J., TOZZI C (2019) U-Th dated speleothem recorded geomagnetic excursions in the Lower Brunhes. *Scientific Reports*, 9(1), 1114.

REGATTIERI E., ZANCHETTA G., ISOLA I., ZANELLA E., DRYSDALE R.N., HELLSTROM J.C., ZERBONI A., DALLAI L., TEMA E., LANCI L., COSTA E., MAGRI F. (2019) Holocene Critical Zone dynamics in an Alpine catchment inferred from a speleothem multiproxy record: disentangling climate and human influences: *Scientific Reports*, 9(1), 1-9.

SASOWSKY I. D. (1998) Determining the age of what is not there. *Science*, 279, 1874.

ZANCHETTA G., DRYSDALE R., HELLSTROM J., FALLICK, AE, ISOLA I., GAGAN MK., PARESCHI, M. (2007) Enhanced rainfall in the Western Mediterranean during deposition of sapropel S1: stalagmite evidence from Corchia cave (Central Italy): *Quaternary Science Reviews*, 26, 279-286.

Age constraints on sea level during the last two glacial terminations based on submerged speleothems from New Caledonia

Isabelle COUCHOUD[1,2], Russell N. DRYSDALE[2], John C. HELLSTROM[3],Hai CHENG[4],
Alan GREIG[3], Vincent LIGNIER[5], Stéphane JAILLET[1],
Laurent MOREL[5] & Jon D. WOODHEAD[3]

(1) EDYTEM, Université Savoie Mont Blanc, Le Bourget du Lac, 73376, France, isabelle.couchoud@univ-smb.fr
(2) School of Geography, University of Melbourne, Melbourne, 3053, Australia
(3) School of Earth Sciences, University of Melbourne, Melbourne, 3053, Australia
(4) Institute of Global Environmental Change, Xi'an Jiaotong University, Xi'an, 710054, China
(5) Laboratoire Ampère, Université Claude Bernard Lyon 1, France

Abstract

Speleothems from coastal caves are useful sources of sea-level data. Ages from submerged speleothems indicate that the relative sea level was lower than the (corrected) elevation of the speleothem, but there is no certainty that the speleothem was still growing during the transgression. More powerful age constraints could be derived if the speleothem were shown to be growing at the time of submergence. We present preliminary results from submerged speleothems in a coastal cenote at Lifou (New Caledonia), located ~150 m from the current coastline. Daily tidal fluctuations in the cenote suggest a physical connection to the ocean. Two speleothems (AeW-11 and AeW-12) were collected in growth position from -42.0 m and -31.6 m, respectively. A thin (few mm) upper growth phase in AeW-11 dates to ~55 ka. The penultimate growth phase ended at ~135 ka, during Termination II. The tip of AeW-12 is dated at ~11.5 ka, during Termination I. We use trace element mapping to determine if the speleothems were active at the time of drowning, then compare their estimated paleo-elevation with the latest reconstructions of relative sea level.

Résumé

Contraintes chronologiques sur le niveau de la mer pendant les deux dernières terminaisons glaciaires à partir de spéléothèmes immergés de Nouvelle-Calédonie. Les spéléothèmes de grottes côtières sont des sources utiles d'information sur les paléo-niveaux marins. Les âges de spéléothèmes submergés indiquent que le niveau marin relatif était plus bas que le spéléothème (son altitude corrigée), mais il n'y a aucune certitude que le spéléothème était toujours actif lors de la transgression. Des points de contrôles chronologiques plus robustes pourraient être obtenus s'il était possible de démontrer que le spéléothème était en cours de croissance au moment de sa submersion. Nous présentons des résultats préliminaires à partir de spéléothèmes submergés d'un cénote côtier de Lifou (Nouvelle Calédonie), situé à ~150 m du rivage actuel. Les fluctuations tidales journalières dans le cénote suggèrent une connexion physique à l'océan. Deux spéléothèmes ont été collectés dans leur position de croissance à -31,6 m et -42,0 m. Le sommet du premier a été daté à ~11,5 ka, durant la Terminaison glaciaire I, tandis que l'avant-dernière phase de croissance du deuxième s'est terminée vers ~135 ka, pendant la Terminaison II. Nous utilisons la cartographie des éléments traces pour déterminer si les spéléothèmes étaient actifs au moment de leur submersion, puis comparons leur paléo-altitude estimée avec les dernières reconstructions des variations du niveau marin.

1. Introduction

Reconstructions of changes in sea level through glacial terminations are based upon a combination of coastal sea-level archives and oxygen-isotope variations in ocean sediments. These geological sea-level records are largely anchored in time by radiometric dating. Corals are the most widely used of the datable sources of sea-level information, but they are often prone to diagenesis once subaerially exposed, which can affect the accuracy of U-Th ages (SCHOLZ et al., 2004; VILLEMANT & FEUILLET, 2003). Besides, individual species can grow over a relatively wide depth range, making precise paleodepth estimates difficult (e.g., DECHNIK et al. 2017). Although

used less frequently, speleothems from coastal caves – stalagmites in particular – have proved to be a useful complementary source of sea-level data because they grow when caves are filled with air and not when they are submerged in sea water or brackish water. Therefore, uranium-thorium ages from the outer surface of a submerged speleothem can provide firm sea-level time-constraints: sea level was necessarily below the tip of the speleothem while it was growing. However, determining if the submersion of the speleothem actually caused its growth cessation would be a more powerful time constraint, but as far as we are aware, this has yet to be

shown in any study employing speleothems as sea-level indicators.

We present preliminary data from two submerged speleothems collected from a coastal cenote (Ani-e-Wee) on the island of Lifou (Loyalty Islands, New Caledonia), in the subtropical western Pacific Ocean (Figure 1). We use trace element patterns to evaluate whether these speleothems were active at the time of submergence and thus capable of yielding more accurate time constraints on paleo sea level.

2. Materials and methods

Lifou is part of the Loyalty islands archipelago, situated east of Grande-Terre, the main island of New Caledonia. The island is an uplifted carbonate platform, measuring 60 km long by 25 km wide, and with a maximum altitude of 104 m asl. Uplift and emergence caused by subduction of the Australia plate under the Pacific plate near the Vanuatu archipelago (BONVALLOT et al., 2012; MAURIZOT and LAFOY, 2004) commenced towards the end of Miocene. The local uplift rate is estimated at approximately 0.13-0.16 m/kyr based on radiometric ages on ~180 ka corals (MARSHALL & LAUNAY, 1978). The platform is strongly karstified as indicated by the lack of surficial runoff and the numerous natural cavities (BOURROUILH, 1972; LIPS et al. 1995).

As with most oceanic islands with significant permeability, Lifou presents at depth a freshwater lens floating on seawater according to Ghysben-Herzberg principle (ORANGE et al. 2008). Ani-e-Wee is a cenote, a water-filled karstic collapse offering an access to the freshwater lens and allowing diving access to the seawater beneath (Fig. 1). It opens into dolomitic limestone on the West coast of the island, 20 m asl, ~150 m inland from the shoreline of Baie du Santal.
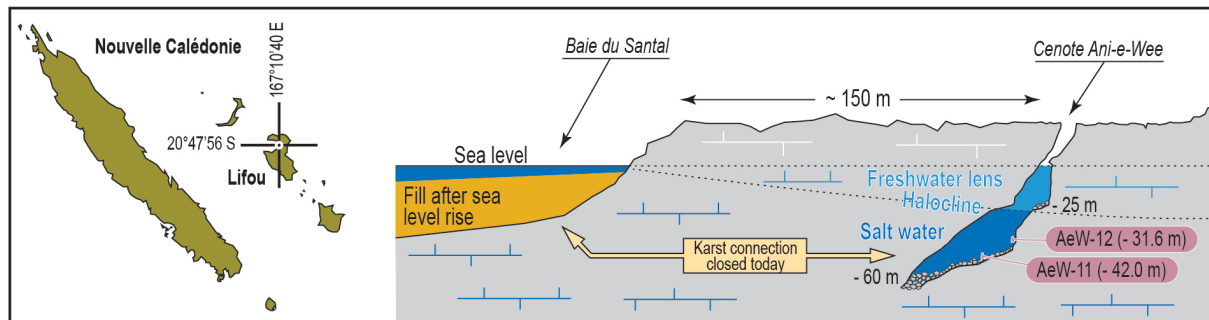

Figure 1: (Left) Location of the Cenote Ani-e-Wee on the island of Lifou, New Caledonia (SW Pacific Ocean). (Right) Cross-section from Baie du Santal (West coast) to the cenote showing the piezometric surface, the freshwater lens and the halocline, and their inferred extension to the sea. The position of the sampled stalagmites is also shown.

It appears as a vast opening on a fault, 30 m long, 15 m wide and 20 m deep (Fig. 1). The water table appears at the base of this vast collapsed entrance, giving access through a flooded pit and a corridor through rock fall to a wide sloping chamber at ~-30 m, which has been explored to -60 m (P. Brunet, pers. com.). An ancient scree slope occupies the chamber, comprising plurimetric blocks and covered in places by more recent rockslides. Many stalactites are visible around -35 m, however stalagmites are less numerous.

Although Ani-e-Wee has no known accessible connection to the open ocean, diurnal tidal changes can be observed. The freshwater lens extends from the water surface to a depth of about -20 m, where it reaches the halocline, which extends to -30 m, after which sea water is reached (LIGNIER et al. 2013). The pH varies abruptly from 8.5 at the surface of the water lens down to 7.8-7.9 at about -8 m then remains stable to a depth of -40 m.

The two speleothems (AeW-11 and AeW-12) were collected in growth position from -42.0 m and -31.6 m respectively (Fig. 1). Both comprise dark compact to light compact and very finely laminated columnar calcite (Fig. 2). They show no visible signs of dissolution despite their long residence time under water, probably due to the fact that they were resting below the halocline.
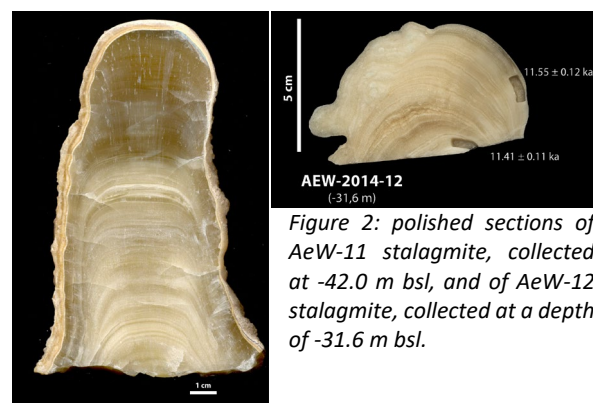

Figure 2: polished sections of AeW-11 stalagmite, collected at -42.0 m bsl, and of AeW-12 stalagmite, collected at a depth of -31.6 m bsl.

Uranium-series dating by MC-ICPMS was undertaken at the School of Earth Science, Univ. of Melbourne, on ~200 mg calcite prisms using the method described by HELLSTROM (2003). In order to determine if AeW-12 was active at the time of submergence, we applied laser-ablation trace-element mapping over its upper part. We used a RESOlution laser-ablation system coupled to an Agilent quadrupole ICP-MS housed at the School of Earth Sciences at the U.

Melbourne. Elemental concentration maps were produced from a grid of 250 parallel raster line scans (104 μm spot, 120 μm spacing). The same mapping will be conducted on AeW-11 in 2021.

3. Results

The U-Th dating results show that the calcite is low in detrital contaminants and with uranium concentration ranging between 0.1 and 0.4 ppm. AeW-12 apparently grew very quickly (within a couple of centuries) at ~11.5 ka BP.

The taller AeW-11 also grew very quickly, as samples taken at the bottom and top of the main and continuous growth phase returned the statistically identical ages at 2σ: 135 ± 1.7 ka BP. A further growth phase of half a centimetre in thickness, visible after a distinct discontinuity, returned an age of 54.8 ± 0.5 ka.

In order to improve the precision of the speleothem chronologies, new dates are programmed for 2021 using higher precision methods.

Trace-element maps were produced for Ca, B, Pb, Ba, Zn, Cl, Mg, Na, I, U, and Mg. The main purpose of the Ca map (Fig. 3) is to display the exact limit between the stalagmite and the resin in where the section was embedded. Among the other maps, the most striking feature is the significant increases in Mg, U and Na concentrations towards the top (Fig. 3); the other elements do not show any such change.

The dating and trace element results will be used to evaluate the reliability of the stalagmites as relative sea level (RSL) indicators by comparing their uplift-adjusted sampling positions to relative sea-level curves.
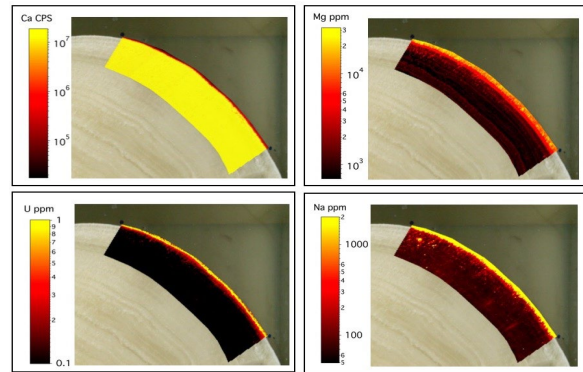

Figure 3: Elemental concentrations of Ca, Mg, U and Na on the top part of AeW-12, showing increased values over the upper few mm. The red band at the top of the Ca map marks the epoxy resin limits.

4. Discussion and Conclusion

The trace element data suggest that AeW-12 speleothem was actively growing at the time it was submerged by the rising freshwater lens. There are at least two lines of evidence to support this. First, the waters of the freshwater lens probably had higher Mg, U and Na concentrations than the drip water that fed the stalagmite due to the longer residence time in the regional karst aquifer. As regional groundwater moves through the karst and becomes exposed to the open atmosphere of the cenote, degassing would promote a shift towards a supersaturated state. This would enable continued calcite growth under subaqueous conditions. Second, the increased concentrations of these elements likely reflect a change in elemental partitioning coefficients as subaerial calcite precipitation is replaced by subaqueous calcite precipitation (DRYSDALE et al., 2019). This has been observed in speleothems from southern Australia, where Mg, U and Na concentrations increase by around a factor of 10 as the speleothem transitions from stalactitic to subaqueous growth (GOULD-WHALEY, 2020). An alternative explanation of the trace element increases in AeW-12 is mineral alteration processes as the speleothem undergoes submergence. Testing these competing hypotheses will be the subject of future investigations using synchrotron X-ray fluorescence. In the meantime, we discuss below the speleothem radiometric age results on the assumption that AeW-12 was active at the time of submergence.

The growth position of both speleothems can be corrected based on uplift rate estimates for Lifou of 14.5 ±1.5 cm/kyr (MARSHALL & LAUNAY, 1978). This returns an adjusted depth of ~-33.3 ± 0.2 m for AeW-12, assuming a top age of

11.5 ka, and of ~-61.6 ±2.2 m for AeW-11, assuming a top age of 135 ka. These estimates must however be treated with caution because of both uncertainties on the speleothem ages (which will be improved with further dating) and the uplift rate estimates, which rely on uncertain sea-level reconstruction and imprecise dating of a single terrace (MARSHALL & LAUNAY, 1978).

Nevertheless, these results can be compared with recent sea-level compilations across glacial Terminations I (LAMBECK et al., 2014) and II (MENVIEL et al. 2019; Fig. 4). The AeW-12 reconstructed position aligns well with relative sea level at the time and supports the notion that it could have been actively growing when it was submerged. AeW-11 grew ~135 ka ago, so the reconstructed position of the speleothem is more sensitive to uncertainties on the uplift rate. Compared with the latest reconstruction available for TII, its position at the time of growth is close, within error, to relative sea level.

Hence, both stalagmites could have been actively growing at the time they were submerged due to sea-level rise. Their top ages could thus be used as a chronological constraint for sea level rise reconstruction in the area, but more robust estimates for uplift rate are needed.

Further dating and geochemical analyses on both speleothems will help reinforcing the argument that they were actively growing at the time of submersion.

Figure 4: Relative sea level curves for Termination I (left, from LAMBECK et al., 2014) and Termination II (right, from MENVIEL et al., 2019). Age and depth uncertainties are shown by X and Y error bars, respectively. The age and uplift-corrected position of AeW-12 (left) and AeW-11 (right) are shown by the red symbols (where X-error bars are 2σ U-Th age uncertainties and Y-error bars are uplift-correction uncertainties; NB: the error bars are too small for Termination I).
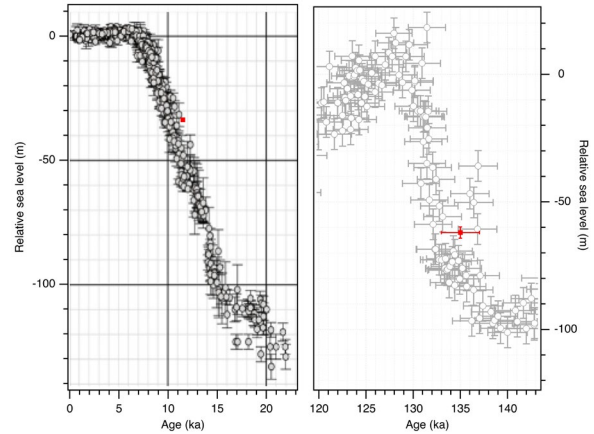
Acknowledgements

References

BOURROUILH F. (1972) Diagenèse récifale : calcitisation et dolomitisation, leur répartition horizontale dans un atoll soulevé île Lifou. Territoire de Nouvelle-Calédonie. *Cahiers ORSTOM* 121–135.

CLUZEL D., MAURIZOT P., COLLOT J., SEVIN B. (2012) An outline of the Geology of New Caledonia; from Permian-Mesozoic Southeast Gondwanaland active margin to Cenozoic obduction and supergene evolution. *Episodes-Newsmag. Int. Geol. Sci.* 35, 72.

DECHNIK B., WEBSTER J.M., Webb G.E. et al. (2017) The evolution of the Great Barrier Reef during the Last Interglacial Period. *Global and Planetary Change*, 149, 53-71.

DRYSDALE R., ZANCHETTA G., BANESCHI I. et al. (2019) Partitioning of Mg, Sr, Ba and U into a subaqueous calcite speleothem. *Geochimica et Cosmochimica Acta* 264, 67-91.

GOULD-WHALEY C. (2020) *Subaqueous speleothems from the Flinders Ranges as palaeoclimate archives for the arid zone*. BSc Honours thesis, University of Melbourne, 136 pp.

LAMBECK K. ROUBY H., PURCELL A. et al. (2014) Sea level and global ice volumes from the Last Glacial Maximum to the Holocene. *PNAS* 111, 15296-15303.

LIGNIER V., MAPES R., HEMBREE D. et al. (2013) Le cénote d'Ani-e-Wee (Lifou, Nouvelle Calédonie) et son .

gisement exceptionnel de Nautilus Macromphalus. *Karstologia*, 61, 37-44

LIPS B., LIPS J., THOMAS C., THOMAS Y., BRUNET, P. (1995) *Grottes de Lifou-Expédition en Nouvelle Calédonie* (Rapport d'expédition), CREI. FFS-FFESSM.

MARSHALL J.F., LAUNAY J. (1978) Uplift rates of the Loyalty Islands as Determined by ^{230}Th/^{234}U Dating of Raised Coral Terraces. *Quaternary Research*, 9, 186-192.

MAURIZOT P., LAFOY Y. (2004) Notice explicative, feuille Lifou, Îles Loyauté. Nouvelle-Calédonie.

MENVIEL, L., CAPRON, E., GOVIN, A. et al. (2019) The penultimate deglaciation: protocol for Paleoclimate Modelling Intercomparison Project (PMIP) phase 4 transient numerical simulations between 140 and 127 ka, version 1.0. *Geoscientific Model Development* 12, 3649-3685.

ORANGE F., ALLENBACH M., LEPILLER M. et al. (2008) La synthèse des travaux sur les îles Loyauté (Nouvelle Calédonie). Problèmes de la gestion de la ressource en eau, in CFH, *Colloque Hydrogéologie et Karst au travers des travaux de Michel Lepiller*. pp. 179–188.

SCHOLZ D., MANGINI A., FELIS T. (2004) U-series dating of diagenetically altered fossil reef corals. *Earth and Planetary Science Letters*, 218, 163-178.

VILLEMANT B., FEUILLET N. (2003) Dating open systems by the ^{238}U-^{234}U-^{230}Th method: application to quaternary reef terraces. *Earth and Planetary Science Letters, 210,* 105–118

Monocrystalline calcite speleothems: an overview and new insights

Jo DE WAELE [1] & Paolo FORTI [2]

(1) BIGEA Department, University of Bologna & La Venta Esplorazioni Geografiche, jo.dewaele@unibo.it
(2) Italian Institute of Speleology via Zamboni 67, 4126 Bologna & La Venta Esplorazioni Geografiche, paolo.forti@unibo.it
 (corresponding author)

Abstract

Since the early 20th century, monocrystalline calcite soda straws and helictites have been described in the literature. Recent observations have also shown that subaerial macrocrystalline speleothems are much more frequent than earlier thought, often occurring in very stable cave environments where slow epitaxial growth can be favored over long time periods. But it appears that their development can also be controlled by frequent small variations in the depositional system (dissolution-precipitation), as opposed to the stationary (depositional) conditions typical of normal speleothems. Despite these short open system conditions, the paleoclimate signal appears to be preserved in these speleothems. High cave air humidity and CO_2 concentration often appear to be triggering factors.

1. Introduction

Many of the currently known cave minerals occur in the cavern environment as euhedral crystals often displaying a single crystal lattice. It is not so difficult to find large euhedral calcite crystals, or other minerals such as gypsum, halite, barite, or fluorite in caves (HILL & FORTI 1997). Generally, but not always, large crystals have a subaqueous, and often thermal, origin (DUBLYANSKY 1997). The development of single large crystals is always related to the very low supersaturation of the depositing fluids, causing epitaxial growth to prevail over nucleation of new crystals (GARCÍA-RUIZ et al. 2007). This is also why subaerial macrocrystalline speleothems were often regarded as diagenetic forms, where laminated structures were slowly recrystallized (FORD & WILLIAMS 1989). However, already since the early 20th Century, monocrystalline calcite soda straws, helictites and, less frequently, stalactites have been described in the literature (PRINZ 1908, SNYDER 1951, HALLIDAY 1953). Until some decennia ago the single described monocrystalline speleothems were those made of calcite. Only at the end of the 20th and, more frequently, at the beginning of the new millennium, monocrystalline speleothems consisting in other minerals than calcite started to be described: the very first were the halite monocrystalline speleothems (mainly stalactites with a single crystal lattice and a plane-parallel twinning) were described and partially studied (DE WAELE et al. 2009).

Recent observations have also shown that subaerial monocrystalline calcite speleothems are much more frequent than earlier thought (CALAFORRA & FORTI 2019). Monocrystalline calcite speleothems often occur in very stable cave environments characterized by high relative humidity and CO_2 concentration, where slow epitaxial growth can be favored over long time periods. In any case, it was also shown very recently that their development could be triggered by frequent small variations in the depositional system (dissolution-precipitation) as opposed to the stationary (depositional) conditions typical of normal speleothems (FORTI & SPRINGER 2020).

In the present paper the different types of monocrystalline calcite speleothems known at present (fig. 1) are shortly discussed on the basis of their genetic mechanisms.

2. Currently known monocrystalline calcite speleothems

Euhedral crystals notwithstanding, the very first studied monocrystalline speleothems were the calcite soda straws and helictites and triangular microgours (PRINZ 1908, 1909). Later monocrystalline stalactites (ONAC 1996) and triangular columns and stalagmites were also described, even if no genetic explanation for them was given (HILL & FORTI 1997). In any case they were speleothems developing in stationary microclimatic and feeding conditions (GONZALES et al. 1992).

Only in the very last few years, new studies on the influence of non-stationary conditions over the development of some peculiar speleothems (Badino et al. 2016), put in evidence the possibility that monocrystalline calcite speleothems may develop even under such conditions. In particular, in 2017 it was proved that some peculiar spheroidal coralloids and pyramidal stalagmites together with other rare monocrystalline speleothems from the Puerto Princesa Underground River in Palawan (Philippines) developed under non-stationary conditions (CALAFORRA & FORTI 2019). The same was shown in 2019 for the "squared soda straws" of the Dry Cave (West Virginia) (FORTI & SPENCER 2020).

3. Monocrystalline speleothems developing in stationary conditions

Tubular speleothems

Calcite soda straws are surely the most common monocrystalline speleothem: they consist of an elongated cylinder, the diameter of which is always around 5.1 mm (corresponding to that of the equilibrium drop just before detaching from the ceiling). Soda straws are the single monocrystalline speleothems developing even if the energy of crystallization is higher than that allowing only epitaxial growth. Their genesis is controlled by water drops falling from the cave roof and normally the supersaturation reached by the dripping water is high enough to promote the competitive selection among the embryonic crystals instead of the simple epitaxial growth, thus allowing, in a very short space (a couple of millimeters as maximum) to create a monocrystalline structure, with the C axis directed along the vertical, which is the direction of growth of this speleothem (MOORE 1962).

Generally speaking, the thickness of the tubular's external wall is very thin (one millimeter or even less) but it is also possible to see soda straws with thicker walls: in fact, sometimes the inner tube exhibits a diameter quite equal to the capillary feeding fissure within the rock.

The tubular's wall thickness and consequently the diameter of the inner tube, is controlled by the dripping frequency: in fact, high drip rates prevent supersaturation to move from the external surface into the dripping core, thus the calcite deposition only occurs along the outer rim of the falling drop. Decreasing the drip frequency will induce a progressive propagation of the supersaturation within the drop, thus causing a progressive increase of the tubular wall's thickness.

The fact that the tubular lattice is one with the C axis always directed along the vertical becomes evident when the speleothem breaks: in fact, the fracture always occurs along a rhombohedron face, no matter the thickness of the tubular's wall.

Soda straws exhibiting external geometrical shapes distinct from the rounded one (triangular, squared, hexagonal) cannot be considered true tubulars but are instead peculiar stalactites, because their shape is the consequence of a water film flowing over their external surface. They will be discussed in the section of the monocrystalline speleothems developing in non-stationary conditions.

Helictites

Monocrystalline calcite helictites are quite common and were the very first speleothem of this type analyzed in detail (PRINZ 1908). Their external shape is always fully independent from the inner capillary feeding tube because their evolution occurs only if no dripping at all occurs from the speleothem tip (MOORE 1982). Their cross-section can be flat or rounded, or even showing several small protrusions parallel to each other, corresponding to the rhombohedron vertexes. The thickness of the helictites varies from less than 1 up to 2-3 cm and is controlled not only by the evaporation rate of the steady drop present at the tip, but also by the possible water film driven by capillary flow over its external surface.

Sometimes the portion close to the apex has an elongated pyramidal shape with a triangular cross-section, corresponding to the vertex of a calcite rhombohedron &/or scalenohedron (MOORE, 1954).

In any case the supersaturation must be constantly kept to a very low value to allow no other depositional mechanisms besides epitaxial growth to be activated.

Pyramidal stalactites

The external shape of the monocrystalline stalactites is normally pyramidal with a rhombohedral cross-section. The tapering angle of these speleothems is far smaller than that of normal conical stalactites (FORTI & SPRINGER 2020). This occurs because the supersaturation of the water film flowing over their external surface must be very scarce, thus avoiding new nucleation and the consequent evolution of a "normal" conical stalactite as a consequence of the competitive selection of the embryonic crystals (MOORE 1962).
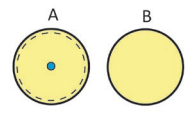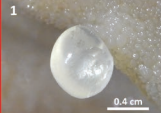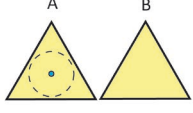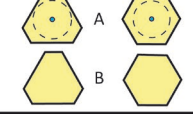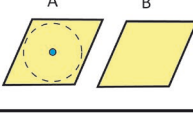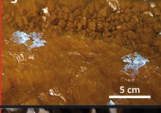

speleothem cross section	speleothem types	examples
A B	A: tubular B: coralloid	1
A B	A: stalactite helictite B: stalagmite column anthodite	2
A B	A: stalactite pseudo-soda straw B: anthodite	3
A B	A: stalactite helictite pseudo-soda-straw B: anthodite	4
	Scintillite	5
	gour	6

Figure 1: Cross-sections of the currently known monocrystalline calcite speleothems. 1- calcite monocrystal spheroid from PPUR, Palawan (photo M. Vattano); 2- Triangular tapering stalagmites from PPUR (photo Vittorio Crobu); 3- Cave grass anthodites from PPUR (photo Alessio Romeo); 4- "squared soda straw" stalactites from Dry Cave (USA) (photo Paolo Forti); 5- "flattened stars" scintillites from PPUR, Palawan (photo Alessio Romeo); 6- triangular gours from PPUR, Palawan (photo Marco Vattano).

Triangular stalagmites and columns

Triangular stalagmites and columns have been described from different caves (HILL & FORTI 1997). They consist of triangular parallelepipeds, whose elongation axis always corresponds to the C axis of the calcite lattice. Sometimes the stalagmite's top consists of a triangular pyramid, corresponding to the rhombohedral calcite crystal with the C axis coincident with the speleothem's elongation axis, but more often it is partially rounded because of the dripping impact. Both these two monocrystalline speleothems develop in a very stationary environment characterized by an extremely stable environment with high CO_2 and very low evaporation rate. As for most of the monocrystalline speleothems the driving factor is the development exclusively by epitaxial growth.

4. Monocrystalline speleothems developing in non-stationary environments

Only in the past few couple of years it was put in evidence that a few of previously known and some of the newly discovered monocrystalline speleothems develop thanks to non-stationary conditions. Actually at least 5 different such types of speleothems are known, two of which are presently only known from the PPUR karst system in Palawan (Philippines).

Triangular gours

They were among the first monocrystalline speleothems described in the literature (PRINZ 1908) even if, at that time, it was not recognized that their development requires non-stationary environments.

Their evolution is controlled by alternation of short periods of fast slightly undersaturated water supply, which fills the cups and rather long ones of drought during which capillary rise and slow evaporation induce epitaxial growth only on the triangular upper rim of the gours. A striking example of triangular gour is that described from the upper levels of the Puerto Princesa Underground River in Palawan (CALAFORRA & FORTI 2019). It was named "champagne cup" being remarkably similar to a flute glass. Its lower part being a normal monocrystalline helictite, which was transformed into a deep triangular gour due to the presence of a undersaturated dripping impacting its tip during the flashy rainfalls which characterize the Palawan Climate.

Hexagonal, triangular, and squared soda straws

The hexagonal and triangular tubulars were firstly described from the U.S. caves by Snyder (1951) and by Halliday (1953), and later by Basset & Basset (1962).

They were wrongly supposed to be soda straws but their evolution, as that of the squared ones, requires the presence of a water layer flowing along their external surface (FORTI & SPRINGER 2020) therefore they must be considered true stalactites. The absence of any kind of tapering is a clear evidence that slight undersaturation-oversaturation migrates along the whole external surface of these speleothems due to local competition among condensation and evaporation (FORTI & SPRINGER 2020)

Spheroidal coralloids

This peculiar type of coralloids, consisting of a monocrystalline calcite spheroid often with a clearly corroded stalk) was described for the first time from PPUR cave in Palawan (CALAFORRA & FORTI 2019) and its non-stationary origin was immediately recognized.

Their genesis and development were proven to be controlled by the peculiar Palawan climate, which is characterized by strong rainstorms followed by rather long dry periods. Capillary flow is active in both periods giving rise to short periods of slight undersaturation (inducing partial re-dissolution of the coralloid) followed by prolonged slight evaporation which allows only epitaxial growth (CALAFORRA & FORTI 2019).

Pyramidal stalagmites with a triangular base

These stalagmites were hitherto described only from PPUR karst system (CALAFORRA & FORTI 2019). They consist of a monocrystalline lattice with the C axis coincident with the stalagmite axis. The body of the stalagmite is shaped as a scalenohedron crystal, while the tip consists of a perfect rhombohedron. These stalagmites differ from the normal monocrystalline stalagmites by their tapering angle.

As the other just described monocrystalline speleothems of the PPUR karst system, their development is controlled by the peculiar Palawan climate.

In particular, their tapering scalenohedral structure is controlled by the alternation of strong rainstorms with rather long dry periods. In fact, during the few days following the rainstorms dripping may result slightly undersaturated thus allowing partial re-dissolution of the upper part and a slight deposition in the lower part of the stalagmite. At the beginning of the dry periods water present on the floor is driven by capillarity forces to the lower part of the stalagmite, where evaporation allows a further deposition of calcite. Both these two processes are evidently able to induce only a very low supersaturation, which explains why a monocrystalline pyramidal structure develops.

Scintillites

Flowstones, stalactites, and stalagmites, generally called "scintillites", due to their ability to reflect light, have been reported from all over the world (HILL & FORTI 1997). They should be considered a peculiar type of monocrystal speleothem due to the fact that reflection occurs in the presence of large flattened rhombic calcite crystals developed over the external surface of a normal speleothem. Recently, scintillites consisting of extremely large crystals have been reported from PPUR cave (DE VIVO et al. 2017). The development of these flattened calcite megacrystals is the result of local non-stationary conditions, allowing the partial re-dissolution of the external surface of the speleothem during the periods of fast water flow, while the development of the scintillites occurs when dripping is absent and feeding is due to both capillary flow and slow evaporation.

5. Conclusion

Recent observations have shown that subaerial macrocrystalline speleothems are much more frequent than earlier thought, and their development is often controlled by frequent small variations in the depositional system (dissolution-precipitation), which is just the opposite of the stationary conditions typical for the development of normal speleothems. High cave air humidity and CO_2 concentration always appear to be triggering factors for their development.

The observation and the research on monocrystalline speleothems developing in non-stationary conditions is still at the beginning and therefore it is highly probable that in the near future, new speleothem types will be discovered. This seems to be the case of the stalagmite sampled in PPUR during the expedition of 2017 (DE VIVO et al. 2017). Apparently, it is just a "normal" rounded stalagmite with well-defined accretion layers… but it resulted to be also completely monocrystalline. Moreover, preliminary U/Th dates and stable isotope analyses (DE WAELE unprinted data) showed that its internal chronology was unaffected by recrystallization processes.

This means that the process transforming the layered structure of the stalagmite into a monocrystalline one must be quite simultaneous, suggesting a possible (seasonal? or even shorter) alternation of a "normal" evolution (with the development of an accretion layer, characterized by a palisade arrangement of the calcite crystals) with a subsequent recrystallization of this single layer which was transformed into an epitaxial accretion of the stalagmite monocrystalline lattice. In fact, this mechanism alone can ensure that the geochemical characteristics of each layer will be maintained also after the recrystallization. Inside the PPUR karst system this fast alternation is controlled, as already said, by its peculiar climate characterized by short strong rainstorms alternated to long dry periods.

References

BADINO G., CALAFORRA J.M., DE WAELE J., FORTI P. (2016) The ribbed drapery of the Puerto Princesa Underground River (Palawan, Philippines): morphology and genesis. *International Journal of Speleology* **46**, pp. 93-97.

BASSET W.A., BASSET A.M. (1962) Hexagonal Stalactite from Rushmore Cave, South Dakota. *National Speleological Society Bulletin* **24**, pp. 88-94.

CALAFORRA J.M., FORTI P. (2019) The climate driven peculiar speleothems of the Natuturingam Cave (Puerto Princesa Underground River, Palawan, Philippines): a review. *Atti e Memorie Comm. Grotte E. Boegan* **48, pp.** 3-22.

DE VIVO A., FORTI P. PICCINI L. (Eds.) (2017) *Support for Sustainable Eco-Tourism in the Puerto Princesa Underground River Area, Palawan, Philippine*. Report on the second expedition to Palawan. Tintoretto, 172 p.

DE WAELE J., FORTI P., PICOTTI V., ZINI L. (2009) Halite macrocrystalline stalactites of the Atacama caves (Chile). *Proceedings 15th International Speleological Congress*, Kerrville Texas, **1**, pp. 296-299

DUBLYANSKY Y.V. (1997) *Hydrothermal cave minerals In Hill C.A., Forti P. Cave Minerals of the World*. National Speleological Society, pp. 252-255.

FORTI P., SPRINGER G.S. (2020) Genesis and evolution of the "square" soda straws of Dry Cave, West Virginia, USA. *Journal of Karst and Cave Science* **82(3)**, pp. 169-182.

GARCÍA-RUIZ J.M., VILLASUSO R, AYORA C, CANALS A, OTÁLORA F. (2007) The Formation of Gypsum Megacrystals in Naica, Mexico. *Geology* **35(4)**, pp. 327-330

GONZALES L.A., CARPENTER S. J., LOHMAN K.C. (1992) Inorganic calcite morphology: roles of fluid chemistry and fluid flow. *J. of Sedimentary Petrology* **62(3)**, pp.382-399

HALLIDAY W.R. (1959). Holocrystalline Speleothems. *National Speleological Society Bulletin* **21**, 15(10), pp. 2.

HALLIDAY W.R. (1953) Holocrystalline stalactites. *California Caver* **5(10)**, p. 2.

HILL C.A., FORTI P. (1997) Monocrystalline and macrocrystalline speleothems. In HILL C.A., FORTI P. *Cave Minerals of the World National Speleological Society*, pp. 248-251.

MOORE G. W. (1954) The origin of helictites. *NSS Occasional paper* 1, 16 p

MOORE G.W. (1962) The growth of Stalactites. *National Speleological Society Bulletin*, **24**, pp. 95-106.

ONAC B. (1997) Crystallography of Speleothems In HILL C.A., FORTI P. Cave Minerals of the World. *National Speleological Society*, pp. 230-236.

PRINZ W. (1908) *Les cristallisations des grottes de Belgique*. Bruxelles, Hayez, 90 p.

PRINZ W. (1909) *Les Cristallisations des grottes de Belgique* (Supplement). Bruxelles, Hayez, pp. 379-395.

SNYDER F.G. (1951) An unusual stalactite from Saltville, Virginia. J. *Sedimentary Petrology* **25(1)**, 26-27

FORD D., WILLIAMS P. (1989) *Karst geomorphology and hydrology*. Ed. Unwin Hyman Ltd. London, 601 p.

Exotic tufa and speleothem deposits on the calcareous island of Lismore, Argyll, Scotland

Trevor FAULKNER [1] & John CRAE [2]

(1) GEES, University of Birmingham, Edgbaston, Birmingham, B15 2TT, UK. e-mail: trevor@marblecaves.org.uk
(2) Grampian Speleological Group, 9, Links Place, Leith, Edinburgh, EH6 7EZ, UK. e-mail: john.crae@hes.scot.

Abstract

Tufa deposits are rare in Scotland. This paper reports deposits of cool freshwater tufa, which are ubiquitous on the calcareous island of Lismore in Loch Linnhe, Argyll. They occur there in several morphological varieties and locations, some being exotic and rarely reported in Britain or more widely. In particular, the tufa commonly occurs in a coastal environment, where it can form distinctive terraced mounds resembling cave gour pools, but with associated plant growth. Many indentations, fracture openings and short, probably hybrid karstic / marine, littoral caves have also formed on raised shore platforms, especially on the west coast of Lismore. These commonly contain stalactites, stalagmites, flowstones or pillars at entrances and in the daylight zone, some appearing remarkably massive. Thin deposits of tufa were also observed on the cliffs of the west coast. Speleothems resembling tufa deposits occur in the daylight zone of some of the larger littoral caves. A single example of a deposit of calcite pearls in the open air in front of a carbonate cliff has morphological and likely genetic affinities to deposits of cave pearls.

1. Introduction

The calcareous island of Lismore lies in Loch Linnhe, SW of Fort William in the Grampian Highlands of Scotland. It is 16 km long, c. 1.6 km wide, reaching 127 m a.s.l. (Fig. 1). The island is beside the Great Glen Fault (GGF) at the western extremity of the Dalradian Supergroup of metamorphic and igneous rocks within the Grampian Terrane (STEPHENSON *et al.*, 2013).
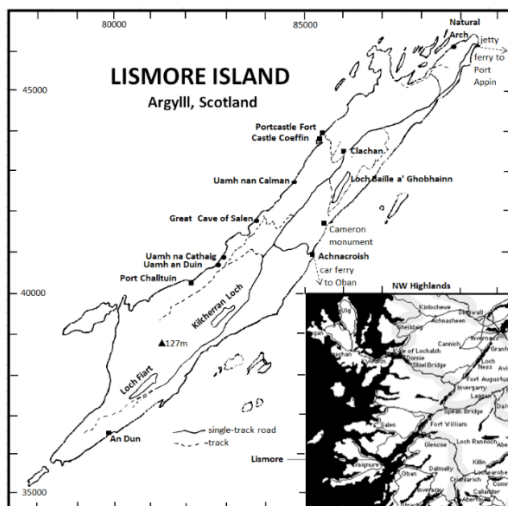

Figure 1: Lismore Island, showing caves and place names.

Comprising the >1 km-thick Lismore Limestone Formation, the island has the longest tract of coastal limestone in northern Scotland. This is a mainly greenschist facies metacarbonate (low grade marble), which deformed in the Ordovician during the Grampian Orogeny. The lithological strike is commonly aligned NE–SW, parallel to island ridges and the GGF. The surviving bedding is commonly vertical or contorted. Dense swarms of vertical igneous dykes up to 3 m wide and of various ages and lithologies intrude the whole outcrop orthogonally, which have created both small ravines and linear stacks (Fig. 2).

Figure 2: A vertical igneous dyke above type D tidal dam deposits on the west coast. Photo by JC.

Some dykes are adjacent to littoral caves, which were first reported on the raised Main Rock Platform at 9–11 m a.s.l. by CORBEL (1957). Littoral caves in marble are rare in Scotland and elsewhere, especially as some on Lismore contain large speleothems. GRAY & IVANOVICH (1988) attempted to date the Platform using calcite deposits from caves and cliff indentations. Most samples were contaminated with detrital thorium, for which Holocene ages were assumed, but one sample yielded an imprecise age of 103.3+28.4/-20.0 ka. This short paper introduces the widespread calcareous deposits on Lismore recorded during a visit by the authors (FAULKNER & CRAE, 2018). Most are in a steep coastal environment, some being exotic and near sea level, whose present tidal range varies throughout the year from 1–4 m.

Lismore glaciation and geomorphology

Lismore was subjected to multiple Quaternary glaciations. Intact surface deposits from pre-Devensian glaciations probably no longer exist, having been overridden at the Last Glacial Maximum (LGM: 27–18 k years ago), but some raised shorelines and littoral caves might have survived that erosion. The island was under a large ice stream occupying Loch Linnhe during the LGM, shown by many far-travelled erratic granite boulders and by depressions that underlie three large inland lakes. Mull to the SW was deglaciated by 17.5±1.0 ka (SMALL *et al.*, 2017) and Lismore followed that, perhaps at c. 16 ka. The rarity of other surficial deposits might arise from ice streaming and be partly the result of marine re-working. Being only 55 km SW from the centre of the Scottish ice dome, isostatic depression caused the local sea level to reach a deglacial marine limit c. 40 m a.s.l. This was perhaps during a late readvance before the Lateglacial Interstadial at 14.7 ka (BALLANTYNE & STONE, 2012), after which Lismore remained unglaciated, being then west of the ice margin. However, there are no littoral caves at the 40 m level.

2. Speleothems, travertine and tufa

Speleothem is the term for all cave chemical precipitates. There is some confusion about the definitions of travertine and tufa, especially regarding the extent of biological and hydrothermal influences (LOWE & WALTHAM, 2002; BRASIER, 2011). This paper regards travertine as primarily a hard, non-biological, calcite deposit that forms in the open air in a similar way to a cave speleothem, and tufa as a softer or spongy and porous variety that is biologically assisted by the photosynthetic removal of CO_2 and the use of plants as a platform for deposition, perhaps assisted by cyanobacteria and algal colonies. Calcitic deposits form primarily by degassing of CO_2 from saturated dripwater (FAIRCHILD & BAKER, 2012, who also discussed biological influences) or recharging spring water. More rarely, they form by evaporation in a warm, well-ventilated, cave passage or when spring water meets warmer open air, to create distinctive coralloid precipitates, with a popcorn morphology. Surface deposits commonly form at waterfalls that can build up terraces like gour dams in caves. Warm weather can increase deposition slightly because CO_2 and calcite solubility reduce as temperature increases. Indeed, FORD (1989) pointed out that supersaturation is needed for precipitation, and that might only occur a kilometer downstream, if the spring temperature is low.

Lismore tufa

FAULKNER & BRAZIER (2016) counted only eight known Scottish tufa sites, all inland. Petrifying springs and the hardness of Lismore water were mentioned by CORBEL (1957). Over 70 tufa deposits were recorded there during the authors' visit, some with exotic morphology and locations. Most occur at the coasts, with some even being near the tidal range and many more being subject to sea spray. Only a few references to tufa forming at temperate latitudes near sea level were given by FORD & PEDLEY (1996). Many morphological varieties of tufa have previously been classified (CHAFETZ & FOLK, 1984; PEDLEY, 1990; PENTECOST, 1993). The authors' identifications of tufa on Lismore are broadly based on the classification of autochthonous tufas A–H provided by PENTECOST (1995).

Lismore karst

There are no known inland caves on Lismore, but the island exhibits allogenic underground stream courses ≤300m long, with vertical ranges ≤15m. Other karst springs and seepages are probably risings from autogenic recharge. They are commonly identified by plentiful growths of yellow flag irises and sporadically by fluviatile crust tufa deposits. This superficial karst hydrology probably developed after deglaciation, assisted by open fracture creation or reactivation during isostatic rebound, as proposed in Norwegian marbles (FAULKNER, 2006). Houses and farms extract abundant supplies of fresh water from shallow wells and boreholes that can be 40m deep. These probably resurge invisibly under the sea (CORBEL, 1957). The deeper flow systems also likely follow faults or neotectonic fractures, some of which, together with some dykes, created weaknesses in the bedrock for the formation of the littoral caves. The present climate is damp (>1600mm precipitation per year) and mild, with little winter freezing or snow.

They can all be active or inactive or intermittently active at present. The genetic processes and the arising petrology of tufa deposits are discussed in several of the cited references. In advance of similar studies, all the Lismore calcareous surface deposits are treated as tufa, and the quite large speleothems in or near the entrances of the short littoral caves, some being vegetated, are probably biologically-assisted.

No deposits seem to fit the type A, perched springline, morphology exactly. However, many tufa deposits below assumed or relict perched springlines do occur. Several thin white crusts on vertical cliffs were recorded, but only along the west coast and not on any inland cliffs, all within 100m of the sea, with bases from 10–21 m a.s.l. They commonly have a sharp upper limit (Figure 3), suggesting that they are fed along narrow horizontal joints in the bedrock by unseen perched springlines.

One distinctive group of 'speleothems' was observed below an apparently inactive superficial overhanging perched springline on the east coast, in the bank of a small stream just above the sea (Figure 4). Large numbers of cliff 'speleothems' occur just outside cave entrances or in various indentations, from 3–25 m a.s.l., especially on the west coast. These are assumed to have formed below unseen joints in the bedrock (Fig. 5 and 6). Type C, cascade tufa, occurs on both coasts, descending to sea level (Figures 7 and 8). One series of type D, non-tidal dams, are inland, along a small stream. Two remarkable type D tidal dams were observed at 0–8 m a.s.l. That on the east coast is covered in green vegetation with some sea pinks (Fig. 9), below a perched springline nourishing yellow flag irises that does not immediately deposit tufa. The visited site on the west coast comprises a longer and larger feature (Figure 2). Where types C and D tufa reach the sea, they become green in colour. Three inland type E, fluviatile crust, deposits occur along stream beds below springs up to 50 m a.s.l., with three more near the coasts. Type F lacustrine crusts rich in calcifying algae have been separately observed beside one of the marl lakes.

Figure 3: Type A cliff deposits surrounding small holes.

Figure 4: Type A tufa speleothems below inactive perched springline just above the sea on the east coast. Figure for scale.

Figure 5: Type A tufa flowstone beneath a cliff fracture and beside the entrance to the Great Cave of Salen. Photo by JC.

Figure 6: Large type A tufa pillar that partially blocks the entrance to Uamh na Cathaig. Figures for scale.

Figure 7: East coast type C cascade deposit descends to the sea.

FORD (1989, p. 39) and FORD & PEDLEY (1996) confirmed the occurrence of tufa-like speleothems inside many cave entrances in Britain and worldwide. Such deposits are all classified herein as type S internal cave speleothems, in or near the daylight zone on cave floors 10–20 m a.s.l. A few

flowstones display a spikey popcorn surface, suggestive of some deposition by evaporation rather than by CO_2 degassing. Some type S deposits appeared to be inactive and sporadically covered in vegetation and not visibly dripping (Figure 10), but others were pristine and bright white, suggesting active precipitation.
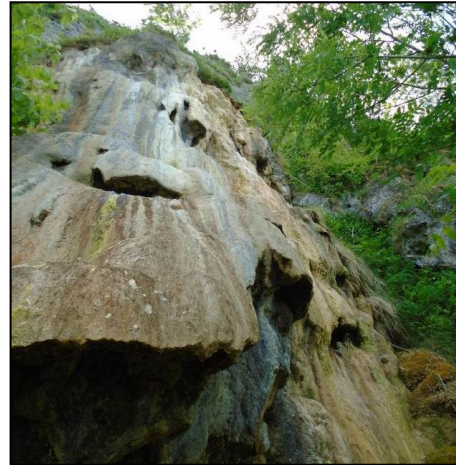
Figure 8: Massive type C cascade, c. 8 m high, overhanging the sea on the west coast. Photo by JC.

Figure 9: Type D vegetated tidal dam tufa with sea pinks.

Figure 10:   Vegetated type S speleothems just inside the entrance to a littoral cave at the head of a 10m-deep gorge. Photo by JC.

Figure 11: Two adjacent nests of white calcite pearls in a tiny stream bed on a raised shore platform in front of a marble cliff on the west coast. Boot for scale.

Calcite pearls

Underground cave pearls are well-known, although there is no comprehensive study of their worldwide distribution and characteristics. The occurrence of similar calcite pearls on the ground surface is less well reported. The discovery of

two closely-adjacent nests of rather flat white calcite pearls on the surface of Lismore (Figure 11) is significant for Scotland. They lie in the bed of a tiny intermittent stream that is probably saturated with calcite when it rises from the base of a marble cliff a few meters away.

3. Discussion

Tufa deposits, littoral caves, bedrock orifices and indentations are commonly associated and sporadically near igneous dykes on Lismore. Coastal tufa types C and D are close enough to sea level for marine inundation during high tides and storms. The sheltered location within high mountains and the mild climate appear to prevent them being washed away. Tufa types A, C, D and E occur at 0–10 m a.s.l. and might be related to the present or a previous shoreline. They likely started to form after the LGM: either in the Lateglacial Interstadial after the amelioration of permafrost and the growth of vegetation, perhaps without surviving Younger Dryas periglaciation, or during the Holocene. The active type C, D, and coastal E tufas are rather small, compared with international deposits. This suggests they are in dynamic equilibrium between growth and destruction by the sea or by dissolution following heavy rain, which would send a plume of aggressive water through the fractures.

No coastal tufa, caves, undercuts or conduits were found >25 m a.s.l. This suggests they did not exist at the readvance just prior to 14.7 ka, when a seasonally-frozen sea accelerated coastal erosion and cut the 40 m shoreline. Otherwise, caves and undercuts should be preserved, because the final Lismore deglaciation was at c. 16 ka and sea level has fallen since. Thus, the land probably remained permafrosted immediately prior to 14.7 ka, so that there were no seepage waters and plants to promote calcite deposition as tufa and no karstic dissolution to create conduits, if that was necessary prior to any subsequent enlargement by marine abrasion. Thin type A cliff deposits were only observed close to the NW coast, at ≥10 m a.s.l. This tufa is probably promoted by the evaporation of sea spray borne by the prevailing SW winds. The containing cliffs were eroded back during glaciation, so that the earliest that most high and massive tufas and speleothems could have formed is in the Lateglacial Interstadial. However, the sample with an MIS5 age was collected from a stalactite in a "deep undercut" 19 m a.s.l. It possibly survived if it formed in a littoral cave passage that was mostly removed by glacial erosion before the end of the LGM. Similarly, the massive column in the entrance to Uamh na Cathaig (Figure 6), which is 3 m in diameter and 8 m tall, might have formed at MIS5e inside a paleo cave passage that was later eroded to leave a 5 m-deep gorge that starts about 30 m in front of the existing cave entrance and runs to the sea. Another cave heads a short 10 m-deep gorge (Figure 10). These three sites could be examples of roofless caves, which have rarely been reported in Britain. Other interesting research queries were also discussed by FAULKNER & CRAE (2018).

Acknowledgements

References

BALLANTYNE C.K., STONE J.O. (2012) Did large ice caps persist on low ground in north-west Scotland during the Lateglacial Interstade? *Journal of Quaternary Science* 27, 297-306.

BRASIER A.T. (2011) Searching for travertines, calcretes and speleothems in deep time: Processes, appearances, predictions and the impact of plants. *Earth-Science Reviews* 104, 213-239.

CHAFETZ H.S., FOLK R.L. (1984) Travertines: Depositional morphology and the bacterially constructed constituents. *Journal of Sedimentary Petrology* 54 (1), 289-316.

CORBEL J. (1957) *Autour du Ben Nevis. In Les Karsts du Nord-ouest de l'Europe*, Université de Lyon, 276-278, Figures 55-62.

FAIRCHILD I.J., BAKER A. (2012) *Speleothem Science: From process to past environments*. Wiley-Blackwell. 432pp.

FAULKNER T. (2006) Tectonic inception in Caledonide marbles. *Acta Carsologica* 35 (1) 7–21.

FAULKNER T., BRAZIER V. (2016) Tufa deposits at Inchrory and Glen Suie, Moray, Scotland. *Cave and Karst Science* 43 (1) 17-20.

FAULKNER T., CRAE J. (2018) Distribution of tufa and speleothem deposits on the island of Lismore, Argyll, Scotland. *Cave and Karst Science* 45 (3) 101-110.

FORD T.D. (1989) Tufa – the Whole Dam Story. *Cave Science* 16 (2), 39-49.

FORD T.D., PEDLEY H.M. (1996) A review of tufa and travertine deposits of the world. *Earth-Science Reviews* 41, 117-175.

GRAY J.M., IVANOVICH M. (1988) Age of the main rock platform, western Scotland. *Palaeogeography, Palaeoclimatology, Palaeoecology*, 68, 337-345.

LOWE D., WALTHAM T. (2002) Dictionary of Karst and Caves. Cave Studies Series (10) *British Cave Research Association*. 40pp.

PEDLEY H.M. (1990) Classification and environmental models of cool freshwater tufas. *Sedimentary Geology* 68, 143-154.

PENTECOST A. (1993) British travertines: a review. Proceedings of the Geologists' Association 104, 23-39.

PENTECOST A. (1995) Quaternary travertine deposits of Europe and Asia Minor. *Quaternary Science Reviews* 14, 1005-1028.

SMALL D. and 8 others. (2017) Cosmogenic exposure age constraints on deglaciation and flow behaviour of a marine-based ice stream in western Scotland, 21–16ka. *Quaternary Science Reviews* 167, 30-46.

STEPHENSON D. and 4 others. (2013) Special Issue: The Dalradian Rocks of Scotland. *Proceedings of the Geologists' Association* 124 (1-2). 409pp.

Prospecting for Last Interglacial speleothems in Vercors

Charlotte HONIAT[1], Stéphane JAILLET[2], Christoph SPÖTL[1], Tanguy RACINE[1], Serge CAILLAULT[3], François LANDRY[4], R. Lawrence EDWARDS[5] & Hai CHENG[6]

(1) Institute of Geology, University of Innsbruck, 6020 Innsbruck, Austria
charlotte.honiat@student.uibk.ac.at (corresponding author)
(2) EDYTEM, Université Savoie Mont Blanc, CNRS, 73390 le Bourget du Lac, France
(3) Spéléo magazine, 38700 Corenc, France
(4) Interclubs Chuats, CDS 26, France
(5) Department of Earth Sciences, University of Minnesota, Minneapolis, MN, USA
(6) Institute of Global Environmental Change, Xi'an Jiaotong University, Xi'an 710054, China

Abstract

The Last Interglacial (LIG, ~130–116 ka) was one of the warmest interglacials of the past 800,000 years. Speleothems offer superior age control and a few LIG records are available from the Eastern Alps. In order to prospect for LIG speleothems in the Western Alps, we drilled small diameter cores at the base of stalagmites. In the Vercors, we sampled 27 speleothems in 6 different caves and dated them using the U-Th method. Here, we present the results of these reconnaissance drilling campaigns. Although, to our surprise, we did not identify stalagmites of LIG age, the resulting ages provide useful chronological information on the individual karst settings.

Among these 27 ages, 5 are Holocene, the others belong to Marine Isotope Stage 2 (5 samples), 3 (2), 5a (1) and 5c (1), 8 (1), 9 (2), 11 (4), 12 (1), 13 (1) and 4 are beyond the U-Th dating limit. These dates can help to re-assess the age of certain cave conduits and the evolution of this well-documented karst region. In addition, they may serve as a basis for future speleothem-based paleoclimate studies of the Vercors.

Résumé

À la recherche de spéléothèmes du Dernier Interglaciaire dans le Vercors. Le Dernier Interglaciaire (LIG, ~130-116 ka) a été l'un des interglaciaires les plus chauds des 800 000 dernières années. Les spéléothèmes offrent la possibilité d'une excellente chronologie pour cette époque et quelques enregistrements sont disponibles dans les Alpes orientales. Afin de trouver des spéléothèmes LIG dans les Alpes occidentales, nous avons foré des carottes de petit diamètre à leur base. Dans le Vercors, nous avons carotté 27 spéléothèmes dans 6 grottes différentes qui ont ensuite été datés par la méthode U-Th. Nous présentons ici les résultats de ces campagnes de forage de reconnaissance. Bien que, à notre surprise, n'ayons pas identifié de stalagmites d'âge LIG, les âges obtenus fournissent des informations chronologiques utiles pour la connaissance du karst. Parmi ces 27 âges, 5 sont holocènes, les autres appartiennent au stade isotopique marin 2 (5 échantillons), 3 (2), 5a (1) et 5c (1), 8 (1), 9 (2), 11 (4), 12 (1), 13 (1) et 4 sont au-delà de la limite de datation U/Th. Ces dates peuvent aider à réévaluer l'âge de certains conduits et l'évolution de ce karst de moyenne montagne. En outre, elles peuvent servir de base pour de futures études paléoclimatiques du Vercors à partir des spéléothèmes.

1. Introduction

The Last Interglacial (LIG ~130–116 ka), equivalent to Marine Isotope Stage (MIS) 5e and considerably warmer than the current interglacial, is a useful test bed for the future course of the Holocene (Anthropocene). In the foreland of the European Alps, the LIG has been studied using pollen preserved in mires and lake sediments. While these records document the succession of tree and other plant species across the LIG, they are very poorly constrained chronologically. Speleothems in caves offer superior age control and a few records are already available from the Austrian Alps (SPÖTL et al., 2002; MOSELEY et al., 2015) and the Swiss Alps (HÄUSELMANN et al., 2015; WILCOX et al., 2020). The aim of the project was to find speleothems of LIG ages in the French Alps and thus extend our knowledge about this period across the entire Alps. Mountains are of particular interest for climate science because they are highly sensitive and show higher amplitudes of climate change than surrounding regions (Mountain Research Initiative EDW Working Group, 2015). Site selection was based on previous work on the Vercors

(e.g., AUDRA 1994; DELANNOY, 1997) and discussion with colleagues and local cavers. Criteria of this selection included the availability of high-quality sample material and whether the cave has been characterized previously (including geomorphological observations and speleothems of different age).

Sites description

The four study sites (6 caves) are presented from north to south (Fig. 1). At 1144 m a.s.l. the **Antre de Vénus** is a horizontal cave of 850 m length. It partially intersects the Croix Perrin anticline and at the time of its formation, it drained the vast Méaudre-Autrans depression. It is interpreted as one of the ponors of a vast paleo-poljé and is the witness of a higher base level of the hydrographic network during the Neogene (DELANNOY et *al.*, 1998). The Coulmes karst, northwest of the Vercors, is a multi-level cave system that has recorded the landscape evolution since the Neogene. **Pra l'Etang** (1220 m a.s.l., 300 m length) is a cave marking a former higher perched base level. Three samples were taken there. Nearby, at a lower elevation, in the **Gournier system** (572 m a.s.l., 18 km length), an underground river which can be followed up to 680 m a.s.l. Six samples were collected in the first fossil gallery of this cave. Next to it, the **Coufin/Chevaline network** (580 m a.s.l., 32 km length) also hosts two underground rivers. Samples were collected in the so-called "gruyères" sectors. The **Pabro cave** (840 m a.s.l., 100 m length) is a decapitated cave facing the Coulmes karst and perched above the gorges de la Bourne. Six samples were taken in the main room.

Finally, the **Chuats system** was the subject of preliminary investigations. It is an important and recently explored network of 43 km length (LANDRY et *al.*, 2019) that
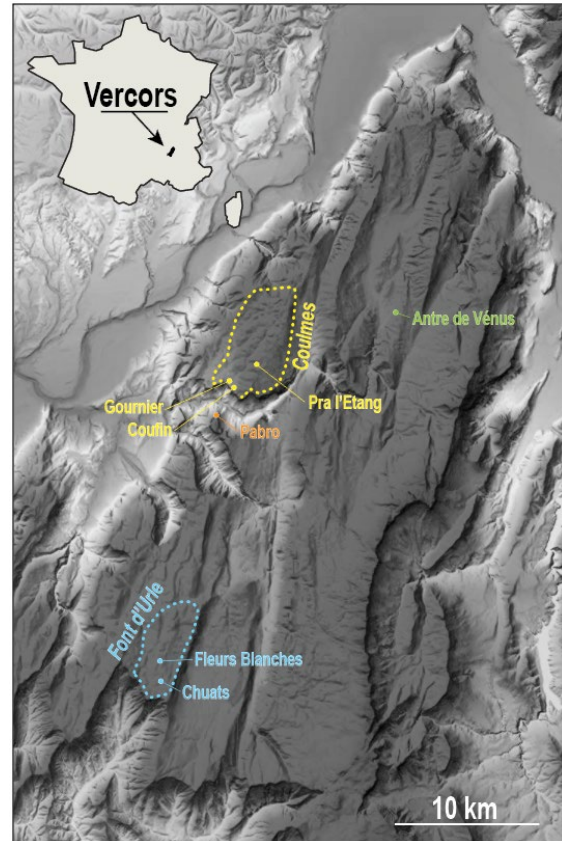

Figure 1: Map of the Vercors region with sampled caves

comprises 5 known entrances. Three samples were taken from the Chuats II chasm in the sectors near the base of the entrance shafts series. These are the first dated speleothems in this major cave system of the southern Vercors.

2. Materials and methods

Figure 2: Sampling of a calcite core in a stalagmite with a hand-held drill and a water flushing unit.

Figure 3: Example of small core pieces used for dating. Both pictures: Serge Caillault

Our sampling approach of taking drill cores instead of entire dripstones minimizes the impact on the cave environment (Fig. 2) (SPÖTL and MATTEY, 2012). In order to search for LIG speleothems, we drilled small-diameter cores (Fig. 3) at the base of 21 speleothems (stalagmite and flowstone) and exclusively retrieved broken stalagmites (6 in total). We targeted the central axis of the stalagmites and sampled the innermost part of each core.

The cores were then cleaned in an ultrasonic bath before being drilled and dated using the U-Th method. Between 30 and 70 mg were analysed at the University of Minnesota and the Xi'an Jiatong University following the same procedure (EDWARDS et al., 1987). All measurements were performed on a ThermoFisher Neptune Plus MC-ICP-MS using the technique described by CHENG et al. (2013).

3. Results

Among the 27 analyzed speleothem samples 5 are Holocene in age, and the others fell into Marine Isotope Stages 2 (5 samples), 3 (2), 5a (1) and 5c (1), 8 (1), 9 (2), 11 (4), 12 (1), 13 (1), while 4 are beyond the U-Th dating limit (older than 650 000 years). The ages are given in year before present (BP) in table 1.

Sample Number	^{238}U (ppb)	^{232}Th (ppt)	$^{230}Th / ^{232}Th$ (atomic x10^{-6})	$\delta^{234}U^*$ (measured)	$^{230}Th / ^{238}U$ (activity)	^{230}Th Age (yr) (uncorrected)	^{230}Th Age (yr) (corrected)	$\delta^{234}U_{Initial}^{**}$ (corrected)	^{230}Th Age (yr BP)*** (corrected)	
ADV-01	259.4 ±0.6	13671 ±275	294 ±6	-30.2 ±2.2	0.938 ±0.004	420669 ±25855	418950 ±25449	-99 ±10	418881	±25449
ADV-02	186.4 ±0.3	13159 ±264	297 ±6	190.0 ±2.0	1.273 ±0.004				Beyond U/Th Limit	
ADV-03-BOT	253.5 ±0.4	2733 ±55	1902 ±38	169.9 ±1.8	1.244 ±0.003				Beyond U/Th Limit	
ADV-04-BOT	115.8 ±0.2	218 ±5	9881 ±229	108.0 ±1.9	1.128 ±0.003	434526 ±18286	434482 ±18281	368 ±20	434413	±18281
COU-01	430.5 ±0.8	1865 ±38	4218 ±85	85.1 ±2.0	1.108 ±0.003	506997 ±33601	506895 ±33573	356 ±35	506826	±33573
COU-02	378.8 ±0.7	5369 ±108	1233 ±25	87.1 ±2.0	1.059 ±0.003	325705 ±6444	325365 ±6429	218 ±6	325296	±6429
COU-03	17.1 ±0.0	150 ±4	1769 ±54	37.5 ±1.9	0.944 ±0.011	251873 ±11203	251634 ±11183	76 ±5	251565	±11183
COU-04	122.1 ±0.2	177974 ±3566	13 ±0	41.8 ±1.9	1.187 ±0.005				Beyond U/Th Limit	
COU-06	108.4 ±0.2	117829 ±2364	16 ±0	46.8 ±2.0	1.042 ±0.005	421933 ±25213	390143 ±30279	141 ±13	390074	±30279
GO-13-Bot	236.7 ±0.3	19251 ±386	38 ±1	356.2 ±2.1	0.190 ±0.001	16324 ±86	14585 ±1234	371 ±3	14517	±1234
GO-14	313.2 ±0.5	12650 ±254	63 ±1	284.8 ±2.2	0.154 ±0.001	13862 ±91	12951 ±651	295 ±2	12883	±651
GO-15	314.5 ±0.5	691 ±14	874 ±18	200.3 ±2.1	0.116 ±0.001	11088 ±66	11035 ±76	207 ±2	10967	±76
GO-16	150.9 ±0.2	11337 ±227	34 ±1	143.5 ±2.1	0.154 ±0.001	15701 ±159	13782 ±1367	149 ±2	13714	±1367
GO-17	107.7 ±0.1	3197 ±64	83 ±2	184.1 ±2.2	0.150 ±0.002	14745 ±192	14018 ±549	192 ±2	13950	±549
GO-18	603.4 ±1.2	155 ±4	8194 ±206	300.1 ±2.3	0.127 ±0.000	11207 ±49	11201 ±50	310 ±2	11133	±50
PLG-01	194.0 ±0.3	4245 ±85	133 ±3	115.1 ±2.1	0.176 ±0.001	18741 ±129	18172 ±423	121 ±2	18103	±423
PLG-03	168.7 ±0.2	697 ±14	350 ±8	103.9 ±2.0	0.088 ±0.001	9012 ±91	8903 ±119	107 ±2	8834	±119
PLG-04	192.6 ±0.4	1734 ±35	56 ±2	-26.5 ±2.1	0.030 ±0.001	3455 ±96	3186 ±214	-27 ±2	3117	±214
PB-19	73.2 ±0.1	448 ±9	979 ±23	41.1 ±2.4	0.363 ±0.005	46662 ±728	46492 ±736	47 ±3	46424	±736
PB-20-Bot	79.2 ±0.1	1291 ±26	433 ±10	66.5 ±2.0	0.429 ±0.004	55717 ±661	55276 ±728	78 ±2	55208	±728
PB-21-Bot	96.2 ±0.1	64 ±3	2179 ±106	34.3 ±2.2	0.088 ±0.002	9642 ±223	9623 ±224	35 ±2	9555	±224
PB-22	106.1 ±0.1	34993 ±701	32 ±1	34.5 ±1.7	0.646 ±0.006	106120 ±1588	96534 ±6960	45 ±2	96466	±6960
PB-23	106.3 ±0.2	9943 ±199	174 ±4	7.5 ±2.3	0.988 ±0.008	416445 ±45062	413750 ±43912	24 ±8	413682	±43912
PB-24	86.8 ±0.1	10496 ±210	134 ±3	6.9 ±2.0	0.985 ±0.008	406405 ±40974	402901 ±39666	21 ±7	402833	±39666
CHU01-TOP	362.7 ±0.4	793 ±16	5227 ±106	275.0 ±1.8	0.693 ±0.002	82559 ±387	82512 ±388	347 ±2	82443	±388
CHU02-BOT	1785.4 ±6.9	298 ±6	98680 ±2111	0.2 ±2.5	0.999 ±0.005	732945			Beyond U/Th Limit	
CHU04-A	487.8 ±0.5	478 ±10	18678 ±382	126.2 ±1.4	1.110 ±0.002	327917 ±4573	327893 ±4572	318 ±5	327824	±4572

Table 1: U-Th dating results. Ages are reported in Year BP; the error is 2 sigma. ADV: Antre de Vénus; COU: Couffin; GO: Gournier; PLG: Pra L'Etang; PB: Pabro; CHU: Chuat

4. Discussion and conclusion

When compared to the deep-sea $\delta^{18}O$ curve based on benthic foraminifera (Fig. 4), the majority of the stalagmites commenced to grow during interglacial periods: 5 are Holocene in age, 2 are from MIS 9, 4 from MIS 11 and 1 from MIS 13. Some ages indicate growth during interstadials. On the other hand, one sample plots at the onset of the Younger Dryas, another sample plots into a glacial (MIS 12) but overlaps within error with the following major interglacial MIS 11 (Fig. 4). Another sample falls into MIS 8 but again its error bar overlaps with an interglacial, MIS 7. Interestingly, we found no speleothems that formed during the LIG.

Regarding the confidence of the dating, the material originating from stalagmites had almost always a higher Uranium concentration and was cleaner (less detrital thorium) than flowstones from the same area in the cave. The high detrital content of the flowstone from the Coufin/Chevaline river were challenging to date and some samples had to be discarded. Samples with a small $^{230}Th/^{232}Th$ atomic ratio (on the order of tens) should be cautiously considered.

We report these new dates to serve as (a) minimum ages for speleogenetic studies of these caves (e.g. to assess the minimum age of certain conduits), and (b) as pilot data for future paleoclimate studies of this part of France. Some of these dates will later be integrated in local studies on these cave systems.
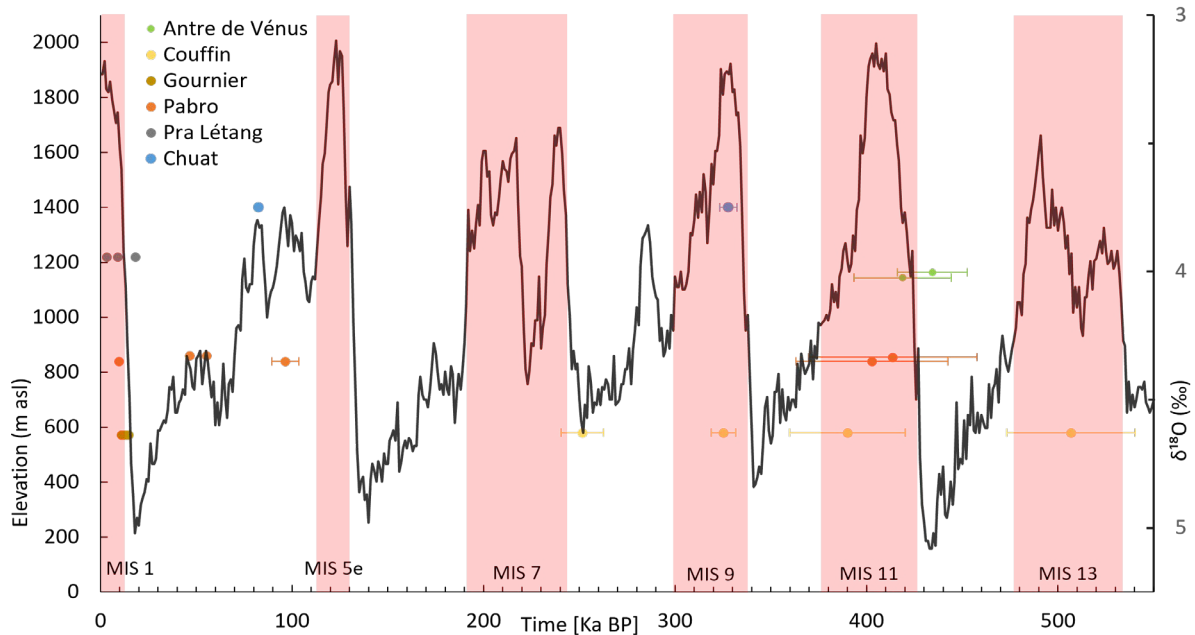
Acknowledgments

Figure 4: Basal ages with 2 sigma error bars of sampled speleothems from the Vercors arranged according to their approximate elevation (cave entrance), compared to the deep-sea δ¹⁸O curve (LISIECKI and RAYMO, 2005). Interglacials are highlighted in purple.

References

AUDRA P. (1994) Karsts alpins-Genèse de grands réseaux souterrains. Karstologia Mémoires 5, 280p.

CHENG H. et al. (2013) Improvements in 230Th dating, ²³⁰Th and ²³⁴U half-life values, and U–Th isotopic measurements by multi-collector inductively coupled plasma mass spectrometry. Earth and Planetary Science Letters 371–372, 82–91. https://doi.org/10.1016/j.epsl.2013.04.006

EDWARDS R.L. et al. (1987). Precise timing of the Last Interglacial period from mass spectrometric determination of Thorium-230 in corals. Science 236, 1547–1553. https://doi.org/10.1126/science.236.4808.1547

DELANNOY J.-J. (1997) Recherches géomorphologiques sur les massifs karstiques du Vercors et de la transversale de Ronda (Andalousie) : les apports morphogéniques du karst. Unpublished PhD thesis Université Joseph Fourier - Grenoble 1.

HÄUSELMANN A.D., FLEITMANN D., CHENG H., TABERSKY D., GÜNTHER D. and EDWARDS R.L., 2015. Timing and nature of the penultimate deglaciation in a high alpine stalagmite from Switzerland. Quaternary Science Reviews 126, 264–275. https://doi.org/10.1016/j.quascirev.2015.08.026

LANDRY F., (2019) Fédération française de spéléologie, Comité départemental (Drôme). Le réseau des Chuats : plateau de Font d'Urle - Vercors. Comité départemental de spéléologie de la Drôme,

Valence.https://catalogue.bnf.fr/ark:/12148/cb457428090

LISIECKI L.E. and RAYMO, M.E. (2005) A Pliocene-Pleistocene stack of 57 globally distributed benthic δ18O records. Paleoceanography 20, n/a-n/a. https://doi.org/10.1029/2004PA001071

MOSELEY G.E. et al. (2015) Termination-II interstadial/stadial climate change recorded in two stalagmites from the north European Alps. Quaternary Science Reviews 127, 229–239. https://doi.org/10.1016/j.quascirev.2015.07.012

Mountain Research Initiative EDW Working Group (2015). Elevation-dependent warming in mountain regions of the world. Nature Climate Change 5, 424–430. https://doi.org/10.1038/nclimate2563

SPÖTL C. et al. (2002). Start of the last interglacial period at 135 ka: Evidence from a high Alpine speleothem. Geology 30, 815-818. https://doi.org/10.1130/0091-7613(2002)030<0815:SOTLIP>2.0.CO;2

SPÖTL C. and MATTEY D. (2012) Scientific drilling of speleothems - a technical note. International Journal of Speleology, 41, 29–34. https://doi.org/10.5038/1827-806X.41.1.4

WILCOX P.S. et al. (2020) Exceptional warmth and climate instability occurred in the European Alps during the Last Interglacial period. Communications Earth & Environment, 1:57, https://doi.org/10.1038/s43247-020-00063-w

Crues holocènes et stalagmites corrodées de l'évent de Foussoubie (Ardèche, France)

Stéphane JAILLET [1], Edwige PONS-BRANCHU [2],
Didier CAILHOL [3], Christophe GAUCHON [1]

(1) Laboratoire EDYTEM, Université Savoie Mont Blanc, CNRS, Pôle Montagne, 73 376 Le Bourget-du-Lac, stephane.jaillet@univ-smb.fr (corresponding author)
(2) Laboratoire des Sciences du Climat et de l'Environnement, LSCE/IPSL, CEA-CNRS-UVSQ, Université Paris-Saclay, F-91191 Gif-sur-Yvette, France
(3) Inrap 13 rue du Négoce 31650 Saint-Orens-de-Gameville – didier.cailhol@inrap.fr

Résumé

En amont des Gorges de l'Ardèche, le système karstique de Foussoubie avec 23 km de développement et un bassin d'alimentation de 14,4 km² se caractérise par un drain dominant alimenté à partir d'une perte unique. Il est caractérisé par des crues importantes affectant une zone épinoyée bien développée. L'exutoire du système (l'Event de Foussoubie) est le siège de mises en charge plurimétriques, commandées par un seuil de déversement au droit du porche d'entrée. Deux stalagmites assez détritiques, ont été datées par la méthode U/Th. Quatre dates ont été obtenues entre 2,05 ± 0,4 ka et 3,95 + 3,07 / - 2,37 ka qui placent l'ensemble de ces croissances dans l'Holocène tardif. L'analyse des sections polies des deux échantillons fait apparaitre plusieurs surfaces d'érosion montrant qu'au cours de cette période des phases de crues intenses (comme c'est le cas actuellement) séparent des phases plus calmes autorisant la croissance des stalagmites. Plusieurs interprétations sont proposées : modification du seuil au niveau du porche, changement géométrique de la perte, évolution du couvert végétal sur le plateau ou dans le bassin d'alimentation.

Abstract

Holocene floods and eroded stalagmites from the Foussoubie Cave (Ardèche, France). Upstream of the Gorges de l'Ardèche, the Foussoubie karstic system, with 23 km of development and a 14.4 km² catchment area, is characterized by a dominant drain with a single sink. It is characterized by significant flooding affecting a well-developed epiphreatic zone. An overflow sill at the entrance porch controls the multi-metric flood in the system's spring (the Foussoubie Event). In the section of the gallery between the downstream siphon and the entrance porch, two detrital stalagmites have been dated by the U/Th method. Four dates were obtained, ranging between 2.05 ± 0.4 ka and 3.95 + 3.07 / - 2.37 ka, which place all these growths in late Holocene. Analysis of the polished sections of the two samples reveals several erosion surfaces, showing that during this period, phases of intense flooding (as is currently the case) separate calmer phases allowed the growth of stalagmites. Several interpretations are proposed: modification of the threshold at the porch, geometric change of the sink, evolution of the vegetation cover on the plateau or in the catchment basin.

1. Introduction

Si les stalagmites sont connues pour être des indicateurs pertinents des variations paléo-environnementales, elles s'avèrent aussi de précieux enregistreurs des crues souterraines. Diverses études ont déjà mis en avant l'enregistrement des crues par les stalagmites, essentiellement par piégeage de sédiments détritiques inter-stratifiés dans les lamines (DASGUPTA *et al*., 2010 ; FRAPPIER *et al*., 2014 ; DENNISTON *et al*., 2017). C'est chaque fois plutôt un enregistrement de paléo-mises en charge avec des circulations lentes d'eaux turbides, qui viennent déposer de minces films détritiques. Lorsque la stalagmite est dans le passage du courant d'eau, ce peut être alors des traces érosives laissées par les flux d'eau et qui affectent les stalagmites elles-mêmes en laissant, dans la structure interne, des surfaces d'érosion. C'est le cas

proposé ici à partir de l'exemple du système de Foussoubie. En rive droite des gorges de l'Ardèche, ce système karstique (23 km de développement souterrain, LE ROUX, 1984, fig. 1) est connu pour la violence de ses crues souterraines. Alimentée par un bassin d'alimentation de 14,4 km², la perte unique (la goule), concentre les écoulements dans un drain épinoyé où les mises en charges ont été étudiées et enregistrées sur plusieurs mètres de hauteur (JAILLET *al*., 2012 ; ERGUY *et al*., 2021). A l'aval du système un siphon de 350 m de longueur connait des mises en charges importantes supérieures à 12 m. C'est dans ce tronçon aval que deux stalagmites ont fait l'objet d'une analyse spécifique consistant à les replacer dans leur contexte morphologique, à analyser leurs croissances et à les dater.
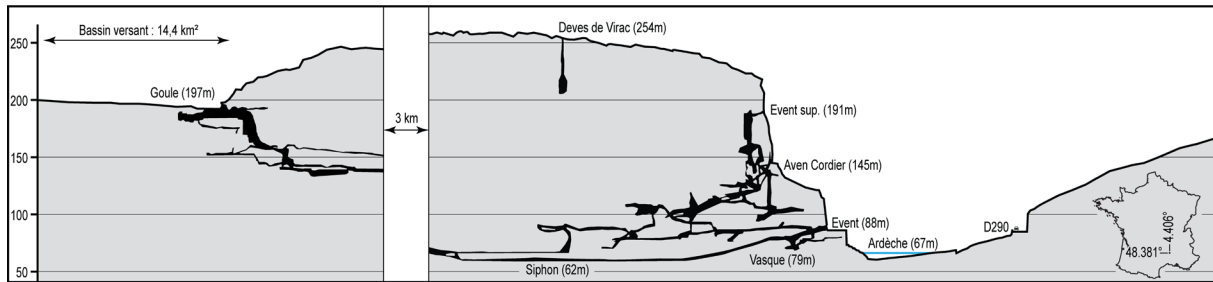
Figure 1 : Le système de Foussoubie en rive droite des gorges de l'Ardèche (23 km) draine un bassin versant de 14,4 km² auquel s'ajoute une alimentation par infiltration. L'évent est l'exutoire temporaire du système.
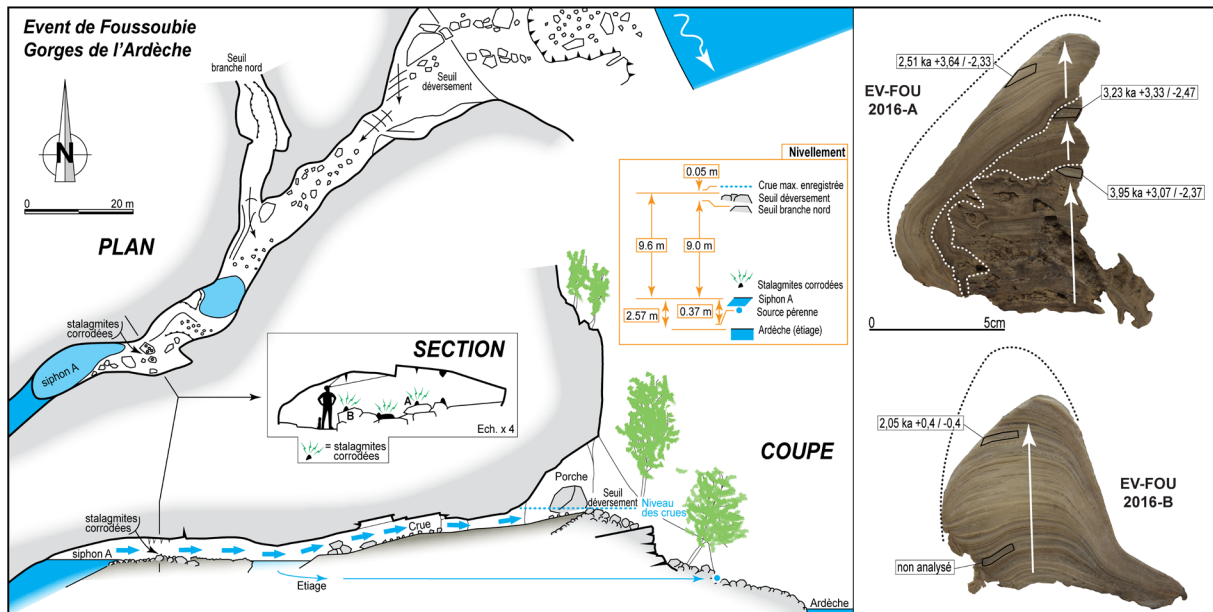

Figure 2 : Plan et coupe détaillée de l'évent de Foussoubie et localisation des stalagmites étudiées dans le tronçon aval du système karstique. Le tronçon de galerie entre le siphon A et le seuil de déversement est le siège de mises en charge récurrentes ennoyant les stalagmites. Les sections polies des stalagmites EV-FOU-2016 A & B montrent les différentes phases d'érosion affectant leur croissance au cours de l'Holocène. Pour EV-FOU-2016-A, des phases de croissances continues sont séparées par des phases de corrosions intenses. La période actuelle est une phase de corrosion.

2. Méthodes : une étude des stalagmites corrodées

L'étude du site a été conduite selon une double approche : (i) topographique et géomorphologique d'une part et (ii) analytique sur les stalagmites d'autres part. Sur place, un relevé topographique de l'évent a été réalisé, en coupe et en plan (fig. 2). Nous avons entrepris un nivellement fin des points clés de déversement des eaux à savoir le siphon A, les seuils, le point d'émergence et l'Ardèche. Ces mesures, réalisées au niveau de chantier, complètent les mesures des hauteurs d'eau réalisées avec des sondes ReefNet au niveau du siphon A. Deux stalagmites corrodées ont été sélectionnées quelques mètres en aval du siphon A (fig. 3). Elles ont connu et connaissent encore des phases érosives majeures. Elles ont été tranchées dans l'axe de la galerie souterraine afin de bien identifier l'alternance des phases érosives et des phases de croissance. Cinq micro-échantillons ont été prélevés et analysés au Laboratoire des Sciences du Climat et de l'Environnement à Gif Sur Yvette.

Ils contiennent une fraction importante d'argile rendant leur datation difficile. La technique de préparation mise en œuvre consiste à dissoudre totalement l'échantillon (fractions carbonatée et argileuse). Des échantillons de 100 à 300 mg ont été dissous en HCl dilué dans des béchers contenant une quantité connue de traceur ^{229}Th ^{233}U ^{236}U. Le résidu argileux non dissous est séparé par centrifugation du surnageant et attaqué par un mélange de HF et HNO$_3$ concentrés, à chaud pendant une nuit puis évaporé et repris en HCl dilué. Les deux fractions ainsi dissoutes sont mélangées puis traitées classiquement pour une datation suivant un protocole présenté dans PONS-BRANCHU et al. 2014. Brièvement, après coprécipitation avec FeOH, les fractions U et Th sont purifiées sur colonne échangeuse d'ions (ici U-TEVA en milieu nitrique). L'analyse est réalisée sur MC-ICPMS Neptune™ +.

3. Résultats : nivellement et mises en charge

Entre le siphon A et le point d'émergence en bordure de l'Ardèche, la dénivellation est de 0,37 m. Celle-ci est à 2,2 m au-dessus du cours de l'Ardèche en étiage. Entre le siphon A et le seuil de débordement au niveau du porche, la dénivellation est de 9,6 m. Ce point commande le moment où l'évent est en crue et déverse par cet orifice temporaire perché (fig. 2). Entre le siphon A et le seuil de débordement au niveau du seuil déversoir en direction de la branche nord et du siphon B, la dénivellation est de 9,01 m. Ce seuil est donc 0,59 m plus bas que le seuil de déversement. Ces éléments altimétriques constituent des seuils clés qui commandent les mises en charge du réseau. Ces mises en charge justement ont été analysées à partir d'un enregistrement des hauteurs d'eau au droit du siphon A, grâce à une sonde ReefNet (période 2011 / 2018). Les données analytiques sont présentées dans un travail spécifique (ERGUY *et al.*, 2021) dont nous extrayons les éléments essentiels. Au droit du siphon A, la hauteur maximale enregistrée est 9,65 m, c'est-à-dire 5 cm au-dessus du seuil de déversement. Le siphon C, perché par rapport au siphon A, connaît une mise en charge maximale enregistrée de 8,31 m. Sur la période de 2011 à 2018, il y a en moyenne 47 épisodes par an, de montée des eaux supérieure à 1 m. Les mois qui connaissent le plus de variations sont mars (11), novembre (9), mai (6) et octobre (5). La plupart de ces montées des eaux ne donnent pas lieu à un débordement par le seuil. La moyenne est évaluée à un débordement tous les 3 ans. Enfin, sur les épisodes intenses,

la vitesse de montée de l'eau est comprise entre 4 et 6 cm/mn. Si le débit de pointe à la sortie du siphon A est de 7,3 m³/s (avec évacuation par le seuil), le débit moyen des crues est de l'ordre de 1m³/s (avec évacuation par l'exutoire en bordure de l'Ardèche par des griffons plus ou moins étagés sur 2m de hauteur). Ces éléments permettent d'évaluer correctement la fréquence et l'intensité des crues subies par les stalagmites étudiées, placées quelques mètres en aval du siphon et donc ennoyées plusieurs dizaines de fois par an.

Figure 3 : Un des ensembles stalagmitiques étudiés présente des marques de corrosion importantes, associées aux crues régulières affectant le système. Le prélèvement de deux stalagmites a permis de réaliser des datations et leur analyse sur section polie.

4. Résultats : Datations et surfaces d'érosion

Les données de concentrations, rapports isotopiques et âges (avant et après correction) sont présentées figure 4. Tous les échantillons analysés présentent des caractéristiques similaires : des concentrations en uranium élevées (plus de 700 ppb), une signature isotopique en uranium appauvrie en ^{234}U ($\delta^{234}U$ négatif) et une contribution importante de thorium détritique, marquée par des teneurs élevées en ^{232}Th et des rapports $^{230}Th/^{232}Th$ faibles (pour l'échantillon de la stalagmite B) ou très faibles (échantillons de la stalagmite A). Les âges déterminés doivent donc être corrigés de cette fraction détritique. Pour l'échantillon B, une correction basée sur un rapport ($^{230}Th/^{232}Th$) de 1,5 ± 50% est appliquée, et les incertitudes propagées, donnant un âge brut de 2,87 (±0,02) ka BP avant correction et 2,05 (±0,43) ka BP après correction. Pour les échantillons de la stalagmite A, le contenu en thorium détritique ne permet pas d'envisager une telle correction avec une composition de la phase détritique prédéterminée. Cependant, ces 3 échantillons étant issus de la même séquence, une correction basée sur la détermination de la valeur de correction permettant de rendre compte de l'ordre stratigraphique est possible (routine STRUTage, ROY BARMAN *et al.*, 2016). Pour cette stalagmite, les âges avant correction s'échelonnent entre 33,40 (±0,18) et 16,78 (±0,11) ka BP, avec des inversions stratigraphiques, et après correction entre 2,51 (+3,64/-2,33) et 3,95 (+3,07/-2,37) ka

BP. La valeur du rapport de correction déterminée par la routine STRUTage ($^{230}Th/^{232}Th$ = 0,84 ± 0,10) est compatible avec ce qui est attendu pour des argiles.
L'analyse des sections polies a été réalisée sur deux tranches avec un axe de coupe parallèle au flux d'eau. L'échantillon EV-FOU-2016-A présente trois surfaces d'érosion que les dates encadrent partiellement (fig. 2). L'échantillon EV-FOU-2016-B est plus récent et n'offre qu'une surface d'érosion correspondante à la période actuelle. Ces deux échantillons se succédant partiellement, il est possible d'avancer que les deux échantillons enregistrent la chronique suivante : croissance stalagmitique jusqu'au moins 3,95 (+3,07/-2,37) ka BP suivi d'une phase d'érosion importante. Une seconde phase de croissance stalagmitique est identifiée jusqu'au moins 3,23 (+3,33/-2,47) ka BP suivie d'une nouvelle phase d'érosion intense. Une nouvelle phase de croissance s'étend jusqu'au moins 2,51 (+3,64/-2,33) ka BP pour l'échantillon A et 2,05 (+0,4/-0,4) ka BP pour l'échantillon B. Elle est oblitérée par une troisième phase d'érosion toujours active. Sur la base des dates et de l'emboitement des surfaces, il ne semble pas raisonnable de distinguer les dernières phases de croissance qui finalisent les deux échantillons. Au contraire elles sont plus probablement synchrones. Au final, c'est donc ici 3 phases de croissances et 3 phases d'érosion qui sont enregistrées sur une période couvrant les 5 derniers milliers d'années.

Echantillon	[^{238}U] ppm		δ^{234}UM (‰)		(^{230}Th/^{238}U)		(^{230}Th/^{232}Th)		Age brut (ka BP)		Age corrigé (ka BP)		
EV FOU 2016 A1	0,867	0,007	-6,3	±1,1	0,176	±0,0003	0,93	0,002	21,24	±0,07	3,95*	+3,07	-2,37
EV FOU 2016 A2	0,722	0,006	-8,3	±1,0	0,262	±0,0009	0,69	0,002	33,40	±0,18	3,23*	+3,33	-2,47
EV FOU 2016 A3	1,160	±0,010	-65,9	±1,3	0,133	±0,0006	0,76	0,004	16,78	±0,11	2,51*	+3,64	-2,33
EV FOU 2016 B2	0,934	0,008	-36,8	±0,8	0,026	±0,0001	5,26	0,029	2,87	±0,02	2,05	+0,4	-0,4

*Figure 4 : Données de concentrations, de rapports isotopiques et d'âges U/Th. δ^{234}U= ([^{234}U/^{238}U] – 1) x 1000. Les âges sont exprimés en milliers d'années avant l'année 1950 (ka BP). Les âges * ont été corrigés en utilisant la routine STRUTage (ROY BARMANN et al., 2016). Pour B2, l'âge a été corrigé en utilisant (^{230}Th/^{232}Th $_{det}$) = 1,5 ± 50%.*

5. Conclusions

Il a été possible de montrer que la fréquence des crues affectant le conduit n'est pas une constante. Sur les cinq derniers milliers d'années, des phases calmes, sont séparés par des phases érosives n'autorisant pas cette croissance et affectant les concrétions de manière importante, laissant chaque fois une surface d'érosion caractéristique (fig. 2). La succession des phases d'érosion et des phases de croissance rythme les conditions hydrodynamiques du conduit dont on mesure combien elles évoluent sur des échelles de temps courtes. On a vu que le seuil de déversement est un élément clé du contrôle des mises en charge puisque les crues les plus importantes, celles qui déversent, ne dépassent que de quelques centimètres ce seuil. Il est donc possible d'envisager que la dynamique gravitaire (effondrements) qui affecte le porche, est un élément de contrôle de la variabilité des mises en charge dans la zone aval. Dans cette occurrence, il conviendrait de mieux cerner le rythme de ces effondrements, mais aussi d'expliquer comment après une phase d'effondrement, une évacuation du matériel est suffisante pour expliquer qu'aucune mise en charge ne soit plus possible durant les phases calmes. L'affleurement des calcaires, reconnu de manière peu profonde sous le tablier de bloc ne milite pas pour cette unique explication. Des édifices stalagmitiques identifiés et datés dans la partie amont du réseau montre de même des phases d'érosion alternant avec des phases de croissances (JAILLET *et al*., 2012). Mais les gammes de dates alors reconnues plaçaient ces alternances dans le pléistocène et laissaient donc entendre un contrôle climatique à ces variations. La variabilité de la dimension de la perte (entrée unique des eaux d'infiltration rapide) constitue alors une piste non négligeable pour expliquer l'alternance de phases de croissance et de phases érosives. Le plateau (infiltration lente) comme le bassin versant de la perte (infiltration rapide) sont de même le siège de changements importants de l'occupation de l'espace. On ne peut donc exclure un contrôle lié l'importance du couvert végétale lui-même sous influence climatique et / ou anthropique.

Les stalagmites de l'évent de Foussoubie se retrouvent finalement en position intéressante, au carrefour d'influences variées : (i) locales (dynamique gravitaire du porche et du seuil de déversement), (ii) éloignées mais ponctuelles (dynamique dimensionnelle de la perte à l'amont), (iii) anthropiques (gestion et occupation de l'espace pour le bassin versant et le plateau sus-jacent), (iv) voire climatiques (variabilité à l'échelle du Pléistocène, mais aussi de l'Holocène). Elles enregistrent évidemment une variabilité des conditions hydrodynamiques d'un tronçon de conduit. D'autres analyses permettront de démêler la part des influences externes (hommes, climat) et des contrôles internes (géométrie et seuils dimensionnels) dans cette évolution singulière.

Références

DASGUPTA S., SAAR M.O, EDWARDS R.L. et al. (2010) Three thousand years of extreme rainfall events recorded in stalagmites from Spring Valley Caverns, Minnesota. *Earth Planet Sci Lett* 300(1–2):46–54

DENNISTON R.F., LUETSCHER M. (2017) Speleothems as high-resolution paleoflood archives. *Quaternary Science Reviews* vol. 170, pp. 1-13.

ERGUY M., JOHANNET A., PISTRE S. et al. (2021) Hydrogeological Behaviour Characterization of the Foussoubie Karst Network using Statistical Approaches. *Congrès UIS 2021, Savoie-Technolac, symposium 05*.

FRAPPIER A.B., PYBURN J., PINKEY-DROBNIS A.D. et al. (2014) Two millennia of tropical cyclone-induced mud layers in a northern Yucatán stalagmite reveal: Multiple overlapping climatic hazards during the Maya Terminal Classic "megadroughts" *Geophys Res Lett* 41(14):5148–5157.

JAILLET S., CAILHOL D., ARNAUD J et al. (2012) Les crues du système karstique de Foussoubie (Ardèche, France). Une analyse morphologique et hydrodynamique des circulations dans la zone épinoyée du karst. *Collection Edytem* 13, 115-138.

LE ROUX P. (1984) Système Goule/Event de Foussoubie. Historique résumé de son exploration (Avril 1984). SERAHV n°18, *Soc. d'Et. et de Rech. Arch. et Hist. de Vagnas*, 12-20.

PONS-BRANCHU E., DOUVILLE E., ROY-BARMAN M. et al. (2014) A geochemical perspective on Parisian urban history based on U-Th dating, laminae counting and yttrium and REE concentrations of recent carbonates in underground aqueducts. *Quat. Geochr*. 24, 44-53.

ROY-BARMAN M., PONS-BRANCHU E. (2016) Improved dating of carbonates with high initial 230Th using stratigraphical and coevality constrains on U-Th ages. *Quaternary Geochronology*, 32, 29-39.

Climate and environmental changes at the MIS 5a/4 transition in southwestern Peloponnese (S. Greece)

Isidoros KAMPOLIS [1,2], Bogdan P. ONAC [2], Stavros TRIANTAFYLLIDIS [1], Victor POLYAK [3] & Yemane ASMEROM [3]

(1) School of Mining & Metallurgical Engineering, Department of Geological Sciences, National Technical University of Athens, 9 Iroon Polytechniou, 15773 Athens, Greece kampolisigeo@gmail.com (corresponding author)
(2) Karst Research Group, School of Geosciences, University of South Florida, 4202 E. Fowler Ave., NES 107, Tampa, FL 33620, USA bonac@usf.edu
(3) Department of Earth & Planetary Sciences, University of New Mexico, 221 Yale Blvd., Albuquerque, NM 87131, USA

Abstract

Stalagmite S1 recovered from Selinitsa Cave in SW Peloponnese (Greece) reveals climatic and environmental information for the latest phase of the last interglacial period. The analysis of 182 calcite samples for O and C stable isotopes along the speleothem growth axis sheds light on the hydroclimatic changes that affected the eastern Mediterranean area. The stalagmite spans the time period from 82.5 to 68 ka BP according to eight U-series dating measurements. The stable isotope time series depicts a trend from dry climatic conditions at 82.5 ka to wetter during the Marine Isotope Stage (MIS) 5a and the beginning of MIS 4. A notable environmental change is documented by a stratigraphic hiatus at the bottom of the stalagmite dated at 80.5 ka that appears to coincide with the MIS 5a sea level high stand.

Presentation of the research

Here we present the climatic and sea level record encoded in stalagmite S1 recovered from Selinitsa Cave on the eastern shore of Messiniakos Gulf in SW Peloponnese (Greece). The cave is part of a larger karstic system called ''Selinitsa-Drakos'', which is located 46 km south of Kalamata City. The system comprises Selinitsa and Drakos Underground River caves (PAPADOPOULOU-VRYNIOTI & KAMPOLIS, 2011). It develops in the typical white and grayish, medium bedded, carbonate rocks of Plattenkalk Unit of Upper Senonian - Upper Eocene age. Selinitsa Cave lies mainly above sea level with a minor part being submerged, whereas Drakos Underground River is currently completely underwater (PAPADOPOULOU-VRYNIOTI & KAMPOLIS, 2012). Selinitsa hosts evidence of phreatic origin, yet today the majority of the cave is part of the vadose zone. Selinitsa was once flooded as Drakos nowadays, but due to the tectonic uplift affecting the area, the cave passages are now in the unsaturated zone.

The formation of this karst system is controlled by the regional tectonic activity. The main faults of the area are predominantly NNW-SSE, with a minor secondary E-W direction also present. They have formed mainly during the early Miocene (MARIOLAKOS *et al*., 1985, 1994), affecting the whole central peninsula of south Peloponnese. Selinitsa Cave develops mainly in a WNW-ESE orientation, with a NNW-SSE to NW-SE trend also evident. The former direction is earlier to Late Pliocene and is due to the clockwise rotation of the western branch of the Aegean Arc since Late Miocene (MERCIER & LALECHOS, 1993). On the other hand, the Drakos cave development trends NE-SW, along a

tectonic line, most probably of Mid – Late Pleistocene age (MERCIER & LALECHOS, 1993; PAPADOPOULOU-VRYNIOTI & KAMPOLIS, 2011). The broader area of the system is currently under uplift since the Middle Pleistocene.

The proximity of this cave system close to the Mediterranean Sea makes it attractive for the study of the sea level history and the relevant climatic conditions during the Quaternary. The entrance of Selinitsa Cave is located 18.5 m above present sea level (mapsl) and just 54 m from the Mediterranean Sea (Fig. 1). Therefore, former sea level high stands may have left their imprints on the cave environment.

The 23.5-cm tall S1 was sampled at 615 m from the entrance. We performed eight U-series dating and analyzed 182 calcite powder samples for oxygen and carbon stable isotopes ($\delta^{18}O$ and $\delta^{13}C$) along the growth axis of S1, which spans from 82.5 to 68 ka BP. The $\delta^{18}O$ and $\delta^{13}C$ values vary between −5.42 and −0.14‰ and from −10.83 to −5.47 ‰, respectively. The oxygen isotopic composition of S1 reveals an overall trend from drier conditions at ~82.5 ka to much wetter during the end of MIS 5a and at the onset of MIS 4. We interpreted the $\delta^{13}C$ values to reflect soil biological activity that also suggests changes from drier to wetter climate. Additionally, the presence of a distinct stratigraphic hiatus at the lower part of the stalagmite dated at 80.5 ka is attributed to the MIS 5a sea level high stand. Altogether, this study highlights some important hydro-climatic and environmental changes in the eastern Mediterranean during a less documented time interval.

Figure 1: The entrance (in the middle of the image) and the external environment of Selinitsa Cave.

References

MARIOLAKOS I., PAPANIKOLAOU D., LAGIOS E. (1985) A neotectonic geodynamic model of Peloponnesus based on: morphotectonics, repeated gravity measurements and seismicity, *Geologisches Jahrbuch Band* 50, 3–17.

MARIOLAKOS I., BADEKAS I., FOUNTOULIS I., THEOCHARIS D. (1994) Reconstruction of the Early Pleistocene paleoshore and paleorelief of SW Peloponnesus area, *7th Congress of the Geological Society of Greece*, Vol. XXX/2, 297-304.

MERCIER J.L, LALECHOS S. (1993) The Middle-Late Pleistocene NW-SE extension in Southern Peloponnesus and the kinematics of the seismic fault of the 1986 Kalamata earthquake (Greece), *Proceedings of the 2nd Congress of the Hellenic Geophysical Union*, Florina, 5-7 May 1993, (Seismology), 586-594.

PAPADOPOULOU-VRYNIOTI K., KAMPOLIS I. (2011) The "Selinitsa-Drakos" coastal karstic system in the Messinian Mani Peninsula (southwestern Greece) in relation to the terrestrial geoenvironment, *Geologica Balcanica* 40(1–3), 75–83.

PAPADOPOULOU-VRYNIOTI K., KAMPOLIS I. (2012) Formation and development of a karstic system below and above sea level in Messinian Mani Peninsula (S. Greece), *Speleogenesis & Evolution of Karst Aquifers*, 12, 17-21 (http://www. speleogenesis.info/content/)

Witnesses of former cave glaciation: cryogenic cave carbonates from the Eastern and Southern Alps

Gabriella KOLTAI [1], Christoph SPÖTL [1], Tanguy RACINE [1], Charlotte HONIAT [1], Lukas PLAN [2] & Hai CHENG [3]

(1) Institute of Geology, University of Innsbruck, Innrain 52, 6020 Innsbruck, Austria, gabriella.koltai@uibk.ac.at (corresponding author), christophspoetl@uibk.ac.at, tanguy.racine@student.uibk.ac.at, charlotte.honiat@student.uibk.ac.at

(2) Natural History Museum, Burgring 7, 1010 Vienna, Austria, lukas.plan@nhm-wien.ac.at

(3) Institute of Global Environmental Change, Xi'an Jiaotong University, Xi'an, China, cheng021@xjtu.edu.cn

Abstract

Coarse crystalline cryogenic cave carbonates (CCC for short) are secondary carbonate deposits that form via freezing-induced supersaturation of small water bodies within cave ice and are an important indicator of former cave glaciation. Due to their commonly small size CCC have been overlooked in caves compared to other types of speleothems. Our research has shown that about a dozen of currently ice-free caves in the Eastern and Southern Alps contain such deposits. We observed a spectrum of morphologies from skeletal crystals to complex aggregates. CCC vary from a few mm to several centimetres in size. Most commonly they are translucent, white, amber-coloured or dark brown. CCC are likely more common than previously thought and caves in other parts of the Alps are expected to yield such paleo-ice indicators as well.

Résumé

Témoins d'une glaciation ancienne en grotte : les carbonates cryogéniques de grottes des Alpes orientales et méridionales.
Les 'Cryogenic Cave Carbonates' cristallins grossiers (CCC ci-après) sont des dépôts calcaires secondaires formé par solidification et super-saturation de poches d'eau liquide emprisonnée dans la glace souterraine; ce sont d'importants indicateurs de glaciation souterraine passée. A cause de leur rareté et de leur taille pour la plupart modeste, les CCC ont souvent bénéficié d'une attention moindre par rapport à d'autres types de spéléothèmes. Nos recherches montrent qu'une douzaine de sites à présent dépourvus de glace dans les Alpes du Sud et de l'Est contiennent de tels dépôts. Nous observons une large panoplie de morphologies, de cristaux squelettiques jusqu'à des agrégats plus complexes. La taille des CCC varie de quelques millimètres à plusieurs centimètres. Ils sont communément soit translucides, soit de couleur blanche, ambre ou marron foncé. Les CCC sont plus répandus qu'admis auparavant, et il est attendu que de tels indicateurs de glace ancienne soient identifiés à terme dans d'autres secteurs des Alpes.

1. Introduction

Modern ice caves and caves that were glaciated in the past may contain a unique type of speleothem, known as cryogenic cave carbonates. Two types can be differentiated, fine and coarse crystalline (ŽÁK et al., 2018). The former type forms via fast freezing-induced supersaturation of karst water often in ventilated cave passages and is common in modern-day ice caves. On the other hand, the deposition of the coarse crystalline variety requires a stable microclimate and occurs via very slow freezing of small karst water bodies within cave ice when cave air temperatures are slightly below 0°C (ŽÁK et al., 2012). These mineral deposits only form in caves that contain perennial ice deposits. Consequently, the presence of coarse crystalline cryogenic cave carbonates (hereafter CCC) in ice-free caves provides direct evidence of a former cave glaciation.

In the Eastern Alps, the first CCC were found in Großes Almbergloch (Totes Gebirge) by Reinhold Kreuz in 1976. He took a sample of white powder on a breakdown block, looked at it using X-ray diffractometry and optical microscopy, but was unsure about its origin (KREUZ, 1976). A year later, Helmut Traindl and Rudolf Pavuza, unaware of the report by Kreuz, also took a sample of this crystal accumulation which was later identified as CCC (PAVUZA and SPÖTL, 2017).

In the past two decades, CCC have been extensively studied in Central European caves (e.g. ŽÁK et al., 2012), but reports of CCC in the Western Alps (LUETSCHER et al., 2013), Eastern Alps (SPÖTL and CHENG, 2014; PAVUZA and SPÖTL, 2017) and Southern Alps (COLUCCI et al., 2017) are still scarce. Here, we summarize new discoveries in the Eastern and Southern Alps which suggest that CCC may also be widespread in Alpine caves.

2. Methods

We primarily selected caves that hosted perennial cave ice and/or snow/firn as recent as the 20th century and are now unglaciated. These caves often have extended inner, more isolated passages that are not strongly ventilated, making them good candidates for CCC formation. CCC sites were mapped and documented and samples were examined using optical microscopy. Their cryogenic nature was verified using stable carbon and oxygen isotope analyses.

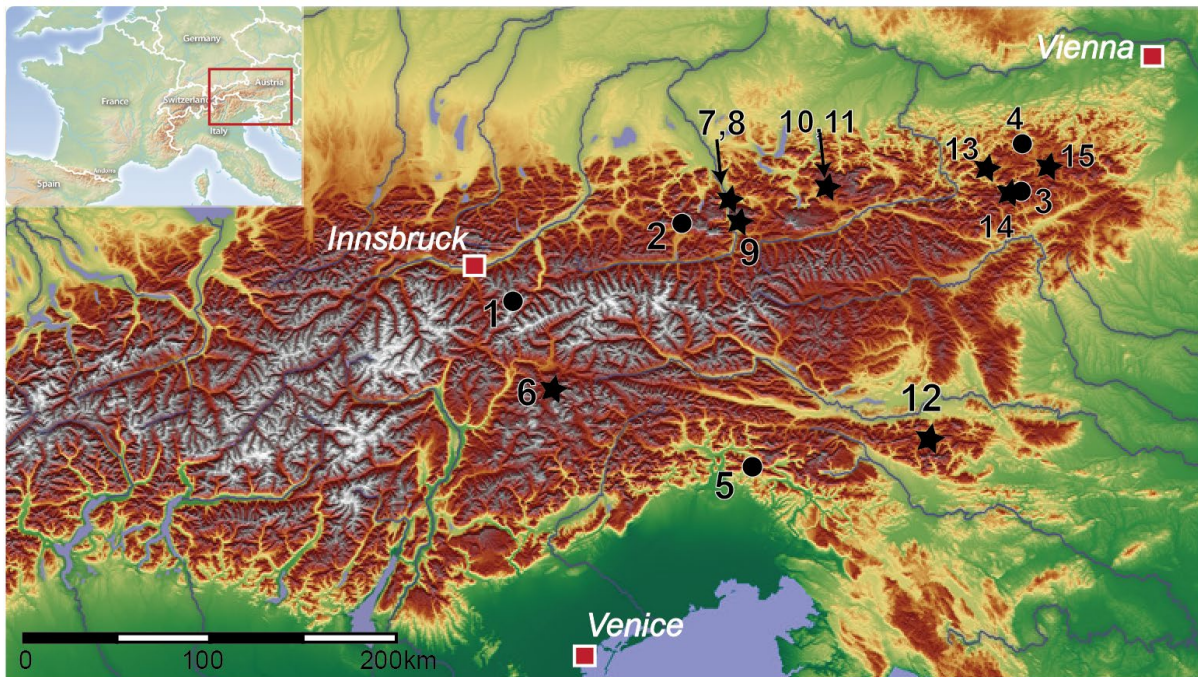## 3. New CCC sites in the Eastern and Southern Alps

Figure 1: Topographic map of the Eastern and Southern Alps showing the currently known locations of CCC. Black circles mark previously known sites (1-Mitterschneidkar Eishöhle, 2-Glaseishöhle, 3-Potentialschacht, 4-Taubenloch, 5-Leupa ice cave). Black stars refer to newly discovered CCC-bearing caves reported in this study (6-Cioccherloch, 7-Frauenofen, 8-Eisriesenwelt, 9-Eiskogelhöhle, 10-Großes Almbergloch, 11-Almberg Höhlensystem, 12-Obir caves, 13-Hochkarschacht, 14-Speikbodenhöhle, 15-Fledermausschacht). Sources: Wikipedia; Geography name

Our research has shown that about a dozen of currently ice-free caves in the Southern and Eastern Alps contains CCC, some hosting multiple occurrences (Fig. 1). The entrances of these caves are located between 1090 and 2275 m a.s.l. The lowest and highest CCC sites were found at approximately 1054 m (Obir caves) and 2225 m a.s.l. (Cioccherloch), respectively. In most caves, CCC are present as loose crystal assemblages (heaps) either on and partially also beneath breakdown blocks (Fig. 2a), or on the cave floor usually in soft sediment (Fig. 2b). Less frequently, CCC are cemented together. Individual heaps usually cover spots of 0.1 to 2 m in diameter.

Dolomites (Southern Alps)
In 2017 CCC were found in Cioccherloch, for the first time in the Dolomites (Fig 1). They occur close to the end of a descending cave chamber. CCC are amber-coloured and their size varies from a few mm to 2.5 cm (Koltai et al., 2018).

Tennengebirge (Eastern Alps)
CCC were identified in three caves in the Tennengebirge (Fig. 1). In Frauenofen four sites were documented. White and translucent colours are most common, and amber-coloured CCC are also present at one site.

In Eisriesenwelt white skeletal crystals and hemispheres were collected at two sites by cavers back in the 1920s and sent to a museum in Salzburg. We re-visited these sites, identified them as CCC (SPÖTL et al., 2020), and found nine additional sites in inner, ice-free parts of this ca. 40 km-long cave, including aggregates as large as 5 cm.

In 2020 translucent, amber-coloured and dark brown CCC were also discovered in a remote ice-free part of Eiskogelhöhle (Fig. 2b). Individual crystals are up to 3.8 cm in length, the largest of their kind from the Eastern Alps so far.

Figure 2: (a) Typical occurrence of loose white skeletal and amber-coloured rhombohedral CCC on breakdown blocks (red arrows, Großes Almbergloch). (b) Individual amber-coloured and dark brown CCC present on the cave floor in fine-grained sediment (Eiskogel cave). Pen tip for scale.

Totes Gebirge (Eastern Alps)

We re-visited the original site of 1976 in Großes Almbergloch (Fig. 2a) and located six more spots of white and amber-coloured CCC. Raft-like CCC were also documented in-situ on a decaying ice body closer to the entrance in 2018. By 2020 this ice has disappeared.

Located a few hundred meters north of the entrance of Großes Almbergloch, the Almberg Höhlensystem yielded one CCC occurrence, where white crystals resembling those in Großes Almbergloch were found in 2020 by speleologists from the Forschungsgruppe Höhle und Karst Franken.

Northern Karawanks (Eastern Alps)

The Obir caves are situated in the Northern Karawanks (Fig. 1) and comprise several individual caves that are sometimes connected by mining adits. White and translucent CCC are present in two caves, known as the Banane and the Rasslsystem. White and translucent crystals were found at four and six sites, respectively.

Tonion (Eastern Alps)

CCC are present at one site as two distinct heaps, 10 m apart from each other at approximately 250 m beneath the surface in Fledermausschacht, part of Tonion Höhlensystem. The crystals are translucent and amber-coloured and range from a few mm to 1 cm, while larger crystal aggregates are up to 2.5 cm.

Göstlinger Alps (Eastern Alps)

In 2020, white CCC aggregates were found in one of the smaller upper chambers of Hochkarschacht that connects to the main cave via inclined, narrow passages. Some of the white porous crystals are overgrown by dark brown dense calcite that is also of cryogenic origin as indicated by its stable isotope composition. Individual crystal sizes vary from 5 to 10 mm and larger aggregates are up to 1.5 cm.

Hochschwab (Eastern Alps)

Speikbodenhöhle is one of the few caves in the Hochschwab massif (Fig. 1) that has extensive horizontal passages. The upper paleo-phreatic level hosts four CCC occurrences. Heaps of white, translucent, amber-coloured, light and dark brown crystals were documented that are often mixed together.

4. Crystal morphologies

For this short morphological description, we use the terminology of RICHTER et al. (2010, 2013). We observed a wide spectrum of morphologies from skeletal crystals to complex multi-aggregates.

Skeletal crystals and hemispheres are usually translucent or white in colour, while rhombic CCC are amber-coloured, light or dark brown. Beak-like and dumbbell habits of both white and amber-colour are also present. Braided forms are often light brown or white. CCC characterised by a light brown core overgrown by dark brown cryogenic calcite were documented in three caves (Eisriesenwelt, Speikbodenhöhle and Hochkarschacht). These changes in colour and often also in porosity reflect variations in the chemical parameters of the slowly freezing water. Similarly, different crystal habits within an individual heap may reflect (i) changes in water chemistry or (ii) different depositional periods. An example for the latter is Eisriesenwelt, where one CCC site yielded multiple CCC generations, whereby the oldest and youngest CCC formed ca. 73,000 and 12,500 years ago, respectively.

Except for two types of large, cm-size individual amber-coloured and dark brown CCC discovered in Eiskogelhöhle (Fig. 2b), crystal habits in the Alpine caves show similar morphologies as those found in Central European caves (e.g. RICHTER et al., 2010, 2013, 2018; ŽÁK et al., 2012; ORVOŠOVÁ et al., 2014).

5. Conclusion and outlook

CCC are key indicators of former cave glaciation. In the last few years, several new sites have been found in the Eastern Alps and one in the Dolomites, whereby the lowest site is located at 1054 m a.s.l. Often multiple occurrences are present in a cave and in some cases, a range of morphologies can be documented within individual CCC spots. Our study

suggests that these unique and hitherto overlooked speleothems are probably quite common also in caves of the Alps, opening the door to learn more about past times of extensive ice coverage including interior parts of today's ice-free caves.

Acknowledgments

References

COLUCCI R.R. et al. (2017) First alpine evidence of in situ coarse cryogenic cave carbonates (CCC_COARSE). *Geografia Fisica e Dinamica Quaternaria*, 40(1), 53–59.

KOLTAI G. et al. (2018) First occurrence of coarsely crystalline cryogenic carbonates in the Dolomites (N Italy). *Geophysical Research Abstracts*, 20, EGU2018-10228.

KREUZ R. (1976) Vermessungsfahrt ins Almbergloch (Grundlsee, Kataster-Nr. 1624/16 a,b) vom 16.4.–18.4.1976. *Höhlenkundliche Mitteilungen Wien*, 32, 149–151.

LUETSCHER M. et al. (2013) Alpine permafrost thawing during the Medieval Warm Period identified from cryogenic cave carbonates. *The Cryosphere*, 7(4), 1073–1081.

ORVOŠOVÁ M. et al. (2014) Permafrost occurrence during the Last Permafrost Maximum in the Western Carpathian Mountains of Slovakia as inferred from cryogenic cave carbonate. *Boreas*, 43(3), 750–758.

PAVUZA R., SPÖTL C. (2017) Neue Daten zu Vorkommen und Entstehung kryogener Calcite in ostalpinen Höhlen. *Die Höhle*, 68, 100–106.

RICHTER D.K. et al. (2010) Cryogenic and non-cryogenic pool calcites indicating permafrost and non-permafrost periods: A case study from the Herbstlabyrinth-Advent Cave system (Germany). *The Cryosphere*, 4(4), 501–509.

RICHTER D. K. et al (2013) Multiphase formation of Weichselian cryogenic calcites, Riesenberg Cave (Süntel/NW Germany). *Zeitschrift der Deutschen Gesellschaft für Geowissenschaften*, 164(2), 353–367.

RICHTER D. K. et al. (2018) Unusual internal structure of cm-sized coldwater calcite: Weichselian spars in former pools of the Zinnbergschacht cave (Franconian Alb/SE Germany). *International Journal of Speleology*, 47(2), 145–154.

SPÖTL C. et al.. (2020) Einblicke in Vereisungsgeschichte der Eisriesenwelt (Tennengebirge). *Die Höhle*, 72, 45-61.

SPÖTL C., CHENG H. (2014) Holocene climate change, permafrost and cryogenic carbonate formation: Insights from a recently deglaciated, high-elevation cave in the Austrian Alps. *Climate of the Past*, 10(4), 1349–1362.

ŽÁK K. et al. (2012) Coarsely crystalline cryogenic cave carbonate - a new archive to estimate the Last Glacial minimum permafrost depth in Central Europe. *Climate of the Past*, 8(6), 1821–1837.

ŽÁK K. et al. (2018) Cryogenic mineral formation in caves. In: *Ice Caves*. Ed. by A. Perşoiu and S.-E. Lauritzen. Elsevier, pp. 123-162

Les remplissages de la phosphatière de Dams, Quercy (Caylus, Tarn-et-Garonne, France)

Carine LEZIN[(1)], Kevin MOREAU[(1)], Sébastien FABRE[(2)], Christian DUPUIS[(3)],
Patrick SORRIAUX[(4)], Gilles ESCARGUEL[(5)], Maeva ORLIAC[(6)],
Pierre Olivier ANTOINE[(6)], Monique VIANEY-LIAUD[(6)] & Thierry PELISSIE[(7)]

(1) Toulouse III | UPS Toulouse · Laboratoire Géosciences Environnement Toulouse - UM 97 (UMR 5563 / UMRD 234) – GET. carine.lezin@get.omp.eu et kevin.moreau.arnage@gmail.com
(2) IRAP, CNRS, Université Paul Sabatier-IRD, 14 Avenue Edouard Belin 31400 Toulouse, France, sfabre@irap.omp.eu
(3) Université de Mons · Department of Geology and Applied Geology, Christian.DUPUIS@umons.ac.be
(4) Spéléo Club du Haut-Sabarthez, psorriaux@gmail.com
(5) Univ. Lyon, Laboratoire d'Ecologie des Hydrosystèmes Naturels et Anthropisés, UMR CNRS 5023, Université Claude Bernard Lyon 1. Gilles.Escarguel@univ-lyon1.fr
(6) Institut des Sciences de l'Évolution, Université de Montpellier-CNRS-IRD-EPHE, maeva.orliac@umontpellier.fr ; pierre-olivier.antoine@umontpellier.fr ; monique.vianey-liaud@umontpellier.fr
(7) UNESCO Global Geopark Causses du Quercy. tpelissie@parc-causses-du-quercy.org

Résumé

Les phosphorites du Quercy, grâce à leur exceptionnel contenu paléontologique, enregistrent, les changements paléoenvironnementaux de quelques 30 Ma autour de la « Grande coupure » de la transition Eocène-Oligocène. Les sédiments piégeant les fossiles ont été peu étudiés et interprétés en regard des contextes géologique et paléoclimatique. Nous proposons une première approche analytique intégrée des sédiments karstiques (sédimentologie, granulométrie, minéralogie, géochimie) des remplissages de la phosphatière de Dams. Ce site montre trois épisodes de dépôt, encadrant la transition Eocène-Oligocène qui se compose de deux fractions principales, l'une détritique, l'autre phosphatée et néoformée. L'apport détritique résulte du transport en masse d'un matériel « sidérolitique » éocène-oligocène présent transitoirement en surface et provenant du remaniement de paléosols latéritiques, formés en amont, directement ou indirectement à partir d'une roche mère cristalline. Le phosphate, précipité sur les parois du karst ou épigénisant les fossiles, livre une signature géochimique marine qui suggère la contribution de l'encaissant carbonaté marin, à la chimie du fluide source. Enfin, les changements climatiques de la Grande Coupure semblent ne se refléter qu'au travers de la dynamique hydrique souterraine enregistrée par les structures, chenaux et fentes de dessiccation, préservées dans les dépôts karstiques.

Abstract

The fillings of the Dams phosphatiere, Quercy (Caylus, Tarn-et-Garonne, France). The « phosphorites du Quercy », thanks to their exceptional paleontological content, record the paleoenvironmental changes over more than 30 Myr encompassing the 'Grande Coupure', at the Eocene-Oligocene transition. The sediments themselves have been little studied and interpreted regarding geological and climatic contexts. We propose here a first integrated analytical approach (sedimentology, granulometry, mineralogy, and geochemistry) of the « phosphorites du Quercy » based on the study of the sedimentary fillings of the DAMS « phosphatière ». This site shows three depositional stages bracketing the « Grande Coupure » event, mainly comprising two parts, one of detrital origin and one of reworked phosphate deposits. The detrital parts result from mass flow infillings of Eocene-Oligocene siderolithic material transitorily lying at the surface and reworked from lateritic paleosols, directly or indirectly developed on upslope crystalline basement rocks. The phosphate, precipitated on cave walls and into bones, yields a REE seawater signature illustrating the marine carbonate host contribution to the chemistry of the source fluid. Finally, climate changes during the «Grande Coupure» seems to be reflected only through hydric sedimentary structures, channels, and mud cracks, preserved in the cave deposits.

1. Introduction

Les phosphatières du Quercy sont des cavités karstiques comblées de dépôts argilo-phosphatés riches en fossiles. Chacune contient un remplissage qui lui est propre et dont la durée de mise en place est estimée à quelques centaines de milliers d'années. Les fossiles extraits des quelques 200 sites reconnus à ce jour, ont permis de reconstituer plus de 30 M.A d'évolution des paysages quercynois de part et d'autre de la transition Eocène-Oligocène (33,9 Ma). Les

sédiments eux-mêmes ont été peu étudiés et leur genèse n'a jamais été replacée dans leurs contextes géologique et climatique. L'étude préliminaire présentée ici concerne la phosphatière de Dams (Fig. 1), la seule identifiée, à ce jour, qui conserve trois épisodes de sédimentation bien distincts du point de vue temporel, de part et d'autre de la limite Eocène-Oligocène et permettant l'analyse, dans une même cavité, de sédiments d'âges différents mis en place sous des contextes climatiques particulièrement distincts.
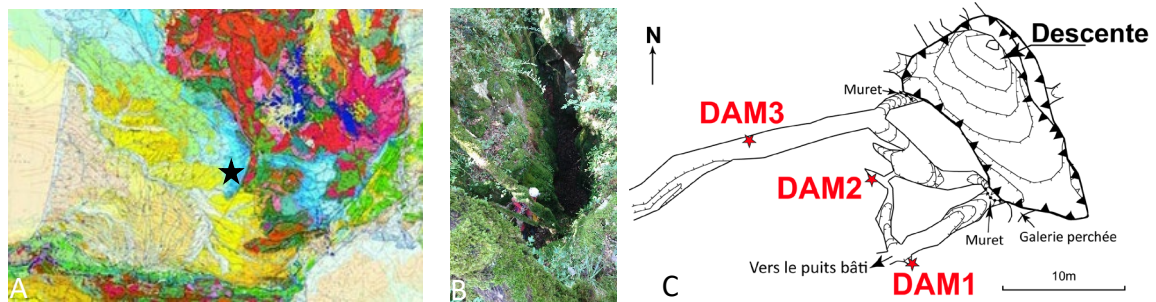
Figure 1 : La phosphatière de Dams. A. Localisation géographique dans le sud du Quercy, à proximité du Massif Central. B. Photo de l'entrée principale de la phosphatière. C. Topographie avec la position des coupes DAMS 1, 2 et 3.

2. Matériel et méthodes

Après le levé stratigraphique et sédimentologique des coupes, l'identification de la source des sédiments et des modalités de dépôt repose sur la minéralogie, la granulométrie et la chimie des échantillons, établies respectivement : par DRX sur la fraction inférieure à 2 µm suivant HOLTZAPFFEL (1985), à l'Université de Mons (Siemens Cristalloflex D5000) et au laboratoire Géosciences Environnement Toulouse (GET ; diffractomètre Bruker D8 Advance du GET), au granulomètre laser LA-950V2 d'Horiba du laboratoire Ecolab de Toulouse, et par spectroscopie de fluorescence X (S2 Ranger de Bruker) au GET.
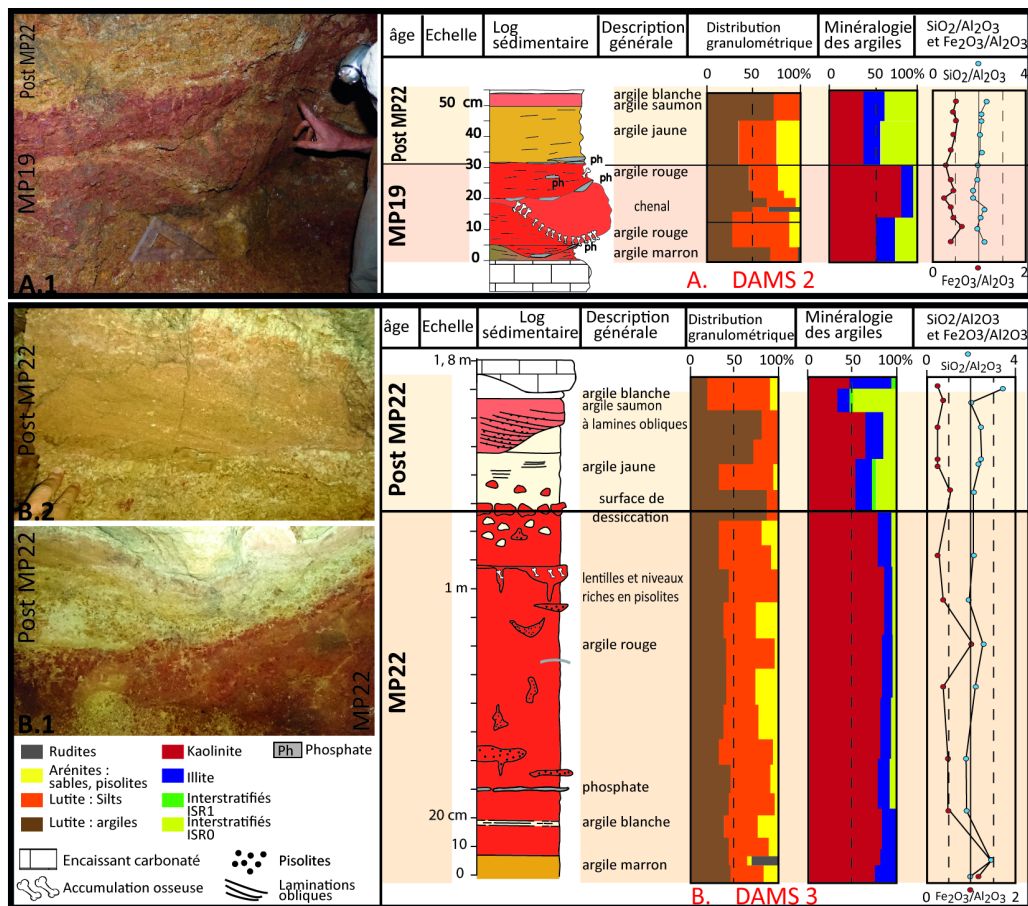

Figure 2 : Illustrations, attributions stratigraphiques, caractérisation sédimentologique, granulométrique, minéralogique et chimique du remplissage DAMS 2 (A) d'âge Eocène supérieur (MP 19) et Oligocène (Post MP22) et du remplissage DAMS 3 (B) d'âge Oligocène inférieur (MP22) et post-MP22. A.1 chenal visible dans le remplissage d'âge MP19 et différence de couleur entre les deux épisodes de remplissages. B.1 différence de couleur entre les deux épisodes de remplissage et illustration de la surface de dessiccation majeure qui les sépare. B.2 lamines obliques visibles dans le remplissage post-MP22.

Pour tracer l'origine du phosphate (e.g., DILL, 1994), les Terres rares (Rare Earth Elements, REE) des composants

phosphatés récoltés (Fig.3) ont été analysées. Les concentrations de REE ont été mesurées par ablation laser couplée à un spectromètre de masse (LA-ICPMS) au GET.

Les données ont été traitées à l'aide du logiciel SILLS (GUILLONG *et al.*, 2008) normalisées au PAAS (TAYLOR & MC LENNAN, 1985), et les spectres obtenus comparés à ceux des sédiments détritiques encaissants et à celui d'un échantillon de phosphate marin.

3. Résultats

3.1. Les dépôts détritiques

Les témoins sédimentaires sont préservés localement dans trois galeries qui les connectent (Fig. 1C). Datations biostratigraphiques et similitudes lithologiques conduisent à distinguer trois ensembles de couches. Le premier, datée de l'Eocène supérieur (MP 19 ; 34,4 Ma) a été reconnu dans les coupes DAMS 1 et DAMS 2 (Fig. 1C & 2A). Le second, datée de l'Oligocène inférieur (MP22 ; 30,2 Ma) est identifié dans la coupe DAMS 3 (Fig. 2B). Le troisième, plus récent, mais non daté précisément (post-MP22), clôture les coupes DAMS 2 et 3 (Fig. 2) (Orliac *et al.,* 2019). Les argiles sableuses éocènes et oligocènes, riches en quartz et oxydes de fer (pisolithes de goethite) (Fig. 2) montrent de nettes similitudes : faible variabilité des rapports SiO_2/Al_2O_3 et Fe_2O_3/Al_2O_3. Le cortège argileux est dominé par la kaolinite (~75%) et l'illite (~20%). Ces deux phases de remplissages diffèrent néanmoins. La phase éocène se marque par l'abondance de phosphate notamment sous forme de croûte laminée (DAMS 1) et une remarquable préservation des ossements fossiles dans les chenaux (DAMS 2 ; Fig.2A). La phase oligocène comprend des corps lenticulaires verticaux ou horizontaux remplis de pisolites et de fragments osseux mis en place localement dans des fentes de dessiccation. Les marques d'un épisode de dessiccation majeur sont visibles au sommet de l'unité (Fig. 2B.1). La phase post-MP22 se démarque par un contenu argilo-sableux plus pauvre en oxydes de fer et une couleur jaune à rose, une teneur en quartz plus élevée et une très faible concentration en phosphate, pisolites et os. Le cortège argileux s'enrichit en smectite au détriment de la kaolinite. Des lamines obliques (Fig. 2B.2) sont localement visibles.

La coexistence de 3 à 4 classes granulométriques sans tendance dans tous les niveaux sédimentaires caractérise un sédiment hétérométrique et sans granoclassement.
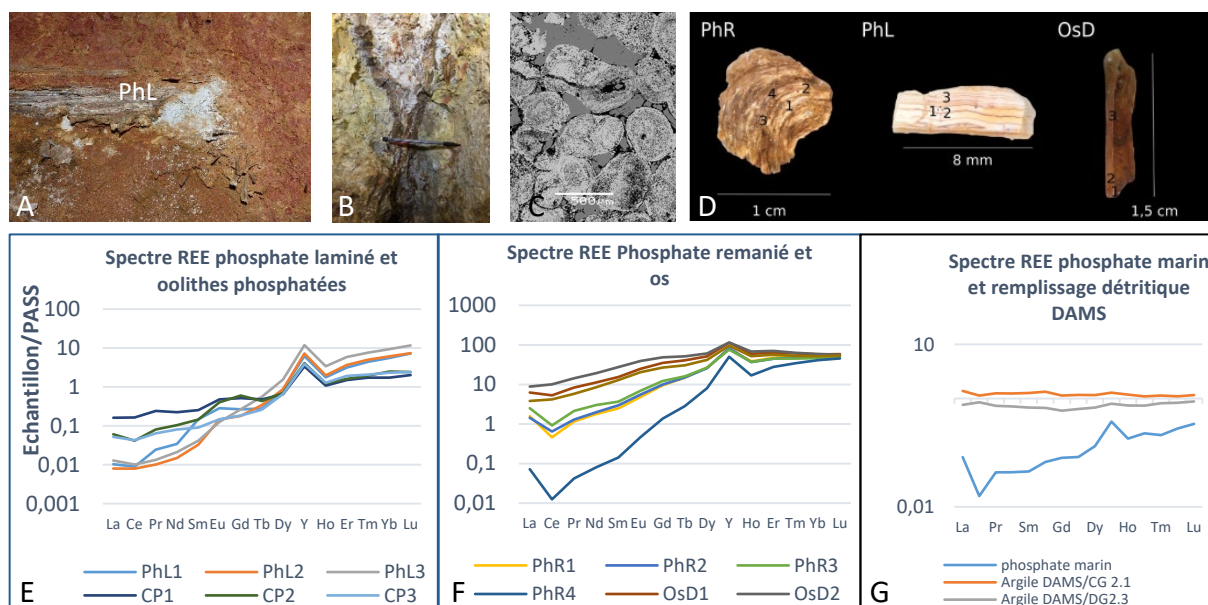

Figure 3 : Les différentes formes de phosphates et leurs spectres REE (terres rares). A. lit de phosphate laminé blanc laiteux (PhL) et ossements, ***B.*** *croûte phosphatée marron qui recouvre les parois du calcaire encaissant, C. oolites phosphatées épigénisées dans la roche encaissante (CP),* ***D.*** *Nodule de croûte phosphatée laminée remaniée qui compose ponctuellement le remplissage sédimentaire argileux (PhR) et ossements (OsD). E et F spectre de REE de tous les échantillons de phosphates. G. spectre de REE d'un échantillon de phosphate marin et de deux échantillons de sédiments détritiques de Dams.*

3.2 Les dépôts phosphatés

Différentes formes de phosphate coexistent à DAMS : lit de phosphate laminé (Figs. 3A, D: PhL), nodule de croûte phosphatée remaniée (Fig. 3D : PhR), encroutement tapissant les parois du calcaire encaissant (Fig. 3B), oolithes de la roche encaissante épigénisées (Fig. 3C: CP), et ossements (Fig. 3D: OsD). Malgré cette diversité de forme et d'origine (précipitation directe versus épigénie), tous ces habitus donnent des spectres de REE très proches, caractérisés par une anomalie négative plus ou moins marquée en Ce, une anomalie positive en Y et un enrichissement significatif en Terres Rares lourdes (Figs 3E & F). Ces motifs sont similaires à celui de l'échantillon de phosphate marin, tandis qu'ils contrastent nettement de ceux de la fraction détritique encaissante qui ne révèlent aucun fractionnement (i.e. spectres « plats » ; Fig. 3G).

4. Interprétation et Discussion

L'analyse sédimentologique, minéralogique et chimique des dépôts détritiques de Dams confirme que la formation sidérolithique Eocène-Oligocène riche en argiles rouges, quartz et pisolithes (GOURDON-PLATEL *et al.*, 2000), et affleurant localement sur le plateau calcaire quercynois, est la source du matériel détritique accumulé dans le karst. Il s'agit de fersialsols remaniés formés sous climat tropical. Ces altérites sont issues de l'intense altération indirecte (sédiment détritique) ou directe (sur le socle) des roches cristallines du Massif Central. Les altérites accumulées dans la phosphatière de Dams ont été transportées en masse par des fluides très visqueux comme en témoigne l'absence de classement et de tri granulométrique. La présence de chenaux et de laminations obliques dans les remplissages indique que le transport tractif joue également un rôle à l'Eocène sup. et post-MP22 suggérant un ennoyage des cavités au cours de ces deux périodes. Dans les sédiments oligocènes, les structures de dessiccation indiquent une importante phase d'aridité. Ainsi, malgré de nettes similitudes lithologiques entre les différents dépôts sédimentaires qui suggèrent une source commune, les divergences observées, en termes de concentration en phosphate, de structure et d'assemblages argileux (kaolinite versus smectite) témoignent d'un contrôle climatique et notamment l'instauration d'un climat plus aride à l'Oligocène inférieur.

Les principales phases minérales phosphatées des karsts sont la fluoroapatite et l'hydroxyapatite dont dérivent des paragénèses alumineuses secondaires à crandallite et perhamite (BILLAUD, 1982). Les spectres de Terres Rares des différents éléments phosphatés de Dams sont typiques de l'eau de mer (e.g., BOHLAR et al., 2004) et suggèrent une origine marine du fluide source. Une telle signature géochimique, en contradiction avec le contexte environnemental continental de la période de phosphatisation, impliquerait la contribution de l'encaissant carbonaté, d'origine marine, sur la chimie du fluide source. Cette hypothèse est confortée par le contexte géologique de formation et de mise à la surface des cavités karstiques à l'origine des phosphatières. ASTRUC et al. (1998) évaluent à 500m l'épaisseur de formations jurassico-crétacées à dominante carbonatée soustraite par altération chimique. Si l'origine marine du phosphore demande encore à être mieux documentée, il apparaît que la dissolution, même partielle, de ces carbonates constitue une source suffisante de calcium et de REE pour former l'apatite. En outre, la préservation exceptionnelle d'ossements, de graines, d'insectes, ainsi que la présence d'organismes momifiés plaident également en faveur de processus de phosphatisation rapides et probablement continus.

5. Conclusion

L'approche multidisciplinaire présentée dans cette étude éclaire d'un jour nouveau le remplissage sédimentaire de la phosphatière de Dams. D'une part, il semble que le contenu sédimentaire à savoir des fersialsols ou « sidérolithique » remaniés aient enregistré les variations hydrologiques ayant eu lieu à proximité de la transition Eocène-Oligocène. D'autre part, la phosphatisation qui a affecté le karst, trouverait son origine dans la dissolution de l'encaissant calcaire mésozoïque, comme en attestent les spectres de Terre Rares typiquement marins.

Remerciements

Références

ASTRUC J.G., CUBAYYNES R., JAUBERT J., PAJOT B., PELISSIE T., MARANDAT B., REY J., SIGE J., SIMON-COINCON R., SOULIER M. (1998) Notice explicative, Carte géol. France (1/50 000), feuille de Caussade (905). BRGM

BILLAUD Y. (1982) Les paragénèses phosphatées du paléokarst des phosphorites du Quercy. Thèse Géologie des ensembles sédimentaires, Univ. Lyon 1, 136 p.

BOLHAR R., KAMBER B.S., MOORBATH S., FEDO C.M., WHITEHOUSE M.J. (2004) Characterisation of early Archaean chemical sediments by trace element signatures: Earth and Planet. Sc. Letters, 222, pp. 43–60.

DILL H.G. (1994) Can REE patterns and U-Th variations be used as a tool to determine the origin of apatite in clastic rocks? Sedimentary Geology 92, 175–196.

GOURDON-PLATEL N., PLATEL J., ASTRUC J. G. (2000) La formation de Rouffignac, témoin d'une paléoaltérite cuirassée intra-éocène en Périgord-Quercy. Géologie de la France, 1, 65-76.

GUILLONG M., MEIER D., ALLAN M., HEINRICH C., YARDLEY B. (2008) SILLS: a MATLAB-based program for the reduction of laser ablation ICP-MS data of homogeneous materials and inclusions. Mineral Assoc Can Short Course 328–333

HOLTZAPFFEL T. (1985) Minéraux argileux : Préparation, analyse diffractométrique et détermination. Société Géologique Nord., n°12, 136 p.

ORLIAC M., ANTOINE P.-O., BLONDEL C., COUETTE S., DUPUIS Ch., et al. (2019) La phosphatière de Dams (Quercy), un nouveau site fossilifère majeur encadrant la Grande Coupure de Stehlin (transition Eocène-Oligocène). Congrès de l'APF, Aix-en-Provence, France.

TAYLOR S.R., MC LENNAN S.M., 1985. The Continental Crust: Its composition and Evolution. Blackwell, Oxford

Mineralogical curiosities:
The "lapis specularis" coins
of the Re Tiberio gypsum cave (Italy)

Marina LO CONTE[1], Massimo ERCOLANI[2] & Paolo FORTI[3]

(1) Speleo GAM Mezzano, Italy
(2) Speleo GAM Mezzano & Federazione Speleologica dell'Emilia-Romagna, Italy
(3) GSB-USB & Istituto Italiano di Speleologia, Dipartimento BIGEA, Università di Bologna, Italy: paolo.forti@unibo.it

Abstract

In 2020 a new peculiar gypsum monocrystal structure was observed in the main gallery of the Re Tiberio gypsum cave (Emilia Romagna Region, Italy), close to its entrance. The new forms consist of a small, extremely flat cylinders (less than 1 cm in diameter and 1 mm in height), which make them remarkably similar to true coins. They were piled one over the other in a small cup just below a narrow fracture filled by clay. The morphological study of the crystals together with that of the fracture, inside which they developed, allowed the definition of their genetic mechanism, which was controlled by two main factors: steric hindrance and epitaxial growth.

Résumé

Des curiosités minéralogiques : les médailles *lapis specularis* de la grotte de gypse de Re Tiberio (Italie). En 2020, une nouvelle structure monocristalline très particulière de gypse a été observée dans la galerie principale de la grotte de gypse de Re Tiberio en Émilie-Romagne, près de l'entrée. Ces formes nouvelles consistent en de petits cylindres très plats (moins d'1 cm de diamètre et 1 mm de haut), ce qui les fait ressembler à de véritables pièces de monnaie. Ils étaient empilés les uns sur les autres dans une petite cupule juste en-dessous d'une fracture étroite remplie d'argile. L'étude morphologique de ces cristaux et de la fracture dans laquelle ils se sont développés permet de préciser le mécanisme de leur formation contrôlée par deux principaux facteurs : la croissance cristalline et l'empêchement stérique.

1. Introduction

Peculiar euhedral gypsum crystals were recently observed within the Re Tiberio cave (Emilia-Romagna Region, Italy). They are extremely flat cylinders making them very similar to gypsum coins. These gypsum crystals are perfectly transparent (like those called "*lapis specularis*" by the Romans) with a diameter ranging between 2 e 3 cm and a thickness from less than 1 up to 2,5 mm (Fig. 1).

The detailed analysis of the area helped define the boundary conditions required for the development of these peculiar crystals, which had hitherto not been observed in any other cave of the world.

Figure 1: Re Tiberio cave: the 3 "lapis specularis coins" just taken at the foot of the subhorizontal fracture where they developed; B: close up view of the coins (A: Φ 16,5-18 mm, B: Φ 16x17 mm, C: Φ 14x14 mm): all of them show just below one half of their upper flat surface the presence of a thin layer of small undefined grains, while in the other half the impurities are far less and extremely close to the external surface. (Photo M. Ercolani).
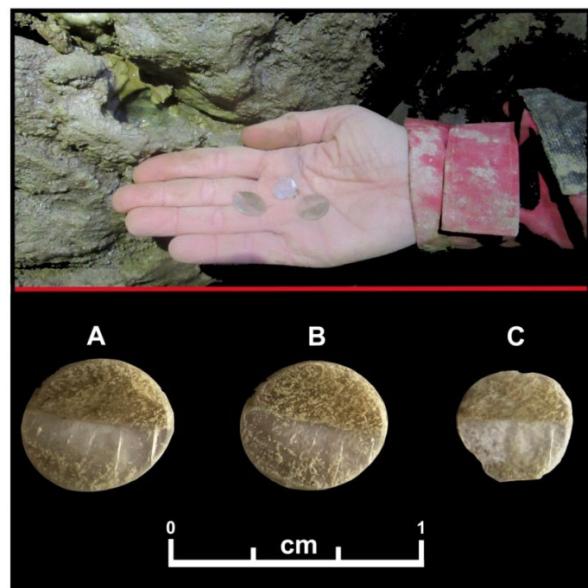
2. The mechanism for the genesis and evolution of the "coins"

The "*lapis specularis*" coins grew within a small open subhorizontal crack located close to a dripping of meteoric seeping water, which is sometime slightly undersaturated with respect to gypsum and consequently able to deposit a thin crust of calcite. Droplets originated by the splash of the dripping water maintain constantly wet the mud filling the crack. During the period of scarce or even absent rainfalls, the slow evaporation of the water trapped within the crack induces a slight supersaturation with respect $CaSO_4 \cdot 2H_2O$, leading to the formation of secondary gypsum.

But the very low energy of crystallization only allows the enlargement of an already existing crystal via bidimensional accretion, rather than new nucleation, a tridimensional mechanism.

In the meantime, the presence of the clay and silt infilling, hindering the development of euhedral crystals, enhance that of lens shaped ones, which are proved to be the most common forms in such contest (FORTI & LUCCI 2016, FORTI 2017).

But why, only in this small fracture, do peculiar crystals (flattened cylinders similar to true coins) develop instead of the "normal" lens-shaped ones?

The single possibility is that the vertical development of the lens-shaped crystal cannot proceed anymore, and that, consequently, the further deposition of gypsum only occurs around its circumference.

As already evidenced for the cubic cave pearls (HILL & FORTI 1997, FORTI & PENSABENE 1989a,b), the single growing mechanism which may cause the development of the gypsum coins is the steric hindrance, which becomes active when the vertical dimension of lens shaped crystal becomes equal to that of the subhorizontal crack (Fig. 2A). Then the crystal is progressively obliged to modify its shape until it becomes a perfect cylinder (Fig. 2B), which, from then on, can only increase its diameter (Fig. 2C).

Even in contact each other and with the crack walls, the different "coins" do not merge due to several concurring factors: among them the presence of clay in between their contact planes and the transient undersaturation occurring during the relative fast water flow during the rainfalls.

Clay particles mechanically avoid crystalline subcritical gypsum particles to stick on the external surface of the coins, thus acting as a "barrier" in between the two gypsum surfaces. Moreover, these particles being free from each other can move back and forth during the wetting and drying cycles, thus they exert some abrasion on the external surfaces of gypsum cylinders.

Anyway, beside these two hindering factors, another makes the merging of two different coins practically impossible: the energy of crystallization, which is, as mentioned above, always extremely low, thus only allowing epitaxial growth. This process is bidimensional; therefore, the crystal lattice grows maintaining the original structure and orientation. Thus twinning &/or growth penetration-crystals cannot develop because they need a higher crystallization energy.

Obviously, the crystal lattice of any gypsum monocrystals is always the same, but its spatial orientation may be different. Statistically this is much more probable than a perfect overlapping of the separate structures thus explaining why two eventually superimposed coins cannot merge to form a single bigger cylinder.

In fact, the different crystal lattice spatial orientation of the piled coins prevents epitaxial accretion to act simultaneously over the two planes in contact and transforming the two coins into one.

But why did the coins pile themselves in the depression just below the crack where they originally developed?

The progressive widening of the crack towards the open space suggests that steric hindrance is still the driving factor. In fact, due to the progressive increase of their diameter, the coins will meet the walls earlier, the closer they are to the inner part of the crack.

This will force a slow, progressive, displacement of the coins towards the exterior, movement which is in turn enhanced by the lubricant presence of the plastic clay.

This process will continue until the coins, extruded over a half from the crack, will fall and accumulates one over the other in the underlying depression (Fig. 3).
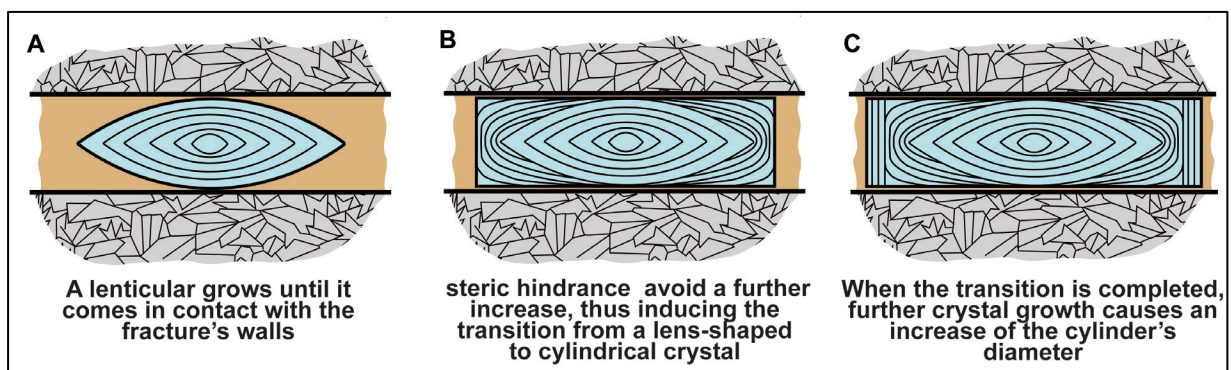

Figure 2: Steric hindrance effect on the lenticular shape of the gypsum crystal (A), which progressively transforms into a cylinder of the same diameter (B), then enlarging it (C).
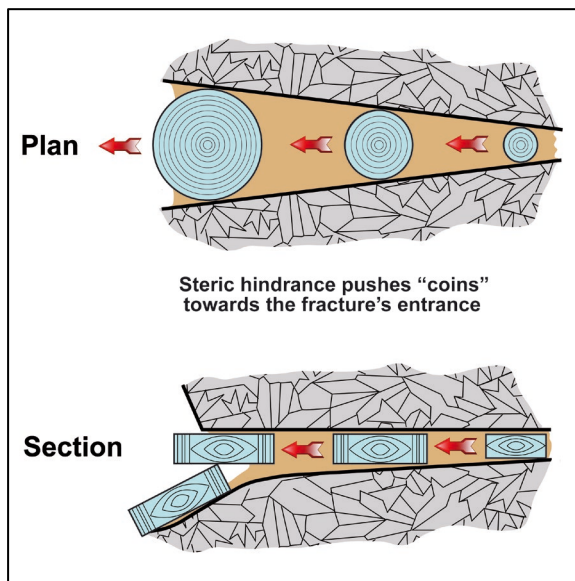
Figure 3: Sketch of coins' migration within the fracture which is controlled by the steric hindrance.

Finally, an explanation is required for the subdivision of the upper surface of all the three coins into two parts (v. Fig. 1, bottom), the first of which shows a high number of very small pale brown to grey inclusions, which were sealed in the gypsum lattice just rather at the end of the accretion process.

The other side of the coins exhibits very few inclusions only, which always restricted to the very outer crown.

The extreme closeness of the pale brown grains to the outer surface of the coins suggests that the inclusion occurred when the development of the monocrystals was nearly completed.

This hypothesis is supported by the with the fact the sealing of the mud and clay grains could not start before the coins were partially pushed out of the fracture. In fact, it is well known and documented that the all the euhedral gypsum crystals, even if developed within clay interbeds, are quite free from solid inclusions and this because the epitaxial growth avoid their incorporation within the crystal lattice. But a further evidence exists that strengthens the hypothesis that incorporation started only after the coins' partial "emersion" from the crack. The boundary between the transparent and the opaque areas is always rectilinear, suggesting that it was coincident with the outer edge of the crack.

Starting from this evidence it is reasonable to think that the last step in the evolution of the coins was controlled by the recurring presence of splash droplets induced by the dripping which feeds the small cup, just below the crack, just after the strong rainfalls.

In fact, the dripping impact, beside supplying the droplets which can land over the upper side of the coins when partially exposed in the open space (Fig. 3 A), have enough energy to mobilize not only silt and clay grains but also small fragments of calcite and/or gypsum.

When these droplets land over the exposed surface of the coin, they leave the carried impurities (Fig. 3 B). Moreover, these droplets were probably still undersaturated as a consequence of the fast seepage after strong rainfalls, such that they could dissolve, even slightly, the surface of the crystals on which they landed.
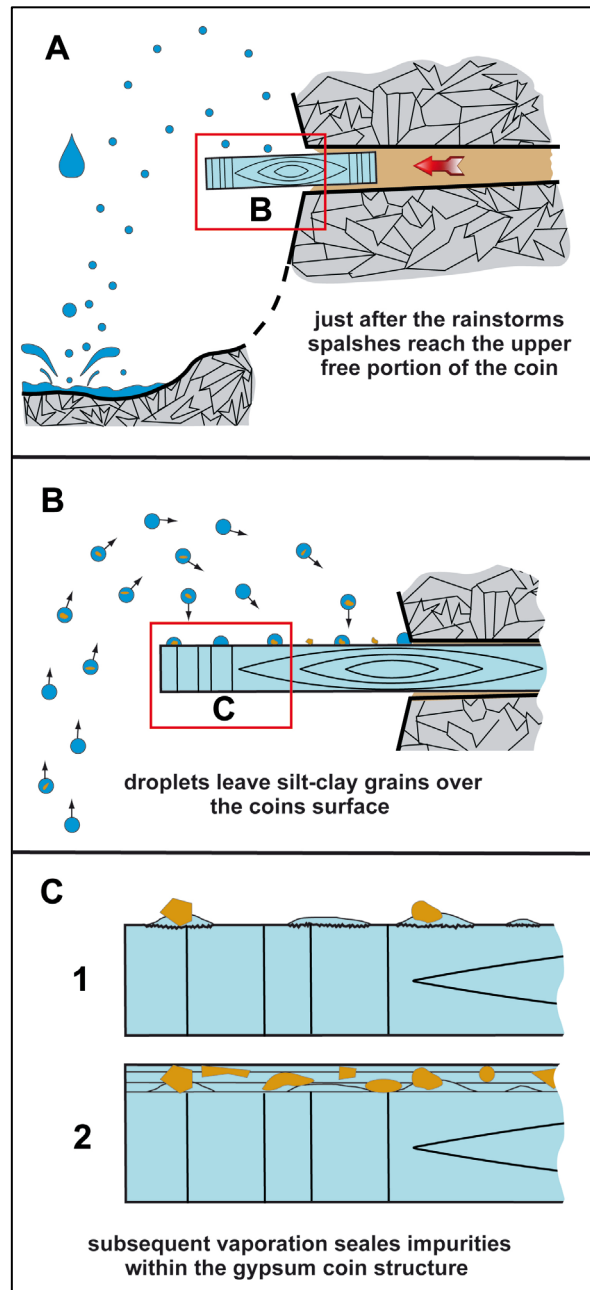

Figure 4: Droplets generated by dripping impact on the cave floor reach the coins' exposed upper surface where small impurity grains are deposited (A). Then evaporation induces gypsum deposition which seals impurities within the coin (B). Several subsequent deposition-evaporation cycles totally bury the grains within the crystal structure (C).

The evaporation starts just after the cessation of dripping, but its rate is very low, as it was during all the process of development of the coins inside the crack. Thus, supersaturation will cause only the gypsum deposition via epitaxial growth, which in turn allows the impurity grains to be sealed linked to the coins' surface (3C1)

The alternation of several rainy periods, with consequent development of splash droplets, to dry periods, with gypsum deposition by evaporation, causes the progressive inclusion of the impurity grains within the crystal lattice (C2).

Thanks to this mechanism the whole external surface of the coins, still consisting of a single crystal, remains completely flat and homogeneous, but the color of the portion over the impurities is quite different, because the transparency of gypsum makes them visible.

Finally, it should be noted that impurity grains are far less numerous in the other parts of the coins, thus suggesting that their fall from the crack occurred recently.

3. Conclusions

The detailed analysis of the area in which the "*lapis specularis*" coins developed allowed the definition the two controlling factors ruling their genesis and evolution: energy of crystallization and steric hindrance.

Finally, before they were completely extruded from the fracture, the splash droplets brought impurity grains over the free portion of their upper surface, where they were later sealed within the crystal lattice. After the complete extrusion and accumulation in the depression below the crack, the accumulation of foreign grains may have started to affect the whole coin upper surface, but it is evident that this process started only a brief time before the coins were observed and studied.

In conclusion the processes which led to the development of these very peculiar gypsum coins was rather complex and this explains why these gypsum crystals were never seen before.

References

FORTI P. (2017) Chemical deposits in evaporite caves: an overview. International Journal of Speleology **46(2)**, 109-135.

FORTI P., LUCCI P. (2016) Come si sviluppano i cristalli prismatici di gesso sulle stalattiti? Memorie dell'Istituto Italiano di Speleologia s.2, **31**, 157-162.

FORTI P., PENSABENE G. (1989) The cubic cave pearls of the Corchia karst system (Apuane Alps, Italy). Proceedings 10th International Speleological Congress, Budapest, **1**, 69-70.

HILL C.A., FORTI P. (1997) Cave minerals of the World National Speleological Society, Huntsville, 464 p

Candlestick stalagmites, a tool to better understand the influence of past earthquakes on natural caves

Aurélie MARTIN[1,2], Thomas LECOCQ[1], Klaus-G. HINZEN[3],
Thierry CAMELBEECK[1], Yves QUINIF[4] & Nathalie FAGEL[2]

(1) Royal Observatory of Belgium, 3 Avenue Circulaire, 1180 Brussels, Belgium, aurelie.martin@oma.be (corresponding author) , thomas.lecocq@oma.be , thierry.camelbeeck@oma.be
(2) AGEs - Département de Géologie - Université de Liège, 14 Allée du Six Août, 4000 Liège, Belgium, nathalie.fagel@uliege.be
(3) Institute of Geology and Mineralogy - University of Cologne, 50674 Cologne, Germany, hinzen@uni-koeln.de
(4) Geology and Applied Geology - Faculty of Engineering - University of Mons, 9 Rue de Houdain, 7000 Mons, Belgium, yves.quinif2@gmail.com

Abstract

Candlestick stalagmites exhibit resonance in the frequency-band of regional earthquake ground motions. An earthquake can break such elongated structures if the ground movement is strong enough. Therefore, the existence of intact stalagmites in caves would indicates that a certain level of ground movement has not been exceeded since they exist. Field surveys were carried out in the Han-sur-Lesse Cave (Belgian Ardennes) to estimate the eigenfrequencies of stalagmites of different sizes and shapes (e.g., Minaret Stalagmite, "Verviétois" gallery) and to explore their reactions to external events such as quarry blasts or earthquakes. The eigenfrequencies of the stalagmites are obtained from direct measurements of ambient seismic noise caused by human activities, microseisms, etc. Seismic sensors were placed on the stalagmites and on the nearby cave floor as well as at various other locations inside and outside the cave. Noise and transient events (e.g., quarry blasts) were recorded during weeks of continuous measurements. 3D laser scans of the stalagmites and Finite Element Modelling allowed constraining the link between their complex shape and their eigenfrequencies.

Résumé

Stalagmites cierges, un moyen de mieux comprendre l'influence des séismes passés dans les grottes naturelles. Certaines stalagmites cierges peuvent entrer en résonances dans la bande de fréquences des mouvements du sol des séismes régionaux. Si celui-ci est suffisamment puissant, les stalagmites peuvent se briser. Dès lors, l'existence de stalagmites intactes dans les grottes indique qu'un certain niveau de mouvement du sol n'a pas été dépassé depuis qu'elles existent. Des études ont été menées dans la grotte de Han-sur-Lesse (Ardennes belges) pour estimer les fréquences propres de stalagmites de différentes tailles et formes (ex : Stalagmite du Minaret, Galerie Verviétois) et pour étudier leurs réactions aux événements transitoire tels que les tirs de carrière ou les tremblements de terre. Les fréquences propres des stalagmites sont obtenues à partir de l'enregistrement du bruit sismique causés par les activités humaines, les microséismes, etc. Grâce aux capteurs sismiques placés sur les stalagmites, sur le sol de la grotte et à l'extérieur de celle-ci, le bruit sismique et les événements transitoires ont été enregistrés sans interruption pendant plusieurs semaines. Les scans laser 3D des stalagmites et la modélisation par éléments finis ont permis de contraindre le lien entre leur forme complexe et leurs fréquences propres.

1. Introduction

Since the 1990s, broken or deformed speleothems have been used as indicators of paleoearthquakes (BECKER *et al.* 2006, for a review) and the usefulness of broken speleothems has been proven to date ceiling collapses and therefore date certain paleoearthquakes (CAMELBEECK *et al.* 2018). However, numerical models and physical experiments pointed out the limits of the link between these deformations and earthquakes (CADORIN *et al.* 2001; LACAVE *et al.* 2004) but did not consider all possible imperfections and weaknesses in the body of the speleothems. Finally, in many cases, it is difficult to prove that the speleothem deformations are linked to seismic events because other phenomena such as frost, ground instability, floods ... can produce similar effects (e.g., BECKER

et al. 2006). To avoid these uncertainties, the study of intact speleothems was favored. The absence of breaks places an upper limit on the ground motion (e.g., GRIBOVSZKI *et al.* 2017) that a specific site may have encountered. These ground motion levels are directly comparable to results of seismic hazard evaluation and of earthquakes ground motion modelling (as for precariously balanced rocks or archaeological objects (BRUNE 1996; SCHWEPPE *et al.* 2017)). Structures can resonate and break at a lower acceleration than predicted, if the ground motions are in the same frequency band as the eigenfrequency of the structure (<20 Hz). The natural frequency and damping factor of the speleothems are fundamental parameters in the study of the response of stalagmites to seismic motion.

Eigenfrequency studies have been conducted with laser or seismic sensors either following a slightly excitation of the stalagmite using a finger or a rubber hammer (LACAVE *et al.* 2000, 2004; GRIBOVSZKI *et al.* 2017, 2018; BOTTELIN *et al.* 2020), or from the ambient seismic noise (i.e., the permanent vibration of the ground surface with different origins depending on the frequency band such as human activities, microseisms, local weather conditions) over a period of 22 days (MARTIN *et al.* 2020). These studies have shown the link between eigenfrequency and the shape of stalagmites (by modeling, 3D scanning, etc.) or the impact of the connection of the stalagmite to the base rock.

This article presents the results obtained during the acquisition campaigns carried out in the Han-sur-Lesse cave (Belgium). The elements that may have an impact on the motion perceived in the cave compared to the surface are presented, namely: eigenfrequencies studies, motion decrease or increase in cave and stalagmites and, the records of external events (earthquakes, quarry blasts).

2. Material and methods

These investigations were made in the karstic system of Han-sur-Lesse, situated in the SSE of Belgium. It is an underground cut-off meander of the Lesse River in the Givetian limestone (Figure 1). From a seismicity point of view, the Han-sur-Lesse cave is situated at a distance of 50–60 km from the Lower Rhine Embayment, which is the most seismically active area in northwestern Europe. However, the closest seismic activity instead comes from the eastern part of the Ardennes at a distance of 30 km (e.g., Verviers: Mw ~6.0, 18 September 1692). In the cave, important roof collapses or slope movement near the river have been linked to regional earthquakes (CAMELBEECK *et al.* 2018).

The study of candlestick stalagmites is currently performed in the "Verviétois" gallery (highlighted in orange on Figure 1) and the first results exploited mainly focus on the "Minaret" stalagmite (red star on Figure 1). The depth of this gallery varies from 60 to 80 m from the ground surface, with the Minaret in the deepest part. The study of the seismic response of the cave is carried out in the tourist part of the cave (yellow dots on Figure 1 indicating the location of seismic sensors), which has among others deeper dry parts (90-100m from the surface), Lesse river crossing areas, rooms of various size and of shapes, different substrates...
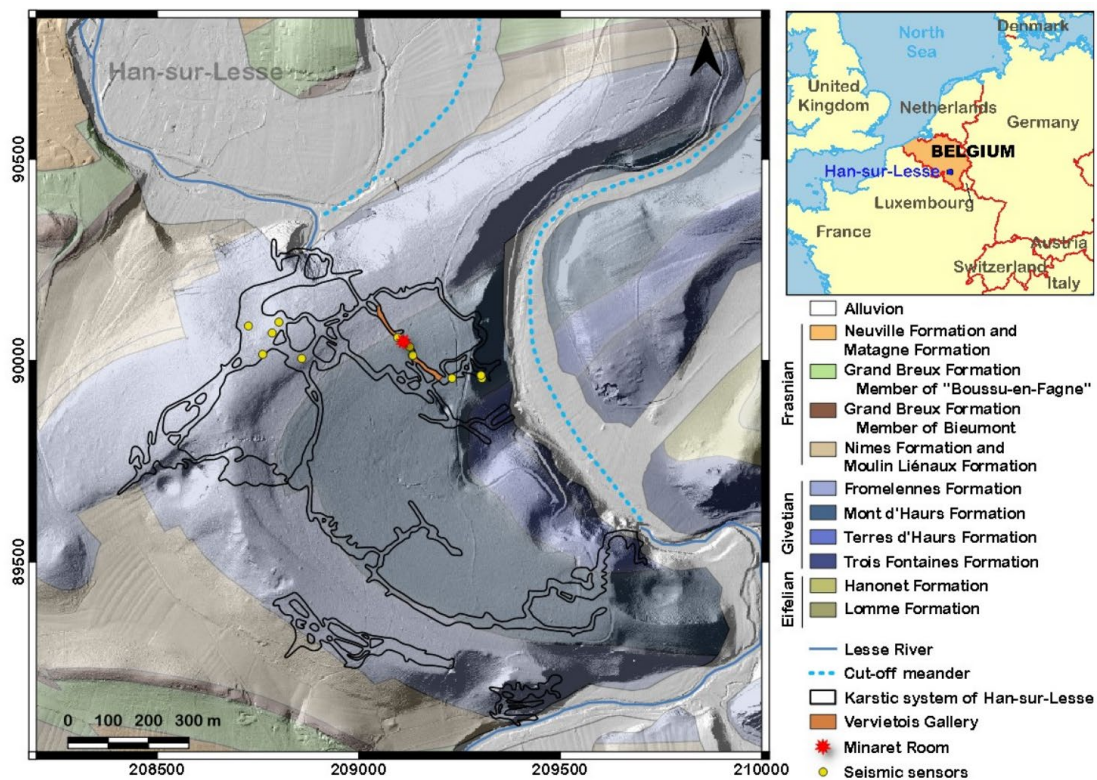

Figure 4: Geological map of the Karstic system of Han-sur-Lesse (Belgian Lambert 1972, in m). The Han-sur-Lesse cave is formed within the Givetian limestone formations (in blue). The cut-off meander (light blue dotted line) can be observed in the alluvial formation (white). The surrounding Eifelian and Frasnian formations are made by shales. The location of the Minaret room is shown by a red star. The "Verviétois" gallery is in orange and the seismic sensors in yellow. This map is based on the new geological map of Wallonia, the Digital Elevation Model (LIDAR) of Wallonia from the Service Public de Wallonie and MARTIN et al. (2020)

Three-components seismic sensors (Smartsolo, Dynamic Technologies – DTCC) were placed on candlestick stalagmites to study their eigenfrequencies and their reaction to external stresses. (see figure 2, bottom left corner). At the same time, sensors were installed at the bottom of the stalagmite, in the centre of the room (if possible) and at the surface (outside the cave). In addition, twenty vertical one-component seismic sensors were placed at the surface and in the cave for 1 month (see figure 2) in rooms of different sizes, shapes, depths, and substrates in order to study the seismic response of the cave.

In parallel with the seismic data, a FARO Focus 3D infrared phase scanner was used to perform a 3D scan of the room of the Minaret and the stalagmites present in this area to capture the shape of the stalagmites and to deduce the possible impact of this on the frequency or the reaction to earthquakes.

Figure 2: Example of seismic sensors in Han-sur-Lesse cave

3. Results

The ambient seismic noise makes it possible to identify the natural frequencies of the candlestick stalagmites present in the cave (Figure 3 (1)). For example, the natural frequencies of the Minaret have been found at 12.2 Hz and 15.2 Hz for the first mode shape. These two frequencies have perpendicular polarization directions (N52E and N142E). The same results were obtained by modelling based on a subsampled point cloud of the 3D laser scan.

Changes in amplitude due to anthropogenic noise were also observed in ambient seismic noise, even in the upper part of the cave (e.g., Minaret room, "Verviétois" Gallery). They are higher during daytime than at night and on weekdays compared to the weekend. They are also more important at the surface than in the cave except for the Minaret. The stalagmite motions are larger compared to the motions measured at its base (21 or 13 times for X and Y components) and at the surface outside the cave (14 or 4 times, respectively).

The use of continuous recording of seismic data also allowed the recording of seismic events such as teleseisms with important magnitude (e.g., MW >6: Turkey, China, Russia, Bering Sea, Caribbean Sea earthquakes). Their frequency bands are usually lower than 2Hz. Quarry blasts have been recorded from the nearby Rochefort quarry in particular (8 km distant); here, the frequency bands are then higher (~2Hz-60Hz). Those frequencies correspond to the eigenfrequencies of the Minaret. The motion recorded on the Minaret clearly shows this event (Figure 3 (2)).
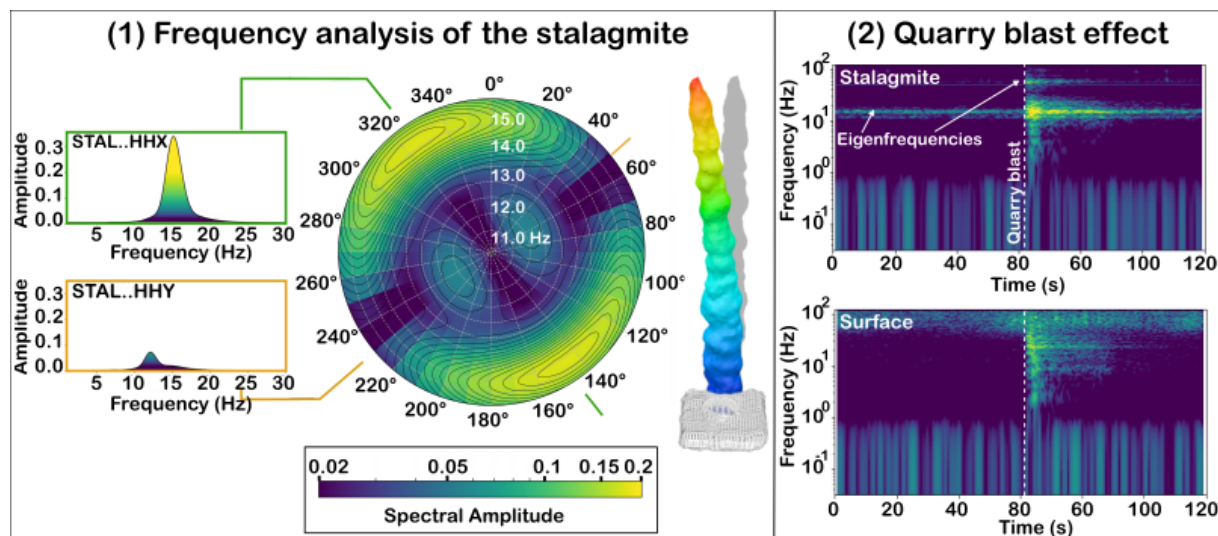

Figure 3: Results obtain with seismic data: (1) Polar spectral plot of the data measured with the sensor on the Minaret stalagmite (STAL). On the left, the spectra of the horizontal directions HHX (N142°E) and HHY (N52°E). On the right, the first type of mode shape of the Minaret stalagmite; the maximal total modal displacement is in red.
(2) Spectrogram of quarry blast event of Rochefort quarry on stalagmite and surface for the horizontal.

4. Discussion and conclusion

The use of ambient seismic noise in natural underground environments showed promising results, mainly to better understand the influence of past earthquakes on stalagmites.

First, the lower eigenfrequencies of the stalagmites could be extracted from the data, thus providing a fundamental parameter in the study of the response of the stalagmites to seismic motion. The use of long-time windows increases the resolution. The model output based on 3D laser scan data shows a good consistency with measured frequencies. The results also highlight the influence of the stalagmite shape and heterogeneities on eigenfrequencies (e.g., by explaining the split frequencies by ellipsoidal cross-section). The small differences between measurements and modelling might be caused by uncertainty on mechanical properties of the stalagmite, heterogeneity in their distribution and the influence of the sensor weight during the measurements which has only a slight influence in the case of the Minaret. These observations can help the study of very fragile candlestick stalagmites, which requires a careful use of adequate seismic sensors, whose installation would be risky.

Second, even if an amplitude decrease of the ground motion amplitudes is observed between the surface and the cave, as it is generally described, the motions recorded on the stalagmite are strongly amplified with respect to the surface motions (4-14 times) or on the ground in the cave. This observation brings strong implications for any seismic hazard validation based on speleothems.

Third, the use of continuous measurements over a long time period gives the opportunity to capture external events over a large frequency band. For example, records show that the Rochefort quarry blasts excite the Minaret's eigenfrequency. This information is encouraging for studies conducted on more slender stalagmites, with lower eigenfrequencies which might be more easily excited by an earthquake.

Acknowledgments

References

BECKER A., DAVENPORT C.A., EICHENBERGER U., GILLI E., JEANNIN P.-Y., LACAVE C. (2006) Speleoseismology: A critical perspective. Journal of Seismology, 10, 371‑388.

BOTTELIN P., BAILLET L., MATHY A., GARNIER L., CADET H., BRENGUIER O. (2020) - Seismic study of soda straws exposed to nearby blasting vibrations. Journal of Seismology, 24, 573-593.

BRUNE J.N. (1996) Precariously balanced rocks and ground-motion maps for Southern California. Bulletin of the Seismological Society of America, 86 (1A), 43‑54.

CADORIN J.F., JONGMANS D., PLUMIER A., CAMELBEECK T., DELABY S., QUINIF Y. (2001) Modelling of speleothems failure in the Hotton cave (Belgium). Is the failure earthquake induced?. Geologie en Mijnbouw, 80 (3‑4), 315‑321.

CAMELBEECK T., QUINIF Y., VERHEYDEN S., VANNESTE K., KNUTS E. (2018) Earthquakes as collapse precursors at the Han-sur-Lesse Cave in the Belgian Ardennes. Geomorphology, 308.

GRIBOVSZKI K., KOVÁCS K., MÓNUS P., BOKELMANN G., KONECNY P., LEDNICKÁ M., MOSELEY G., SPÖTL C., EDWARDS R.L., BEDNÁRIK M., BRIMICH L., TOTH L. (2017) Estimating the upper limit of prehistoric peak ground acceleration using an in situ, intact and vulnerable stalagmite from Plavecká priepast cave (Detrekői-zsomboly), Little Carpathians, Slovakia—first results. Journal of Seismology, 21, 1111‑1130.

GRIBOVSZKI K., ESTERHAZY S., BOKELMANN G. (2018) Numerical Modeling of Stalagmite Vibrations. Pure and Applied Geophysics, 175.

LACAVE C., LEVRET A., KOLLER M. (2000) Measurement of natural frequencies and damping of speleothems. Auckland, New-Zealand, 12th World Conference on Earthquake Engineering.

LACAVE C., KOLLER M.G., EGOZCUE J.J. (2004) What can be concluded about seismic history from broken and unbroken speleothems?. Journal of Earthquake Engineering, 8 (3), 431‑455.

MARTIN A., LECOCQ T., HINZEN K.-G., CAMELBEECK T., QUINIF Y., FAGEL N. (2020) Characterizing Stalagmites' Eigenfrequencies by Combining In Situ Vibration Measurements and Finite Element Modeling Based on 3D Scans. Geosciences, 10 (10), 418.

SCHWEPPE G., HINZEN K.-G., REAMER S.K., FISCHER M., MARCO S. (2017) The Ruin of the Roman Temple of Kedesh, Israel; Example of a Precariously Balanced Archaeological Structure Used as a Seismoscope. Annals of Geophysics, 60 (4), 0444.

Potential cosmogenic ^{10}Be/^{36}Cl dating of fossil guano deposits

Donald A McFARLANE[1] & Joyce LUNDBERG[2]

(1) Keck Science Center, The Claremont Colleges, Claremont CA 91711, USA, *dmcfarlane@kecksci.claremont.edu* (corresponding author)
(2) Dept of Geography and Environmental Studies, Carleton University, Ottawa, Canada. JoyceLundberg@cunet.carleton.ca

Abstract

Recently, there has been renewed interest in sub-fossil bat guano deposits as paleo-archives and repositories. Effective protocols for radiocarbon dating guano samples < 50 ka in age have been developed. However, many subfossil guano deposits of archeological and paleoecological interest exceed the radiocarbon age limit, and no alternative radiometric dating options are currently available. Clastic cave sediments have effectively been dated using the age-dependent changes in relative concentrations of cosmogenically-derived isotopes ^{10}Be and ^{26}Al, but this technique is geochemically unsuited to guano. Here, we test the potential of a novel method for guano: coupled ^{10}Be and ^{36}Cl. Preliminary results demonstrate that measurable quantities of these isotopes are bound to the chitin matrix of ancient insectivorous guano, are immobile in the stratigraphic column, and that the ratio of these isotopes shifts with time over deca-millenial timescales. We further demonstrate appropriate change in isotopic ratio in a small number of independently dated guanos. The half-lives of $3.01 \pm 0.02 \times 10^5$ years for ^{36}Cl and $1.387 \pm 0.012 \times 10^6$ years for ^{10}Be imply a change in ratio of ~25% over 125,000 years, opening the possibility of dating fossil guanos well beyond the radiocarbon limit.

Résumé

L'utilisation des cosmogènes ^{10}Be/^{36}Cl pour dater les guanos fossiles. On a redécouvert récemment l'intérêt des dépôts de guanos de chauves-souris comme archives environnementales. Des protocoles ont été développés pour des datations radiocarbones d'échantillons de guanos jusqu'à 50.000 ans. Or certains dépôts de guanos subfossiles qui présentent un intérêt archéologique et paléoclimatique dépassent cet âge limite et aucune alternative radiométrique n'est actuellement disponible. Des sédiments clastiques prélevés dans les grottes ont été datés en se fondant sur l'évolution des concentrations d'isotopes dérivés des cosmogènes ^{10}Be et ^{26}Al, mais cette technique n'est pas adaptée à la géochimie du guano. Ici, nous testons la possibilité d'une nouvelle méthode couplant ^{10}Be et ^{36}Cl. Les premiers résultats montrent que les quantités mesurables de ces isotopes sont contenues dans la chitine des insectes échantillonnée dans les guanos ; et qu'elles conservent la même place dans la colonne stratigraphique. La demi-vie du ^{36}Cl étant de $3,01 \pm 0,02 \times 10^5$ ans et celle du ^{10}Be de $1,387 \pm 0,012 \times 10^6$ ans, cela implique un changement dans le rapport d'environ 25 % pour 125.000 ans, ce qui ouvre la possibilité de dater des guanos fossiles au-delà de la limite des méthodes radiocarbone.

1. Introduction

In the past few years, there has been renewed interest in ancient bat (and, in SE Asia, cave-dwelling swiftlet – *Collocallia sp.*) guano deposits as paleo-archives and repositories (CLEARY & ONAC, 2020). These deposits can be as much as 10 m in thickness, and under suitable environmental conditions may preserve intact insect chitin for tens of thousands of years (WURSTER *et al.,* 2010). Exhaustive work by WURSTER *et al.* (2009) has now established effective protocols for radiocarbon dating guano samples < 50 ka in age. However, many subfossil guano deposits of archeological and paleoecological interest exceed the radiocarbon finite-age limit, and no alternative radiometric dating options in this age range are currently available. Clastic cave sediments have effectively been dated using the age-dependent changes in relative concentrations of cosmogenically-derived isotopes ^{10}Be and ^{26}Al but this technique is geochemically unsuited to guano. JOHNSTON *et al.* (2010) report on coupled ^{14}C and ^{36}Cl analyses of a Holocene guano, but encountered difficulties

with the latter, apparently because they used bulk guano samples in which most of the chlorine was likely to have derived from percolating fluids. Here, we present exploratory data on the use of coupled ^{10}Be and ^{36}Cl cosmogenically-derived isotope ratios with the potential for absolute dating of ancient bat and swiftlet guano deposits considerably beyond the range of carbon dating.

Cosmogenic ^{10}Be (created in Earth's atmosphere by high energy cosmic particles, rained out, and incorporated into surface materials) is typically present in organic matter at concentrations of 10^6-10^{10} atoms ^{10}Be/g organic matter (WILLENBRING & BLANCKENBURG, 2010) Our own ICPMS measurements of total Be in bat guanos have yielded values in the range of 0.1-0.8 ppm, which translates to 10^6-10^7 atoms ^{10}Be/g guano. Total chlorine levels in fossil and subfossil bat guanos are quite high. JOHNSTON *et al.* (2010) report total chlorine concentrations of 4000-5000 ppm, and ^{36}Cl values of 1.7- 4.7×10^{11} atoms/g in Holocene fossil bat guano from Romania. However, only a small, but still

significant, amount of Cl is matrix-bound and resists the acid and alkali washes that remove mobile Cl.

Since the zero-age concentration of both ^{10}Be and ^{36}Cl would be unknown in an ancient guano accumulation, we have used the age-dependent change in relative concentrations of these isotopes. Since bats and swiftlets of the same species often frequent the same locations today, we can use modern guano samples to establish a zero age isotope ratio for these accumulations. Correlation with Late Pleistocene ^{14}C-dated guano from the site can be used to establish the validity of the technique

Half-lives of 3.01 ± 0.02 x 10^5 years for ^{36}Cl and 1.39 ± 0.01 x 10^6 years for ^{10}Be (KORSCHINEK *et al.,* 2010) imply a potential change in ratio of ~25% over 125,000 years.

Figure 1: Sequence of old guano deposits in Niah Great Cave, Sarawak, Borneo

2. Materials and methods

Guano samples were collected from Niah Cave, Niah Cave National Park, Sarawak, Malaysia (Fig. 1), under permit from the Forestry Department (99.JHS.NCCD.600-7.2.107). Samples were analyzed for ^{10}Be and ^{36}Cl at the Rare Isotope Measurement Laboratory, Purdue University, Indiana. Accelerator mass spectrometer radiocarbon analyses were performed by Beta Analytic, Miami, Florida.

Samples were pretreated with acid, alkali, and chloroform/methanol washes as per WURSTER (2009). Splits were prepared for ^{14}C (1 gram) and ^{10}Be and ^{36}Cl. For Be and Cl analysis, paired 6-gram splits were ashed at 900° C and dissolved in sulfuric/nitric and hydrofluoric acids in Teflon crucibles. After addition of a stable Cl isotope spike, Be and Cl were selectively precipitated with a Be carrier and barium nitrate. Final separation of chlorine from sulfate was by ion exchange chromatography.
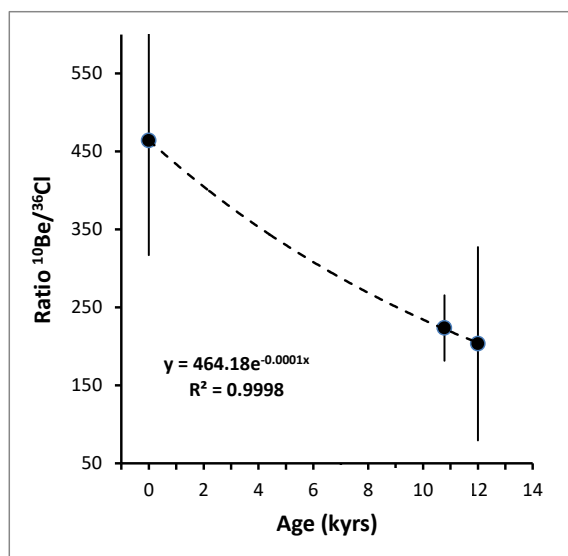

Figure 2: Change in ratio of ^{10}Be/B$_{total}$ and ^{36}Cl/Cl$_{total}$ over time.

3. Results

Isotopic measurements are shown in Table (Fig. 3), and the plot of ^{10}Be/B$_{total}$ and ^{36}Cl/Cl$_{total}$ against time (Fig. 2) shows an excellent correlation.

Age	^{36}Cl/Cl $_{total}$	^{10}Be/B $_{total}$	^{10}Be:Be/ ^{36}Cl:Cl
0	5.54E-15	2.57E-12	463.90
10780	2.65E-15	5.92E-13	223.40
12000	1.64E-15	3.34E-13	203.23

Figure 3: ^{14}C ages and isotopic ratios.

4. Discussion and Conclusion

This proof-of-principle analysis has demonstrated that measurable quantities of chitin-bound ^{10}Be and ^{36}Cl can be recovered from ancient guano deposits. Furthermore, the change in isotope ratio with time is highly correlated with known age derived from accelerator mass spectrometry radiocarbon dating over at least 12,000 years. Further analyses will be required to demonstrate the relationship out to the radiocarbon finite-age limit of ~45 ka. Currently, nothing is known about the retention or selective leaching of ^{10}Be and ^{36}Cl from ancient bat guanos. However, in dry guano accumulations, the original structure of the chitin fragments is retained over the full span of the ^{14}C timescale. Thus, there is reason to suppose that an intact, matrix-bound ^{10}Be and ^{36}Cl record may be retained. If this is the case, then, by combining a radiometrically dated sequence with established techniques of recovering environmental ^{13}C records from bat guanos (c.f. WURSTER et al., 2008; 2010; CLEARY & ONAC, 2020), there is a potential, using this novel dating method of coupled ^{10}Be and ^{36}Cl, to examine environmental histories beyond the radiocarbon dating limit.

Acknowledgments

References

CLEARY D.M., ONAC B. (2020) Using ratios in cave guanos to assess past environmental changes. Geological Society, London, Special Publications, 507, 21 (DOI: https://doi.org/10.1144/SP507-2020-13).

JOHNSTON V.E., MCDERMOTT F., TAMAS T. (2010) A radiocarbon dated bat guano deposit from N.W. Romania: Implications for the timing of the Little Ice Age and Medieval Climate Anomaly. Palaeogeography, Palaeoclimatology, Palaeoecology, 291, 217-227.

KORSCHINEK G., BERGMAIER A., FAESTERMANN T., GERSTMANN U.C., KNIE K., RUGEL G., WALLNER A., DILLMANN I., DOLLINGER G., LIERSE VON GOSTOMSKI CH., KOSSERT K., MAITI M., POUTIVTSEV M., REMMERT A. (2010) A new value for the half-life of ^{10}Be by Heavy-Ion Elastic Recoil Detection and liquid scintillation counting. Nuclear Instruments and Methods in Physics Research B, 268, 187–191.

WILLENBRING J.K., VON BLANCKENBURG F. (2010) Meteoric cosmogenic Beryllium-10 adsorbed to river sediment and soil: applications for Earth-surface dynamics. Earth Science Reviews, 98 (1-2) 105-122.

WURSTER C.M., PATTERSON W.P., MCFARLANE D.A., WASSENAAR L.I., HOBSON K.A., BEAVAN ATHFIELD N., BIRD M.I., (2008) Stable carbon and hydrogen isotopes from bat guano in the Grand Canyon, USA, reveal Younger Dryas and 8.2 ka events. Geology, 36, 683-686.

WURSTER C.M., BIRD M.I., BULL I., BRYANT C., ASCOUGH P. (2009) A Protocol for Radiocarbon Dating Tropical Subfossil Cave Guano. Radiocarbon, 51, 977-986.

WURSTER C.M., SAIZ G., CALDER A., BIRD M.I. (2010) Recovery of organic matter from mineral- rich sediment and soils for stable isotope analyses using static dense media. Rapid Communications in Mass Spectrometry, 24, 165-168.

WURSTER C.M., BIRD M.I., BULL I.D., CREED F., BRYANT C., DUNGAIT J.A.J., PAZ V. (2010) Forest contraction in north equatorial Southeast Asia during the Last Glacial Period. Proceedings of the National Academy of Sciences, USA, 107, 15508-15511

Techniques de carottages sur calcite souterraine. Enjeux et méthodes.

Gaël MONVOISIN[(1,6)], Arnaud DAPOIGNY[(2,6)], Eglantine HUSSON[(3,6)], Stéphane JAILLET[(4,6)], Emmanuel MALET[(4,6)], Alexandre ZAPPELLI[(5,6)], Edouard REGNIER[(2,6)] et Julia GARAGNON[(2,4,6)]

(1) GEOPS, UMR 8148, Bâtiment 504, Rue du belvédère, Université Paris Saclay, 91405 Orsay, France
gael.monvoisin@universite-paris-saclay.fr
(2) LSCE, UMR 8212, Bâtiment 714, Orme des merisiers, Université Versailles St Quentin – Paris Saclay, 91190 St Aubin, France
(3) BRGM, 3 avenue Claude-Guillemin - BP 36009, 45060 Orléans Cedex 2, France
(4) EDYTEM, UMR 5204, Université Savoie Mont Blanc, Pôle Montagne, 73 376 Le Bourget du Lac, France
(5) CEREGE, UMR 7330, Université Aix Marseille, Technopôle de l'Arbois-Méditerranée, BP 80, 13545 Aix en Provence, France
(6) Réseau de métiers CNRS MSK « Milieux Souterrains et Karsts »

Résumé

Le développement de techniques analytiques permettant d'étudier des échantillons de calcite souterraine (datations U/Th, U/Pb, analyses chimiques et isotopiques, morphoscopie…) amène à multiplier les prélèvements d'échantillons sous terre. Cependant le souci de conservation du milieu souterrain, les enjeux d'un impact paysager limité, la nécessité d'une documentation efficace du prélèvement sont autant d'éléments qui militent pour le développement de techniques de carottage adaptées. Ces techniques, présentées ici, couvrent trois types d'échantillonnage : (i) diamètre 4 à 10 mm, longueur 65/80 mm adapté aux bases de stalagmites ; (ii) diamètre 28 à 32 mm, longueur 30 cm à 1 m adapté aux petits planchers et bases de stalagmites ; (iii) diamètre 80 à 112 mm, longueur 0,3 à 2 m adapté aux planchers et coulées stalagmitiques. Un groupe d'études techniques du réseau de métiers CNRS « Milieux Souterrains et Karsts » propose ici une synthèse des retours d'expérience et de tests menés sur le terrain. Les contraintes du carottage (grotte protégée), d'accessibilité au site (karst profond), d'extraction (conditionnement) en fonction du type d'échantillonnage et de leur documentation sont discutées. L'objectif final est de proposer un guide méthodologique adapté aux différents enjeux et situations rencontrées sous terre.

Abstract

Core drilling techniques on subterranean calcite. Issues and methods. Several analytical techniques are available to study underground calcite samples (U/Th, U/Pb dating, chemical and isotopic analyses, morphoscopy...). This leads to an increase of the number of samples taken from the caves. However, the conservation of the underground environment, a limited landscape impact and efficient documentation of the sampling are all elements that militate in favour of the development of adapted coring techniques. These techniques, presented here, cover three types of sampling: (i) diameter 4 to 10 mm, length 65/80 mm adapted to stalagmite bases; (ii) diameter 28 to 32 mm, length 0.3 to 1 m adapted to small floors and stalagmite bases; (iii) diameter 80 to 112 mm, length 0.3 to 2 m adapted to stalagmite floors and flowstones. A technical study group of the CNRS "*Milieux Souterrains et Karsts*" trade network offers here a synthesis of feedback and tests carried out in the field. The constraints of coring (protected cave), site accessibility (deep karst), extraction (conditioning) according to the type of sampling and their documentation are discussed. The final objective is to propose a methodological guide adapted to the different issues and situations encountered underground.

1. Introduction

Les analyses d'échantillons de calcite souterraine sont de plus en plus utilisées pour travailler sur des sujets majeurs comme les datations absolues (U/Th, U/Pb), les analyses chimiques fines de traces et ultra-traces et les analyses isotopiques permettant de discriminer les différentes sources d'éléments chimiques et leur histoire géologique ou climatique. Une partie de ces applications est tournée vers les grottes ornées à haute valeur patrimoniale ou vers les études paléoclimatologiques, mais également vers des études plus expérimentales sur l'histoire de ces cavités et de leur développement. Les carottages sont un moyen fiable de réaliser les échantillonnages. Il est possible de travailler avec de petits carottiers, légers et adaptés aux prélèvements de parois sensibles (grottes ornées) ou en karst profond (portage important). Très peu d'articles et de documentations techniques traitent des carottages souterrains à part l'article de SPÖTL & MATTEY (2012).

Un groupe d'études techniques du réseau de métiers CNRS « Milieux Souterrains et Karsts » propose ici une première synthèse de retours d'expérience et de tests menés sur le terrain prenant en compte les contraintes du carottage (cavités sensibles), d'accessibilité au site (karst profond), d'extraction des carottes (conditionnement) en fonction du type d'échantillonnage et de leur documentation.

2. Des techniques adaptées à différents enjeux de conservation

Les contraintes d'accès aux sites de travail, l'image donnée par des scientifiques prélevant et cassant des concrétions, l'impact visuel des dégradations de concrétions et l'importance patrimoniale de parois ornées imposent une réflexion spécifique. Le groupe d'études techniques s'est donné pour objectif d'avoir cette approche globale incluant ces questions de conservation.

Figure 1 : Différents types de matériels utilisés (couronnes diamantées (4 à 112 mm), rallonges, têtes d'injection).

Parmi ces enjeux, la détermination de l'âge des voiles de calcite scellant l'art pariétal est sujet à discussions (PONS-BRANCHU *et al.*, 2014 ; VALLADAS *et al.*, 2017 ; PONS-BRANCHU *et al.*, 2020). Sur ces sites, il n'est souvent pas envisageable de prélever des échantillons complets de parois ou de concrétions. Il importe cependant de pouvoir prélever suffisamment profond pour recueillir toutes les couches de dépôts à étudier. L'utilisation de micro-carottiers est alors plus adaptée. Il est également possible de forer encore plus fin, avec un système de dremmell ou une perceuse avec une mèche de 1-2 mm, mais l'absence de système de carottage et la dureté de la calcite ne facilitent pas ces échantillonnages. On ne récupère alors que la poudre sans possibilité de distinction exacte de l'échantillon. Cette technique sera préférentiellement

utilisée pour micro-échantillonner les carottes de retour au laboratoire. Dans le domaine de la paléoclimatologie, les échantillons prélevés doivent recouvrir des périodes différentes et les analyses des isotopes de l'Oxygène et du Carbone permettent par exemple de reconstituer les conditions environnementales au moment de leurs dépôts.

Figure 2 : Mise en œuvre d'un perforateur sur accus avec carottier 32 mm (ici deux rallonges) et refroidissement à eau (grotte Pallas 3, Ardèche). Photo S. Jaillet.

3. Des techniques adaptées à différents usages

Le groupe d'études techniques du réseau de métiers CNRS « Milieux Souterrains et Karsts » travaille sur un large éventail de carottiers et de modèles de perforateurs adaptés aux carottiers (fig. 1). Les diamètres internes des carottiers vont de 4 mm à 112 mm, pour des longueurs entre 65 mm et 400 mm, avec parfois des rallonges permettant d'atteindre 1 m de profondeur. Tous les carottiers sont dotés de couronnes diamantées. Ils sont connectés à des perforateurs portatifs de tailles et de puissances variables et adaptées. Les perforateurs ne sont jamais utilisés en mode percussion. Pour les petits carottages (4 à 10 mm), un perforateur léger (ex : Bosch GBH 18V EC) ou une visseuse (ex : Makita DDF484 18V) sont utilisés. Un perforateur plus puissant (ex : Hilti TE-6A 36V ou Bosch GBH 18V) est mis en œuvre pour les carottages moyens (28 à 40 mm) (fig. 2) et un carotteur nécessitant une alimentation électrique

extérieure (ex : Hilti-DD100 220V) est nécessaire pour les plus gros diamètres (80 à 112 mm). Les contraintes majeures des carottages sont (i) ne pas casser ou bloquer le carottier pendant le forage, (ii) extraire la carotte de calcite en un minimum de morceaux, (iii) la sortir du carottier et (iv) parfois pouvoir l'orienter afin de retrouver sa position initiale une fois extraite. Tous les prélèvements par carottage se font nécessairement avec injection d'eau pour deux raisons : (i) évacuation des boues de forage, (ii) évitement de l'échauffement, pour éviter d'user prématurément ou de casser la couronne diamantée, voire d'avoir des conséquences importantes sur les échantillons (datations U/Th/He notamment). La tête de la couronne diamantée, d'un diamètre légèrement supérieur, permet de maintenir un espace entre carottier et paroi pour la remontée de l'eau et des boues. Un opérateur est dévolu

uniquement à cette gestion de l'eau. Dans certains sites, pour éviter des contaminations, des eaux du commerce sont utilisées. Souvent, utiliser l'eau de la grotte (rivière ou mieux piégée dans un gour) permet de résoudre le problème. Lors d'un atelier dédié à ces méthodes, nous avons testé 3 ensembles de matériels adaptés aux situations rencontrées.

Pour les prélèvements de petit diamètre (4 à 10 mm interne), la profondeur d'investigation permet d'atteindre 80 mm sans difficulté particulière (fig. 3). Les problèmes rencontrés sont l'amorce du forage (impliquant qu'un opérateur tienne la tête au début du travail). Sur les très petits diamètres, la carotte se fragmente et remonte dans la tête d'injection, gênant la possibilité de reconstituer correctement la carotte. Le dosage de l'injection d'eau (pouvant être réalisé avec un pulvérisateur ou une bouteille PET) doit être fait avec soin. La pression sur l'outil doit être adaptée. Ces éléments militent pour une formation de l'opérateur surtout pour des sites à forts enjeux patrimoniaux.

Figure 3 : Carottage de petit diamètre (ici 4 mm intérieur) mis en œuvre avec une visseuse et un pulvérisateur de jardin (Aven d'Orgnac, Ardèche). Photo S. Jaillet.

Les tests réalisés sur diamètre moyen (28 à 40 mm) se sont révélés concluants. Sans colonne de guidage et avec deux rallonges, en 32 mm, il est assez aisé d'atteindre 1 m de profondeur (fig. 2). Les principaux problèmes rencontrés sont de casser les tronçons de carottes à la base du carottage et d'extraire la carotte. Cette difficulté augmente à chaque ajout d'une rallonge. Une longue tige métallique

rigide peut être utile pour casser la carotte. Aspirer dans le tuyau d'injection d'eau peut parfois permettre de maintenir la carotte dans le carottier dans la phase d'extraction. Notons qu'à partir de ces diamètres, la consommation d'eau devient importante (au moins 10 litres pour 1 m de carotte).

L'utilisation de diamètres plus importants (80 mm ou plus) implique le recours à une colonne de guidage fixée au sol (gougeons ou scellement) (fig. 4). La méthode permet d'ajouter plusieurs rallonges et d'envisager des carottages de plus de 2 m (QUINIF, 1991). L'impact visuel et environnemental, le recours à un matériel plus lourd, la nécessité d'utiliser le 220 V, milite pour limiter ces opérations à des cas particuliers (analyse morphologique des lamines par exemple, demandant une largeur minimale de la carotte).

Figure 4 : Carottier 80 mm sur colonne de guidage et refroidissement à eau, ici mis en œuvre sur une grosse stalagmite couchée (Aven d'Orgnac, Ardèche). Photo P. Crochet.

4. Prélever pour analyser, communiquer, échanger

La question de l'impact visuel est importante et suscite d'autres réflexions. En effet les spéléothèmes participent à l'esthétique de la grotte. Il est donc indispensable d'accompagner chaque prélèvement d'une réflexion préliminaire sur l'intérêt de l'échantillonnage, le choix de la

zone retenue et l'impact visuel final. En premier lieu, pourquoi prélever sur ce point ? Quelles analyses seront faites sur l'échantillon et à quelles questions scientifiques cela permettra de répondre ? Comment organiser la restitution des données et comment intégrer les résultats

dans les bases de données qui se mettent en place ? Ces questions sont de plus en plus d'actualité dans la communauté scientifique, à l'heure d'un développement croissant des échanges de données (CNRS, 2020).

L'impact visuel peut être limité avec plusieurs approches potentielles. Doit-on cacher le prélèvement ? Si oui, il n'est pas impossible de boucher le trou avec des matériaux inertes, le temps et les écoulements recouvriront la cicatrice rapidement si la concrétion est encore active. Il est également possible d'envisager de montrer explicitement le trou en documentant le travail, par exemple avec une pancarte expliquant pourquoi, par qui et quand ce prélèvement a été réalisé. Ces messages peuvent avoir deux effets : (i) ne pas laisser les visiteurs devant un trou sans explication et (ii) sensibiliser aux questionnements scientifiques et aux modes de travail. Une troisième possibilité est de reproduire un fac-similé du prélèvement, lorsque la concrétion entière a été prélevée, mais cette possibilité n'est plus d'usage si l'on se limite à un carottage plutôt qu'un prélèvement de la concrétion complète.

Conclusions

À travers cette note préliminaire, nous avons voulu présenter les premiers résultats de ce groupe de travail sur les carottages sur calcite au sein du réseau de métiers MSK du CNRS.

Ces premiers tests montrent que le diamètre 4 mm est délicat à mettre en œuvre et doit sans doute être réservé à des enjeux particuliers. Le diamètre 10 mm permet, avec une visseuse et une bouteille PET, d'avoir un matériel simple, polyvalent et efficace (poids total 3 kg), notamment pour des datations prospectives. L'utilisation de carottiers de 32 mm avec un perforateur 18, 24 ou 36 V permet d'atteindre aisément 1 m de profondeur dans des conditions satisfaisantes, là encore avec un encombrement raisonnable (poids total 7 kg). Il est toutefois important d'avoir un perforateur (ou une visseuse) avec un couple de serrage de bonne qualité (minimum 40 N/m) et des batteries de fort ampérage, pour l'autonomie. Parmi les différents modèles de têtes diamantées que nous avons testés, la société ODS (Saint-Leu-la-Forêt, 95) a démontré la performance de ses couronnes diamantées sur mesure, notamment sur des forages avec rallonges.

Loin de limiter ces réflexions à des aspects techniques, nous souhaitons les élargir à des problématiques plus vastes qui sont celles des enjeux de conservations des milieux souterrains et à la question du partage des données. La seconde phase de ce travail sera donc de confronter, au cours d'un atelier thématique à venir, les différents utilisateurs de spéléothèmes. L'objectif sera de comparer les avantages et inconvénients des différentes techniques utilisées et utilisables, puis de former et sensibiliser les débutants aux questions posées. À plus long terme, l'objectif final de ce travail sera de proposer un guide méthodologique adapté aux différents enjeux et situations rencontrées sous terre.

Remerciements

Références

CNRS (2020). Plan Données de la Recherche du CNRS https://www.science-ouverte.cnrs.fr/wp-content/uploads/2020/11/Plaquette-Plan-Donnees-Recherche-CNRS_16112020.pdf

PONS-BRANCHU E., BOURRILLON R., CONKEY M., FONTUGNE M. and FRITZ C. (2014). Uranium-series dating of carbonate formations overlying Paleolithic art: interest and limitations. *Bull. Soc. Préhist. Franc*, 111 (2), pp.211-224.

PONS-BRANCHU E., SANCHIDRIAN J.L., FONTUGNE M., MEDINA-ALCAIDE M.A., QUILES A., THIL F. and VALLADAS H. (2020). U-series dating at Nerja cave reveal open system. Questioning the Neanderthal origin of Spanish rock art. *Journal of Archaeological Science*, 117.

QUINIF, Y. (1991) La série stalagmitique de la galerie des Vervietois (Han-sur-Lesse, Belgique). *Speleochronos* n°3, CERAK, Univ. Mons, pp. 29-44.

SPÖTL C. and MATTEY D. (2012). Scientific drilling of speleothems – a technical note. *International Journal of Speleology*, 41(1), 29-34.

VALLADAS H., PONS-BRANCHU E., DUMOULIN J.P., QUILES A., SANDRICHIAN J.L. and MEDINA-ALCAIDE M.A. (2017). U/TH and 14C cross dating of parietal calcite deposits: application to Nerja cave (Andalusia, Spain) and future perspectives. *Radiocarbon*, Vol 59 (6), p 1955–1967.

Natural and anthropogenic cave sediments: the example of the Apuan Alps (Central Italy)

Alessia NANNONI[1], Leonardo PICCINI[1], Pilario COSTAGLIOLA[1], Nicolò BATISTONI[1], Pietro GABELLINI[1], Gabriele PRATESI[2] & Silvia BUCCI[2]

(1) Department of Earth Science, Università degli Studi di Firenze, Via La Pira 4, 50121 Florence, Italy, alessianannoni@gmail.com (corresponding author)
(2) Agenzia Regionale per la Protezione Ambientale – Toscana (ARPAT), Via N. Porpora 22, 50144 Florence, Italy

Abstract

The Apuan Alps represent an important karst area of Central Italy characterized by large karst systems fed mainly through autogenic recharge. For this reason, cave sediments are not abundant and are usually associated with allogenic recharge through sink holes. An important source of cave sediments is currently represented by the carbonate powder produced during the quarrying of the famous "Carrara" marble. This material has a grain-size ranging from fine sands to silt that can be transported by meteoric waters into karstic network as a very fluid slurry through fissures and cavities crosscut by quarries. Samples of sediments have been collected in some caves and springs fed by the major Apuan karst systems. Composition, grain-size, and morphological features of these sediments have been compared with those of the anthropogenic carbonate powder. Marble slurries and spring sediments show some differences in their mineralogical compositions: the former deposits are composed mainly by calcite grains, whereas the latter show variable proportions of calcite, dolomite, and silicates particles.

1. Introduction

Carbonate aquifers are extremely vulnerable to contamination due to the presence of fast infiltration flow paths such as solutional-enlarged fracture and cavities (WORTHINGTON et al., 2000). Moreover, the yield of these aquifers is not constant neither in time nor in space because of the high heterogeneity and anisotropy of permeability (BAKALOWICZ, 2005). Human activities can potentially damage karst aquifers, including quarrying. The Apuan Alps is a mountain range famous for the extraction of the precious "Carrara" white marble. These mountains are made up of both metamorphosed and non-metamorphosed carbonate rocks arranged in different tectonic units (CARMIGNANI *et al.*, 2006, CONTI et al., 1993). The structural setting and the lithological heterogeneities determined complex hydrodynamic behaviors of the local karst aquifers which represent an important drinking water supply for the coastal urban areas (PICCINI *et al.,* 2019). Quarries are widespread in the metamorphosed sectors of

the mountain range (Fig. 1). Large marble blocks are extracted by sawing the rock with belt, wire and chain saws. The powder produced during extraction and squaring of the blocks is collected and disposed in repositories but a significant fraction of it infiltrates before it is removed during sawing operations, representing a pollutant that can propagate into the karst systems through enlarged fractures when precipitations occur. The input of this contaminant in the groundwater systems changes the physical and mineralogical properties of transported sediments and causes episodic increases of turbidity in karst springs during heavy rains and floods (DRYSDALE et al., 2001). This work proposes the Apuan Alps as a case study to characterize the impact of this physical pollutant on sediments transported and stored in karst aquifers. With this aim, the features of sediments collected in caves and karst springs presumably contaminated by the marble slurry are presented and discussed.

2. Hydrogeological setting, materials and methods

An extensive network of karstic cavities has developed in the metamorphosed carbonate units of the Apuan Alps, with a total length of more than 325 km (DOVERI et al., 2019). The major carbonate aquifer consists of a succession made up of dolostone, dolomitic marble, marble, and cherty meta-limestone. The carbonate aquifer is laterally and vertically confined by impermeable basement rocks (schists) and clastic sedimentary covers. The metamorphosed carbonate succession is arranged in contiguous but distinct drainage systems. Most of the springs fed by the metamorphic aquifers have very irregular regimes, typical of vadose and

epiphreatic flow systems (DOVERI *et al.,* 2019). The sampling sites were chosen to study the mineralogical, morphological and grain size characteristics of the anthropogenic marble powder, the cave deposits, and the spring sediments. Samples were collected in some of the quarries where the marble powder is produced. Care was taken to collect samples of powder produced with different sawing techniques. Cave sediments were sampled in vadose passages (active and relict ones) of the Monte Corchia cave. This is one of the most extensive caves in Italy (length of about 65 km). Samples were also collected at some of the

major springs variably contaminated by the marble slurry (Fig. 1). Cave sediment samples mainly transported in phreatic conditions were collected close to the outlet and grouped with the spring samples. 1 dm^3 of sediment was collected in a LDPE bag at each site using a Teflon spoon. The samples were dried, passed through a 2.8 mm sieve to remove impurities. The fraction passing a 0.25 mm sieve was analyzed with XRD, SEM-EDX and an automated optical microscope for grain size analysis.
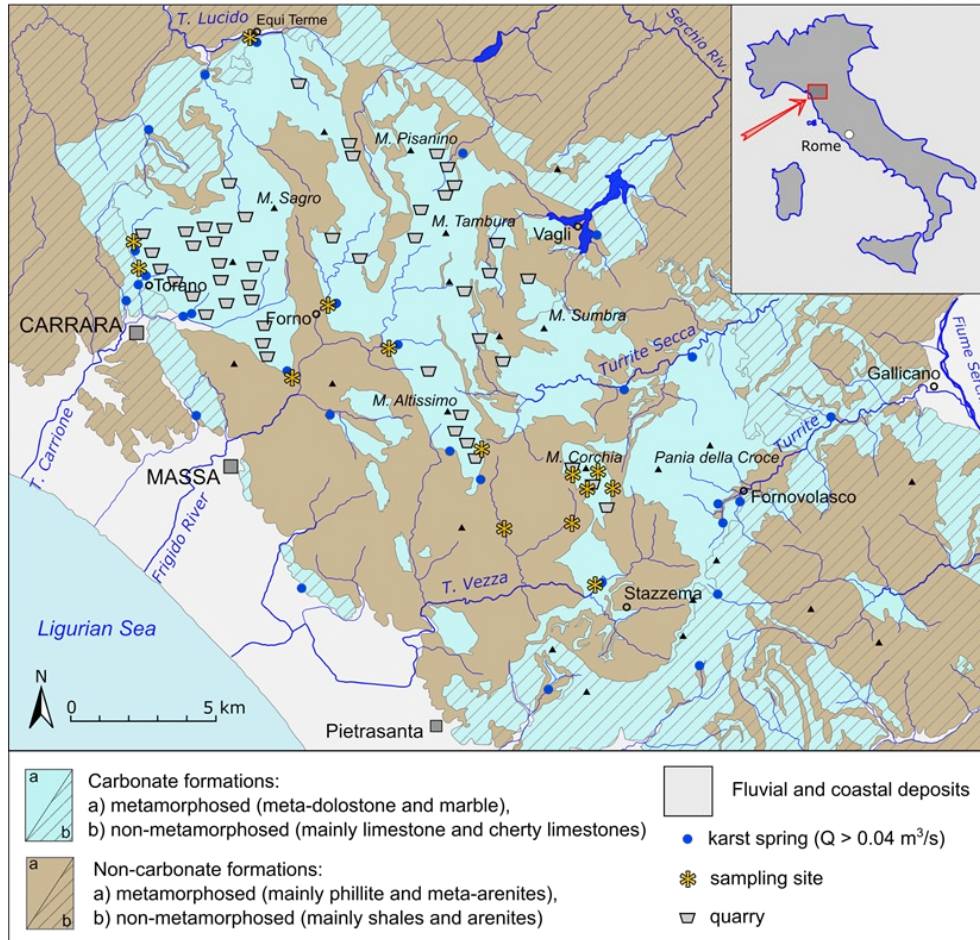

Figure 1: Simplified hydrogeological map of the Apuan Alps (modified after PICCINI et al., 2019).

3. Results

In order to measure the granulometric composition of the samples by optical methods, we removed the sediment fraction that had a diameter larger than 0.25 mm (grain size φ = 1). The marble slurry has a grain size distribution of a silt with variable amounts of fine sands. Spring and cave deposits have a mean grain size of a fine sand, with variable amounts of silt, whereas the clay fraction is volumetrically irrelevant in all the sediments. The XRD analyses revealed that the marble powder has a mineralogical composition totally or predominantly composed by calcite. SEM micromorphometric analyses showed that the particles composing the marble powder have angular contours and no signs of chemical alteration (Fig. 2a). Cave and spring deposits are mostly made up of calcite grains with variable proportion of dolomite and silicates, in particular quartz, muscovite (and albite in some cases). The highest concentrations of silicates are found in the spring samples. Dolomite is frequent in cave samples. Calcite and dolomite grains show different superficial morphologies. In particular, some calcite grains and most of the dolomite grains show irregular surfaces caused by dissolution phenomena (Fig. 2b). However, angular calcite grains with no evidence of dissolution are also present in all cave and spring samples, except than in cave sediments collected in ancient relict passages (Fig. 2c).
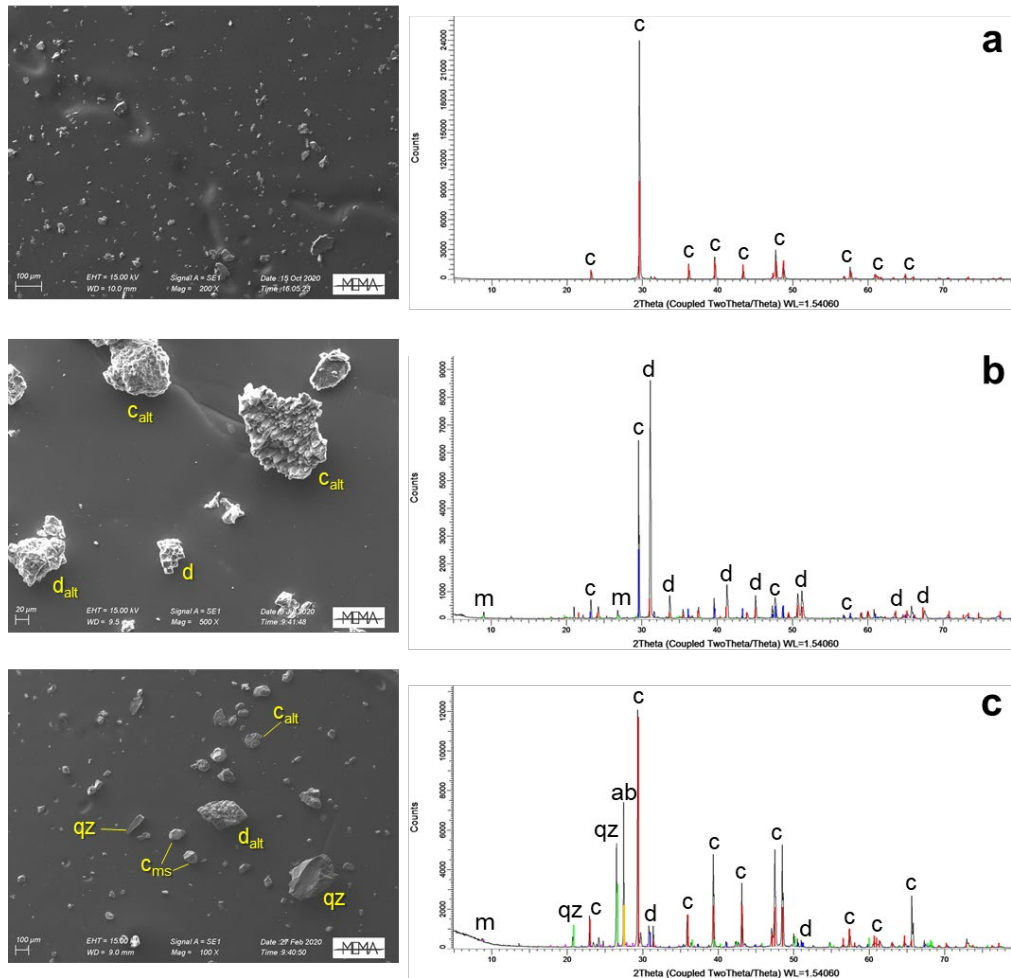
Figure 2: Examples of SEM pictures (left) and diffractograms (right) for a marble powder sample (a), a cave sediment (b), and a spring sample (c). Labels on SEM pictures: c_{ms} = particle of marble slurry (calcite), c_{alt} = weathered calcite, d = dolomite, d_{alt} = weathered dolomite, qz = quartz. Labels on diffractograms: c =calcite, d = dolomite, m = muscovite, qz = quartz, ab = albite.

4. Discussion

The mineralogical composition of the cave and karst spring sediments depends upon the geology of the catchments feeding their internal drainage systems. Calcite, dolomite, and silicate grains are the main constituents, and can be produced by the natural weathering and physical degradation of the rocks outcropping in the study sites. In particular, dolomite particles are produced by the partial dissolution of the dolostone occurring in the epikarst, forming a fine dolomitic sand that can be easily mobilized by the percolating waters. The vadose cave samples from Monte Corchia cave have variable proportions of dolomite grains because dolostone outcrops only in specific sectors of the system so that sediment supply can be either calcic/siliciclastic or a mixture of the three mineral groups (Fig. 3a). However, some samples collected in cave sectors that develop mainly in the dolomitic portions of the aquifer contain a relevant and unexpected amount of calcite grains. Therefore, these samples could be the evidence of marble powder contamination originated from quarries. As expected, major springs have the highest concentrations of silicates because their catchments embrace also relevant sectors of non-carbonate rocks.

A closer observation at specific grain size intervals is useful to highlight differences between the marble slurry and the natural to variably contaminated sediments. It appears that the marble slurry is finer than the karst sediments, although covering a wide dimensional range (Fig. 3b). Marble powder samples are very dispersed in grain size because they were produced with different sawing methods and did not undergo transport. There are no clear differences in grain size between the springs and the cave sediments (Fig. 3b). It is worth to mention that a fine silt fraction is absent in springs that have recently experienced clear episodes of contamination by marble powder. This can be addressed either to 1) the fact that it is not volumetrically relevant independently from other factors or, 2) although it represents a significant volume fraction, it cannot be found because it easily washed away as suspended load during floods, or 3) it was already deposited upstream of the sampling site.
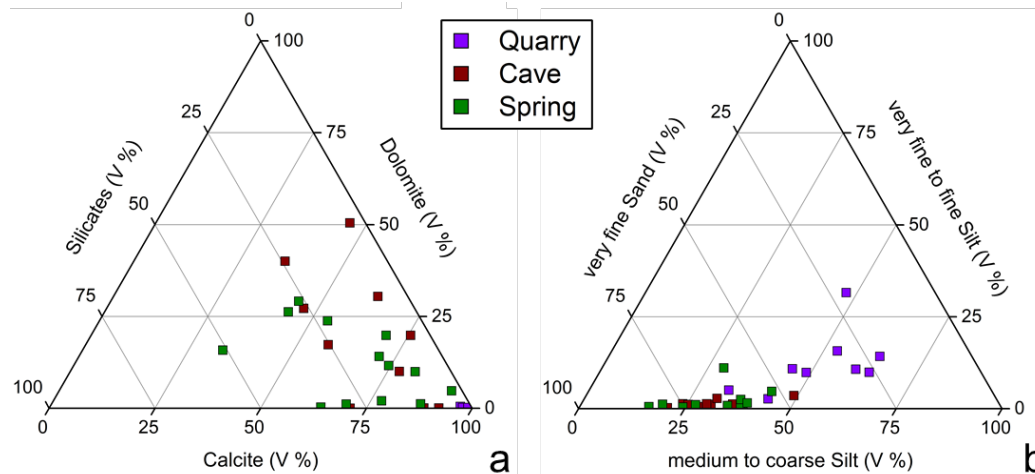
Figure 3: Ternary diagram of the mineralogical composition (a), and of the grain size distribution (b) relative to the very fine to fine silt (φ = 6 − 8, μm = 15.63 − 3.9) − medium to coarse silt (φ = 4 − 6, μm = 62.5 − 15.63) - very fine sand (φ = 3 − 4, μm = 125 − 62.5) interval of the sediments, both expressed in volume percentage.

5. Conclusion

This study confirms a homogeneous calcite composition for the anthropogenic marble powder, whereas cave and spring deposits are mineralogically more heterogeneous, although calcite is always the prevalent constituent. For this reason, the occurrence of calcite alone is not indicative of contamination, but the comparison of mineralogical and textural features and a detailed knowledge of the local geology were useful to recognize the presence of the marble slurry in the Apuan karst systems. Grain size analysis of specific fractions showed that this contaminant is generally finer and less sorted respect to the karst groundwater sediments because the deposition of the latter depends on the hydrodynamic conditions through the systems. The

extreme temporal and spatial variability of the hydrodynamic behavior of these systems justify the heterogeneity of the morphological and compositional characteristics of cave and spring sediments, even for a single system.

In conclusion, marble slurry does not influence much the grain size distribution of cave and spring sediments, except than for a few, very contaminated samples. However it increases the amount of anthropogenic calcite grains, whose morphology is characterized by the absence of dissolution features differently from those produced by natural weathering processes.

References

BAKALOWICZ M. (2005). Karst groundwater: A challenge for new resources, Hydrogeol. J., 13, 148–160.

CARMIGNANI L., CONTI P., MASSA G., VASELLI L., MANCINI S. (2010). Lineamenti geologici delle Alpi Apuane. Acta apuana 5, pp. 9-23.

CONTI P., DI PISA A., GATTIGLIO M., MECCHERI M. (1993). Pre-Alpine basement in the Alpi Apuane (Northern Apennines, Italy). In: Von Raumer JF, Neubauer F (eds.) Pre-Mesozoic geology in the Alps. Springer, Berlin, pp. 609–621.

DOVERI M., PICCINI L., MENICHINI M. (2019). Hydrodynamic and geochemical features of metamorphic carbonate aquifers and implications for water management: The Apuan Alps (NW Tuscany, Italy) case study. Karst Water Environment. Springer, Cham, pp. 209-249.

DRYSDALE R., PIEROTTI L., PICCINI L., BALDACCI F. (2001). Suspended sediments in karst spring waters near Massa (Tuscany), Italy. Environmental Geology, 40(8), pp. 1037-1050.

PICCINI L., DI LORENZO T., COSTAGLIOLA P., GALASSI, D. M. P. (2019). Marble slurry's impact on groundwater: the case study of the Apuan Alps karst aquifers. Water, 11(12), 2462.

WORTHINGTON, S. R. H., FORD, D. C. AND BEDDOWS, P. A. (2000). Porosity and permeability enhancement in unconfined carbonate aquifers as a result of solution in speleogenesis. In: Klimchouk, A. Ford, D. C. Palmer, A. N. and W. Dreybrodt (eds.), Evolution of karst aquifers, National Speleological Society, Inc., Huntsville, AL, USA, pp. 463–472

Climate Variability reconstructed from La Cueva Chica speleothems: implication for Megafauna and Human settlements in South Patagonia, Chile

Carole NEHME[1], Dominique TODISCO[1], Sebastian BREITENBACH[2],
Isabelle COUCHOUD[3], Igor GIRAULT[1], Fabiana MARTIN[4],
Luis BORRERO[5], John HELLSTROM[6], Rik TJALLINGII[7], & Philippe CLAEYS[8]

(1) Identités et Différenciations des Espaces, de l'Environnement et des Sociétés UMR6266 CNRS, Université de Rouen Normandie, France. dominique.todisco@univ-rouen.fr ; carole.nehme@univ-rouen.fr (corresponding author)

(2) Faculty Engineering and Environment, Dep. Geogr. and Envir. Sciences, Northumbria Univ., Northumbria upon Tyne, U-K.

(3) Environnements, Dynamiques et Territoires de la Montagne, UMR 5204 CNRS, Université Savoie Mt-Blanc, France.

(4) Centro de Estudios del Hombre Austral, Instituto de la Patagonia, Universidad de Magallanes, Punta Arenas, Chile.

(5) Departamento de Investigaciones Prehistoricas y Arqueológicas (CONICET), Universidad de Buenos Aires, Argentina.

(6) School of Earth Sciences, The University of Melbourne, Australia.

(7) GFZ German Research Centre for Geosciences, 14473, Potsdam, Germany.

(8) Analytical, Environmental and Geo- Chemistry, Vrije Universiteit Brussel, Belgium.

Abstract

Investigating new palaeoclimate records is of major importance for evaluating the impact of past forcing factors on the evolution of ecosystems as well as megafauna, and human dispersal, especially in Southern Patagonia (Chile) where few records are available. The Cueva Chica, located in the Cerro Benitez (Ultima Esperanza) is partially filled with postglacial deposits that preserve the oldest palaeontological evidence of palaeofauna in the region and is sealed by calcite flowstones. The study relies on a 40 cm long flowstone core S6 and stalagmite S8. The samples were radiometrically (U-Th & ^{14}C) dated to build an age-depth model for the proxy series (stable isotopes, chemical composition). The objectives of this work are to: i) reconstruct past climate variations from geochemical analyses, and ii) assess the palaeoclimatic context of megafauna extinction and human settlements in the area. Core S6 grew discontinuously from 13 to 1 ka with several possible hiatuses. Sample S8 grew from 6.8 to 5.8 ka and at *ca.* 1.2 ka. The results show a change from a wet phase prior to the Holocene to a drier phase during the mid-Holocene likely related to the westerlies dynamics in the Southern Hemisphere. Based on these results, we further discuss the possible implications of climate changes on the megafauna extinction in the area.

Résumé

Variabilité climatique reconstituée à partir des spéléothèmes de La Cueva Chica : implication pour la mégafaune et les établissements humains dans le sud de la Patagonie, au Chili. L'étude des enregistrements paléoclimatiques est d'une importance majeure pour évaluer l'impact des forçages passés sur l'évolution des écosystèmes, la mégafaune et la dispersion humaine, en particulier dans le sud de la Patagonie (Chili), où peu d'archives naturelles carbonatées sont disponibles. La Cueva Chica, située dans le Cerro Benitez (Ultima Esperanza) est partiellement remplie de dépôts postglaciaires livrant parmi les plus anciens vestiges de paléofaune dans cette région. Ces dépôts sont scellés par un plancher de calcite. L'étude repose sur les datations Uranium-Thorium et l'analyse pétrographique et isotopique de la carotte S6 (40 cm de long) prélevé du plancher et de la stalagmite S8. Cette étude a pour objectifs de: i) reconstituer les variations climatiques passées à partir des analyses géochimiques, et ii) évaluer le contexte paléoclimatique de l'extinction de la mégafaune ainsi que des premiers établissements humains dans la région. La carotte S6 couvre une période allant 13 à 1 ka BP, marqués par plusieurs hiatus. La stalagmite S8 couvre une plus courte période, de 6,8 à 5,8 ka et *ca.* 1,2 ka. Les résultats montrent un changement climatique avec une phase humide et chaude de 13 à 9 ka et une phase plus sèche de 8,5 à 5,8 ka, et un retour vers un climat plus humide de 3,0 à 2,5 et *ca.* 1,2 ka. Sur la base de ces résultats, les implications possibles des changements climatiques sur l'extinction de la mégafaune dans la région seront discutées.

1. Introduction

Studying new palaeoclimate records is of major importance for evaluating the impact of past forcing drivers on the evolution of ecosystems and extinction of megafauna, especially in Southern Patagonia where few records are available. The Cerro Benitez (Ultima Esperanza) hosts more than 13 caves and rockshelters with the oldest

palaeontological evidence of palaeofauna in the region (MARTIN et *al.,* 2013; 2015). Two caves (Cueva Lago Sofía 1; Cueva del Medio) host two of the oldest archaeological records of Patagonia, dated between 13.6 and 10.6 ka cal BP, while Cueva Chica hosts the oldest paleontological record of the region, a *Lama gracilis* astragale dated 18,500-17,930 cal BP. The famous Cueva del Milodón comprises the paleontological remains of the extinct ground-sloth *Mylodon*. Cueva Chica is a 73 m long cave located in the southeastern part of Cerro Benitez and comprises the earliest known megafaunal occupation (*e.g. Lama gracilis*) at *ca.*16 ka cal BP. The Cerro Benitez was fully covered by a piedmont ice lobe during the last glacial at *ca.*40 ka. After several glacier retreats and advances from 30 ka to 18 ka, the caves of the Cerro Benitez, including Cueva Chica, were

open and partially sediment filled (TODISCO et *al.,* 2018). Underground galleries were then occupied by megafauna as evidenced by fossil remnants in the cave deposits. We investigated La Cueva Chica as the cave comprises laminated deposits partially sealed with a thick calcite flowstone (Fig. 1). As no stalagmites are preserved in the cave, a 40 cm core was drilled in the flowstone at the end of the cave (Fig. 1C). The calcite core S6 and the stalagmite S8 were radiometrically dated (U-Th,[14]C). Petrographical and geochemical analyses (δ^{18}O, δ^{13}C, chemical composition), combined with monitoring data were used to reconstruct a high-resolution paleoclimate record spanning the Holocene and assess the palaeoclimatic context of megafauna extinction and first human settlements in this area.
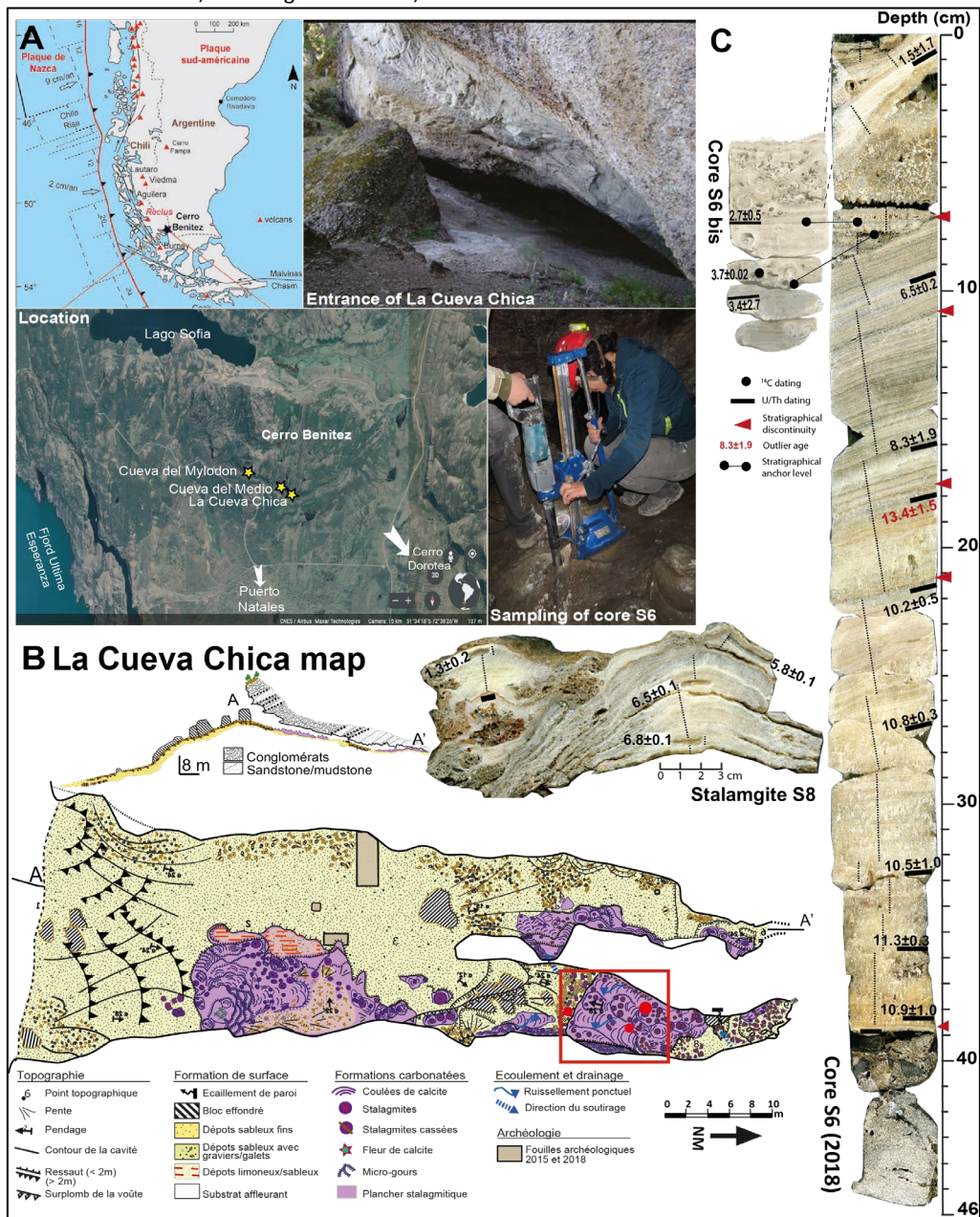

Figure 1: Location of Cerro Benitez and Cueva Chica in SW Patagonia, Chile (A). The map of La Cueva Chica shows the location of the samples (B). The image of stalagmite S8, and cores S6 and S6bis highlights dating points and potential discontinuities. The ages are reported in BP 1950.

2. Materials and methods

Both cores S6 and S6bis were sampled using a Makita drill. The cores and stalagmite S8 were cut along their growth axes and polished using 120–4000 μm silicon carbide sandpaper. 16 ages were obtained on a Nu Instruments MC-ICPMS at the Geochemistry Laboratory, Earth Science Department, University of Melbourne (Australia) using an internally standardized parallel ion-counter procedure and calibrated against the HU-1 secular equilibrium standard following the procedures of Hellstrom (2003). Correction for detrital Th content was applied using initial activity ratios of detrital thorium ($^{230}Th/^{232}Th)_i$ of 0.93 ±0.73. the ^{14}C date was obtained through the analysis of 10 mg of charcoal sampled on core S6bis. A stratigraphical correspondence combined with U-Th dates from core S6bis permits the inclusion of the radiocarbon date into the age model.

12 thin sections of 80-100 μm thick were prepared at the department for Sediment and Isotope Geology, Ruhr University Bochum, Germany. A preliminary petrographic analysis was conducted with a Leica optical microscope to determine the stratigraphical characteristics of core S6 (e.g., fabric, structure, inclusions, discontinuities/hiatuses).

381 stable isotope samples were taken along the growth axis of core S8 (Fig. 1) for $\delta^{13}C$ and $\delta^{18}O$ measurements. Samples were also drilled along the stalagmite growth axis at 1 mm resolution using a Merchantek Micromill mounted on a Leica microscope. The samples were analysed using either a Nu Carb carbonate device coupled to a Nu Perspective mass spectrometer (MS) at the Vrije Universiteit Brussel or a Thermo Gasbench II connected to a Thermo MAT253plus MS in continuous flow mode at the Sediment and Isotope Geology department, Rhur University Bochum, Germany.

Preliminary monitoring data were collected with loggers continuously measuring temperature both outside and inside the cave. Additionally, 16 seepage and water samples were collected from La Chica cave and nearby caves, springs and lakes in December, 2016, 2017, and 2018 for $\delta^{18}O$ and δD measurements in hermetically sealed glass bottles. Isotope measurements were performed at Vrije Universiteit Brussel on a Picarro L2130-i analyzer using cavity ringdown spectroscopy (CRDS). The sensitivity of the proxies to hydrological changes and prior carbonate precipitation (PCP) is further tested with indicators using μXRF element data. The S6 core was scanned using the Bruker M4 Tornado μXRF scanner at the GFZ-Potsdam, Germany to determine relative concentrations of Sr and S (Sr/Ca; S/Ca).

With this on-going study, further dating points will be analyzed to refine the age model and plotted later against the stable isotopes and XRF element records. A detailed petrographic analysis is ongoing to determine growth stops. At this stage, only a linear age model is interpolated between the dated levels in order to reconstruct a preliminary paleoclimatic time series.

3. Results

Flowstone S6 grew discontinuously from *ca.*13 ka to *ca.*1 ka with several possible hiatuses at *ca.*10 ka, from 5.7 to 3.0 ka and 2.5 to 1.8 ka (interpolated ages). Sample S8 grew from 6.8 to 5.8 ka and at *ca.*1.2 ka. Several hiatuses are found between 29 and 70 mm, at 80-, 218- and 385-mm depth (Fig.2).
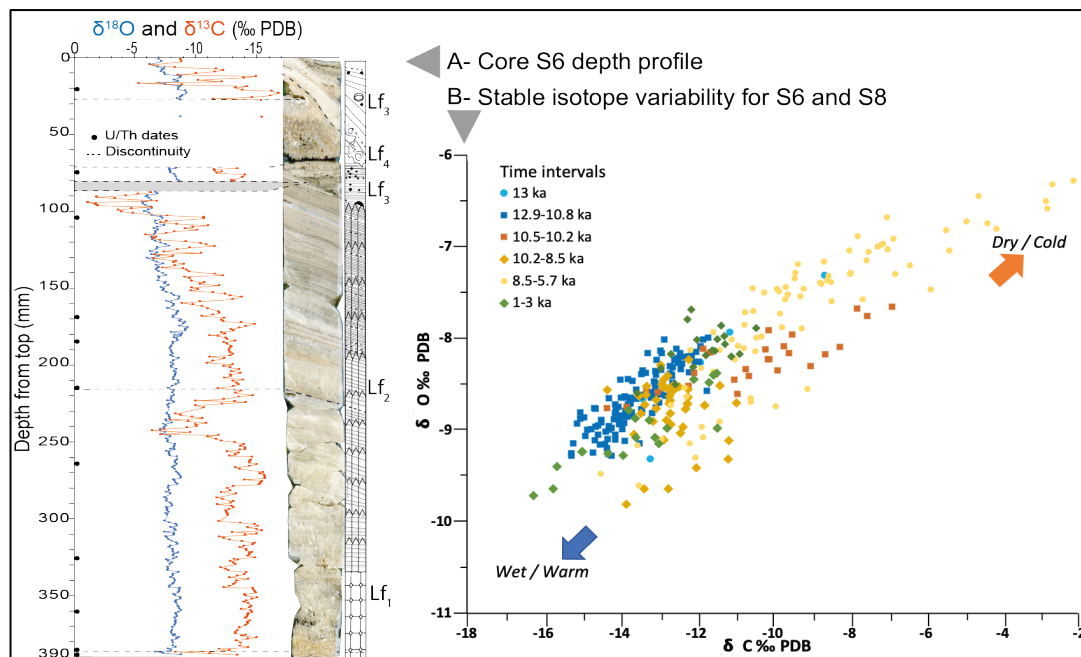

Figure 2: Stable isotope measurements on both S6 and S8 samples. **A.** *Stable isotope depth profile measured along the S6 core with the lithofacies legend and* **B.** *Stable isotopes variability for S6 and S8 plotted against a linear age model.*

Petrographic analysis of thin sections shows that core S6 is mainly composed of columnar calcite, which ranges from poorly-to-well laminated to massive, often with a persistent detrital and allochthonous component and other impurities. Based on clastic content, fabrics, visual appearance, and colour of the calcite, four lithofacies are defined in core S6 from the base to the top (Fig. 2): lithofacies Lf_1 is rich in clastic material and characterised by yellowish calcite with a poorly laminated and more porous structure imbedded in a microgour structure. Low but significant content of oxides, rutile and calcite fragments (micrite, sparite) fill the voids between the calcite crystals comparing to other levels. Lithofacies Lf_2 is composed of compact, elongated columnar calcite with highly laminated structure. Few empty voids are reported comparing to Lf_1. The basal part of Lf_2 shows few impurities and more, well recognizable, fluid inclusions. The upper part of Lf_2 shows more impurities and higher number of hiatuses. Lithofacies Lf_3 is less-clearly laminated but comprises the highest amount of impurities, minerals, bones fragments and remains of organic material in the entire record. Oxides, rutiles, pyroclasts are the most common minerals preserved in this part. Lithofacies Lf_4 is not laminated but rather a primary subaqueous calcite formed in a sub-aqueous environment. Stable isotopes analyzed at sub-centennial resolution show a 3 ‰ range for $\delta^{18}O$, and more than 14‰ for $\delta^{13}C$. These changes; mostly in carbon, are likely caused by kinetic fractionation and prior calcite precipitation (PCP), controlled by changes in moisture availability and cave air humidity. The $\delta^{13}C$ record varies closely in-phase with the $\delta^{18}O$ record but with different degrees of compression (*vs* distance) for the same oscillations (Fig. 2). The sensitivity of the proxies to hydrological changes and PCP is further tested with Sr/Ca acquired by μXRF element scanning. The Sr/Ca record is consistent with the $\delta^{18}O$ profile showing an anti-phase correlation. The basal part of core S6 up to 176 cm depth shows low Sr/Ca ratios with more negative $\delta^{18}O$ values. The mid and upper parts of the core (from 176 cm to 86 cm, and from 27 cm to the top) show higher Sr/Ca ratios and more positive $\delta^{18}O$ values.

4. Discussion & conclusions

The multiproxy record from La Cueva Chica suggests a wet phase from *ca.*13 to 9 ka, likely related to strong southern westerlies, preceded by a short dry/cold spell at *ca.*13 ka. This wet phase was followed by colder/drier conditions from 8.5 to 5.8 ka, likely related to weaker westerlies, especially during the mid-Holocene. High precipitation and strong westerlies prevailed from 3.0 to 2.5 ka and during Medieval times. Our paleoclimate record implies that the presence of extensive megafauna, the development of *Nothofagus* forest and human arrival (METCALF et al., 2016), all occurred during a climatically favorable wet/warm period *ca.* 13 to 9 ka, after the Antarctic Cold Reversal (ACR). However, the deterioration of the vegetation cover at the Cerro Benitez coinciding with high $\delta^{13}C$ values excursions was initiated since *ca.*11 ka. Previous studies suggest an extinction of major megafauna species (e.g. *Mylodon, Smilodon, Panthera onca meembrina*) during this wet/warm period.

Such climate-driven changes likely reduced open ecosystem environment and may have led to local decline of herbivore populations. Later cooling/drying at *ca.*9 ka may have contributed to the disappearance of other mammal species along with human activities. Finally, a charcoal layer dated at *ca.*4 ka in core S6 indicates possible human activities inside La Cueva Chica, well after the megafauna' extinction. The speleothems S6, S6bis and S8 from La Cueva Chica provide a new palaeoclimate record from high-latitude Southern Patagonia (Chile). The constructed time series span most of the Pleistocene-Holocene transition and the Holocene period. This preliminary work reports several proxy records (stable isotopes; chemical composition). Additional U-Th dating will refine the age model. Petrographic, monitoring and statistical analyses will be completed to assess the consistency of the proxy time series and the significance of the reconstruction at regional scale.

Acknowledgments

References

MARTIN F., SAN ROMÁN M., MORELLO F., TODISCO D., PREVOSTI F.J., BORRERO L.A., 2013. Land of the ground sloths: recent research at Cueva Chica, Ultima Esperanza, Chile. Quaternary International, 305, 56-66.

MARTIN F., TODISCO D., RODET J., SAN ROMAN M., MORELLO F., PREVOSTI F., STERN C., BORRERO L.A., 2015. Nuevas excavaciones en Cueva del Medio. procesos de formacion de la cueva y avances en los estudios de interaccion entre cazadores recolectores y fauna extinta. Magallania, 43, 165-189.

METCALF J.L., TURNEY C., BARNETT R., MARTIN F., BRAY S.C., VILSTRUP J.T., ORLANDO L., SALAS-GISMONDI R., LOPONTE D. et al., 2016. Cooper A. Synergistic roles of climate warming and human occupation in Patagonian megafaunal extinctions during the Last Deglaciation. Science Advance, 2, e1501682.

TODISCO D., RODET J., NEHME C., MARTIN F., BORRERO L.A., 2018. Les cavités du Cerro Benitez (Patagonie, Chili). Hypothèses génétiques glacio-karstiques. Karstologia, 67, 31-42

Record of the Pyrenean climate since the last Interglacial by two stalagmites from Moulis Cave (Ariège, S. France)

Christine PERRIN[1, 2], Lilian LATAPIE[2], Charlotte HONIAT[3]
& Laurent PRESTIMONACO[4]

(1) Muséum National d'histoire Naturelle, HNHP UMR7194, CERP Tautavel Avenue Léon-Jean Grégory 66720 Tautavel France cperrin@mnhn.fr (corresponding author)
(2) CNRS, SETE UMR 5321, 2 Route du CNRS, 09200 Moulis France
(3) Institute of Geology, University of Innsbruck, Innrain 52, 6020 Innsbruck, Austria
(4) Aquila Conseil, Parc Industriel de la Piche, Avenue Pierre Semard, 31600 Seysses, France

Abstract

Two small stalagmites from the northern Pyrenean piedmont in SW France provide a discontinuous record of past climates between the last interglacial and the Holocene. Aims of the present work are twofold : 1. To evaluate the potential of the studied stalagmites as reliable paleoenvironmental / paleoclimatic archives; 2. To describe the various spelaean facies and their significance in terms of growth history and hydrological information about the infiltration conditions and drip-rate feeding the speleothems at time of their formation. For this purpose, we used a set of petrographical-geochemical techniques to characterize the successive growth units and internal architecture of stalagmites.

Results show that stalagmite grew discontinuously from MIS 5 to 3.8 kyrs and presents several surfaces of growth interruption, some of which correspond to important hiatus evidenced by U-Th dating. Three active and relatively fast growth phases correspond to the MIS 5a-b , the Bølling-Allerød and Younger Dryas and to the Lower Holocene (11.6 to 6.2 kyrs). During the uppermost phase (between 6.2 and 3.8 kyrs), the stalagmite growth rate decreases drastically.

Résumé

Enregistrement du climat pyrénéen depuis le dernier interglaciaire par deux stalagmites de la Grotte de Moulis (Ariège, S. France). Deux petites stalagmites provenant d'une grotte du piémont nord pyrénéen dans le sud-ouest de la France ont fourni un enregistrement discontinu du paléoclimat entre le dernier interglaciaire et l'Holocène. Les objectifs de ce travail sont: 1) d'évaluer le potentiel des stalagmites étudiées en tant qu'archives paléoenvironnementales / paléoclimatiques; et 2) de décrire les différents faciès de ces spéléothèmes et leur signification en termes d'histoire de croissance et d'informations hydrologiques sur les conditions d'infiltration et les variations de débit d'alimentation des spéléothèmes au moment de leur formation. Pour cela, nous avons utilisé un ensemble de techniques analytiques pétrographiques et géochimiques pour caractériser les unités de croissance successives et l'architecture interne des stalagmites.

Les résultats montrent que le spéléothème s'est développé de manière discontinue entre le MIS 5 et 3,8 ka et présente plusieurs surfaces d'arrêt de croissance, dont certaines correspondent à un hiatus important mis en évidence par les datations U-Th. Trois phases de croissance active et relativement rapide correspondent respectivement au MIS 5a-b, au Bølling-Allerød et au Dryas Récent, ainsi qu'à l'Holocène inférieur (11.6 - 6.2 ka). Au cours de la phase la plus récente (entre 6,2 et 3,8 ka), le taux de croissance de la stalagmite a diminué considérablement.

1. Introduction

This paper reports on two small stalagmites from the northern Pyrenean piedmont in SW France, which provide a discontinuous record of past climates between the last interglacial and the Holocene. The high potential of speleothems as reliable recorders of paleoclimate and environmental conditions is largely recognized and, for this purpose, there are a number of proxies which can be extracted from their petrography and geochemistry. The objectives of this work are twofold : 1. To evaluate the potential of the studied stalagmite as a reliable palaeoenvironmental / palaeoclimatic archive spanning various time-slices since the last interglacial. 2. To describe the various spelaean facies and their significance in terms of growth history and hydrological information about the infiltration conditions and drip-rate feeding the stalagmite at the time of its formation.

2. Setting, materials and methods

Moulis cave is located a few kilometers SW of the small city of Saint-Girons (Ariège), on the northern side of the Pyrenean range, and is developed in the Jurassic limestones and dolostones of the Arize massif sedimentary cover (Fig. 1). The two stalagmites presented here, MOU 4 and MOU 5 were found broken in a small gallery close to the entrance of the cave. The methodological approach used for the study of Moulis speleothem is basically the one described in PERRIN *et al.* (2019) for optimizing subsampling in speleothems, combined with more classical petrographical – geochemical analysis and also methods recently developed for understanding controls on the internal architecture of stalagmites (RAILSBACK 2013, PERRIN *et al.* 2014, MUÑOZ-GARCÍA *et al.* 2016, MARTÍN-CHIVELET *et al.* 2017). Large thin sections prepared continuously along the median growth axis of both stalagmites were observed with an optical petrography microscope and a fluorescence microscope. Raman microspectrometry was performed on thin sections to confirm and complete mineralogical identifications obtained from observations of thin sections with the petrographic microscope. SEM observations and EDS-microanalysis complete this dataset.

The stalagmite MOU 4 was sampled for U-Th dating. Ten subsamples were analyzed with a MC-ICP-MS at the Geotop (Montreal, Canada). Ages are reported in kyrs BP.
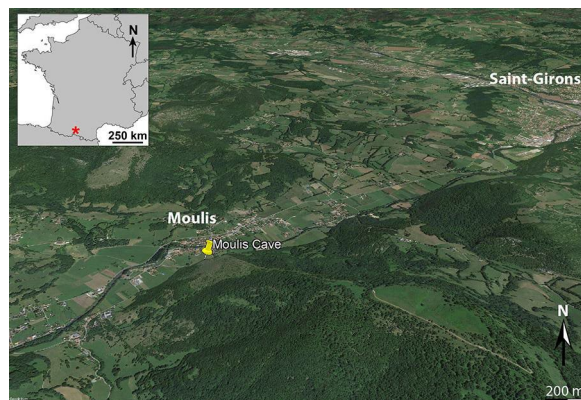

Figure 1: Location of Moulis Cave (aerial view Google Earth).

3. Results

Mineralogical species and potential diagenesis
The spelaean material consists of calcite, with no aragonite detected in the two stalagmites. Detrital material includes dolomite, quartz, iron oxides and hydroxides.
Neither detailed petrographical observations and SEM-EDS analyses, or Raman microspectrometry data have shown presence of aragonite or indication of recrystallization of aragonite into calcite. In both samples, calcite is therefore essentially primary. The two stalagmites are considered in a good state of preservation although partial dissolution processes have been evidenced at level of some discontinuities and at the base of MOU 5.

Facies and lamination
Several types of calcite are observed in both speleothems, the most common of which being the compact columnar calcite and the open columnar calcite. These form the major part of MOU 4 and upper part of MOU 5 and show a brown-green aspect in polished sections. Elongated columnar calcite is present at some levels and often bears some laminated layers of brown color in transmitted light and white-cream aspect in polished sections. These layers are rich in tiny elongated pores and organic components. The basal part of MOU 5 consists of coralloid knobs formed by radial-fibrous calcite (*sensu* KENDALL 1985).
Petrographical and luminescence microscopy, together with SEM imaging and EDS microanalysis, reveal the presence of different types of laminae (Fig. 2): visible laminae resulting from contrasting density of micropores (GENTY & QUINIF 1996), luminescent laminae and geochemical laminae expressed by slight differences in Mg-content.

Lamination occurs at different scales, the finest alternance of laminae (both visible and luminescent laminae) being annual.

Discontinuities
Three types of surfaces have been recognized in the two stalagmites. These are type E bounding surfaces associated with partial dissolution (RAILSBACK *et al.* 2013), growth interruption marked by a detrital clay deposit and discontinuities resulting from abrupt facies change (PERRIN *et al.* 2014, MARTÍN-CHIVELET *et al.* 2017).
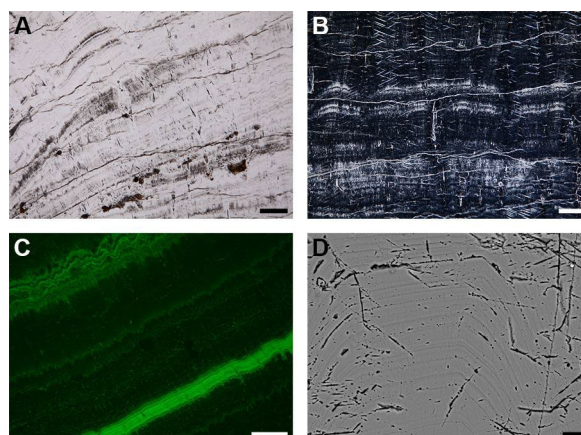

Figure 2: Lamination. A. Visible laminae, transmitted light, scale 500 µm. B. Visible laminae, dark field, scale 500 µm. C. Luminescent laminae, reflected light and GFP filter, scale 100 µm. D. Geochemical laminae, SEM BSE image, scale 10 µm.

Ten major surfaces have been identified in MOU 4 and five in MOU 5. These surfaces represent the boundaries of the major growth units. In both samples, additional minor surfaces occur (Fig. 3).
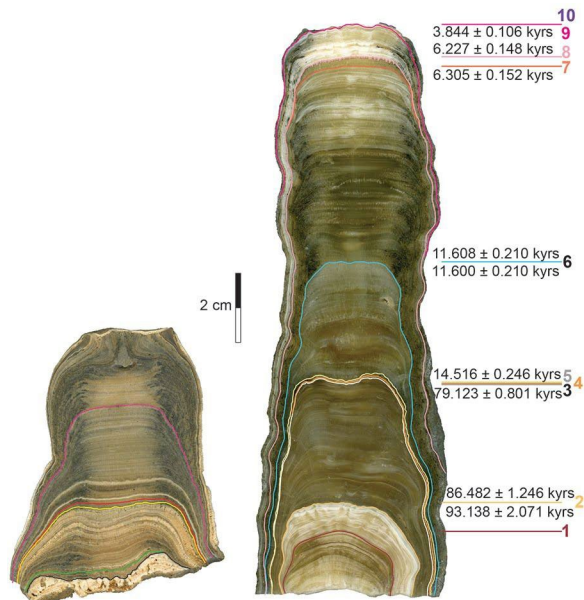

Figure 3: Median polished slabs of stalagmites MOU 4 (right) and MOU 5 (left) with major discontinuities (colored lines) and U-Th ages of MOU 4.

U-Th dating
Ten subsamples were selected in MOU 4 for U-Th dating. U-Th analyses provided ages ranging between 3.8 ± 0.1 kyrs

and 93.1 ± 2.1 kyrs. These results show the occurrence of two major hiatus, both corresponding to major discontinuities during the development of MOU 4.
The second major surface corresponds to a growth interruption of about 6-7 kyrs while the group of discontinuities 3-5 represent a condensed level of about 6465 kyrs (Fig. 3).

Evolution of apex morphology and stacking pattern.
Both stalagmites nicely show that morphology of their apex and stacking pattern of growth layers have evolved through time. We have analyzed these variations in detail in order to get information about drip rate conditions during stalagmite growth.
After the first growth phase of coralloid knobs at the base, MOU 5 adopts a rimmed-shape apex morphology with a marked progradational stacking pattern. This gradually evolves into a flat-topped stalagmite with a retrograde geometry. Above the youngest major discontinuity, the apical morphology changes back to a rimmed shape during a mostly aggradational growth phase (Fig. 3).

MOU 4 consists of ten growth units bounded by major discontinuities. These units successively record changes from globular to irregular flat-topped, and rimmed apical shape before 79 kyrs. After the main condensed level and until the end of Pleistocene, apex morphology varies from rimmed to flat-topped and growth is characterized by largely dominated aggradational and retrograde trends. From the beginning of Holocene until 6.2 kyrs, the morphology of MOU 4 changes gradually from a rimmed to a flat top while the stalagmite widths vary from slightly progradational to aggradational with brief periods of retrograde stacking pattern.

4. Climate and hydrological record

The internal architecture, microstratigraphy and petrography of both samples express changes in the feeding patterns of both stalagmites in terms of drip rate variability, supersaturation state of feeding water relative to calcite, and infiltration events.

The lower half of MOU 5 records a higher drip rate variability relative to its upper part, periods of high infiltration associated with higher concentration in organic compounds. The upper part of MOU 5 is characterized by more homogeneous conditions with low and constant drip rate and low drip rate variability.

The basal unit of MOU 4 reflects changing conditions of drip rate variability and infiltration pattern and supersaturation state. During the interstadials 5b-5a of the last interglacial (86.5 – 79.1 kyrs), MOU 4 developed with a rather moderate growth rate and stable drip rate conditions. The full glacial

period corresponds to a condensed level (79.1 to 14.5 kyrs) and three successive major growth interruptions in the stalagmite. MOU 4 resumed its growth at the beginning of the Bølling (14.5 kyrs) which was accompanied by a marked increase of warmth and moisture. The constant and moderate drip rate and low drip rate variability favored a relatively high growth rate for MOU 4. The Younger Dryas is recorded petrographically by a change from compact columnar calcite to open columnar calcite and an increase in drip rate variability. The lower Holocene until 6.2 kyrs corresponds to the period of highest growth rate for MOU 4. Hydrological conditions are rather stable and homogenous during the lower half of this unit and gradually become more variable toward the top. During the uppermost growth phase (between 6.2 and 3.8 kyrs), the growth rate of MOU 4 decreased drastically as a result of increasing frequency of high infiltration events and a decrease in supersaturation relative to calcite.

Acknowledgments

References

GENTY D., QUINIF Y. (1996) Annually laminated sequences in the internal structure of some Belgian stalagmites – importance for palaeoclimatology. Journal of Sedimentary Research, 66, 275–288.

KENDALL A.C. (1985) Radiaxial fibrous calcite: a reappraisal. In: Schneidermann N. & Harris P.M. (Eds.), Carbonate cements. Society of Economical Paleontology, Mineralogical Special Publication, 36, 59-77.

MARTÍN-CHIVELET J., MUÑOZ-GARCÍA M.B., CRUZ J.A., ORTEGA A.I., TURRERO M.J. (2017) Speleothem Architectural Analysis: Integrated approach for stalagmite-based paleoclimate research. Sedimentary Geology, 353, 28–45.

MUÑOZ-GARCÍA M.B., CRUZ J., MARTÍN-CHIVELET J., ORTEGA A.I., TURRERO M.J., LOPEZ ELORZA M. (2016) Comparison of speleothem fabrics and microstratigraphic stacking patterns in calcite stalagmites as indicators of paleoenvironmental change. Quaternary International, 407, 74-85.

PERRIN C., PRESTIMONACO L., SERVELLE G., TILHAC R., MAURY M., CABROL P. (2014) Aragonite–Calcite Speleothems: Identifying Original and Diagenetic Features. Journal of Sedimentary Research, 84, 245–269.

PERRIN C., TILHAC R., PRESTIMONACO L. (2019) Optimizing subsampling strategies for U/Th dating and geochemical proxies in carbonate speleothems. Sedimentary Geology, 389, 91-102.

RAILSBACK L., AKERS P., WANG L., HOLDRIDGE G., VOARINTSOA N.R. (2013) Layer-bounding surfaces in stalagmites as keys to better paleoclimatological histories and chronologies. International Journal of Speleology, 42, 167–180.

Speleothems in iron ore caves in the Carajás National Forest, southeast Amazon

Luís PILÓ[1], Enrico BERNARD[2], Rafael SCHERER[3] & Allan CALUX[4]

(1) Departamento de Zoologia – UFPE, Av. Moraes Rego, s/n, CEP. 50670-420, Recife, Brazil. lbpilo7@gmail.com (corresponding author)
(2) Departamento de Zoologia – UFPE, Av. Moraes Rego, s/n, CEP. 50670-420, Recife, Brazil. enricob2@gmail.com
(3) Grupo Espeleológico de Marabá - GEM, Av. Alameda Atlântica, Q10, Lote 1, CEP.68502-110, Marabá, Brazil. schererafael@gmail.com
(4) Carstografica, Rua Adamastor Tymburibá, 01/610, CEP. 31170-320, Belo Horizonte, Brazil. ascalux@gmail.com

Abstract

In the Carajás National Forest, about 1,500 caves in iron ore and canga deposits have been identified. The speleothems in these caves are all relatively small in size. Crusts and coralloids prevail, but draperies, small rimstone dams, irregular forms known as *pingentes* hanging from the ceilings, similar to stalactites, are also present. These speleothems are mainly formed of hematite, goethite and gibbsite, derived from the weathering of the cave bedrock. In caves with guano deposits, speleothems are larger and more abundant. Corralloids, crusts, stalactites, draperies, stalagmites and columns predominate, and are composed of phosphate, especially leucophosphite, phosphosiderite, strengite and spheniscidite. Sulphate crusts are present and consist of gypsum, aluminite and felsőbányaite. Phosphate and sulphate minerals are related to leaches resulted from the bacterial decomposition of guano, which react with rock or sediment to form speleothems. Using radiocarbon dating, guano trapped in a 17 cm long phosphate stalagmite was dated to 10.2 cal kyr BP (bottom) and 3.8 cal kyr BP (top), providing, to our knowledge, the first dates for phosphate speleothems in caves, and giving us a reference for the growth rate of these rare formations.

1. Introduction

The Carajás National Forest (CNF) covers an area of 411,949 ha and is located in the southeastern Brazilian Amazon, approximately 540 km south of Belém, the Pará State capital. Geologically, the Carajás Formation stands out, as a Neoarchean metavolcanosedimentary sequence within the Grão Pará Group. It is composed of banded iron formations (BIF) represented by jaspilites. The iron formation is covered by iron breccia generically known as canga, which act as caprock on plateau tops, regionally represented by the Carajás Ridge. The average temperature is 23°C and annual rainfall reaches 2,400 mm (PILÓ *et al*. 2015). Over 1,500 small caves have already been identified in the CNF some of which host more than 100,000 insectivorous bats (*Pteronotus gymnonotus* and *Pteronotus personatus*) and there are important guano deposits in them. In general, the caves are small, on average 30 m long. Dripping is significant inside the caves due to their proximity to the surface and porosity of the canga. Some caves function as springs. Temporary drainage channels can also occur. Speleothems of CNF caves have been reported by MAURITY & KOTSCHOUBEY (1995), PILÓ & AULER (2011), SCHERER *et al*. (2017), ALBUQUERQUE *et al*. (2018) and FIGUEIRA, *et al*. (2019). This work presents studies on speleothems from 36 caves in the region, totalling 91 samples of speleothems and 22 samples of guano for chemical, mineralogical and chronological analyses.

2. Materials and methods

To characterize the speleothems, the study selected 36 of the caves in the Carajás Ridge including 11 with large guano deposits (bat caves). Ninety-one samples of speleothems were collected for mineralogical and chemical analysis. The analyses were performed at the technological characterization laboratory of the Polytechnical School at the University of São Paulo – USP. The mineralogical analyses used the powder method and a Panalytical X-ray diffractometer (X'Pert model with an X'Celerator detector). The chemical analyses (oxides) used an XRF spectrometer manufactured by Malvern Panalytical (Zetium model). Twenty-two guano samples were analysed at the Organic Correctives, Fertilizers and Residues Laboratory of the Luiz de Queiroz Higher School of Agriculture - ESALQ/USP. The determinations and methods used were: Phosphorus (P_2O_5) using a spectrophotometer and a vanadomolybdenic solution; Potassium (K_2O) and Sodium (Na) using flame photometry; Sulphur (S) using gravimetric technique with precipitation of Barium sulphate; Calcium (Ca), Magnesium (Mg), Copper (Cu), Manganese (Mn), Zinc (Zn), Iron (Fe) using extraction with HCl for atomic absorption photospectrometry. ^{14}C dating of eight guano samples and two stalagmite samples was carried out at the Beta Analytic Laboratory, Miami (USA), using Accelerator Mass Spectrometry (AMS) technique. In the stalagmite, the dated carbon originates from guano, deposited and intercalated with laminations of phosphate minerals (Figure 2).

3. Results

The main speleothems identified in the iron ore caves were coralloids, crusts, flowstones, *pingentes*, stalactites, stalagmites and columns (PILÓ & AULER, 2011, PILÓ *et al*. 2015). The coralloids are small, may be nodular, globular, botryoidal or coral-like in shape and situated mainly on walls, floors and boulders on the cave floor. Coralloids colours vary; they may be whitish, red, yellowish, dark brown or light grey. Coralloids can consist of iron oxide-hydroxide, especially hematite and goethite or of phosphates particularly strengite, $Fe^{3+}(PO_4)\cdot 2H_2O$), leucophosphite, $KFe^{3+}_2(PO_4)_2(OH)\cdot 2H_2O$, and phosphosiderite, $Fe^{3+}(PO_4)\cdot 2H_2O$ (usually associated) and less often, spheniscidite, $(NH_4)Fe^{3+}_2(PO_4)_2(OH)\cdot 2H_2O$, taranakite, $K_3Al_5(PO_3OH)_6(PO_4)_2\cdot 18H_2O$), rodolicoite, $Fe^{3+}(PO_4)$, and hureaulite - $Mn^{2+}_5(PO_3OH)_2(PO_4)_2\cdot 4H_2O$. Two sulphates were also detected among the coralloids, gypsum, $Ca(SO_4)\cdot 2H_2O$, and jarosite - $KFe^{3+}_3(SO_4)_2(OH)_6$.

Coralloids composed exclusively of iron phosphates usually present from 36% to 38% of P_2O_5 and 38% to 40% of Fe_2O_3. Phosphates associated with sulphates may contain up to 13.6% of SO_3. The crusts are relatively frequent in the caves and may cover small areas or in some cases, practically the entire cave. They are generated by seeping and flowing water. Crusts mainly cover the floors, but they can also cover walls, ceilings and boulders. They may be compact, laminated, banded or microbreccia and can be up to a few centimetres thick. Crusts can be red, yellow, white or dark grey. Crusts predominantly consist of hematite, Fe_2O_3, goethite, $FeO(OH)$, and phosphates (strengite, phophosiderite, leucophosphite taranakite, hannayite, $(NH_4)_2Mg_3(PO_3OH)_4\cdot 8H_2O$, spheniscidite and variscite - $Al(PO_4)\cdot 2H_2O$. Crusts formed by bayerite, $Al(OH)_3$, were also documented. Crusts formed by sulphates alone (gypsum, aluminite, $Al_2(SO_4)(OH)_4\cdot 7H_2O$, and felsőbányaite, $Al_4(SO_4)(OH)_{10}\cdot 4H_2O$, were identified as well as others associated with phosphate (francoanellite - $K_3Al_5(PO_3OH)_6(PO_4)2\cdot 12H_2O$. Crusts formed exclusively by phosphates (newberyite, $Mg(PO_3OH)\cdot 3H_2O$, and monetite, $Ca(PO_3OH)$ consisted of 21.7% MgO, 40% P_2O_5 and 3.4% CaO. Other speleothems present in the caves are flowstones on the walls, originating from solutions seeping from fractures and small conduits known as canaliculi. The flowstones may form draperies and small rimstone dams on sloping walls, their colours being predominantly red, yellow and light brown.

The flowstones are mainly composed of Fe and Al oxyhydroxides (goethite, hematite, gibbsite, $Al(OH)_3$, lepidocrocite - $Fe^{3+}O(OH)$, and bayerite - $Al(OH)3$. Flowstones composed exclusively of phosphates (associations of phosphosiderite, spheniscidite and strengite), were less common. A sample of flowstone composed of iron and aluminium oxides and hydroxides consisted of 80.8% F_2O_3 and 2.9% Al_2O_3. The *pingentes* are downward projections from the ceiling or sloping walls consisting of ferruginous material similar to stalactites but with no central canal or concentric lamination. In general, they have many empty spaces inside them. They are either red or reddish brown and can be up to 30 cm long but just a few centimetres wide. Analysis of samples indicated a composition of oxides and hydroxides of iron (hematite, goethite and lepidocrocite) and aluminium (gibbsite). Stalactites and stalagmites are the most surprising forms in the iron ore caves (Fig. 1). The stalactites have a central canal, concentric growth layers and lengths of up to 1.5 metres. These rare speleothems are usually either dark brown, yellowish or reddish in colour.

Figure 1: Stalactites, stalagmites and columns of phosphatic minerals in cave S11B-0094. Photo: Ataliba Coelho.

The stalagmites have convex lamination and may take the shape of a cone or a candle. They are less frequent in occurrence than the stalactites and may reach a height of 50 cm. There are also some columns in the caves. The analysis of 18 samples of stalactites and stalagmites only identified phosphatic minerals paragenesis: spheniscidite-leucophosphite, strengite-phosfosiderite, leucophosphite-spheniscidite-phosphosiderite and leucophosphite-phosphosiderite-strengite-spheniscidite. In some of the samples, however, only a single phosphate was identified (leucophosphite or strengite). One iron phosphate stalactite registered 37.5% of P_2O_5 and 41.3% of Fe_2O_3.

Significant guano deposits were identified in the bat caves; they are rich in organic matter, high concentrations of C (40.1%), N (11.7%), P_2O_5 (1.9 to 22.9%), Fe_2O_3 (1.2 to 22.3%) and minor but important content of K_2O (0.1 to 1.7%), CaO (0.03 to 4.8%) and SO_3 (0.1 to 6.4%). Guano pH ranged from 2.1 to 5.6. Phosphate minerals (spheniscidite, leucophosphite, hannayite, biphosphammite, $(NH_4)H_2(PO_4)$, and brushite, $Ca(PO_3OH)\cdot 2H_2O$, sulphates (gypsum, syngenite, $K_2Ca(SO_4)_2\cdot H_2O$, aphthitalite, $K_3Na(SO_4)_2$, and bassanite, $Ca(SO_4\cdot 0.5H_2O)$ and a nitrate gwihabaite, $(NH_4)(NO_3)$, have been identified in acid guano. ^{14}C dating of eight guano samples taken from the base of the deposits in six bat caves first identified two of them as dating from the end of the Pleistocene: 22,876 – 22,469 cal yr BP (Beta 544608) and 18,191 – 17,857 cal yr BP (Beta 521294). One sample corresponded to the upper Holocene 7,891 – 7,878 cal yr BP (Beta 521292). All the other sample datings were for the period of the last 4 thousand years 3,450 – 3,323 cal yr BP (Beta 544609), 2,464 – 2,305 cal yr BP (Beta 521293),

2,183 – 2,015 cal yr BP (Beta 521295), 2,018 – 1,890 cal yr BP (Beta 544607) and 1,882 – 1,728 cal yr BP (Beta 527797). Two ages were obtained from the guano that was intercalated with phosphate from a 17 cm long stalagmite (Figure 2). The base was dated as 10,296 - 10,187 cal yr BP (Beta 534951) and the top as 3,892 – 3,694 cal yr BP (Beta 534952).

4. Discussion

Speleothems in iron ore caves with no extensive guano deposits are of local occurrence and small, possibly due to the low dissolution of iron (III). In these caves there can be occurrences of coralloids, flowstones and crusts, mainly constituted of Fe and Fe/Al oxides and hydroxides, but there may be occurrences of phosphates associated to small, dispersed guano occurrences. The source of Fe and Al is undoubtedly the surrounding iron-bearing bedrock. The presence of Al is more marked in the canga (PILÓ & AULER, 2011). According to MAURITY & KOTSCHOUBEY (1995), the slow dissolution of oxides and hydroxides in the canga enables the mobilisation of Fe and Al in the form of colloids that flocculate after limited transport by the water flows, generating thin deposits of gels.

Figure 2. Sectioned phosphatic stalagmite showing the locations where samples were taken from for radiocarbon dating to obtain the ages.

The dehydration and crystallization of those amorphous products resulted in the generation of the speleothems in the Carajás caves. KAMP & CURI (2000) underscored that the main processes for the dissolution of iron are protonation, reduction by microorganisms and complexation by organic ligands. The soluble Fe (II) can circulate in the caves, oxidise and re-precipitate, generating secondary minerals. PARKER *et al.* (2013) demonstrated the action of reducing bacteria on Fe (III) in iron ore caves of Carajás. However, the greater diversity, abundance and size of speleothems is found in the bat caves. In those caves, which are larger than the regional average, it is possible to encounter stalactites, stalagmites, columns, coralloids and crusts sometimes almost entirely covering the floor, walls and ceilings. Phosphate speleothems predominate but sulphates also occur to a lesser extent. The phosphatic minerals in the bat caves are derived from guano, given that the banded iron formation of Carajás has very low P_2O_5 content (an average of 0.01%), according to MACAMBIRA & SCHRANK (2002). A variety of complex reactions takes place in the guano, especially bacterial decomposition, liberating nitric, phosphoric and sulphuric acids which react with rock or the sediments to form the secondary minerals (ONAC & FORTI, 2011; AUDRA *et al*. 2019). Inside the guano deposits the sulphuric acid reacts with the rock to form sulphates, notably gypsum, and the reaction with phosphoric acid produces phosphates (ONAC & VERES, 2003; HILL & FORTI, 1997). The guano deposits are acidic (pH 2.1 to 5.6) and samples from the base of the deposits are the most acidic, as already observed by WURSTER *et al.* (2015). In addition to expressive P_2O_5 and Fe_2O_3 content the guano has K_2O, CaO, Na_2O, and SO_3 availability. Added to that, in the bat caves, are high humidity, high temperatures (>30°C in the inner zones) and the presence of ammonia originated from decomposition of bat urea. Those conditions have made the formation of a whole set of diversified phosphate and sulphate minerals possible, including rare ones like rodolicoite and hureaulite. Radiocarbon dating of guano samples indicates ages ranging from the end of the Pleistocene (22.0 cal kyr BP) testifying to the long duration of the presence of bat colonies in the caves. Another dating registered was for the beginning of the Holocene (8.0 cal kyr BP). Five ^{14}C in different bat caves placed the beginning of their guano deposits at times more recent than 3.5 cal kyr BP. None of the identified deposits were thicker than 1 m. Given the intense water activity (dripping and small flows) in most of the bat caves the guano deposits are being eroded and transported out of the caves. The identification of the most ancient deposits awaits a more ample prospection. Guano included in a well-laminated phosphatic stalagmite 17 cm long was dated, which gave an age for its base at 10.2 cal kyr BP and at the top 3.8 cal kyr BP. Not considering possible interruptions in the dripping of phosphate rich water and other variables such as climate, then the growth rate of that phosphatic stalagmite was 0.026 mm/year.

5. Conclusion

Most of the speleothems in the iron ore caves of the CNF are relatively small features mainly formed of hematite, goethite and gibbsite, derived from the weathering of the iron-bearing rock with a predominance of crusts and coralloids. In the active or inactive bat caves with deposits of guano, the speleothems are larger more abundant and more diversified. Coralloids, crusts, stalagmites and stalactites predominate, largely composed of phosphate, most notably, the minerals leucophosphite, phosphosiderite, strengite and spheniscidite. Sulphate crusts are also present consisting of gypsum, aluminite and

felsőbányaite. The sulphate and phosphate minerals are related with the bacterial decomposition of guano which reacts with the rocks or sediments to form the speleothems. Radiocarbon dating in guano deposits indicate ages from around the end of the Pleistocene (22.0 cal kyr BP) to the Holocene (1.8 cal kyr BP), evidence of the long duration of bat colonies presence in the caves. One 17 cm-long phosphate stalagmite was dated thanks to the 14C dating of included guano layers, producing a first age information for phosphate speleothems in caves and a reference for the growth rate of these rare formations.

Acknowledgments

References

ALBUQUERQUE A.R.L., ANGÉLICA R.S., GONÇALVES D.F. and PAZ S.P.A. (2018) Phosphate speleothems in caves developed in iron ores and laterites of the Carajás Mineral Province (Brazil) and a new occurrence of spheniscidite. *International Journal of Speleology*, 47 (1), 53-67.

AUDRA P., DE WAELE J., BENTALEB I., CHROŇÁKOVÁ A., KRIŠTŮFEK V., D'ANGELI I.M., CARBONE C., MADONIA G., VATTANO M., SCOPELLITI G., CAILHOL D., VANARA N., TEMOVSKI M., BIGOT J.Y., NOBÉCOURT J.C., GALLI E., RULL F. and SANZ-ARRANZ A. (2019) Guano-related phosphate-rich minerals in European caves. *International Journal of Speleology*, 48 (1), 75-105.

FIGUEIRA R.L., HORBEB A.M.C., ARAGÓN F.F.H. and GONÇALVES D.F. (2019) Exotic sulphate and phosphate speleothems in caves from eastern Amazonia (Carajas, Brazil): Crystallographic and chemical insights. *Journal of South American Earth Sciences*, 90, 412–422.

HILL C. A. and FORTI P. (1997) *Cave Minerals of the World*. National Speleological Society - NSS, 463 p.

KÄMPF N. e CURI N. (2000) Óxidos de ferro: Indicadores de ambientes pedogênicos. Tópicos em ciência do solo, Viçosa, MG, *Sociedade Brasileira de Ciência do Solo*, 2000. v.1. p.107-138.

MACAMBIRA J.B. e SCHRANK A. (2002) Químio-estratigrafia e evolução dos jaspilitos da Formação Carajás (PA). *Revista Brasileira de Geociências*, 32(4), 567-578.

MAURITY C. e KOTSCHOUBEY B. (1995) Evolução recente da cobertura de alteração no Platô N1 – Serra dos Carajás-PA. Degradação, pseudocarstificação, espeleotemas.

Boletim do Museu Paraense Emilio Goeldi. Série Ciências da Terra, n° 7, 331-362.

ONAC B.P. and VERES D.S. (2003) Sequence of secondary phosphates deposition in a karst environment: evidence from Māgurici Cave (Romania). *European Journal of Mineralogy*, 15, 741-745.

ONAC B.P. & FORTI P. (2011) Minerogenetic mechanisms occurring in the cave environment: an overview. *International Journal of Speleology*, 40 (2): 79-98.

PARKER C.W., AULER A.S., SENKO J., SASOWSKY I.D., PILÓ L.B., SMITH M., JOHNSTON M. and BARTON H. (2013) Microbial iron cycling and biospeleogenesis: cave development in the Carajás Formation, Brazil. *ICS Proceedings*, Brno, 442–446.

PILÓ L.B. e AULER A. (2011) *Mineralogia dos espeleotemas das cavernas ferríferas da região de Carajás*, PA. Golder Associates, RT-017_099-515-5006_00-B, 47 p. Unpublished.

PILÓ L.B., AULER A. and MARTINS F. (2015) Carajás National Forest: iron ore plateaus and caves in *Southeastern Amazon. Landforms and landscapes of Brazil*. New York: Springer, 273-283.

SCHERER R., PILÓ L.B. SOUZA-FILHO W.M., BARATA A.S. e SCHERER, B. (2017) Ocorrência de espeleotemas e feições morfológicas raras em cavernas ferríferas da Serra dos Carajás, no Pará. *Congresso Brasileiro de Espeleologia*, 34, 2017. Ouro Preto. Anais SBE, 409-416.

WURSTER C.M., MUNKSGAARD N., ZWART C. and BIRD M. (2015) The biogeochemistry of insectivorous cave guano: a case study from insular Southeast Asia. *Biogeochemistry*, 124 (1-3), 163-175.

Spéléothèmes des grottes *vs* spéléothèmes des systèmes anthropiques (carrières, souterrains …). Problèmes chronologiques et apport des éléments traces pour étudier et reconstruire les climats et/ou l'occupation ou l'utilisation des sols dans le passé.

Edwige PONS-BRANCHU[1], Louise BORDIER[1], Philippe BRANCHU[2], Arnaud DAPOIGNY[1], Eric DOUVILLE[1], Laurine DRUGAT[1], Emmanuel DUMONT[2], Gaël MONVOISIN[3], Jean-Pascal DUMOULIN[4], Jules QUERLEUX[5] & Nadine TISNERAT-LABORDE[1]

(1) Laboratoire des Sciences du Climat et de l'Environnement, LSCE/IPSL, CEA-CNRS-UVSQ, Université Paris-Saclay, F-91191 Gif-sur-Yvette, France, France, edwige.pons-branchu@lsce.ipsl.fr (corresponding author)
(2) GEOPS Bat. 504 - Universite Paris-Saclay, 91405 Orsay Cedex, France
(3) CEREMA, 12 Rue Teisserenc de Bort, 78197 TRAPPES-en-Yvelines Cedex
(4) Lab. de Mesure du Carbone 14 (LMC14), LSCE/IPSL, CEA-CNRS-UVSQ, Univ. Paris-Saclay, F-91191 Gif-sur-Yvette, France
 (5) IGC, Inspection générale des Carrières - 86 rue Regnault, 75013, France.

Résumé:

Les spéléothèmes (de grottes ou de systèmes anthropiques comme les carrières ou les souterrains) sont utilisés depuis plus de 40 ans pour les reconstructions paléoclimatiques ou paléo-hydrologiques. Plus récemment, ils ont montré leur utilité pour retracer des changements dans l'occupation et l'utilisation des sols. Nous montrerons à travers plusieurs exemples, que si dans de nombreux cas des chronologies fiables peuvent être obtenues en utilisant les séries de l'uranium (U/Th), dans d'autres situations il est nécessaire de coupler des méthodes complémentaires (i.e. avec le ¹⁴C ou le comptage des lamines par exemple). Une attention particulière sera portée sur l'utilisation des éléments traces et notamment les terres rares pour reconstruire les changements environnementaux ou climatiques passés. Nous comparerons en particulier leur étude dans un spéléothème de grotte (Sud de la France) et dans des spéléothèmes prélevés en milieu urbain (Paris), avec dans un cas la caractérisation du rôle et de la contribution des sols en fonction des changements du climat et dans l'autre celle de l'occupation du sol et son utilisation (activités anthropiques).

Abstract

Cave speleothems vs. speleothems in anthropogenic systems (quarries, underground ...). Chronological problems and the contribution of trace elements to the study and reconstruction of climates and/or land use in the past. Speleothems (from caves or from anthropogenic systems such as quarries or undergrounds) have been used for more than 40 years in paleoclimatic or paleo-hydrological reconstructions. Lately, they have shown their usefulness for the reconstruction of land use change. We will show through several examples, that if in many cases, reliable chronologies can be obtained by using uranium (U/Th) series, in others cases it is necessary to use several methods (i.e. cross analysis with ¹⁴C or laminae counting for example). Particular attention will be given to the use of trace elements and especially rare earths elements for environmental reconstructions. Speleothem from a natural cave setting in southern France will be compared to speleothems-like deposit from urban areas (Paris), with in one case the reconstruction of soil activity according to climate variations and in the other that of land use (human activities).

1. Introduction

Les spéléothèmes sont de formidables archives climatiques. D'une part car ils peuvent, dans de nombreux cas être datés de manière absolue par la méthode uranium-thorium sur les derniers 600 000 ans (LI *et al*. 1989 ; HELLSTROM 2003) ou sur des périodes plus courtes par des méthodes relatives (PONS-BRANCHU *et al.,* 2014). D'autre part, l'analyse de traceurs géochimiques nous renseigne sur les conditions environnementales régnant au moment de leur dépôt. Les

indicateurs environnementaux étudiés dans ces archives sont principalement les isotopes stables du carbone et de l'oxygène (LABEYRIE *et al.,* 1967, FOHLMEISTER *et al.*, 2020), mais aussi les teneurs ou rapports en éléments mineurs et traces (FAIRCHILD & TREBLE, 2009). Parmi ces éléments, les lanthanides, du nom du premier élément de cet ensemble (lanthane) auquel s'ajoutent l'Yttrium et le Scandium pour former le groupe des terres rares (rare earth elements-REE en anglais) sont encore très peu étudiées dans les spéléothèmes (BOURDIN *et al.*, 2011). Les terres rares se caractérisent par des propriétés géochimiques relativement similaires. Elles sont par exemple toute trivalentes dans les conditions oxydo-réductrices de surface, à l'exception du Cérium (divalent ou trivalent), état spécifique de cet élément souvent à l'origine d'une anomalie négative ou positive dans un spectre de terres rares normalisées. Du fait de leurs rayons ioniques diminuants avec leur masse, les terres rares trivalents se distribuent et s'alignent sur un spectre normalisé, différemment selon leur comportement au cours des processus d'altération ou d'incorporation dans les minéraux. Les terres rares sont très utilisées dans les études de géochimie de surface, notamment pour l'étude des processus d'altération (CULLERS *et al.*, 1987). Cependant, elles sont encore très peu étudiées dans les spéléothèmes.

Dans cet article, nous comparons l'utilisation des terres rares dans trois cas d'études différents, provenant de sites contrastés : un spéléothème de grotte naturelle (grotte de la Salamandre, Gard), un spéléothème de souterrain à Paris (aqueduc de Belleville) et un spéléothème souterrain d'une carrière au sud de Paris (Carrière de la Brasserie). Les deux premiers cas sont tirés de publications récentes (DRUGAT *et al.*, 2019 ; PONS-BRANCHU *et al.,* 2014) et le troisième est une étude inédite.

2. Matériel et méthodes

Les 3 sites de prélèvement, ont en commun d'être peu profonds. Les spéléothèmes ici étudiés se forment à partir d'infiltrations d'eau pluviales et sont tous laminés.

   -**Salam 3** est une stalagmite de 50 cm de hauteur, prélevée dans l'Aven de la Salamandre (Gard), qui s'est développée pendant près de 2500 ans au cours de la transition entre la dernière période glaciaire et l'Holocène (DRUGAT *et al*., 2019). La chronologie a été déterminée par la méthode uranium thorium (U/Th), classiquement utilisée pour les spéléothèmes de plusieurs milliers d'années, avec correction de la fraction détritique par la méthode stratigraphique (ROY-BARMAN & PONS-BRANCHU 2016).

   -**Bel 2** est une concrétion de 4 cm d'épaisseur prélevée dans l'aqueduc de Belleville (au nord de Paris) et dont la croissance couvre les derniers 300 ans (PONS-BRANCHU *et al.,* 2014). La chronologie a été déterminée par comptage des lamines et datations absolues (U/Th). Le croisement des 2 méthodes a permis de valider que la lamination des spéléothèmes de ce site en zone très urbaine est bi-annuelle comme dans les sites « naturels » des zones climatiques similaires.

   -**Bras 1**, de 1 cm d'épaisseur seulement a été prélevé dans la carrière de la Brasserie à Paris (Figure 1) taillée dans les calcaires du Lutétien. Le concrétionnement était actif au moment du prélèvement (année 2012). Les lamines bien que présentes, sont peu marquées et leur comptage peu évident. Cet échantillon étant trop mince pour effectuer des prélèvements d'assez de matériel pour réaliser des datations U/Th, et son développement certainement très récent font que cet échantillon est un mauvais candidat pour utiliser cette méthode de datation.

10 mg de poudre ont été prélevés au sommet de la concrétion Bras 1 pour une analyse ^{14}C. L'objectif est ici d'évaluer la quantité de carbone mort pour tester la faisabilité de la datation ^{14}C dans ces concrétions. Les analyses ont été réalisées par l'équipe du Laboratoire de mesure du carbone 14 (LMC14) sur l'instrument national Artemis, suivant le protocole décrit dans DUMOULIN *et al*. (2017). Sur 3 niveaux, environ 3 mg ont été prélevés pour les analyses des éléments traces. Les échantillons ont été dissous dans l'acide nitrique (HNO$_3$ 0.5N) afin d'obtenir des solutions à 100 ppm de calcium avant d'être analysés par ICP-QMS. Le protocole utilisé est celui décrit dans BOURDIN *et al.* (2011).

Figure 1 : Carrière de la Brasserie (Paris), site de prélèvement

3. Résultats et discussion

3.1. ^{14}C et discussion sur l'opportunité de datation sur les échantillons jeunes

Les données ^{14}C obtenues sur Bras 1 sont présentées dans le tableau (figure 2). L'échantillon analysé étant prélevé au sommet d'un spéléothème actif en 2012, le niveau d'une dizaine de mg couvre 5 à 6 lamines, soit environ 3 ans si les lamines sont bi-annuelles comme dans le cas des spéléothèmes de l'aqueduc du nord de Paris (PONS-BRANCHU *et al*., 2014).

N° SacA	Echantillon	pMC	Age ans BP
55096	Bras 1 - 15	61,69 ± 0,18	3880 ± 30

Figure 2 : résultat de l'analyse ^{14}C sur Bras 1. pMC ; pourcent de carbone moderne.

Sur la figure 3, le ^{14}C mesuré dans l'échantillon est comparé au ^{14}C atmosphérique de l'hémisphère nord (HUA *et al.* 2013). La différence entre les deux implique ici une quantité importante de carbone mort, de l'ordre de 40%. Cette proportion de carbone mort est ici particulièrement marquée. A titre de comparaison, elle varie entre 2.5 et 10% pour l'Aven de la Salamandre (GENTY *et al.*, 2001) et, en région parisienne (Paris-Versailles) dans un contexte urbanisé, celle-ci a été évaluée à deux fois moins (17-22%) pour des spéléothèmes de souterrains de Versailles et Paris (PONS-BRANCHU *et al.*, 2018). Dans ces derniers cas, une chronologie relative des spéléothèmes urbains a pu être établie en retraçant le signal ^{14}C du « pic des bombes » des années 1960s, avec un transfert rapide du carbone atmosphérique vers le sous-sol et l'influence probable d'une petite fraction de «*vieux carbone*» lié à l'utilisation de ressources fossiles (effet Suess). Dans le cas présenté ici (Bras 1), la proportion de carbone mort est beaucoup plus importante, et l'utilisation du « pic des bombes » pour établir la chronologie de cette concrétion dépendra fortement de l'importance de l'atténuation de ce pic et d'un possible temps de délai entre les variations atmosphériques et le transfert du carbone atmosphérique vers la concrétion. De nouvelles analyses sont nécessaires et pourront permettre de contraindre ces paramètres.
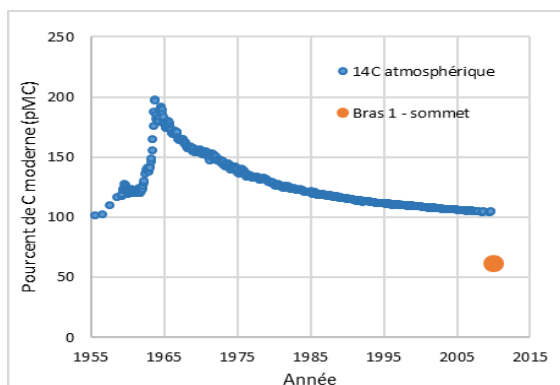

Figure 3 : comparaison entre le ^{14}C atmosphérique (HUA et al., 2013) et la mesure du ^{14}C au sommet de Bras 1.

3.2. Les terres rares
Seuls les lanthanides sont discutés ici. L'Europium (Eu) étant interféré par la présence de Baryum (interférences isobariques) lors de la mesure en spectrométrie de masse, cet élément n'est ici pas présenté.
Les concentrations mesurées dans Bras 1, varient de 1,7 à 27,8 ppb. Leurs teneurs ont été normalisées à celles d'une référence pour les roches sédimentaires (NASC, GROMET *et al.*, 1984) pour représenter en figure 4 le spectre en terres rares correspondant. Pour comparaison, les données normalisées au NASC des 2 autres échantillons (Bel 2 et Salam 3), ont également été ajoutées à cette Figure. Pour Bel 2, les données issues de 3 niveaux uniformément répartis suivant l'axe de croissance ont été reportés. Pour Salam 3, les moyennes correspondant aux 3 périodes climatiques enregistrées (Bølling–Allerød - réchauffement en fin de période glaciaire; Dryas récent - retour bref aux

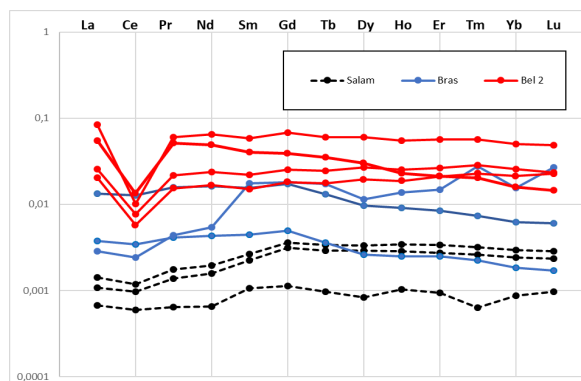conditions glaciaires; Holocène - climat interglaciaire actuel) sont reportées.

*Figure 4 : Spectres de terres rares normalisés (NASC) pour les échantillons de calcaire Bel 2 (*PONSBRANCHU *et al., 2004), Salam 3 (*DRUGAT *et al., 2019) et Bras 1 (ce travail).*

L'échantillon Salam 3 de l'aven de la Salamandre, présente les teneurs les plus faibles en terres rares, tandis que l'échantillon Bel 2, qui a incorporé pour les niveaux les plus jeunes des terres rares issues des activités anthropiques (PONS-BRANCHU *et al.,* 2014) présente les teneurs les plus élevées. L'échantillon Bras 1 de la carrière de la Brasserie présente des teneurs intermédiaires. Une anomalie négative marquée en Cérium est observée seulement pour Bel 2 (figure 4). Cette anomalie témoigne d'un effet de conditions oxydantes en amont de la percolation dans l'aqueduc. Cette anomalie n'est pas observée dans l'échantillon de la carrière de la brasserie comme dans celui du site naturel (aven de la Salamandre). La différence majeure entre l'échantillon de grotte naturelle et celui de la carrière sous le bois de Vincennes est « l'allure » générale du spectre des terres rares avec un enrichissement en terres rares lourdes et plus prononcé pour Salam 3 et à l'opposé un enrichissement en terres rares légères pour Bras 1 dans 2 échantillons sur les 3 analysés. Dans Salam 3, les différentes allures des spectres pour les 3 périodes s'expliquent par des proportions différentes de ces éléments traces en provenance du sol et/ou de la roche mère reflétant un lien direct avec les changements climatiques (DRUGAT *et al*., 2019).
La différence entre les spectres de Salam 3 et Bras 1 peut s'expliquer par i) une origine des terres rares différente (roche mère et/ou sol) ; ii) un fractionnement différent du fait de processus géochimiques contrastés (modes et temps de dissolution de l'encaissant, précipitation primaire dans l'épikarst, vitesse de croissance des spéléothèmes) ; iii) un effet marqué du milieu urbain comme pour le site du Nord de Paris (Aqueduc de Belleville). La poursuite de l'étude devra inclure l'analyse de la roche mère de la carrière de la Brasserie ainsi que celle du sol sus-jacent. La fraction importante de carbone mort mise en évidence pour Bras 1 peut être un argument en faveur de processus géochimiques longs et complexes dans le sol et l'épikarst pour le site de la Brasserie.

5. Conclusion

Cette étude a permis de comparer trois spéléothèmes prélevés sur des sites très contrastés : un spéléothème d'une grotte du Sud de la France, un spéléothème d'aqueduc du Nord de Paris dans une zone urbanisée et un spéléothème d'une carrière parisienne, sous le bois de Vincennes. Les deux premiers échantillons avaient pu être datés par la méthode uranium/thorium malgré la présence de thorium détritique. Dans l'échantillon de la carrière parisienne, la méthode U/Th n'a pu être appliquée. La mesure du ^{14}C sur un dépôt actuel, montre une très forte proportion de carbone mort (~40 %) qui pourrait rendre difficile l'utilisation de cette méthode pour ce site, utilisée dans de nombreux cas pour les échantillons très récents (recherche du « pic des bombes » des années 1960s). La comparaison des spectres des terres rares des 3 échantillons montre que i) l'échantillon de la carrière parisienne sous le bois de Vincennes présente des teneurs comprises entre les fortes concentrations de l'échantillon « urbain » et les faibles concentrations de l'échantillon de grotte naturelle ; ii) tout comme l'échantillon de grotte, l'échantillon de carrière ne présente pas d'anomalie en cérium contrairement à celui du site urbain ; iii) pour deux échantillons sur trois, la concrétion calcaire de la carrière de Vincennes présente un enrichissement en terres rares légères (par rapport aux lourdes) pouvant être comparé à ceux observés en zone urbanisée (Belleville)

Des études complémentaires en cours dans le cadre de l'ANR HUNIWERS permettront de comparer ces spectres aux sources de terres rares potentielles (sol, encaissant). Nous pourrons ainsi déterminer si cette formation peut être utilisée comme une archive environnementale à l'image des spéléothèmes étudiés précédemment.

Références

BOURDIN C., DOUVILLE E., GENTY, D. (2011) Alkaline-earth metal and rare-earth element incorporation control by ionic radius and growth rate on a stalagmite from the Chauvet Cave, SE France. Chem. Geol. 290, 1–2), 1–11.

CULLERS R.L., BARRETT T., et al. (1987) Rare-earth element and mineralogic changes in Holocene soil and stream sediment: a case study in the Wet Mountains, Colorado, USA. Chemical geology, 63(3-4), 275-297.

DRUGAT L., PONS-BRANCHU E., et al. (2019) Rare earth and alkali metal elements in stalagmite, as marker of Mediterranean environmental changes during Termination I. Chemical Geology, 525, 414-423.

DUMOULIN JP. et al. (2017) Status report on sample preparation protocols developed at the LMC14 Laboratory, Saclay, France: from sample collection to 14C AMS measurement. Radiocarbon, 59(3), 713.

FAIRCHILD I.J., TREBLE P.C., (2009) Trace elements in speleothems as recorders of environmental change. Quaternary Science Reviews, 28(5), 449-468

FOHLMEISTER J., VOARINTSOA N. R. G., et al.. (2020) Main controls on the stable carbon isotope composition of speleothems. Geochimica et Cosmochimica Acta.

GENTY D., et al. (2001) Dead carbon in stalagmites : carbonates bedrocks vs ageing of soil organic matter. Implications for ^{13}C variations in speleothems. Geochimica et Cosmochimica Acta, 65 (20) : 3443-3457

GROMET LP., HASKIN L.A., et al. (1984) The "North American shale composite": Its compilation, major and trace element characteristics. Geochimica et Cosmochimica Acta, 48(12), 2469–2482.

HELLSTROM J., (2003) Rapid and accurate U/Th dating using parallel ion-counting multi-collector ICP-MS. Journal of Analytical Atomic Spectrometry, 18(11), 1346-1351

HUA Q. et al. (2013) Atmospheric radiocarbon for the period 1950–2010. Radiocarbon 55(4):2059–72.

LABEYRIE J., DUPLESSY J.C., et al. (1967) Study of temperatures prevailing in ancient times by measurement of the oxygen-18, carbon-13 and carbon-14 content of concretions in caves. In Radioactive dating and methods of low-level counting.

LI W.X., et al., (1989) High-precision mass-spectrometric uranium-series dating of cave deposits and implications for palaeoclimate studies. Nature, 339(6225), 534-536.

PONS-BRANCHU E., DOUVILLE E., et al. (2014) A geochemical perspective on Parisian urban history based on U-Th dating, laminae counting and yttrium and REE concentrations of recent carbonates in underground aqueducts. Quater. Geochron. 24, 44-53.

PONS-BRANCHU E. DOUVILLE E., et al. (2014) A geochemical perspective on Parisian urban history based on U-Th dating, laminae counting and yttrium and REE concentrations of recent carbonates in underground aqueducts. Quaternary Geochronology 24, 44-53.

PONS-BRANCHU E., BERGONZINI L., et al. (2018) ^{14}C in urban speleothem-like deposits: a new tool for environmental study. Radiocarbon 60(4):1269-1281.

Le remplissage de l'aven du Devès de Reynaud (St-Remèze, Ardèche, S-E France) : rôle du karst dans la conservation des indicateurs sédimentologiques d'un enregistrement chronostratigraphique pléistocène

Simon PUAUD[1], Yves BILLAUD[2], Olivier TOMBRET[1-3], Laurent CREPIN[1], Mélanie LEPENANT[1], MASC[4], Antoine ZAZZO[3], Jean-Jacques BAHAIN[1], Christophe FALGUERES[1], Matthieu LEBON[1], Lisa GARBE[1], Évelyne DEBARD[5], Jean-François PASTRE[6]

(1) UMR 7194 HNHP (CNRS, MNHN, UPVD) / Département Homme & Environnement MNHN. Musée de l'Homme 17, place du Trocadéro F-75 116 Paris – France. puaud@mnhn.fr (corresponding author), otombret@mnhn.fr, laurent.crepin@mnhn.fr, melanie.lepenant@gmail.com, jean-jacques.bahain@mnhn.fr, falgueres@mnhn.fr, lebon@mnhn.fr, lisagarbe@hotmail.fr

(2) UMR 5138 arar (CNRS, Univ. Lyon 2, UCBL Lyon 1). DRASSM 147, place de l'Estaque F-13 016 Marseille – France. yves.billaud@culture.gouv.fr

(3) UMR 7209 AASPE (CNRS, MNHN) / Département Homme & Environnement MNHN. 55, rue Buffon F-75 005 Paris – France. otombret@mnhn.fr, antoine.zazzo@mnhn.fr

(4) Montélimar Archéo-Spéléo-Club, Service de la Vie Associative 1, avenue Saint-Martin F-26 200 Montélimar – France. audouard.jean-jacques26@orange.fr

(5) 25, rue Paul Chevrel F-69 370 Saint-Didier-au-Mont-d'Or – France. evelyne.debard@free.fr

(6) UMR 8591 LGP-Environnements Quaternaires et Actuels (CNRS, Univ. Paris 1, UPEC). Bâtiment Y, 1, place Aristide Briand F-92 195 Meudon – France. jean-françois.pastre@lgp.cnrs.fr

Résumé

L'intérêt du remplissage de l'aven du Devès de Reynaud est reconnu depuis la fin du XIXème siècle. Ces dépôts ont été exploités, comme dans d'autres cavités de la région pour leur contenu en ossements (« la ruée vers les phosphates »). La stratigraphie actuellement accessible, outre son contenu paléontologique, montre 2 niveaux de retombées volcaniques. Ces téphras constituent 2 rares indicateurs exceptionnellement conservés par le karst, de l'activité de la province volcanique du Vivarais. Le montage du projet TéphrArd (2019) a rendu possible une mission destinée à relever cette séquence et à en effectuer le prélèvement pour établir son cadre chronostratigraphique : en précisant la nature et le contexte de mise en place des dépôts ; en contraignant chronologiquement la séquence, il existe plusieurs types de support de datation (os, dents, sédiments, spéléothèmes) ; en apportant de nouveaux éléments paléoenvironnementaux par l'étude des restes fauniques. Les dépôts caractérisent le fonctionnement d'un cours d'eau hypogé peu compétent, laissant peu de place à la dynamique gravitaire. Les téphras occupent une position secondaire. La chronologie couvre une période discontinue depuis les MIS 9/10 jusqu'à la fin du Pléistocène.

Abstract

The Devès de Reynaud infilling (St-Remèze, Ardèche, SE France): role of the karst in the conservation of the sedimentary indicators of a Pleistocene chronostratigraphical record. The interest of the Devès de Reynaud infilling is known since the end of the 19th century. The infilling has been exploited, like in other caves of this area for their bone richness ("phosphate rush"). The currently outcropping stratigraphic sections contain not only faunal remains but 2 volcanic ash falls too. These tephras are 2 scarce indicators of regional volcanic activity, exceptionally preserved by the karst. With the TephrArd's project (2019), it has been possible to organize a field mission into the Devès de Reynaud Cave. The aims were to study and sample sections to establish the infilling's chronostratigraphic frame by characterizing sediments and their depositional conditions; to constrain chronologically the sequence, using the different dating supports available (bones, teeth, sediment, speleothems); and to provide new paleoenvironmental elements through the study of faunal remains. Sediments result of underground stream dynamic with low competence. Sediments deposited by gravity are uncommon. Tephras are in secondary position. Chronology covers a discontinuous period from MIS 9/10 until the end of Pleistocene.

1. Introduction

L'aven du Devès de Reynaud est situé sur la commune de Saint-Remèze (1,5 km au SO de ce bourg) en Ardèche (Fig. 1). Il s'ouvre sur le plateau éponyme, dans les calcaires du Crétacé inférieur (Urgonien) à l'altitude de 385 m.
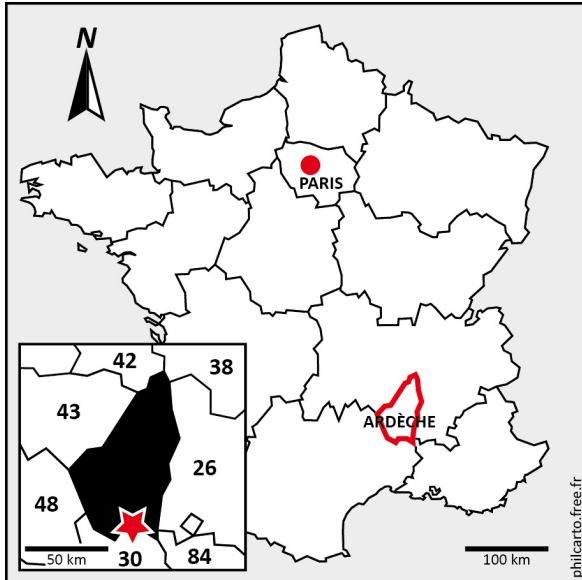

Figure 1 : Le département de l'Ardèche est situé au sud-est de la France. L'aven du Devès de Reynaud (étoile rouge) est localisé à l'extrême sud de ce département en rive gauche des gorges de l'Ardèche qui fait face à la rive gardoise.

Cette cavité est un puits, haut de 58 m recoupant un réseau horizontal à -36 m. À son extrémité sud, une salle contenait un important remplissage qui a livré au cours du dernier quart du XIXème siècle 1 tonne d'ossements de faune quaternaire et 2 retombées volcaniques (Fig.2). MARTEL (1894) relate la descente dans l'aven du préhistorien de Vallon-Pont-d'Arc, Ollier de Marichard. CHANTRE (1901) énumère les taxons fossiles qui ont pu être sauvés de l'aven. Les mineurs semblent avoir aménagé les parois du gouffre pour y installer des structures permettant d'y descendre aisément (BIGOT, 2015). L'épuisement du gisement fait oublier le gouffre. R. de Joly l'explore en 1937 (DE JOLY, 1937) sans retrouver de fossile malgré les fouilles entreprises (au mauvais endroit !). Le gouffre reste néanmoins bien connu des habitants puisqu'il « sert depuis un temps immémorial de dépotoir municipal ! [où] l'odeur est difficilement supportable et rend l'exploration très pénible. » (TRÉBUCHON, 1956). À la fin des années 1970,

l'un de nous (YB) effectue la topographie de l'aven (BILLAUD, 1978). Il y retrouve de la faune et découvre les 2 niveaux de téphra. GUÉRIN (1980) l'attribue à la MNQ 26 (Pléistocène supérieur). L'analyse de la composition du téphra supérieur suggère à J.-F. Pastre que cette retombée provient de l'éruption phréatomagmatique d'un maar de la province vivaroise (DEBARD & PASTRE, 2008).

Figure 2 : Aven du Devès de Reynaud, salle des téphras. La coupe inférieure montre, dans sa partie inférieure l'impressionnante couche de sable noir interstratifiée dans les sédiments limoneux. Le géochronologue donne l'échelle. Cliché Projet TéphrArd 2019.

C'est dans le sillage de ces travaux préliminaires que le projet TéphrArd a été déposé en 2019, dans le cadre de l'AAP fédérateur du Département Homme & Environnement du Muséum national d'histoire naturelle. La finalité de cette étude est de contextualiser le remplissage conservé dans la salle d'où ont été extraits les ossements et dans laquelle on observe encore actuellement les 2 téphras : à partir de l'analyse sédimentologique des dépôts, essayer de comprendre leur mode de mise en place et de restituer un cadre chronologique grâce à la datation des différents supports de datation. L'apport des données obtenues à partir de l'étude des restes fauniques doit également contribuer à cette étude en apportant des éléments d'ordre paléoenvironnemental et (bio)-chronologique.

Le projet a pu financer une mission sur le terrain ainsi que plusieurs datations (^{14}C, U-Th, ESR sur dent).

Cette étude souligne le rôle considérable du karst dans la conservation des séquences sédimentaires.

2. Matériels et méthodes

Le projet TéphrArd s'appuie sur deux éléments essentiels : une mission de terrain qui a permis non seulement de fournir les matériaux destinés aux analyses mais également de permettre de faire le relevé des 2 coupes stratigraphiques de ce qui reste du remplissage sédimentaire ainsi que d'effectuer les observations associées. Le second élément du projet a consisté à l'analyse du matériel au laboratoire : analyses sédimentologiques,

géochronologiques (datations) et paléontologiques. Les résultats tirés de ces dernières feront l'objet d'un article dans ces mêmes actes par l'une d'entre nous (M. Lepenant).

L'intégralité des échantillons a été prélevée lors de la mission réalisée sur le terrain en janvier 2019. Il s'agissait de sédiments, de spéléothèmes et de restes fauniques (os et dents). Les sédiments ont été préparés pour être analysés

par diffraction laser au granulomètre Malvern Mastersizer 2000. Les datations ont été réalisées sur 3 types de support : ossements par la méthode de ^{14}C, spéléothèmes par la méthode des séries de l'uranium (U-Th) et dents d'herbivores (ESR : résonnance électronique de Spin, traitement en cours).

Les analyses ont été réalisées dans les laboratoires de l'UMR 7194 HNHP (Musée de l'Homme et Institut de Paléontologie humaine) pour la sédimentologie, les séries de l'U, le dosage du collagène des os et les datations ESR. Les échantillons destinés aux datations ^{14}C ont été préparés à l'UMR 7209 et mesurés au LSCE (UMR 8212).

3. Résultats

La stratigraphie du remplissage (Fig. 3)

La salle où sont conservés les restes du remplissage a été vidée dans sa quasi-totalité par les ouvriers phosphatiers à la recherche d'ossements. Il subsiste néanmoins 2 témoins séparés par un hiatus de près de 5 m. Chacun d'eux contient une intercalation de sables noirs.

La coupe inférieure est constituée par un ensemble de matériaux fin à rares passées de granules calcaires. On observe une succession de niveaux argilo-limoneux finement lités dans lesquelles se trouve le téphra inférieur (TI). Il s'agit de sables noirs atteignant une épaisseur de 30 à 40 cm, de texture fine à moyenne très bien triés et finement lité. Sa teinte sombre trahit l'abondance du verre volcanique. La qualité du tri et les structures sédimentaires observées montrent qu'il s'agit de retombées volcaniques remobilisées dans le karst par la dynamique fluviatile comme le montre également les autres dépôts de cette séquence. Des arrêts de sédimentations sont marqués par la précipitation de deux planchers stalagmitiques. Les niveaux limono-argileux contiennent 2 zones où se concentrent les ossements.

La coupe supérieure présente une organisation comparable : succession argilo-limoneuse, passées sableuses, le téphra supérieur (TS), peu épais (5 cm) et 3 lits d'ossements. Un plancher stalagmitique clôt la séquence.

Les téphras

Ces 2 dépôts ont une granulométrie (sables bien triés) et une composition comparable (verre sombre et minéraux du socle : quartz, micas). Ces caractéristiques comme celle de la géochimie du verre (DEBARD & PASTRE, 2008) rapprocheraient ces retombées de l'activité phréatomagmatique de la province volcanique du Vivarais.

Les datations (Fig. 4)

La chronologie de la séquence établie à partir des datations actuellement disponibles (^{14}C et U-Th) s'étendrait au-delà des MIS 9/10 et jusqu'à la fin du Pléistocène.

D'après les chronologies établies pour le volcanisme vivarois (GUÉRIN & GILLOT, 2007 ; SASCO *et al.*, 2017) : TI se placerait dans la phase la plus ancienne (> 150 ka) et TS dans les phases les plus récentes (< à 45 ka).

Figure 3 : Coupe stratigraphique synthétique du remplissage de la salle des téphras. Les 2 coupes présentent des faciès limono-argileux où la fraction grossière est rare et où 2 téphras sont interstratifiés (TI : 7 et TS : 27). La coupe supérieure repose sur une coulée stalagmitique. La coupe inférieure, topographiquement sous la coulée est stratigraphiquement au-dessus (pas d'inversion U-Th 1/4). Prélèvements géochronologiques (étoiles) : rouges (U-Th), jaunes (^{14}C), bleu (ESR).

© Y. Billaud (TéphrArd, 2019)
© S. Puaud-TéphrArd, 2019
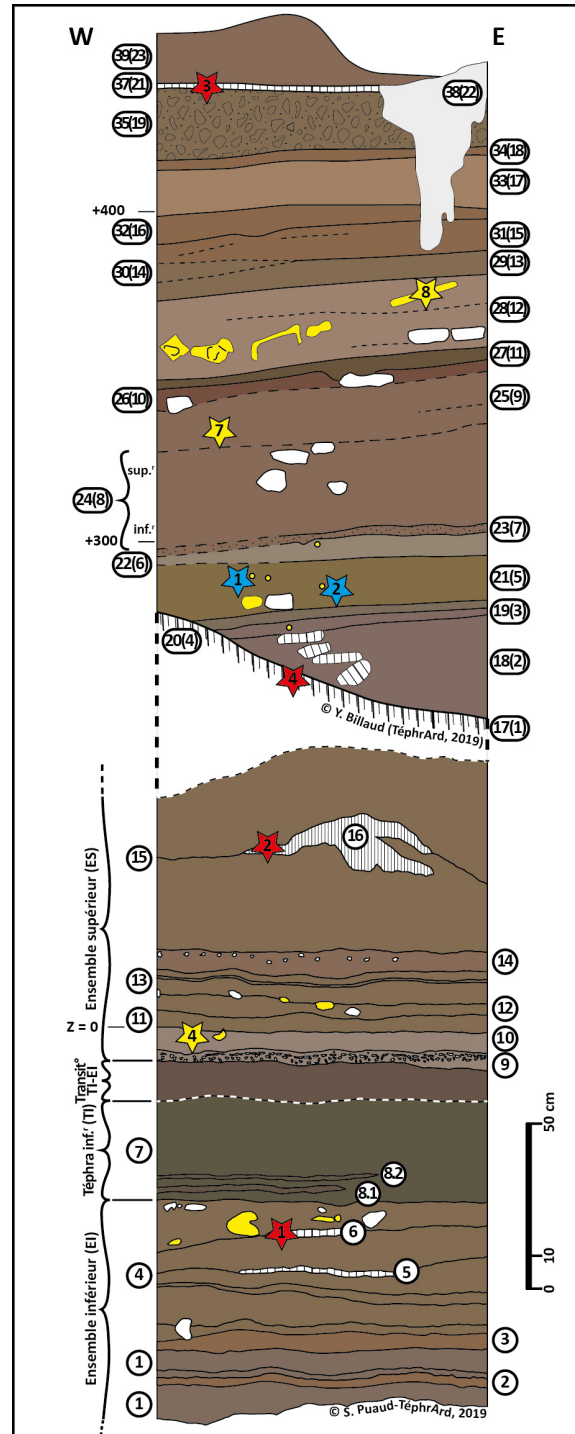
¹⁴C collagène (os)	Codes		Échantillon	Âges		
	ECHoMICADAS	Muséum		yr BP	± 1σ	date calibrée (2σ)
	2676.1.1	MUSE19105	PC14-4	> 45 000	-	-
	2677.1.1	MUSE19106	PC14-7	44 340	665	47 381-44262
	2678.1.1	MUSE19107	PC14-8	41 420	465	43 804-42 098
U-Th spéléothème (calcite)	Échantillon		Âge	+ Erreur -		Âge corrigé
	DdR2019-PUTh1		357 598	165 620	59 313	348 140	355 058
	DdR2019-PUTh2		70 926	2775	2669	59 820	67 402
	DdR2019-PUTh3		14 403	409	407	10 949	13 354
	DdR2019-PUTh4		> 479 923	-	-	-	-

Figure 4 : Résultat des datations effectuées à l'aven du Devès de Reynaud. Les datations ESR sur les tissus dentaires n'ont pas encore livré leur résultat. Tous ces résultats sont localisés sur la coupe stratigraphique de la figure 3.

4. Synthèse et conclusions

L'aven du Devès de Reynaud, situé sur la commune de Saint-Remèze en Ardèche méridionale, conserve dans une salle annexe à son puits d'entrée un remplissage sédimentaire conservant des témoins exceptionnels. Les restes fauniques qui ont rendu cet aven célèbre (voir la communication de M. Lepenant dans ces actes) ont donné notamment des restes de mammouth ou d'hyène. Outre ces témoins fossiles, les coupes encore présentes sur le site montrent 2 niveaux très nets de téphras. Ces retombées volcaniques constituent de très rares témoins des manifestations volcaniques de la province vivaroise. Quoique repris légèrement par la dynamique fluviatile, ces dépôts sont parfaitement caractérisables. Leurs caractéristiques géochimiques, minéralogiques et granulométriques permettent de les attribuer à la phase la plus ancienne et celle la plus récente de l'activité de cette province.

La mise en place de la séquence du Devès doit une part importante à l'activité du karst. Celle-ci se traduisant par l'accumulation des dépôts par le biais d'une rivière souterraine. L'étude des sédiments montre le peu de compétence du cours d'eau : le karst se comble de sédiments fins.

Une question majeure restée en suspens est celle du point d'entrée des ossements. S'agit-il d'un aven-piège ? La salle des téphras est à l'aplomb d'une cheminée actuellement obturée. Néanmoins aucun dépôt corrélatif ne se trouve associé à cette morphologie (cône d'éboulis). Il est également difficile d'invoquer uniquement la dynamique fluviatile afin d'expliquer une telle accumulation d'ossements à cet endroit. Cette question traduit la complexité du fonctionnement de cette cavité.

Remerciements

Références

BIGOT J.Y. (2015) Traces & indices. Enquête dans le milieu souterrain. Contribution à la spéléo-archéologie et à la géoarchéologie. J.-Y. Bigot, Montpellier, 194 p.

BILLAUD Y. (1978) Le plateau de Saint-Remèze. Les nouvelles du M.A.S.C., Bull. MASC (11).

CHANTRE E. (1901) L'Homme quaternaire dans le bassin du Rhône. Étude géologique et anthropologique. Ann. Univ. Lyon (nelle sér., I : Sciences, Médecine) (4) 189 p.

DEBARD É., PASTRE J.F. (2008) Nouvelles données sur les téphras pléistocènes piégés dans les remplissages karstiques ardéchois (SE France). Quaternaire 19(2) 107-116.

GUÉRIN C. (1980) Les rhinoceros (Mammalia, Perissodactyla) du Miocène terminal au Pléistocène supérieur en Europe occidentale. Comparaison avec les espèces actuelles. Doc. lab. géol. Lyon, Univ. Lyon 1 (79) 1182 p.

GUÉRIN G., GILLOT P.-Y. (2007) Nouveaux éléments de chronologie du volcanisme pléistocène du Bas-Vivarais (Ardèche, France) par thermoluminescence. C.R. Géoscience, 339, 40-49.

JOLY (de) R. (1937) Compte-rendu sommaire des explorations faites par divers groupes de la Société Spéléologique de France en 1937. Bull. Spéléo-Club Fr. (Spelunca 2ème sér.) (8) 26-39.

MARTEL É.-A. (1894) Les Abîmes. Éditions Charles Delagrave, Paris VIII-578 p.

SASCO R., GUILLOU H., NOMADE S., SCAO V., MAURY R.-C., KISSEL C., WANDRES C. (2017) ^{40}Ar/^{39}Ar and unspiked ^{40}K-^{40}Ar dating of upper Pleistocene volcanic activity in the Bas-Vivarais (Ardèche, France). J. Volcanol. Geotherm. res., 341, 301-314.

TRÉBUCHON J.C. (1956) Étude spéléologique de la basse Ardèche (commune de Vallon-Pont-d'Arc, Saint-Remèze et Bidon). Annales de spéléologie 11(1) 27-44.

Le remplissage de la grotte de Laang Spean (province de Battambang, Cambodge) : une archive sédimentaire témoin de l'activité du karst et un enregistrement de l'anthropisation en contexte tropical humide au cours du Pléistocène et de l'Holocène

Simon PUAUD[1], Hubert FORESTIER[1], Heng SOPHADY[2], Olivier TOMBRET[1], Christophe FALGUÈRES[1], Valéry ZEITOUN[3], Henry BAILS[1], Cécile MOURER-CHAUVIRÉ[4], Roland MOURER[5]

(1) UMR 7194 Histoire naturelle de l'Homme préhistorique (HNHP) CNRS-MNHN-UPVD, Musée de l'Homme, 17, place du Trocadéro, 75 116 Paris, France, puaud@mnhn.fr (corresponding author), hubforestier@gmail.com, otombret@mnhn.fr, falgueres@mnhn.fr, baills@orange.fr

(2) Ministère de la Culture et des Beaux-arts du Cambodge, 227 Kbal Thnal, boulevard Preah Norodom, Sangkat Tonle Bassac, Khan Chamkar Mon 12305, Phnom Penh, Cambodge, hsophedy@yahoo.com

(3) UMR 7207 Centre de Recherche Paléontologie-Paris (CR2P) CNRS-MNHN-Sorbonne université, Université Pierre et Marie Curie, Tour 46-56, case 104, 4, place Jussieu, 75 252 Paris Cedex 05, France, pythecanthro@gmail.com

(4) UMR 5276 Laboratoire de Géologie de Lyon Université Lyon 1-CNRS, 2 rue Dubois, 69 622 Villeurbanne Cedex, France, cecile.mourer@univ-lyon.fr

(5) 3, rue Julien, 69 003 Lyon, France, roland.mourer@online.fr

Résumé

La région de Battambang est avec celle de Kampot l'autre grand secteur karstique du Cambodge. Le démantèlement de l'épaisse formation carbonatée permienne des « calcaires ouraliens » n'a laissé aujourd'hui que des morphologies résiduelles : les phnoms. Situé à mi-chemin entre Battambang et la frontière thaïe, le phnom Teak Treng, est parcouru par 14 cavités. La plus vaste : Laang Spean (« la grotte des ponts ») est devenue un site préhistorique majeur de l'Asie du Sud-est continentale. La Mission Préhistorique Franco-Cambodgienne poursuit depuis 10 années les travaux initiés par les époux Mourer, à l'origine de la fouille du site dans les années 60. La salle centrale de cette immense caverne a livré un remplissage sédimentaire dépassant 10 mètres de puissance. Il constitue une archive sédimentaire qui a enregistré les modifications paléoenvironnementales et les conséquences d'événements géologiques régionaux depuis près de 400 ka. Outre cet enregistrement conservé par le karst, la stratigraphie livre, 4 niveaux d'occupation : les 2 niveaux les plus anciens (outils frustes sur calcaire et industrie sur silicifications) sont mal caractérisés, les niveaux hoabinhien (11-5 ka BP) et néolithique (~3 ka BP), sont abondants. Ils ont permis de définir une véritable aire d'habitat et un lieu d'inhumation.

Abstract

The Laang Spean Cave (Battambang Province, Cambodia): Pleistocene-Holocene karstic and anthropic records in a wet tropical context. Battambang and Kampot provinces are the main Cambodian karstic areas. The dismantling of the thick Permian carbonate formation of «Uralian limestones» has left some residual morphologies: the phnoms. Located halfway between Battambang and the Thai border, the phnom Teak Treng, is crossed by 14 cavities. The largest: Laang Spean («the cave of the bridges») has become a major prehistoric site of South-East Asia. Since 10 years, the Franco-Cambodian Prehistoric Mission has been continuing the work initiated by the Mourer spouses, who excavated the site in the 1960s. The central room of this immense cavern has a sedimentary filling exceeding 10 meters in thickness. It is a sedimentary archive that has recorded paleoenvironmental changes and the consequences of regional geological events since nearly 400 ka. Besides this sedimentary record controlled by karstic activity, there are 4 levels of occupation: the 2 oldest levels with chipped stone tools on limestone and local silicifications. These are poorly characterized. Hoabinhian levels (11-5 ka BP) and Neolithic (~3 ka BP) are abundant. They allowed us to define real habitat area and a place of burial.

1. Introduction : le site

Laang Spean (*grotte des ponts* en khmer) est située au Cambodge (Fig. 1A), au nord-ouest du royaume, dans la province de Battambang. Depuis cette ville, on suit la RN10 vers la Thaïlande jusqu'au village de Sdao. La grotte est à 5 km à l'ouest du village (Fig. 1B).

Cette cavité se développe à travers le phnom Teak Treang (Fig. 2). Le terme phnom désigne au Cambodge les reliefs (pas toujours karstiques) qui émergent de la plaine. L'exploration spéléologique de ce petit massif de calcaire attribué au Permien a montré l'existence d'un ensemble de 14 cavités (LAUMANNS, 2019). Très peu d'entre elles ont livré du matériel archéologique ; ces cavités ayant été fréquentées par les moines qui s'y installent en ermite ou bien par les villageois qui ont exploité et utilisé les remplissages sédimentaires comme fertilisants.

Celui du gisement de Laang Spean est resté vierge jusqu'à la reconnaissance de sa richesse archéologique par les époux Mourer en 1964. Fouillé lors de 3 campagnes il livrait alors les témoins inédits de l'activité des derniers chasseurs cueilleurs hoabinhiens et de leurs successeurs néolithiques (MOURER & MOURER, 1973 ; MOURER, 1994). La reprise du site, en 2009, par la Mission Préhistorique Franco-Cambodgienne (MPFC) (SOPHADY, 2014) a permis non seulement de mettre au jour des aires d'activité attribuées aux hoabinhiens (FORESTIER *et al.*, 2016), de riches sépultures néolithiques (ZEITOUN *et al.*, 2012 ; SOPHADY, 2016 ; SOPHADY *et al.*, 2016) mais également de découvrir des industries lithiques insoupçonnées obtenues à partir de matières 1ères locales (silicifications et calcaire). Outre ces découvertes, les dimensions imposantes de la cavité : il s'agit d'un couloir dépassant 60 m de long, 20 m de large où la voûte peut culminer à 30 m et la puissance de son remplissage, le substrat a été atteint 13,6 m sous la surface, classent désormais la grotte de Laang Spean parmi les grandes séquences du Pléistocène et de l'Holocène de l'Asie du Sud-Est continentale.
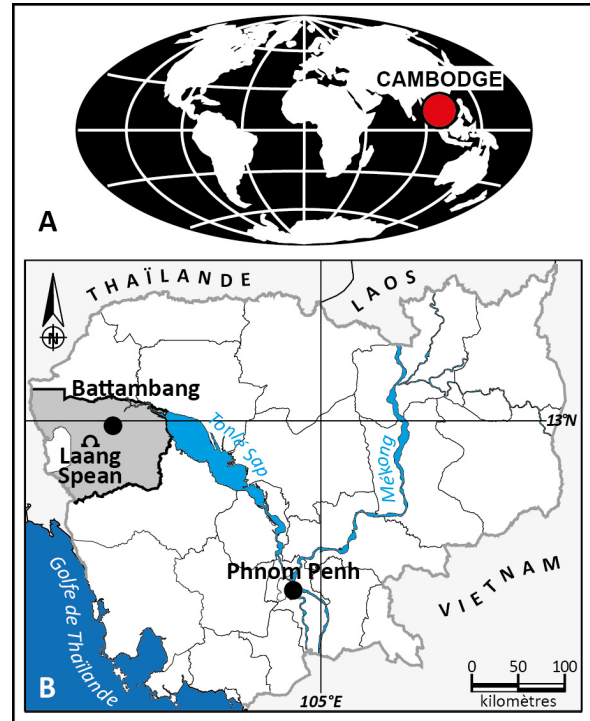

Figure 1 : Localisation du site préhistorique de Laang Spean. A) Le Royaume du Cambodge forme la partie ouest de l'extrémité de la péninsule indochinoise. B) La grotte est située à l'ouest du pays, près de la ville de Battambang entre le Grand Lac (Tonlé Sap) et la frontière thaïlandaise.
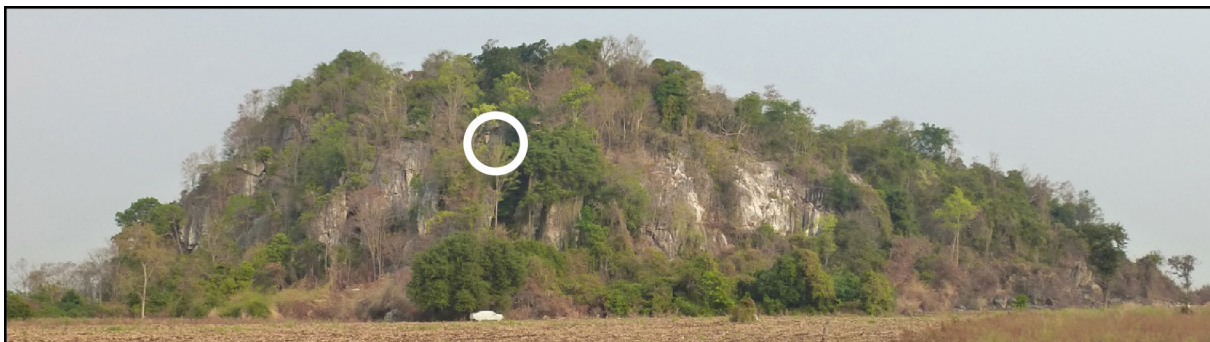

Figure 2 : Vue panoramique du Phnom Teak Treang. Cette morphologie karstique résiduelle abrite la grotte de Laang Spean dont l'entrée, dissimulée par la végétation, est approximativement située au niveau du cercle blanc. Ce relief abrite 13 autres cavités de moindre développement. Peu d'entre elles ont livré du matériel archéologique car les remplissages de ces cavités ont été très bouleversés (aménagement par les moines, vidange par les villageois). (Crédit photo S. Puaud / MPFC 2014)

2. Matériels et méthodes : la fouille

La fouille du site a été entreprise dans la partie centrale de la grotte (salle 2) à l'emplacement des premiers travaux. Son extension s'est effectuée selon un axe transversal (largeur de la salle). Un puits a été foncé en son centre afin de reconnaître l'intégralité de la séquence des dépôts. La stratigraphie a ainsi révélé une épaisseur atteignant 13,6 m.

Le rôle du karst est à souligner car il est à l'origine du piégeage puis de la conservation des ensembles stratigraphiques. Son activité est également responsable d'une grande partie du dépôt du remplissage sédimentaire. On observe non seulement des spéléothèmes mais aussi des dépôts fluviatiles liés à l'activité d'un cours d'eau hypogé.

3. Résultats : la stratigraphie du remplissage sédimentaire

La stratigraphie du remplissage de Laang Spean comporte 30 unités (couches) qui se répartissent en 3 grands ensembles. Chacun de ces ensembles marque un changement dans les conditions de sédimentation.

L'assise sur laquelle repose la pile sédimentaire est constituée par le substratum calcaire. Ces carbonates marins sont attribués au Permien (FONTAINE, 2002). Ils sont recouverts en partie par un faciès carbonaté grisâtre pétris de perles de cavernes (couche 29) ou bien d'une épaisseur métrique de spéléothème (coulée stalagmitique, couche 28). Le spéléothème moule le substratum. Á sa surface, se développe un cortex d'altération noir d'une épaisseur de plusieurs millimètres. Il peut montrer une structure microlaminée où alternent des lits noir et blanc. L'altération affecte, par place, profondément le spéléothème puisque si l'on distingue encore les prismes de la calcite, ceux-ci sont devenus mats. Le faciès devient poreux et friable, il prend un aspect crayeux. Les sédiments de la couche 27 viennent recouvrir l'ensemble des faciès précédent. Il s'agit de sédiments très sombres, dépourvus de fragments grossiers, de structure sédimentaire et de texture sablo-limoneuse. Sa géométrie est complexe car ces dépôts s'observent de part et d'autre du spéléothème, l'intégrant à la faveur de cavités ou le recouvrant.

Le 1er ensemble s'observe entre 10 et 8 mètres de profondeur. Il s'agit d'un ensemble de sédiments sablo-limoneux pauvres en fraction grossière (calcaire, pulvérulent, portant un cortex noir) recouvre l'assise. Il s'y distingue 7 faciès superposés (couches 26 à 20), limités par des contacts érosifs. Outre le cortex noir de la fraction grossière, les transformations chimiques ont affecté le toit de la couche 26. La précipitation des oxy-hydroxydes de fer dans la porosité du faciès sableux est à l'origine des grès de la couche 25.

Le 2ème ensemble s'étend au-delà des couches 21/20, entre 8 et 5 mètres de profondeur. C'est un ensemble de sédiments aux faciès monotones de limons argileux. La base (couche 19) est plus argileuse, puis les sédiments deviennent plus limoneux (couche 18). Dans cet ensemble, les pierres ont perdu leur cortex noir d'altération.

Le 3ème ensemble se développe à partir de -5 m et jusqu'à la surface. La séquence stratigraphique est alors constituée par un ensemble de limons sableux carbonatés (25 % de $CaCO_3$). La fraction grossière devient de plus en plus abondante. Ces dépôts ont enregistré les modifications morphologiques de la grotte. Après un dernier témoin du fonctionnement karstique de la cavité, avec la précipitation du plancher stalagmitique 15/14, la présence de blocs, au-delà de la couche 14, témoigne de l'effondrement de la voûte de la cavité (Fig. 3).

Figure 3 : Vue de Laang Spean depuis l'entrée de la grotte. Le chantier est au 1er plan. Les parois, très dégradées, conservent néanmoins quelques coulées et draperies. Au second plan, l'effondrement du toit est à l'origine des fenêtres et du « pont ». (Crédit photo S. Puaud / MPFC 2015)

Ces changements majeurs ont modifié le mode de sédimentation et la nature du remplissage. C'est également dans cet ensemble que les témoins anthropiques deviennent abondants. Le remplissage est scellé par le dépôt d'écailles de calcaire résultant de la desquamation des parois de la cavité.

4. Synthèse et conclusion

Actuellement, une stratigraphie de 13,6 m a pu être reconnue dans la grotte de Laang Spean. Cette accumulation représente un fait exceptionnel qui rappelle et confirme le rôle prépondérant du karst dans la conservation des archives sédimentaires (MAIRE & POMEL, 1994), dont certaines, par leur rareté (téphras), pourraient s'avérer être des témoins uniques d'événements géologiques majeurs ayant un eu un impact global. La variabilité des faciès des dépôts observée à Laang Spean traduit la diversité des dynamiques sédimentaires responsables de la mise en place du remplissage. Ces dynamiques sont contraintes par les conditions environnementales qui se sont succédé dans la cavité et sa région depuis près de 400 000 ans. Cette date a été obtenue à partir de l'analyse isotopique (U-Th) de la calcite du spéléothème recouvrant le substratum calcaire formant l'assise des dépôts détritiques postérieurs.

Aujourd'hui, le phnom, ses cavités, Laang Spean et son remplissage en particulier sont complètement déconnectés de la plaine qu'ils surplombent de plusieurs 10aines de mètres. L'isolement de ces 2 entités (phnom et plaine) est consécutif à l'abaissement drastique du niveau de base du

réseau hydrographique. Ses fluctuations sont reliées à celles du niveau marin (eustatisme) qui ont pour origine la cyclicité climatique glaciaire / interglaciaire (glacio-eustatisme). Dans le cas du contexte géologique régional de la péninsule indochinoise on ne peut négliger l'influence de la tectonique himalayenne et son rôle tectono-eustatique (DEMANGEOT & SCHNEIDER, 1971 ; CARBONNE, 1972 ; TAPPONNIER *et al.*, 1990 ; HUTCHISON, 2014). En effet, l'assise, le 1er et le 2ème ensemble sont le résultat de l'activité du karst. Ce fonctionnement implique que la plaine se situait au-dessus de son niveau actuel. La variation du niveau de base est à l'origine de l'arrêt progressif de l'alluvionnement karstique et de l'érosion de la plaine. L'effondrement du plafond de la cavité, qui a permis en outre de sceller le remplissage et de le préserver de l'érosion, peut également être consécutif à cette variation : le dégagement du phnom et son assèchement entraînent la détente de ses parois prédisposant ainsi la cavité à s'ébouler.

Ces premiers jalons sur l'interprétation de la séquence de Laang Spean réaffirment l'intérêt que peut susciter cette cavité. Si les témoins d'occupations préhistoriques confèrent au site une indéniable valeur patrimoniale, ses dépôts sédimentaires pourraient également devenir les marqueurs de grands événements géologiques d'ampleur régionale.

Remerciements

Références

CARBONNEL J.-P. (1972) Le IVaire cambodgien. Structure et stratigraphie. Mém. ORSTOM 60, Paris, 248 p.

DEMANGEOT J., SCHNEIDER B., (1971) Observation sur l'évolution du karst du Cambodge méridional. In: A. Semmel (ed.) Neue Ergebnisse der Karstforschung in den Tropen und im Mittelmeerraum, Karstsymposiums, Frankfurt, 1971. Erdkundliches Wissen, 32, 17-24.

FONTAINE H. (2002) Permian of Southeast Asia: an overview. J. Asian Earth Sci., 20(6), 567-588.

FORESTIER H., SOPHADY H., PUAUD S., CELIBERTI V., FRÈRE S., ZEITOUN V., MOURER CHAUVIRÉ C., MOURER R., THAN H., BILLAULT L. (2016) The Hoabinhian from Laang Spean Cave in its stratigraphic, chronological, typo-technological and environmental context (Cambodia, Battambang province). J. Archaeol. Sci.: Reports, 3, 194-206.

HUTCHISON C.S. (2014) Tectonic evolution of Southeast Asia. Bull. Geol. Soc. Malaysia, 60, 1-18.

LAUMANNS M. (2019) International Speleological Projects to Cambodia 1995/96–2017 (Provinces of Kampot, Siem Reap, Kampong Speu, Stoeng Treng, Banteay Meanchey, Odda Meanchey and Battambang). Berliner Höhlenkunliche Berichte, 77, 271 p.

MAIRE R., POMEL S. (1994) Enregistreurs et indicateurs de l'évolution de l'environnement en zone tropicale. Concepts et méthodologie. In : R. Maire, S. Pomel, J.-N. Salomon (dir.), Enregistreurs et indicateurs de l'évolution de l'environnement en zone tropicale. Presses universitaires de Bordeaux, Bordeaux, 11-26.

MOURER R. (1994) Contribution à l'étude de la préhistoire du Cambodge. Étud. thémat., EFEO, Paris, 1, 143-195.

MOURER C., MOURER R. (1973) Recherche sur le gisement préhistorique de Laang Spean, phnom Teak Treang, (Province de Battambang), Cambodge. Annales de l'Université royale des Beaux-Arts de Phnom Penh, 2, 25-44.

SOPHADY H. (2014) The case of Phnom Teak Treang and Laang Spean: the potential for World Heritage site nomination in Cambodia, the significance of the site for human evolution in Asia, and the need for international cooperation. World Heritage papers, UNESCO, Paris, 39, 166-183.

SOPHADY H. (2016) Archaeo-stratigraphy of Laang Spean prehistoric site (Battambang Province): a contribution to Cambodian prehistory. Th. Doct. MNHN, Paris, 470 p.

SOPHADY H., FORESTIER H., ZEITOUN V., PUAUD S., FRÈRE S., CELIBERTI V., WESTAWAY K., MOURER R., MOURER-CHAUVIRÉ C., THAN H., BILLAULT L., TECH S. (2016) Laang Spean cave (Battambang province): a tale of occupation in Cambodia from the Late Upper Pleistocene to Holocene. Quat. Int., 416, 162-176.

TAPPONNIER P., LACASSIN R., LELOUP P.-H., SHÄRER U., ZHONG DALAI, WU HAIWEI, LIU XIOHAN, JI SHAOCHENG, ZHANG LIANSHANG, ZHONG JIAYOU (1990) The Ailao Shan/Red River metamorphic belt: tertiary left-lateral shear between Indochina and South China. Nature, 343(6257), 431-437.

ZEITOUN V., FORESTIER H., SOPHADY H., PUAUD S., BILLAULT L. (2012) Direct dating of a Neolithic burial in the Laang Spean cave (Battambang Province, Cambodia): First regional chrono-cultural implications. C.R. Palevol, 11, 529-537.

Ice-free alpine caves during Pleistocene glaciations

Christoph SPÖTL[1], Jens FOHLMEISTER[2,3], Gabriella KOLTAI[1], Charlotte HONIAT[1], Gina MOSELEY[1], Martin TRÜSSEL[4] & MARC LUETSCHER[1,5]

(1) Institute of Geology, University of Innsbruck, 6020 Innsbruck, Austria, christoph.spoetl@uibk.ac.at (corresponding author)
(2) Potsdam Institute for Climate Impact Research, Telegrafenberg, 14473 Potsdam, Germany
(3) GFZ German Research Centre for Geosciences, Section Climate Dynamics and Landscape Development, Telegrafenberg, 14473 Potsdam, Germany
(4) Stiftung Naturerbe Karst und Höhlen Obwalden, 6065 Alpnach, Switzerland
(5) Swiss Institute for Speleology and Karst Studies (SISKA), 2301 La Chaux-de-Fonds, Switzerland

Abstract

Caves located above the timberline are characterised by low temperatures and the local presence of perennial ice accumulations. It is thus not surprising that early analyses of such high-elevation caves suggested that speleothem growth occurred primarily during climate periods at least as warm as the present interglacial. More recent studies confirm preferential formation of stalagmites and flowstones during comparably warm and humid climate epochs allowing vegetation and soil formation at these altitudes. Some caves, however, provide compelling evidence that speleothems also formed during much colder and less humid times of the Pleistocene, conditions which would lead to freezing conditions in the karst. This enigma of caves warm enough to allow the presence of liquid water and the growth of speleothems during glacial times can be resolved invoking the superposition of the caves by temperate glaciers.

This contribution provides a concise overview of how a glacier above a cave can lead to non-freezing conditions in the cave, how glacial-age speleothems can be identified, and what they tell us about the highly dynamic history of the long ice ages in the Alps.

Résumé

Grottes des Alpes non englacées durant les glaciations pléistocènes. Les grottes situées au-dessus de la limite de la forêt se caractérisent par de basses températures et par la présence locales d'accumulations pérennes de glace. Aussi n'est-il pas surprenant que les premières analyses de ces cavités d'altitude aient suggéré que la croissance des spéléothèmes avaient commencé lors de périodes au moins aussi chaudes que l'interglaciaire actuel. Des études plus récentes ont confirmé la formation des stalagmites et des planchers durant des époques au climat suffisamment chaud et humide pour permettre le développement de sols et de végétation à ces altitudes. Toutefois, certaines grottes recèlent des preuves convaincantes que des spéléothèmes se sont aussi formées durant des périodes plus froides et moins humides du Pléistocène, conditions favorables à la présence de gel dans les grottes. Cette énigme des grottes suffisamment chaudes pour que l'eau liquide y circule et pour que les spéléothèmes se forment pendant les périodes glaciaires peut être résolue si l'on pense que les massifs pouvaient être occupés par des glaciers tempérés.

Cette communication fait le point sur la façon dont un glacier surmontant une grotte peut créer les conditions de circulation d'eau, sur l'identification de spéléothèmes contemporains de périodes glaciaires et sur ce que ces spéléothèmes nous apprennent sur les dynamiques sur le long terme de l'englacement dans les Alpes.

1. Introduction

Alpine caves, i.e. caves located above the timberline, are commonly close to the 0°C isotherm. Climate cooling will therefore profoundly affect their microclimate and their hydrology. Severe climate deterioration will lead to three possible scenarios, mainly controlled by the regional hydroclimate and the local topography: (a) permafrost will develop in the catchment above the cave, (b) a temperate glacier will form on the karst terrain, or (c) a small ice cap frozen to the ground will develop on top of the karst. The first and third case may lead to perennial ice formation inside the karst.

Speleothems provide a direct record of drip water availability and hence ice-free conditions in the subsurface. An increasing number of studies utilising stalagmites and flowstones dated by U-series techniques reveals an unexpected pattern: speleothems in alpine caves are not restricted to interglacials of similar or greater warmth as the Holocene; they also formed during colder climate periods including stadials. In some caves such cold-climate speleothems appear in fact to be more abundant than warm-climate ones, although this may be due to the fact that glacial periods comprised some 85% of the time of the

last half million years while interglacials were underrepresented.

Paradoxically, non-freezing and hence ice-free caves during glacial periods can be explained by burial underneath glacier

2. Concept

In order to prevent an alpine cave from freezing during a cold climate, a temperate glacier has to be present on top of the cave. The base of such a glacier is at the melting point and meltwater available during the ablation season will find its way into the karstic subsurface. Warm-based glaciers dominate the alpine cryosphere today. They were also abundant during glacials and sculptured the mountains by carving U-shaped valleys and cirques, leaving behind smoothed and striated rock surfaces. The karst beneath such a glacier is prevented from freezing because of two processes, insulation from the winter chill by the snow, firn and ice blanket, and meltwater transferring latent heat during the summer into the karstic rock underneath the glacier. This meltwater can also entrain clastic sediment and may even result in paragenetic cave enlargement.

Speleothems are the best recorders of such periods of ice-free conditions in a karst system, provided that the galleries are not filled by sediment and/or seasonally flooded. Growth of speleothems at temperatures barely above the freezing point in a subglacial setting requires special conditions because of the absence of soil-derived carbon dioxide as the starting point for karstification. These conditions are met in rocks that contain finely disseminated pyrite. These microscopic sulphide crystals form early diagenetically in sediment that contains dispersed organic

ice. And if the host rock of the cave contains finely disseminated pyrite, common in dark grey limestones and marls, these times in the Pleistocene may be precisely registered by speleothems.

matter. This is commonly the case in grey limestones and dolomites and in particular in dark grey marls. In light grey carbonate rocks, however, pyrite is usually absent. Upon contact with water containing dissolved oxygen, pyrite weathers and gives rise to sulphuric acid which dissolves the carbonate rock. These redox reactions also take place when the catchment of the cave is unglaciated and covered by vegetation. During the warm climate regime, however, karst dissolution by pedogenic carbon dioxide overwhelms pyrite oxidation because of the abundance of soil carbon dioxide compared to the generally small amount of pyrite present in the host rock and its slow reaction kinetics.

To summarise this concept, alpine caves can stay above 0 °C and speleothem growth does not need to stop at the onset of climate cooling if a warm-based glacier covers the cave and pyrite is present in the host rock.

Unfortunately, modern subglacial caves are very rare in the Alps and we are unaware of monitoring data of such a system. The proof-of-concept, however, was provided already some four decades ago by a pioneering study of Castleguard Cave, a large cave that extends underneath the Columbia Icefield of the Canadian Rocky Mountains and features both active drip sites and speleothems (ATKINSON et al., 1983).

3. How to recognise « glacial » speleothems in alpine caves

There is currently no field-deployable instrument that allows determination of the age of a speleothem nor the climate conditions under which it formed back many thousands of years in the past. The answers to both questions can only be found via sophisticated laboratory analyses. There is, however, one field observation that provides a first hint on whether glacial-age speleothems can in principle be expected in a given cave, i.e. the presence of secondary gypsum. This evaporite mineral indicates the presence of sulphides in the host rock which give rise to dissolved sulphate in the seepage water upon oxidation. Gypsum precipitation requires evaporative concentration of these solutions, typically enhanced by the cave wind.

Five main lines of evidence exist to identify speleothems that formed in subglacial settings, i.e. without soil, during glacial climates. They are ideally applied in combination and these criteria cannot be transferred to other climate regions without significant adjustments.

Chronology

Speleothems can be accurately dated by U-series techniques. Although precision worsens with age and becomes poor beyond about half a million years, younger speleothems can be dated with very small uncertainty. This is further improved by obtaining multiple ages,

documenting the growth history of individual speleothems in detail. Comparing a speleothem or a growth period therein with well-established climate records provides an important first step to assess the climate of a given time interval registered by a speleothem. The most widely used reference for the Quaternary period (and beyond) are the Marine Isotope Stages (MIS), which are based on deep-sea sediments and are of global significance. Even-numbered stages designate glacials and if a stalagmite from an alpine cave formed e.g. during MIS 6, the penultimate glacial, then chances are high that this growth would not have been possible without a glacier covering the catchment.

Oxygen isotopes

A second line of evidence utilises the stable isotopic composition of oxygen of the speleothem calcite. This parameter is a function of the cave air temperature and the oxygen isotopic composition of the drip water. The main control in alpine caves is the latter which reflects the water that enters the karst and which itself carries climate information. Studying speleothems of different age and climate from a cave system allows the identification of the oxygen isotopic composition of warm-climate speleothems, e.g. those of Holocene age. Pleistocene speleothems with significantly lower oxygen isotope values from the same or

neighbouring caves are thus a strong indication that they formed during a considerably colder climate. If a cave today is already close to 0°C then it is difficult to explain speleothem growth during a colder climate without invoking superposition by a warm-based glacier.

Carbon isotopes

Probably the strongest argument in favour of speleothem deposition in a subglacial setting are stable carbon isotope values close to or even exceeding the values of the host carbonate rocks (which in the Alps are exclusively of marine origin and thus show characteristic carbon isotope values). The carbon isotope composition of speleothems is sensitive to the influx of carbon from the soil giving rise to negative values. Care must be taken if the rock overburden is very thick and/or the mean travel time of the drip water is long. Both factors buffer the carbon isotope signature of the drip water towards the higher host rock values and may disguise a soil provenance.

Petrography

Speleothems formed without a soil cover commonly, but not exclusively, are composed of dense crystalline and often semi-transparent calcite showing a very low abundance of impurities. This may seem counterintuitive considering the model of subglacial meltwater entering the karst. What this may indicate, however, is that subglacial speleothems are fed by seepage water using very slow flow routes, where the water is in contact with finely disseminated pyrite. In contrast, glacier meltwaters preferentially use fractures and larger karst conduits.

Growth rate

The model of very slow seepage as opposed to fracture flow feeding subglacial stalagmites is consistent with the observation that these speleothems may show extremely slow growth rates, down to about 1 micron per year (e.g., WENDT et al., 2020). In contrast, warm-climate stalagmites in alpine caves show rates of a few tens of microns up to about a tenth of a millimeter per year. Importantly, and in contrast to warm-climate speleothems, subglacial stalagmites do not exhibit systematic changes in growth rate across even large and abrupt climate transitions. This underscores the decoupling of calcite precipitation dynamics from surface conditions as long as liquid water is present in the subglacial karst system.

4. Case studies

Results from five caves in the Eastern and Western Alps are briefly summarised below. These caves developed in host rocks (limestone, marble) containing sulphides and detailed studies of speleothems have shown that the temperature in these caves remained above the freezing point even during some glacial periods.

Kleegruben Cave

The first duplicated record of stalagmites that very likely formed during times of glacier ice coverage emerged from Kleegruben Cave, Zillertal Alps, which opens at 2165 m. Today, the cave interior air temperature is 2.4°C. The stalagmites grew across stadial-interstadial climate shifts of MIS 3, including Heinrich 5, a major cold event in the North Atlantic realm (SPÖTL et al., 2006). There is no change in growth rate between interstadials and stadials but the oxygen isotope composition of the stalagmites registers these climate swings at high resolution.

Spannagel Cave

Located about 1 km south of Kleegruben Cave with the main entrance at 2524 m, this 12 km-long system yielded several stalagmites and flowstones that record growth at times when the nearby glacier was sliding over this cave. As recent as 1850 AD about two thirds of the cave was underneath the glacier tongue. Today's temperature in this cave is 1.8-2.2°C. Times when Spannagel Cave was covered by temperate glacier ice include MIS 3, 7, 8, 9 and 10 (SPÖTL & MANGINI, 2007). Interestingly, there are no records of glacial maxima (i.e. MIS 2 or 6). This might suggest that during these extreme periods the glacier above this high-alpine cave becomes partly cold-based.

Sieben Hengste cave system

This extensive system north of Lake Thun yielded a replicated set of stalagmites that grew continuously across MIS 2, broadly equivalent to the Last Glacial Maximum (LUETSCHER et al., 2015). Today's cave temperature at the sampling point is 4.2°C and its elevation is 1540 m (surface at 1755 m), i.e. about 1 km lower than at Spannagel Cave. The Sieben Hengste stalagmites record millennial-scale climate swings by their oxygen isotopic composition, while the carbon isotope values lack a soil signal. No change in growth rate occurred during millennial- to centennial-scale climate shifts. Speleothem deposition, however, ended abruptly at 14,700 years ago, precisely at the time of major northern hemispheric warming. This event most likely records the melting of the ice cover and the lack of soil on this barren land to promote karstification and warm-climate speleothem growth.

More recent work has shown evidence of a persistent talik, at least affecting some parts of this cave, during MIS 6, the penultimate glacial (HONIAT et al., 2018), as well as during parts of MIS 10 and 12 (M. LUETSCHER, unpublished data).

Klaus Cramer Cave

Located at 1964 m in the Allgäu Alps of Austria close to the border to Germany, today's air temperature in this cave is 1-2°C. A small stalagmite yielded a 17,400 year-long record covering the transition from the prominent Greenland Interstadial 19 to the long stadial equivalent to MIS 4. This is a time when the alpine glaciers advanced significantly, possibly even into their foreland. Deposition of this stalagmite continued uninterruptedly across this large

climate shift and shows no change in growth rate either (BOCH et al., 2011).

Ongoing research on other stalagmites yielded evidence of ice-free conditions in this cave also during earlier glacials, including MIS 10 and 12 (C. SPÖTL & G. MOSELEY, unpublished data).

Melchsee-Frutt cave system

A series of large caves is located between about 1300 and 2450 m in the Melchsee-Frutt region of central Switzerland

(mean cave air temperature 2.9°C). Drill cores as well as fully recovered stalagmites from three of these caves (Schratten cave, Betten cave, Neotektonik cave) yielded evidence of speleothem growth during interglacials including the Holocene but more abundantly during glacial periods: MIS 2, 3, 4, 5, 6, 8 and 10 (FOHLMEISTER et al., 2019, and unpublished data). The oxygen isotope records of these stalagmites register fine-scale climate swings and the carbon isotope signature attests a soil-free catchment, likely overlain by a temperate glacier during cold periods.

5. Conclusions

Speleothems from cold high-elevation caves are sensitive paleoenvironmental archives because they form close to the freezing point of water, and alpine soils - the source of carbon dioxide for karstification - are thin and vulnerable. Climate cooling is therefore widely considered to result in speleothem growth stops. This widely, however, ignores the fact that climate cooling will lead to a lowering of the equilibrium line altitude and the expansion of glaciers. A temperate glacier overflowing a karst system can prevent the latter from freezing. Although glacials were generally less humid than interglacials, alpine caves had a much higher chance of being glacier-covered during the ice ages (and hence being kept "warm") than caves at lower elevation elsewhere which were often in the permafrost zone. Times of non-freezing conditions in caves overlain by temperate glaciers cannot be recorded by speleothems unless the host rock contains disseminated pyrite. It is therefore not surprising that alpine caves carved in rather pure limestone

(e.g. Wetterstein and Dachstein Formations in the Eastern Alps) lack glacial-age speleothems. In contrast, speleothem growth in limestones interlayered with marls e.g. of Cretaceous age, wide-spread in the Western Alps, recorded ice-free conditions in the karst during times of superposition by glaciers.

Subglacial speleothems provide unique and precise windows into how alpine caves behaved during the long glacial periods. Combining them with the study of warm-climate speleothems controlled by soil dynamics (e.g., MOSELEY et al., 2020; WILCOX et al., 2020) as well as cryogenic cave carbonates (as robust indicators for the presence of cave ice accumulations), allows for the interpretation of alpine caves on glacial-interglacial time scales in addition to the production of extremely valuable information about climate and landscape evolution precisely registered by well-protected speleothems in the subsurface.

References

ATKINSON T.C. (1983) Growth mechanisms of speleothems in Castleguard Cave, Columbia Icefields, Alberta, Canada. Arctic and Alpine Research, 15, 523-536.

BOCH R. et al. (2011) NALPS: a precisely dated European climate record 120-60 ka. Climate of the Past, 7, 1247-1259.

FOHLMEISTER J. et al. (2019) Stalagmitenwachstum der letzten 200000 Jahre in den Karsthöhlen der Melchsee-Frutt (Kerns OW). Akten des 14. Nationaler Kongress für Höhlenforschung, Sinterlaken 2019, 179-184.

HONIAT C. et al. (2018) Toward a reconstruction of the Riss glaciation from Sieben Hengste Cave System stalagmites in Switzerland. International Symposium on Karstology, 27 June 27- 2 July 2018, Chambery, DOI: 10.13140/RG.2.2.29986.07366.

LUETSCHER M. et al. (2015) North Atlantic storm track changes during the Last Glacial Maximum recorded by Alpine speleothems. Nature Communications, 6: 6344, DOI: 10.1038/ncomms7344.

MOSELEY G.E. et al. (2020) NALPS19: Sub-orbital-scale climate variability recorded in northern Alpine speleothems during the last glacial period. Climate of the Past, 16, 29-50.

SPÖTL C. & MANGINI A. (2007) Speleothems and paleoglaciers. Earth and Planetary Science Letters, 254, 323-331.

SPÖTL C. et al. (2006) Chronology and paleoenvironment of Marine Isotope Stage 3 from two high-elevation speleothems, Austrian Alps. Quaternary Science Reviews, 25, 1127-1136.

WENDT K.A. et al. (2020) Precise timing of MIS 7 sub-stages from the Austrian Alps. Climate of the Past Discussions, DOI: 10.5194/cp-2020-145.

WILCOX P.S. et al. (2020) Exceptional warmth and climate instability occurred in the European Alps during the Last Interglacial period. Communications Earth & Environment, 1:57, DOI: 10.1038/s43247-020-00063-w.

Sedimentary evolution of the Bruniquel Cave, France

Sophie VERHEYDEN[1], Serge DELABY[2], Hubert CAMUS[3] & Jacques JAUBERT[4]

(1) Department of Earth History of Life, Royal Institute of Natural Sciences (RBINS), Brussels (RBINS) Belgium, sverheyden@naturalsciences.be
(2) UNESCO Global Geopark Famenne-Ardenne, Belgium, serge.delaby@geoparkfamenneardenne.be
(3) PROTEE-EXPERT, CENOTE sarl., France, camus.hubert@laposte.net
(4) PACEA- University of Bordeaux - CNRS UMR 5199, France, jacques.jaubert@u-bordeaux.fr

Abstract

The Bruniquel Cave along the Aveyron River in southern France, is known to be a remarkable archaeological site with its Neanderthal structures of broken stalagmites dated at 176.5 ± 2.1 ka and revising our knowledge of Neanderthal behaviour. Besides the archaeological finds, the cave also contains important natural detrital deposits of several meters thick and several generations of speleothems. The study and dating of the deposits indicate a long sedimentary history of at least 400 ka as indicated by the oldest ages obtained from a remobilised stalagmite lying on the present-day cave floor. At least three detrital infill and speleothem deposition cycles are observed. Flowstone U-Th dating suggests that the cave displays its current environment since 130 ka (MIS 5), while the good preservation of the anthropogenic Bruniquel structures suggests that no important sedimentary changes occurred in the cave since ~ 176 ka (MIS 6).

Résumé

Evolution sédimentaire de la grotte de Bruniquel, France. La grotte de Bruniquel, située le long de l'Aveyron dans le sud de la France, est connue pour être une "grotte archéologique" intéressante. Elle contient des structures de stalagmites brisées datées de 176,5 ± 2,1 ka et attribuées à l'Homme de Néandertal, ce qui contribue à réviser nos connaissances sur le comportement de Néandertal. Outre les découvertes archéologiques, la grotte contient d'importants dépôts détritiques naturels de plusieurs mètres de haut et plusieurs générations de spéléothèmes. L'étude et la datation des dépôts indiquent une longue histoire sédimentaire d'au moins 400 000 ans, comme l'indiquent les âges les plus anciens obtenus à partir d'une stalagmite remobilisée reposant sur le sol actuel de la grotte. Plusieurs, et au moins trois, cycles de "dépôts de sédiments détritiques et de spéléothèmes" sont observés. La datation U-Th de la calcite suggère que la grotte n'a pas beaucoup changée depuis 130 000 ans (SIM 5), tandis que la bonne préservation des structures anthropogènes de Bruniquel suggère qu'aucun changement sédimentaire important n'a eu lieu dans la grotte depuis ~ 176 ka (SIM 6).

1. The Bruniquel Cave, anthropogenic structures and animal traces.

The Bruniquel Cave is situated in front of the medieval Bruniquel village, nearby the 'confluence of the Vère river with the Aveyron River. The cave (Fig 1) develops in Bajocian limestone at approximately 50 meters above the Aveyron River. The cave was discovered in the early nineties by the Société Spéléo-Archéologique de Caussade, a local caving club. At 300 meters from the entrance, several strange, roughly circular structures of broken stalagmites were discovered. The cave is structured as a single, rather straight gallery, in general 15 meters large and 2 to 5 meters high. The gallery is, rich of warmly coloured speleothems and several large rimstone basins. Several bear hollows are observed along the cave. A first archaeological study, led by F. Rouzaud and M. Soulier (ROUZAUD et al., 1997), including a ^{14}C dating of a burnt bone fragment, indicated an age of at least 47 000 years (ROUZAUD et al., 1995). In 2016, uranium-thorium dating of the stalagmites inside the largest structure during a second archaeological study led by JAUBERT, VERHEYDEN and GENTY et al. (2016), indicated an age of 176 500 years with an uncertainty of ±2 100 years. The age came as a surprise and changed our perception of Neanderthals as the first cavers, mastering perfectly well their underground environment. Besides, the discovery indicates that these humans perfectly mastered fire and had already strong social bands, regarding the complexity of the constructions.

The structures, although well preserved, seem to have undergone some damage, likely due to gravity, flooding or the presence of bears. To better understand the history of these structures, as well as of the entire cave, the study of the cave and its deposits is one aspect of the general study of the site. The gallery formed through the limestone hill surrounded by the river and suggests two possible entrances. Indeed, the current entrance was opened by digging in the sediments and the limestone. The cave is rich in speleothems and several phases of speleothem deposition are clearly observed. Complex sedimentary profiles and a wide range of speleothem ages suggest a rich cave history prior to the construction of the structures. First observations and mapping of the cave deposits, combined with U-Th dating of speleothems, give some first insights in the successive infilling phases in the cave. A preliminary simplified model of the general sedimentary dynamics and resulting endokarstic landscapes is proposed.
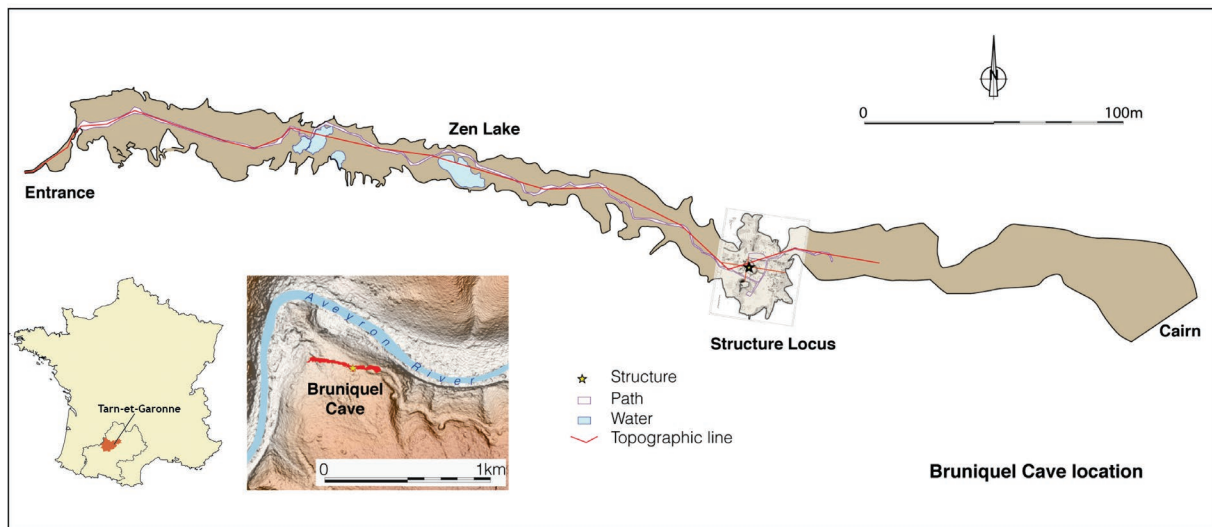
Figure 1: Location and map of the Bruniquel Cave.

2. Speleothem growth over five Glacial-Interglacial cycles

The BR-stm-8 stalagmite (Fig. 2) was found, completely embedded in clay, lying on the pathway just before the massive fallen limestone rock called the 'Chaos' area. This area is situated at ~100 m from the entrance. The stalagmite has two distinct basal 'crowns' suggesting a partial sedimentary burial and restart of speleothem growth on this new ~10 cm detrital layer. The internal sedimentary structure of the stalagmite confirms a significant cave infilling at ~347.9 (± 8.0) ka as demonstrated by the remaining detrital layer between two calcite layers and the more recent speleothem on top of it (Fig. 2, circle). Several other 'detrital episodes' are detected in the stalagmite during the final phase of the Interglacial ~MIS 11 and the Glacial, ~MIS 10 periods (Fig. 3). A final, more stable and rapid, calcite growth occurred from 335.1 ± 3.1 ka up to the top of the stalagmite at 330.4 ± 4.0 ka, in agreement with ~MIS 9 interglacial conditions.

In total, already ~100 speleothem ages were obtained from speleothems in the Bruniquel cave since the start of this study in 2014. The ages indicate speleothem growth over 5 Glacial-Interglacial cycles (Fig. 3). This is in agreement with in-cave observations of several speleothem phases alternating with or embedded in detrital infills, identified during mapping of the cave, demonstrating a multiphase sedimentation history.

Figure 2: Bruniquel Cave – Internal section of the BR-stm-8 stalagmite (middle) found ex-situ (left) in vicinity of the 'Chaos'. Right: MC-ICP-MS U-Th dating results (Hai Cheng, Xi'an Jiaotong University). The circle indicates incorporated detrital sediments with new stalagmite growth on top of it.

3. Relation with regional climate

The alternating detrital and speleothem deposition in temperate regions is known to be closely linked to climate, more specifically to alternating warm and cold periods (QUINIF et al., 2006). Figure 3 shows the U/Th ages obtained from speleothems in the cave against Northern Hemisphere climate reference curves. Results reveal speleothem deposition during Glacial and Interglacial periods with, however, limited speleothem deposition during the coldest glacial episodes and with several detrital infill episodes during declining interglacial and glacial periods as suggested by BR-stm-8. Further work will focus on the relation between warm phases (Interstadials) of glacial periods and speleothem deposition.
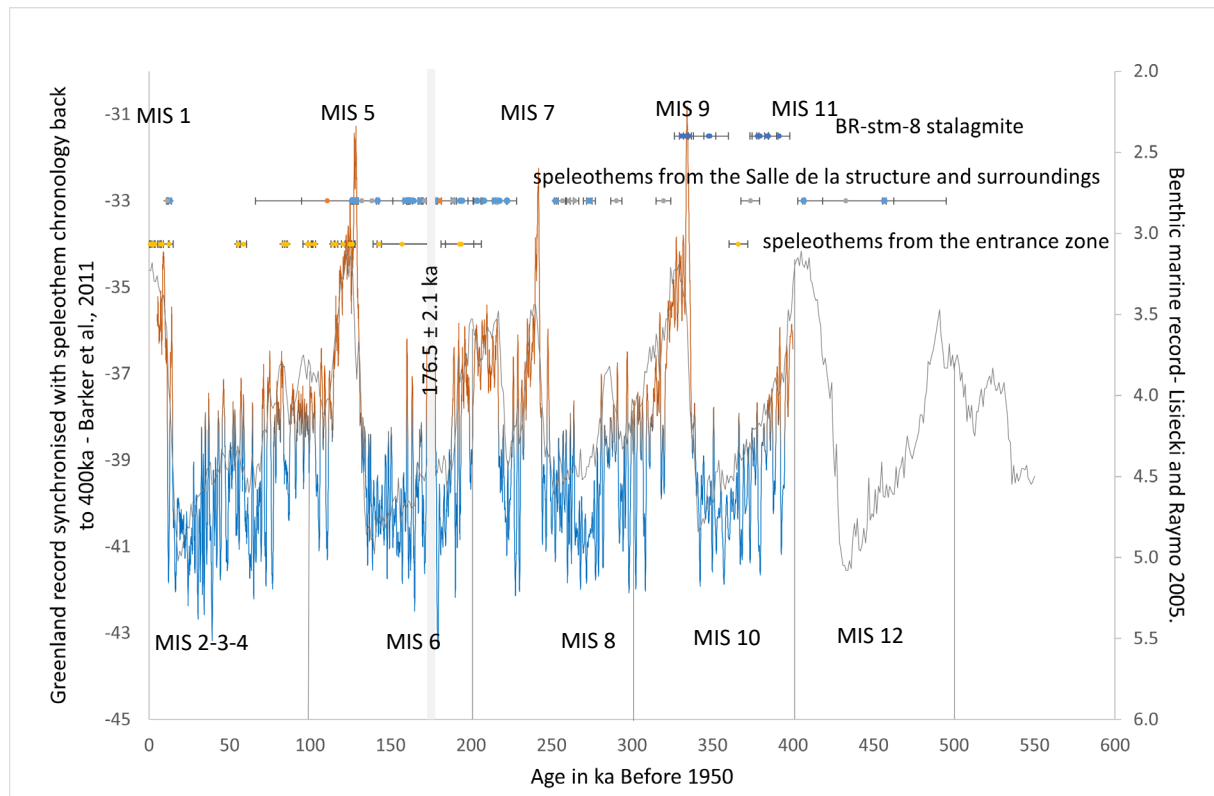
Figure 3: Bruniquel Cave – Speleothem ages reported on the northern hemisphere climatic curve. The succession of Interglacial (IG)(MIS 1, 5, 7,..) and Glacial (G) (MIS 2-3-4, 6, 8, 10) periods are highlighted by the red and blue colours respectively. The age of the Neanderthal structure (176.5 ka) including its uncertainty (±2.1 ka) is indicated by the grey vertical bar. The ages of other dated speleothems in the cave are indicated as dots above the climatic curve and their uncertainties are shown as horizontal lines at each side of the dot. The BR-stm-8 stalagmite for example, was deposited during the IG-G-IG periods ~MIS 11-10-9.

4. Multiphase sedimentary dynamics in the Bruniquel Cave – a first model

Besides the indications for past regular flooding of the cave in the BR-stm-8 stalagmite, other observations on the sedimentary dynamics can be made. No cobbles or gravel are found in the cave, with exception of those found in the entrance collapse. Fine grained deposits are found on horizontal limestone ledges, even several meters high. Moreover, at several places in the cave and especially more than 300 meters from the current entrance, indications occur for suffosion, i.e. where loose material is drained by percolation water and disappears in underlying voids. Remnants of clay deposits, slumping of the clay, destabilized stalagmites, and swallow holes are strong indications for the existence of an active drainage underneath the main gallery of the Bruniquel Cave.

Since no indications are found up to now for a main high-energetic river flowing through the gallery, we hypothesis detrital deposition by low energy floods, during higher basal levels (*cf.* QUINIF, 1989). The suffosion holes in the gallery may therefore have functioned as 'sources' for upcoming water and the main gallery may have played the role of an overflow gallery resulting in the multiphase sedimentation (Fig. 4).
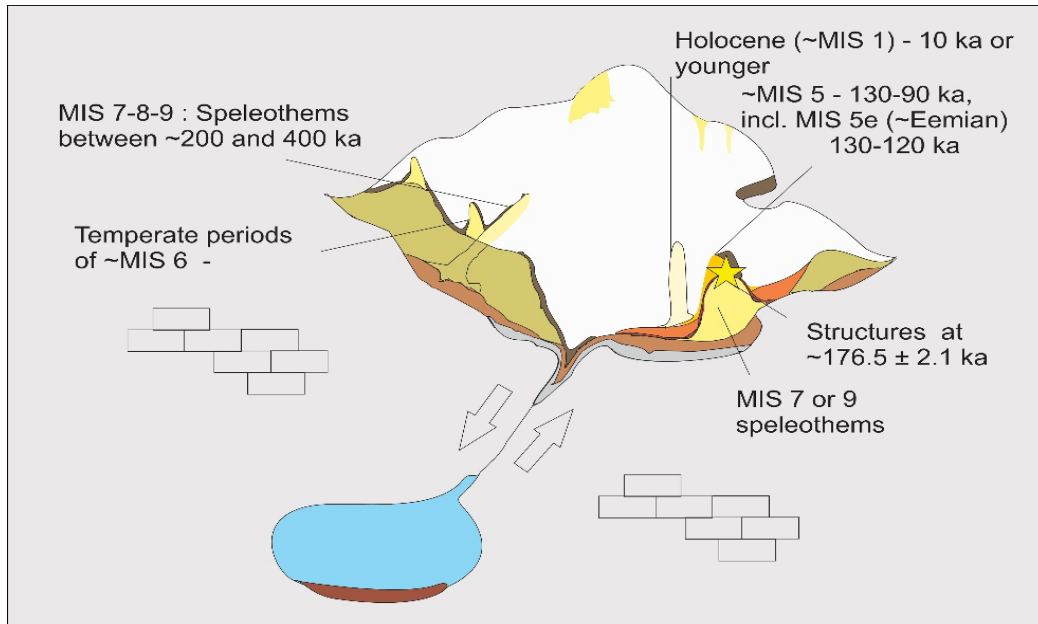
Figure 4: Bruniquel Cave –Simplified model of sedimentary dynamics in the cave leading to the current endokarstic landscape.

5. General conclusions and perspectives.

A first assessment of the sedimentary deposits in the Bruniquel cave leads to a preliminary model for the sedimentary dynamics in the cave. The generally fine-grained deposits observed up to now in the cave and the absence of clear high energetic river morphologies suggest a multiphase sedimentation due to successive flooding related to changes of water base levels, eventually climate driven. An active karstic system underlying the main gallery seems responsible for suffosion phenomena and could have played a role in successive flooding of the main gallery, which could have functioned as an overflow of the karstic system. Within this cave evolution, the 'anthropogenic' period is strictly constrained between 174 ka and 179 ka. Further studies will look for the underlying active system, continue mapping and dating of sediments and explore in detail the relation with climate. The dating of speleothems together with detailed morpho-stratigraphic observation is crucial in the elaboration of an environmental evolution model of the cave and its surroundings.

Acknowledgments

References

BARKER S, KNORR G, EDWARDS R.L, PARRENIN F, PUTNAM A.E, SKINNER L.C, WOLFF E, ZIEGLER M (2011) 800,000 Years of Abrupt Climate Variability. Science, 334, 347-351.

JAUBERT J, VERHEYDEN S, GENTY D, SOULIER M, CHENG H, BLAMART D, BURLET Ch, CAMUS H, DELABY S, DELDICQUE D, EDWARDS R. L, FERRIER C, LACRAMPE-CUYAUBÈRE F, LÉVÊQUE F, MAKSUD F, MORA P, MUTH X, RÉGNIER É, ROUZAUD J.-N, SANTOS F (2016). Early Neanderthal constructions deep in Bruniquel Cave in southwestern France. Nature, n° 534, 111-115.

LISIECKI L.E, RAYMO M.E (2005) A Plio-Pleistocene Stack of 57 Globally Distributed Benthic 18O Records. Palaeoceanography, n° 20, 17 pp PA1003.

QUINIF Y (1989) La notion d'étages de grottes dans le karst belge. Karstologia, n° 13, 41-49.

QUINIF Y (2006). Complex stratigraphic sequences in Belgian caves. Correlation with climatic changes during the middle, the upper Pleistocene and the Holocene. Geologica Belgica, 9/3-4, 231-244.

ROUZAUD F, SOULIER M, LIGNEREUX Y (1995) La grotte de Bruniquel. Spelunca, n°60, décembre 95, 27-34.

ROUZAUD F, SOULIER M, LIGNEREUX Y (1997) La structure paléolithique de la grotte de Bruniquel (Tarn-et-Garonne, France) Intern. Congress of Speleology, La Chaux-de-Fonds, n°3, S2, Archaeology and Palaeontology in Caves, 71-74.

The barite conundrum: active growth of non-hydrothermal BaSO$_4$ speleothems in Lechuguilla Cave (New Mexico, USA)

Max WISSHAK[1], Hazel A. BARTON[2], Katey E. BENDER[2] & Harvey R. DUCHENE[3]

(1) Senckenberg am Meer, Marine Research Department, 26382 Wilhelmshaven, Germany, max.wisshak@senckenberg.de (corresponding author)
(2) University of Akron, Department of Biology, Akron, OH 44325-3908, USA
(3) PO Box 362, Lake City, CO 81235, USA

Abstract

Barite (BaSO$_4$) speleothems have been reported from caves around the globe and interpreted to have chiefly formed in phreatic, hypogene, hydrothermal settings. Here, we report two contrasting types of barite speleothems – bluish tabular pool crystals and actively dripping greenish stalactites – which today form at lower temperatures in the non-hydrothermal environment of Lechuguilla Cave, New Mexico, USA.

SEM analysis, together with energy- and wavelength-dispersive X-ray spectroscopy (EDS, WDS) as well as X-ray diffraction (XRD), characterize the habit and chemical composition as barite. In both elements, fractionation of the minor element calcium is related to growth along different crystal faces whereas variations in strontium are mirrored in blue color zoning of the pool crystals.

Two possible modes of non-hydrothermal barite precipitation are discussed: (1) intense evaporation driven by thermal atmospheric convection cells, or (2) mixing of barium-rich, sulfate-poor water with water rich in sulfate. Both processes, in isolation or in combination, lead to supersaturation and could explain formation of the investigated barite speleothems. Observations of three types of microbes on the pool barite crystals showing evidence of incrustation raises the question whether (3) there is a potential involvement of microbial activity in the temperate barite precipitation in Lechuguilla Cave.

1. Introduction

The formation of barite (BaSO$_4$) in continental settings is usually associated with hydrothermal activity supporting the formation of massive barite as a component of ore deposits (HANOR 2000). Remobilization and phreatic reprecipitation of barite in a hypogene hydrothermal karst environment is believed to be responsible for the majority of the known occurrences of barite as a cave mineral (HILL & FORTI 1997). For at least some of those occurrences, a hydrothermal origin has been demonstrated by analysis of fluid inclusions and/or sulfur stable isotope analyses (for review, see DUBLYANSKY 1997).

Barite speleothems that formed in the vadose zone under subaerial conditions in caves are rare (e.g. MALTSEV & MALISHEVSKY 1990, HILL & FORTI 1997, ONAC *et al.* 2014) and active formation has not been demonstrated for any of these occurrences. The fact that barite can form in non-hydrothermal settings in the ocean (GRIFFITH & PAYTAN 2012), such as cold vent sites (GREINERT *et al.* 2002, STEVENS *et al.* 2015), has raised the question whether barite could also form in caves under non-hydrothermal conditions. In a recent paper (WISSHAK *et al.* 2020) we have characterized two such types of actively growing barite speleothems in a temperate environment (normal-temperature cave setting = 5-25°C sensu DUBLYANSKY 1997), both discovered in Lechuguilla Cave, New Mexico, USA. Lechuguilla Cave is among the world's largest cave systems and has recently surpassed 150 miles (~240 km) of survey (WISSHAK 2020). The cave formed in the carbonate rocks of the Permian Capitan Reef Complex in the Guadalupe Mountain uplift through hypogene sulfuric acid speleogenesis (HILL 2000). Substantial deposits of gypsum were left behind as a byproduct and their secondary dissolution and reprecipitation led to the formation of a wide variety of speleothems (e.g. DAVIS 2000, POLYAK & PROVENCIO 2001). Lechuguilla Cave contains many rare cave minerals, many of which are directly or indirectly related to sulfuric acid speleogenesis (DUCHENE 1997, DAVIS 2000, POLYAK & PROVENCIO 2001). This inventory includes greenish barite stalactites that drip water, first identified in an area called 'Frostworks', and bluish barite crystals forming at the bottom of a calcite-lined pool in an area called 'Blanca Navidad'. Our detailed analysis of samples taken from these two sites has employed a combination of crystallographic investigation, micro-structure analysis, and elemental mapping (WISSHAK *et al.* 2020). Based on the results and circumstantial evidence from the geological and speleological setting we have discussed potential modes of these types of non-phreatic and non-hydrothermal barite precipitation.

In this proceedings paper, we briefly summarize our findings and provide an outlook on our anticipated future research on these and related unusual speleothems.

2. Materials and methods

A database of all suspected and confirmed occurrences of barite and celestine in Lechuguilla Cave was compiled from expedition reports and the mineral inventory database maintained by the Carlsbad Cavern National Park.

Two samples were taken from barite speleothems, one piece of a broken stalactite from 'Frostworks' and one subaqueous crystal from a pool in 'Blanca Navidad'.

Samples were air-dried, photographed, and subsamples were prepared for scanning electron microscopy (SEM) undertaken with a Tescan VEGA3 xmu at 20 keV.

Samples were ground to powder for X-ray diffraction (XRD) analysis on a Philips PW1729 X-ray generator with a 2200 Watt 60 keV Cu X-ray source. Analyses were run at 40 keV and 30 mA in a 2 Theta range from 15 to 60°.

High-resolution elemental mapping of resin-embedded and polished samples with wavelength dispersive X-ray spectroscopy (WDS) was carried out on a JEOL Superprobe JXA-8200 electron microprobe. Elemental maps were produced on a 5 to 10 µm grid with a 10 µm probe diameter at 100 ms dwell time, 15 keV acceleration voltage and a beam current of 100 nA. Detailed maps were acquired on a 1 µm grid at the margin of the crystals, with a 1 µm probe diameter at 100 ms dwell time, 15 keV acceleration voltage and a beam current of 100 nA. Quantitative transects were logged in 5 to 10 µm spacing across overview maps, and 1 µm spacing across detail maps, applying 5 or 1 µm probe diameters, respectively, at 15 keV acceleration voltage, 50 nA beam current.

3. Results

Numerous greenish to greenish-bluish stalactites were found within a perimeter of about 500 m in the western branch of the cave. They are up to 20 cm in length, have moist surfaces, actively drip water, in some cases form greenish splash points below (Fig. 1A-B). Our sample is composed of an aggregate showing parallel crystallites resulting from parting, tabular to the pinacoid base c {001} in the orthorhombic system. The outer surface of the stalactite primarily shows faces of the prism m {210} and pinacoid a {100} (see Fig. 2 for a diagram of the crystallographic properties). Several hundred bluish tabular crystals, up to 2 cm in size, were found growing in a shallow pool, lined with calcite spar, in the 'Blanca Navidad' area (Fig. 1C), situated also in the western branch of the cave. Our sample is a nearly idiomorphic platy crystal, tabular to the pinacoid base c {001} in the orthorhombic system, and lateral faces are formed by the prism m {210}. Along the latter, the crystal shows a blue color zonation.

Mineral identification of both samples via XRD analysis in the 15° to 60° (2θ) range matches the peak signature of barite. No other mineral was detected in the samples.

High-resolution element mapping via WDS shows a homogeneous distribution of the major elements Ba, S, and O, in a stoichiometric relationship corresponding to that of barium sulfate ($BaSO_4$). This applies also to the outer margin of the crystal, which was mapped and profiled with 1 µm resolution, thereby excluding the presence of a detectable layer of witherite ($BaCO_3$). Calcium (Ca) and strontium (Sr) were the only detected trace elements; other elements that can substitute for Ba in barite (Ca, K, Ra, Pb, and more rarely Fe, Cu, Zn, Ag, Ni, Hg, V; HANOR 2000, GRIFFITH & PAYTAN 2012), were not detected. Concentrations of Ca and Sr vary with growth along the prism m {210} faces, reaching concentrations of up to 4,820 ppm and 26,200 ppm, respectively, in the case of the pool crystals. Calcium concentrations are higher in parts that grew along the pinacoid face c {001}, whereas Sr was found relatively depleted in these zones, thus showing an inverse pattern. The respective Sr/Ca ratios cluster accordingly. Concentrations of Sr mirror the blue color zoning in the pool crystals in that the outermost (youngest) zone shows the highest Sr concentrations and most intense coloration.

Figure 1: One of several greenish barite stalactites in the Frostworks area (A), another one with a greenish splash point below (B), and subaqueous barite crystals with blue color zoning in a shallow pool in Blanca Navidad (C).
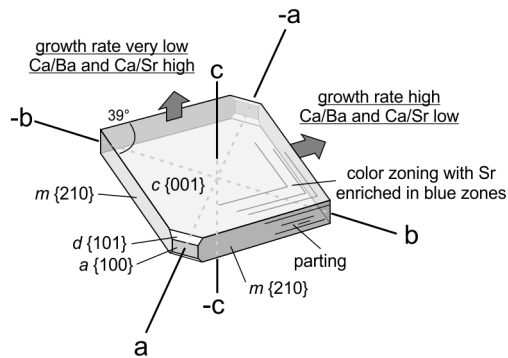
Figure 2: Mineralogical properties of the sampled barite speleothems: The crystallographic axes and principal faces are shown for an idiomorphic tabular crystal prismatic to the pinacoid base c {001}. Parting occurs parallel to c {001} and color zoning (pool crystals only) parallel to the prism faces m {210}. High growth rates along m {210} and a {100} show low Ca concentrations, whereas slow growth along m {210} leads to relatively high Ca concentrations.

4. Discussion

The classical interpretation of barite speleothems as a result of phreatic hydrothermal activity can be excluded for both the barite stalactites and the barite pool crystals that are likely still forming today in the vadose and temperate environment of Lechuguilla Cave (see our discussion in WISSHAK *et al.* 2020). For tackling this conundrum, we discuss three possible underlying processes of non-hydrothermal barite precipitation that might be active, in isolation or in combination, in Lechuguilla Cave: 1) evaporation, 2) mixing of water rich in barium with water rich in sulfate, and 3) microbial activity:

1) Evaporation model: Significant evaporation can lead to supersaturation with respect to barite, leading to precipitation until saturation is reached. Prominent thermal atmospheric Rayleigh-Benard convection cells in Lechuguilla Cave have long been identified as drivers for condensation and evaporation, controlling the formation of corrosion residues / ferromanganese deposits and leading to directional growth of speleothems, respectively (e.g. QUEEN 1994). In 'Frostworks', corrosion residues at the ceiling and aragonite frostwork on calcite popcorn at the bottom, together with the observation of significant airflow in the area, suggest that condensation and evaporation take place. Evaporation is also conceivable for the barite pool in 'Blanca Navidad', where recharge and discharge of water is via discrete seepage from flowstone only, complemented by occasional drips from overlying stalactites, so that the retention time in the pool is considerable. This part of 'Blanca Navidad' is rich in aragonite frostwork and other speleothems that are indicative of surface diffusion and evaporation. The observed Sr concentrations and color zoning might provide circumstantial evidence for episodes of increased evaporation and a temporarily closed system, as Ba is removed preferentially over Sr from aqueous solutions (HANOR 2000).

Three types of microbial morphology were identified on, and partly embedded within the sampled barite pool crystal: Type 1 microbes form filaments 0.3-0.4 µm in diameter and were found collapsed on the surface with associated coccoidal cells or spores. Some filaments enter or exit deep trenches or angular holes formed by crystal overgrowth.

Type 2 microbes are only evident where the barite has grown around the original organic filaments, leaving incrustations that mimic their structure. These incrustations suggest unbranched filaments, 0.2-0.4 µm in diameter, meandering on the surface of the crystal and originating from a circular central area. Individual furrows or the entire structure are partially overgrown by younger barite crystallites, along with barite precipitating between filaments to form micro-terraces.

Evidence of Type 3 microbes are rod-shaped incrustation structures, three to five microns in length and about one micron in diameter, observed in broken sections of the crystal.

However, considering the poor solubility of barite in water (2.2 mg/l at 18°C; SEIDELL 1940), this scenario requires immense amounts of water to evaporate to form barite speleothems the size of the documented stalactites.

2) Mixing model: An alternative model is mixing of waters from two different sources, one rich in Ba^{2+} and devoid of SO_4^{2-}, the other rich in SO_4^{2-}. Mixing of such waters would result in supersaturation with respect to barite and instant precipitation until saturation is reached (HANOR 2000, GRIFFITH & PAYTAN 2012). In Lechuguilla Cave, this scenario is conceivable where condensation water meets percolating meteoric water, or at mixing points of meteoric waters with different pathways. An obvious source of sulfate is contact with the abundant secondary gypsum deposits, whereas barium ions might derive from the host rock, corrosion residues, ore deposits, or other sources to be identified.

3) Microbe model: The discovery of microbes associated with the barite pool crystals (we cannot exclude their presence in the case of the stalactites) raises the question whether there could be microbial involvement in the precipitation of these barite speleothems, or whether the documented association is coincidence. There is a growing body of evidence that microbial activity is an integral component of barite formation, particularly in the marine realm (STEVENS *et al.* 2015 and references therein), but also in terrestrial settings (SENKO *et al.* 2004). For instance, some bacteria mediate barite precipitation by means of sulfur/sulfide-oxidation. In the latter context, the recent discovery of massive gypsum and a substantial deposit of elemental sulfur only few meters above the barite speleothems in 'Barite Boulevard' is a puzzling finding that may hold a key for the understanding of the barite precipitation below in terms of microbial sulfur-oxidizing activity.

5. Outlook

In a future project, we plan to study the closely related sulfate mineral celestine ($SrSO_4$). Barite and celestine form a solid solution series (see HANOR 2000 for a review) and both occur and form speleothems in Lechuguilla Cave. This provides a unique opportunity to study the two minerals in concert.

Plans are being made for two research expeditions that revisit most of the confirmed or suspected occurrences of barite and celestine in the cave. Detailed documentation of the minerals in situ together with targeted sampling will allow a mineralogical and geochemical 'fingerprinting'

(stable isotope signatures and trace element concentrations) and, as far as technically possible, age determinations of these occurrences. Water samples, together with evaporation experiments and autonomous data loggers, will provide the essential environmental data and information on the water chemistry for assessing the contribution of three potential modes of mineralogenesis in the cave, and for evaluating the value of barite and celestine speleothems as a geochemical archive for environmental change.

References

Davis D.G. (2000) Extraordinary features of Lechuguilla Cave, Guadalupe Mountains, New Mexico. Journal of Cave and Karst Studies 62: 147-157.

Dublyansky Y.V. (1997) Hydrothermal cave minerals. In: Hill C.A., Forti P. (Eds.), Cave minerals of the world. 2nd edition, National Speleological Society, Huntsville, p. 252-255.

DuChene H.R. (1997) Lechuguilla Cave, New Mexico, USA. In: Hill C.A. & Forti P. (Eds.), Cave minerals of the world. 2nd edition, National Speleological Society, Huntsville, p. 343-350.

Greinert J., Bollwerk S.M., Derkachev A., Bohrmann G., Suess E. (2002) Massive barite deposits and carbonate mineralization in the Derugin Basin, Sea of Okhotsk: precipitation processes at cold seep sites. Earth and Planetary Science Letters 203: 165-180.

Griffith E.M., Paytan A. (2012) Barite in the ocean – occurrence, geochemistry and palaeoceanographic applications. Sedimentology 59: 1817-1835.

Hanor J.S. (2000) Barite–celestine geochemistry and environments of formation. In: Alpers C.N. et al. (Eds.), Sulfate minerals: crystallography, geochemistry and environmental significance. Reviews in Mineralogy and Geochemistry 40: 193-275.

Hill C.A. (2000) Overview of the geologic history of cave development in the Guadalupe Mountains, New Mexico. Journal of Cave and Karst Studies 62: 60-71.

Hill C.A., Forti P. (1997) Cave minerals of the world. 2nd edition, National Speleological Society, Huntsville, 463 p.

Maltsev V.A., Malishevsky D.I. (1990) On hydrothermal phases during later stages of the evolution of Cup

Coutunn Cave System, Turkmenia, U.S.S.R.. NSS Bulletin 52: 95-98.

Onac B.P., Fornós J.J., Merino A., Ginés J., Diehl J. (2014) Linking mineral deposits to speleogenetic processes in Cova des Pas de Vallgornera (Mallorca, Spain). International Journal of Speleology 43: 143-157.

Polyak V.J., Provencio P. (2001) By-product materials related to H2S-H2SO4-influenced speleogenesis of Carlsbad, Lechuguilla, and other caves of the Guadalupe Mountains, New Mexico. Journal of Cave and Karst Studies 63: 23-32.

Queen J.M. (1994) Influence of thermal atmospheric convection on the nature and distribution of microbiota in cave environments. In: Sasowsky I.D., Palmer M.V. (Eds.), Breakthroughs in karst geomicrobiology and redox geochemistry. Karst Waters Institute, Special Publication 1: p. 62-64.

Seidell A. (1940) Solubilities of inorganic and metal organic compounds. 3rd edition, volume 1, D. Van Nostrand Company, New York, 1689 p.

Senko J.M., Campbell B.S., Henriksen J.R., Elshahed M.S., Dewers T.A., Krumholz L.R. (2004) Barite deposition resulting from phototrophic sulfide-oxidizing bacterial activity. Geochimica et Cosmochimica Acta 68: 773-780.

Stevens E.W.N., Bailey J.V., Flood B.E., Jones D.S., Gilhooly W.P., Joye S.B., Teske A., Mason O.U. (2015) Barite encrustation of benthic sulfur-oxidizing bacteria at a marine cold seep. Geobiology 13: 588-603.

Wisshak M., Barton H.A., Bender K., DuChene H.R. (2020) Active growth of non-hydrothermal subaqueous and subaerial barite (BaSO4) speleothems in Lechuguilla Cave (New Mexico, USA). International Journal of Speleology 49: 11-26.